Development of photocatalytic ceramic membrane for the removal of pharmaceuticals from water

L Sawunyama

orcid.org/0000-0003-3494-8118

Thesis accepted in fulfilment of the requirements for the degree Doctor of Philosophy in Chemistry at the North-West University

Promoter: Prof DC Onwudiwe

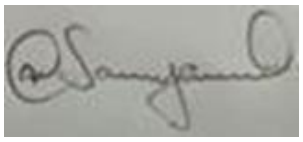
Co-Promoter: Dr OA Oyewo

Assistant-Promoter: Dr MF Bopape

Graduation: May 2025

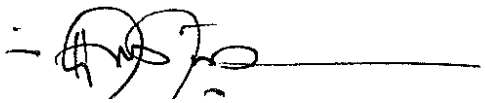
CERTIFICATION

This is to certify that the thesis titled “Development of photocatalytic ceramic membrane for the removal of pharmaceuticals from water” is an authentic research work carried out by SAWUNYAMA LAWRENCE under the supervision of Prof. Damian Chinedu Onwudiwe at the Chemistry department of the North-West University, Faculty of Natural and Agricultural Sciences, South Africa.



Date: 20-03-2025

L. Sawunyama



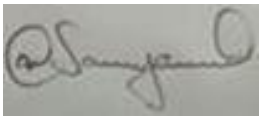
Date: 21-03-2025

Prof. D.C. Onwudiwe

DECLARATION

I declare that this doctoral thesis titled: "***Development of photocatalytic ceramic membrane for the removal of pharmaceuticals from water***" is solely owned by me, and has not been submitted to any other institution for the purpose of obtaining a degree or qualification, and all sources cited are acknowledged by comprehensive referencing where any information has been derived from other sources.

Sawunyama Lawrence

Signature:  20-03-2025

DEDICATION

This thesis is dedicated to my beloved wife, Sandra; my son, Zayden Akudzweishe; and my parents, Henry and Georgina.

ACKNOWLEDGEMENT

I want to express my heartfelt gratitude to the individuals and institutions that have guided and supported me throughout my PhD studies at North-West University. First and foremost, I thank the Lord for the gift of life and for keeping me in good health throughout my studies. I am particularly grateful for His protection during the countless long journeys from Masvingo, Zimbabwe, to Mafikeng, South Africa, and back.

I extend my deepest appreciation to my supervisor, Prof. Damian C. Onwudiwe, for granting me the opportunity to pursue my PhD in the Inorganic and Material Science Research Group. Your unwavering encouragement and support have been invaluable. Your passion and exemplary approach to your work highlight that outstanding achievements are the result of hard work and dedication. Thank you for being an exceptional mentor and making significant contributions to my academic journey. I also want to express my sincere appreciation to my co-supervisors, Dr. Opeyemi and Dr. Bopape. Your significant contributions, especially in proofreading the manuscripts, have greatly enhanced the quality and clarity of the work.

I also wish to thank members of the Department of Chemistry at NWU for their invaluable support. I am particularly thankful to Mr. Sizwe, Mr. Peter, and Ms. Murendeni for their assistance in analyzing the samples. To all members of the research group (Dr Chris, Nozipho, Azeezat, Simangile, Fando, Amanda, Lucky and Hassan) working alongside you has been a pleasure, and your encouragement has been greatly appreciated.

I am also deeply grateful to my friends mukoma E. Hweru and mudhara A. Dube. Your continuous support and check-ins have been incredibly motivating. I would like to express sincere appreciation to Dr Timothy Ajiboye and his family for their generous assistance in helping me settle in Mafikeng. Your warm welcome and support made my transition to this new environment much easier and more pleasant. I am truly grateful for your kindness.

To my beautiful wife, Sandra thank you for your continuous support throughout my PhD studies. Your encouragement and empathy have been a constant source of strength. Your dedication and sacrifices have made this journey possible, and I am grateful for everything you have done. Lastly, I extend my utmost acknowledgements to my parents, Henry and Georgina, and all my siblings for their love and support throughout my studies.

LIST OF PUBLICATIONS

1. **Sawunyama, L.**, Oyewo, O. A., Seheri, N., Onjefu, S. A., & Onwudiwe, D. C. (2023). Metal oxide functionalized ceramic membranes for the removal of pharmaceuticals in wastewater. Surfaces and Interfaces, 38, 102787 https://doi.org/10.1016/j.surfin.2023.102787

2. **Sawunyama, L.**, Ajiboye, T. O., Oyewo, O., & Onwudiwe, D. C. (2023). Ceramic-polymer composite membranes: synthesis methods and environmental applications. *Ceramics International*. https://doi.org/10.1016/j.ceramint.2023.11.337

3. Ajiboye, T. O., **Sawunyama, L.**, Ravele, M. P., Rasheed-Adeleke, A. A., Seheri, N. H., Onwudiwe, D. C., & Mhlanga, S. D. (2023). Synthesis approaches to ceramic membranes, their composites, and application in the removal of tetracycline from water. *Environmental Advances*, *12*, 100371. https://doi.org/10.1016/j.envadv.2023.100371

4. **Sawunyama, L.**, Olatunde, O. C., Oyewo, O. A., Bopape, M. F., & Onwudiwe, D. C. (2024). Application of coal fly ash based ceramic membranes in wastewater treatment: A sustainable alternative to commercial materials. *Heliyon*. https://doi.org/10.1016/j.heliyon.2024.e24344

5. **Sawunyama, L.**, Oyewo, O., Onwudiwe, D. C., & Makgato, S. S. (2023). Photocatalytic degradation of tetracycline using surface defective black TiO_2–ZnO heterojunction photocatalyst under visible light. *Heliyon*, *9*(11). https://doi.org/10.1016/j.heliyon.2023.e21423

6. **Sawunyama, L.**, Oyewo, O. A., Bopape, M. F., & Onwudiwe, D. C. (2024). Fabrication and characterization of low-cost ceramic membranes from coal fly ash and natural sand. *Sustainable Chemistry for the Environment*, *8*, 100165.https://doi.org/10.1016/j.scenv.2024.100165

7. **Sawunyama, L.**, Oyewo, O. A., Makgato, S. S., Bopape, M. F., & Onwudiwe, D. C. (2025). TiO_2–ZnO functionalized low-cost ceramic membranes from coal fly ash for the removal of tetracycline from water under visible light. *Discover Nano*, *20*(1), 1. https://doi.org/10.1186/s11671-024-04178-3

Other articles that are not included in this thesis

8. Ajiboye, T. O., Mafolasire, A. A., **Lawrence, S.**, Tyhali, N., & Mhlanga, S. D. (2024). Composite and Pristine Silver Bismuth Sulphide: Synthesis and Up-to-Date Applications. *Journal of Inorganic and Organometallic Polymers and Materials*, *34*(2), 433-457. https://doi.org/10.1007/s10904-023-02838-y

9. Olatunde, O. C., **Sawunyama, L.**, Yusuf, T. L., & Onwudiwe, D. C. (2024). Visible light driven $CuBi_2O_4$ heterostructures and their enhanced photocatalytic activity for pollutant degradation: A review. *Journal of Water Process Engineering*, *66*, 105890. https://doi.org/10.1016/j.ceramint.2023.11.337

Conference papers/Symposiums/Presentations

1. **Sawunyama Lawrence** and Damian C. Onwudiwe**,** "Functionalized low-cost ceramic membranes from coal fly ash for the removal of antibiotics from water under visible light, US-Botswana Workshop on Research Technologies in Water and Energy Needs for Remote, Austere Locations 2024 (WORTHWEEDS 2024), Cresta Maun Hotel, Maun, Botswana 22 - 25 July 2024 (*Oral presentation*).

2. **Sawunyama Lawrence** and Onwudiwe D.C (2024) Preparation and characterization of TiO_2-ZnO/CFA-NS photocatalytic ceramic membranes for the photocatalytic degradation of tetracycline under visible light. WaterNet/WARFSA/GWP-SA Symposium 2024 held 30th of October to 1st of November 2024 Avani Maseru Hotel, Maseru, Lesotho. Won the *First Prize for Outstanding Presentation by a Young Water Scientist* at the symposium

3. Presented at the North-West University Postgraduate Student Poster Presentation Competition, the poster titled 'TiO_2-ZnO Functionalized Low-Cost Ceramic Membranes from Coal Fly Ash for the Removal of Tetracycline from Water Under Visible Light' was showcased on October 3, 2024."

ABSTRACT

The use of advanced hybrid wastewater treatment techniques in the elimination of emerging contaminants such as pharmaceuticals has recently attracted significant interest as a viable technique for industrial scale wastewater treatment. Advanced hybrid wastewater treatment techniques are based on the integration of different advanced wastewater treatment techniques such as membrane technology, advanced oxidation processes and bioremediation. Each approach addresses different aspects of contaminants removal, resulting in a robust system that enhances efficiency by minimizing the drawbacks of individual technique and enhancing their advantages. The aim of this study was to prepare a hybrid wastewater treatment technique involving photocatalysis and ceramic membrane technology and evaluate their efficiency in the removal of tetracycline as a model wastewater pollutant by utilising both photocatalysis and filtration processes. The main technical barriers hindering the application of photocatalysis at industrial scale are: (1) limited utilization of solar spectrum by most photocatalysts; (2) high electron and hole recombination rate, which lowers quantum efficiency and photocatalytic activity; (3) poor adsorption towards non-polar organic pollutants; (4) challenging recovery of the used nanoparticles from the uniform suspension; and (5) low thermal stability. Therefore, this work focused on the fabrication of surface defective heterojunction nanocomposites from TiO_2 and ZnO in order to enhance the photocatalytic activity through improved light absorption capabilities and charge separation process. High energy requirements for sintering, high cost of starting materials, and limited effectiveness in pollutant mineralization are identified as significant drawbacks in the industrial application of ceramic membrane technology. Therefore, this study focussed on fabrication of affordable and sustainable ceramic membranes from coal fly ash, an industrial solid waste product, and natural sand, a commonly available and inexpensive natural material.

Firstly, surface defective TiO_2-ZnO heterojunction nanocomposite were synthesized using the conventional sol-gel approach, coupled with aluminium foil-assisted $NaBH_4$ reduction. Titanium tetra-isopropoxide and zinc acetate were used as precursors at different molar ratios while isopropyl alcohol and water were used as solvents. Subsequently, ceramic membranes were fabricated by the uniaxial compaction of the starting material (coal fly ash, natural sand, dextrin (pore former) and carboxymethyl cellulose (binder)) using a manual hydraulic pressing machine. The coal fly ash and natural sand were mixed in different proportions and the fabricated ceramic membranes were sintered at different temperatures of 800, 100, and 1200 ℃. Finally, the novel TiO_2-ZnO functionalized coal fly ash-based ceramic membrane was fabricated utilizing co-pressing and co-sintering processes. The photoactive layer was formed by placing the grounded mixture of pre weighed photocatalyst (TiO_2-ZnO) and pre-weighed ceramic membrane precursor material on the mold's base, and the supporting layer was formed by adding pre-weighed ceramic membrane precursor material to the mold. The structure, morphology, surface properties, and optical characteristics of the synthesized materials were studied using Fourier transform infrared spectroscopy (FTIR), X-ray diffraction (XRD), UV–vis absorption spectra, Scanning electron microscopy (SEM), Energy-dispersive X-ray spectroscopy (EDS), Thermogravimetric analysis (TGA) and Transmission electron microscopy (TEM). The

properties of the optimized membranes were further studied to ascertain their mechanical strength, chemical stability, porosity, water absorption, water permeability, and shrinkage behaviour.

The XRD analysis confirmed the successful formation of black $BTiO_2$–ZnO heterostructure, while SEM revealed the structural morphology as pseudo-spherical with slight agglomeration. $BTiO_2$–ZnO was found to be more efficient than $BTiO_2$ and BZnO for the removal of tetracycline with degradation efficiencies of 63, 58, and 56 % respectively. The effects of process parameters such as the amount of photocatalyst, pollutant's concentration, and the initial solution pH on photocatalytic degradation study were systematically explored. The results confirm that the formation of the heterostructure from $BTiO_2$ and BZnO could offer a facile route to improving the catalytic degradation of tetracycline. X-ray fluorescence (XRF) analysis of the starting materials (coal fly ash and natural sand) confirmed the presence of SiO_2 and Al_2O_3, two key inorganic materials required for the fabrication of ceramic membranes. ICP OES analysis revealed that coal fly ash contains heavy metals, including arsenic (As), cadmium (Cd), chromium (Cr), copper (Cu), nickel (Ni), lead (Pb), and mercury (Hg). The levels of arsenic and chromium exceeded the WHO limits. Therefore, the heavy metals present in the raw coal fly ash were successfully leached out using acetic acid prior to the fabrication process. The membrane fabricated with 20 wt% sand content and at 1000 °C sintering temperature had pore size of 0.64 µm and 34.7% porosity, exhibited good mechanical strength (7.71 MPa), and exceptional chemical stability. The membrane also showed a remarkable water permeability of 32.23 $L/m^2/h$. The ceramic membrane functionalized with 0.5 g of TiO_2 -ZnO and sintered at 850 °C exhibited good thermal, chemical stability, and porosity required for ultrafiltration applications. The optimum photocatalytic efficiency of the functionalized photocatalytic substrate achieved within 100 min under the visible light was estimated at 77% and removal efficiency by filtration was estimated at 57%. Moreover, the functionalized membrane was found to be stable with 73% photocatalytic degradation efficiency after 5 consecutive cycles of reusability test, with negligible loss of efficiency. In the filtration studies, tetracycline was simply adsorbed and filtered without degradation complicating desorption from surface-active areas.

The scale-up of photocatalytic ceramic membranes and their utilization in real industrial applications will confirm their robustness when used in a hybrid photocatalysis and filtration reactor system that optimize its synergistic photocatalytic, adsorption, and filtration properties. In general, the use of advanced hybrid wastewater treatment techniques, specifically through the use of photocatalytic ceramic membranes fabricated from cost-effective starting materials, presents a promising and sustainable alternative for the removal of pharmaceuticals from water.

Keywords: **Metal oxide; Functionalized membranes; Pharmaceuticals; Photocatalysis; Coal fly ash**

LIST OF ABBREVIATIONS

%R- Percentage rejection

%RE- Percentage removal efficiency

AOP- Advanced oxidation process

CB- Conduction band

CFA- Coal fly ash

ECs- Emerging contaminants

EDX- Electron dispersion spectroscopy

FTIR- Fourier transform infrared spectroscopy

Mt- Metric ton

ICP-OES- Inductively coupled plasma optical emission spectroscopy

NS- Natural sand

PL- Photoluminescence

SDGs- Sustainable development goals

SEM- Scanning electron microscopy

TC- Tetracycline

TEM Transmission electron microscopy

TGA- Thermo-gravimetric analysis

THMs- Trihalomethanes

UF- Ultrafiltration

UV- Ultraviolet

VB- Valence band

XRD- X-ray diffraction analysis

XRF- X-ray fluorescence

Contents

CERTIFICATION ii

DECLARATION iii

DEDICATION iv

ACKNOWLEDGEMENT iv

LIST OF PUBLICATIONS v

ABSTRACT vii

LIST OF ABBREVIATIONS ix

PREFACE xvi

CHAPTER ONE 1

Introduction and general background 1

1.0 Problem statement 1

1.1 Motivation and rationale 2

1.2 Research aim and objectives 3

1.3 References 4

CHAPTER TWO 5

Literature review 5

2.0 Pharmaceuticals as emerging contaminants in wastewater 5

2.1 Tetracycline as emerging contaminant 10

2.1.2 Toxicity of tetracycline on plants and animals 11

2.1.1 Removal methods for tetracycline in water 13

2.2 Membrane technology 14

2.2.1 Ceramic membrane technology in wastewater 16

2.2.2 Advantages and disadvantages of ceramic and polymeric membranes 17

2.2.3 Challenges facing ceramic membrane technology and the remedial actions 18

2.2.3.1 Ceramic membrane cost 19

2.2.3.2 Fouling and concentration polarization 20

2.2.4 Coal fly ash as a sustainable alternative to commercial materials in membrane fabrication 21
2.2.4.1 Coal fly ash 21
2.2.4.2 Synthesis of coal fly ash-based ceramic membranes 23
2.2.4.3 Synthesis of coal fly ash ceramic membranes by pressing method 24
2.2.4.4 Synthesis of coal fly ash ceramic membranes by extrusion method 25
2.2.4.5 Synthesis of coal fly ash ceramic membranes by slip casting method 26
2.2.4.6 Synthesis of coal fly ash ceramic membranes by Tape casting method 27
2.2.5 Coal fly ash based ceramic membrane cost analysis 32
2.2.6 Application of coal fly ash in ceramic membrane for wastewater treatment 34
2.2.6.1 Membrane precursor 34
2.2.6.2 Sintering additive 35
2.2.6.3 Membrane filler 36
2.2.6.4 Membrane filters 37
2.2.7 Factors affecting the physical properties and performance of coal fly ash based ceramic membranes 39
2.2.8 Factors that affect separation efficiency of coal fly ash-based ceramic membranes 43
2.2.9 Management of fouling on coal fly ash based ceramic membranes 44
2.3. Metal oxide functionalized ceramic membranes 46
2.3.1 Synthesis of metal oxide functionalized ceramic membranes 49
2.3.2 Application of metal oxide functionalized ceramic membranes in the degradation of pharmaceuticals in wastewater 50
2.3.3 Photodegradation mechanism and products 51
2.3.4 Strategies for improving the efficiency of metal oxides in functionalized ceramic membranes 55
2.3.5 Factors that affect pharmaceutical removal by metal oxide functionalized membranes 58
2.4 References 61
CHAPTER 3 84

Photocatalytic degradation of tetracycline using surface defective black TiO_2-ZnO heterojunction photocatalyst under visible light 84
3.0 Introduction 84
3.1 Experimental 86
3.1.1 Materials 86
3.1.2 Synthesis of ZnO nanoparticles 86
3.1.3 Synthesis of TiO_2 nanoparticles 86
3.1.4 Synthesis of TiO_2-ZnO heterojunction nanoparticles 87
3.1.5 Synthesis of $BTiO_2$, BZnO and $BTiO_2$-ZnO nanoparticles 87
3.1.6 Characterization of synthesized nanocomposites 87
3.1.7 Photocatalytic degradation of tetracycline in water 87
3.2 Results and discussion 88
3.2.1 Fourier transforms infra-Red (FT-IR) spectroscopy 88
3.2.2 X-ray diffraction (XRD) analysis 89
3.2.3 Optical properties of the binary metal oxides and composite oxides 92
3.2.4 Morphological study 94
3.2.5 Photoluminescence (PL) study 99
3.2.6 Photodegradation of tetracycline 99
3.2.7 Influence of TC Solution pH on the degradation efficiency 100
3.2.8 Influence of photocatalysts dose 103
3.2.9 Influence of initial concentration of tetracycline on the degradation process 105
3.2.10 Degradation efficiency and kinetics of the degradation process by $BTiO_2$-ZnO, $BTiO_2$ and BZnO 106
3.2.11 Photocatalytic Mechanism 108
3.3 Conclusion 109
3.5 References 111
CHAPTER 4 118

Fabrication and Characterization of Low-Cost Ceramic Membranes from Coal Fly Ash and Natural Sand 118
4.0 Introduction 118
4.1 Experimental 120
4.1.1. Materials 120
4.1.2. Leaching of heavy metals present in coal fly ash 121
4.1.3. Ceramic membrane fabrication 121
4.1.4 Water uptake 123
4.1.5 Chemical stability 123
4.1.6 Water absorption and Porosity 123
4.1.7 Pure water permeation and mean pore radius 124
4.1.8 Linear firing shrinkage and loss on ignition 124
4.1.9 Average crystallite size 125
4.1.10 Ceramic membrane characterization 125
4.2 Results and Discussion 126
4.2.1 X-ray fluorescence (XRF) analysis and Leaching studies 126
4.2.2 Material composition and appearance of the fabricated ceramic membrane. 127
4.2.3 Shrinkage and Loss on ignition 128
4.2.4 Water absorption, open porosity and water permeability 128
4.2.5 Chemical and mechanical stability 130
4.2.5.1 Chemical stability 130
4.2.5.2 Mechanical stability 130
4.2.6 Fourier transform infrared (FTIR) spectroscopic studies 132
4.2.7 X-ray diffraction (XRD) analysis 133
4.2.8 Thermogravimetric analysis (TGA) 136
4.2.9 Morphological study 137
4.2.9.1 SEM and EDX analysis of ceramic membranes sintered at different temperatures. 137

4.2.9.2 SEM and EDX analysis of ceramic membranes fabricated from different natural sand compositions. 139
4.3 Conclusion 142
4.4 References 143
CHAPTER 5 149
TiO_2-ZnO functionalized low-cost ceramic membranes from coal fly ash for the removal of tetracycline from water under visible light 149
5.0. Introduction 149
5.1. Experimental 151
5.1.1 Materials 151
5.1.2. Synthesis of TiO_2-ZnO heterojunction 151
5.1.3 Thermal Treatment of Coal Fly Ash and Leaching of Heavy Metals from Coal Fly Ash 152
5.1.4. Preparation of TiO_2-ZnO functionalized CFA/NS ceramic membrane 152
5.1.5. Characterization of the photocatalytic ceramic membranes 154
5.1.6 Water absorption, Porosity and Pore size 154
5.1.7 Chemical and Mechanical stabilities 155
5.1.8 Pure water permeability and Tetracycline removal by filtration studies 156
5.1.9 Procedure for photocatalytic degradation of tetracycline 157
5.2 Results and discussion 158
5.2.1 Physical observations 158
5.2.2 Water absorption, Porosity and Pore size 158
5.2.3 Chemical and mechanical Properties 160
5.2.4 Fourier transform infrared spectra 161
5.2.5 Structural studies 162
5.2.6 Thermal analysis 163
5.2.7 Morphological studies 164
5.2.8 Photocatalytic activity of the functionalized ceramic membranes 166
5.2.8.1 Effect of solution pH 166

5.2.8.2. Effect of Tetracycline concentration 167
5.2.8.3 Effect of photocatalyst loading 169
5.2.8.4 Synergistic effect of adsorption and photocatalysis 169
5.2.8.5 Reusability of the functionalized ceramic membrane 171
5.2.9 Synergistic effect of adsorption and filtration performance 171
5.2.10 Photocatalytic mechanism 172
5.3 Conclusion 173
5.3 References 174
Chapter 6 179
Conclusion and recommendation 179
6.0 Conclusion 179
6.1 Recommendation 180

PREFACE

This thesis was written using the article format. All experimental works and drafting of initial manuscript were done by Sawunyama Lawrence. Prof. D. C. Onwudiwe, Dr. Oyewo, and Dr Bopape supervised the research work and proofread the manuscripts. All articles included in this thesis are published with the consent of the journal editors and co-authors.

LIST OF FIGURES

Chapter 2

Figure 1: A schematic diagram showing possible pharmaceutical pollution sources, routes, and receptors in the environment. **9**

Figure 2: Structures of representative members of the tetracycline family. **11**

Figure 3: Types of membrane employed in the wastewater treatment sectors **16**

Figure 4: The typical cross-section of (a) symmetrical ceramic membrane and (b) an asymmetrical ceramic membrane **17**

Figure 5: Representation of different raw materials in studies of low-cost ceramic membranes **19**

Figure 6: Schematic Illustration of the structure of coal fly ash **22**

Figure 7: :(a) Changes in global coal consumption (b) various uses of coal fly ash **23**

Figure 8: Schematic illustration for the preparation of coal fly ash based ceramic fabrication by dry pressing method **25**

Figure 9: Fabrication of coal fly ash based ceramic membrane via extrusion method. **26**

Figure 10: Schematic illustrations of the slip casting technique for fabricating ceramic membranes **27**

Figure 11: Schematic illustrations of the tape casting technique for fabricating ceramic membranes **28**

Figure 12:(a) Fabrication cost of coal fly ash based ceramic membrane as percentages of manufacturing cost and equipment cost and (b) factored in manufacturing expenses **33**

Figure 13: (a)Variation of average pore size with sintering temperature, (b) picture of membranes sintered at four different temperatures, (c) variation of flexural strength with sintering temperature (d) XRD spectra at different sintering temperatures, and (e) variation of porosity with sintering temperature **40**

Figure 14:(a) Relationship between the mechanical strength of the membrane and the content of the pore-forming agent as well as the temperature of sintering. (b) SEM images of Coal fly ash ceramic membrane with Wt% of dextrin (i) 0, (ii) 3, (iii) 6, and (iv) 9 sintered at 1150 °C **42**

Figure 15: Mechanism of photocatalysis **46**

Figure 16: Illustration of the integrated photocatalyst on the surface and embedded membrane. Orientation of light source: (a) inside the reactor, (b) outside the reactor, and (c) vertical inside the reactor **48**

Figure 17: Scheme of the preparation of TiO_2 functionalized Al_2O_3 porous ceramic membrane **48**

Figure 18: Photodegradation mechanism and products for amoxicillin using TiO_2 nanoparticles coupled with a novel submerged porous ceramic membrane reactor **50**

Figure 19: Photodegradation mechanism and products for ibuprofen via α-Al_2O_3/$CoFe_2O_4$ catalytic membrane **53**

Figure 20: The mechanism of non-metal and metal ion doping on metal oxide semiconductor. **56**

Figure 21: Classification of semiconductor heterostructures, their configurations, and electron migration: type I heterojunction, type II heterojunction, and type III heterojunction **57**

Figure 22: Schematic illustration of the different types of photocatalyst defects **58**

Chapter 3

Figure 1: FTIR spectra of (a) pristine TiO_2, (b) $BTiO_2$, (c) pristine ZnO, (d) BZnO, (e) TiO_2-ZnO, and (f) $BTiO_2$-ZnO. **89**

Figure 2: X-ray diffraction patterns of (a) overlaid pristine ZnO and BZnO synthesized at 300 ℃, 350 ℃ and 400 ℃, (b) overlaid pristine TiO_2 and $BTiO_2$ synthesized at 300 ℃, 350 ℃ and 400 ℃, and (c) TiO_2-ZnO and $BTiO_2$-ZnO synthesized at 300 ℃, 350 ℃ and 400 ℃. **91**

Figure 3: Optical spectra of overlapped (a) ZnO and BZnO synthesized at 300 ℃, 350 ℃ and 400 ℃, (b) pristine TiO_2 and $BTiO_2$, synthesized at 300 ℃, 350 ℃ and 400 ℃, and (c) TiO_2-ZnO and $BTiO_2$-ZnO synthesized at 300 ℃, 350 ℃ and 400 ℃ while d, e and f are the tauc plots respectively. **93**

Figure 4: SEM micrographs of (a) $BTiO_2$, (b) BZnO, (c) TiO_2-ZnO, (d) $BtiO_2$-ZnO synthesized at 300 ℃, (e) $BTiO_2$-ZnO synthesized at 350 ℃, and (f) $BTiO_2$-ZnO synthesized at 400 ℃. **94**

Figure 5: (a) TEM image, (b) EDX spectra, (c) elemental mapping showing (d) Zn, (e) Ti, and (f) O elements of Black TiO_2-ZnO prepared at 350 ℃ for 1 h. **95**

Figure 6: TEM image, (b) particle size distribution histogram, (c) EDX spectra, and (d) elemental mapping showing (e) O, and (f) Zn elements of black TiO_2. **96**

Figure 7: TEM image, (b) EDX spectra, (c) elemental mapping showing (d) Zn, (e)Ti, and (f) O elements of Black TiO_2-ZnO prepared at 400 ℃ for 1 h. **97**

Figure 8: TEM image, (b) EDX spectrum, (c) elemental mapping showing (d) Zn, (e)Ti, and (f) O elements of Black TiO_2-ZnO prepared at 300 ℃ for 1 h. **97**

Figure 9: (a) TEM image, (b) EDX spectra, (c) elemental mapping showing (d) Zn, (e)Ti, and (f) O elements of Black TiO_2-ZnO prepared at 350 ℃ for 1 h. **98**

Figure 10: TEM image, (b) EDX spectra, (c) elemental mapping showing (d) Zn, (e)Ti, and (f) O elements of Black TiO_2-ZnO prepared at 400 ℃ for 1 h. **98**

Figure 11: Photoluminescence spectra of $BTiO_2$, BZnO, TiO_2-ZnO and $BTiO_2$-ZnO. **99**

Figure 12**:** UV-vis absorption spectra of photocatalytic degradation of TC using $BTiO_2$-ZnO synthesized at (a) 300℃), (b) 350℃ and (c) 400℃ (d) percentage degradation of TC under visible light (50 mg/L dye concentration and catalysts dosage 100 mg/L. **100**

Figure 13: Absorption spectra of TC (50 mg/L) at different time using 100 mg/L of $BTiO_2$-ZnO at pH values of (a) pH 4, (b) pH 7 and (c) pH 10, (d) rate of decomposition, and (e) the kinetics graph of the decomposition process. **101**

Figure 14**:** Zeta potential of (a) BZnO, (b) $BTiO_2$, (c) $BTiO_2$-ZnO (all under natural pH) and (d) $BTiO_2$-ZnO under acidic, neutral, and alkaline conditions **102**

Figure 15: Absorption spectra of TC showing its photolysis at different pH (a) 4, (b) 7, (c) 10, (d) Kinetic graphs at different pH values, and (e) percentage degradation of TC under visible light (TC initial concentration: 50 mg/L, catalyst dosage 100 mg/L). **103**

Figure 16: Absorption spectra of TC showing its photodegradation by $BTiO_2$-ZnO nanocomposite at catalyst loading concentrations of (a) 0, (b) 75, (c) 100, and (d) 125 mg/L, and (e) percentage degradation of TC under visible light (TC initial concentration: 50 mg/L, pH: 7), and (f) kinetics of graphs of the decomposition process. **104**

Figure 17: Absorption spectra of TC showing its photodegradation by $BTiO_2$-ZnO nanocomposite at initial TC concentrations of (a) 25, (b) 50, and (c) 75 mg/L. (d) the kinetics graph of the decomposition process. **105**

Figure 18:(a-c) Absorption profile, (d) percentage degradation, and (e-g) kinetics graphs of BZnO, $BTiO_2$, and $BTiO_2$-ZnO, respectively and (100 mg/L photocatalyst, 50 mg/L TC and pH = 7Table 2: Comparison of TC degradation using the prepared $BTiO_2$-ZnO with other different TiO_2 or ZnO based advanced oxidation process catalysts earlier reported. **107**

Figure 19: Proposed mechanism for the photocatalytic degradation of Tetracycline with $BTiO_2$-ZnO. **109**

Chapter 4

Figure 1: Schematic diagram of the fabrication process of the ceramic membranes by the pressing technique. **122**

Figure 2: Images of the fabricated ceramic membranes illustrating the typical differences in the visual aspects of different sintering temperatures. (A, B, C and D represents ceramic membranes fabricated from CFA: NS ratios of 90/0, 80:10, 70:20 and 60:30 respectively while subscripts 1, 2 and 3 represent sintering temperatures of 800, 1000, 1200 ℃ respectively). **127**

Figure 3: Pure water flux of different fabricated ceramic membranes sintered at 1000 °C for 2 h: (A2) CFA (90%); NS (0%), (B2) CFA (80%); NS (10%), (C2) CFA (70%); NS (20%) and (D2) CFA (60%); NS (30%). **129**

Figure 4:(a) Flexure strain vs. flexure load and (b) Flexural strength of different fabricated ceramic membranes sintered at 1000 °C for 2 h (A2) CFA (90%); NS (0%), (B2) CFA (80%); NS (10%), (C2) CFA (70%); NS (20%) and (D2) CFA (60%); NS (30%). (c) Flexure strain vs. flexure load and (d) Flexural strength of ceramic membranes fabricated from CFA (70%); NS (20%) and sintered at (C1) 800 ℃, (C2) 1000 °C and (C3) 1200 °C for 2 h. **131**

Figure 5 : FTIR spectra of ceramic membrane samples fabricated from different ratios of coal fly ash and natural sand, (a) CFA (90%); (b) CFA (80%), NS (10%); (c) CFA (70%), NS (20%); and (d) CFA (60%), NS (30%) all sintered at 800 °C, 1000 °C, and 1200 ℃ for 2 h. **133**

Figure 6:X-ray diffraction patterns of ceramic membrane samples fabricated from different ratios of coal fly ash and natural sand (a) CFA (90%), NS (0%); (b) CFA (80%), NS (10%); (c) CFA (70%), NS (20%); and (d) CFA (60%), NS (30%); all sintered at 800, 1000 and and 1200 ℃ for 2 h. (α-quartz (♥), mullite (♦), anorthite (●), hematite (©), corundum (♠), cristobalite (♣) and albite (◦) **135**

Figure 7:TGA-DTG curve for the ceramic membrane starting material (60%CFA;20% NS) **136**

Figure 8: SEM surface micrographs (a-c), SEM cross-sectional micrographs (d-f), and EDX spectra (g-i) of ceramic membranes fabricated from 30% natural sand and 60% coal fly ash and sintered for 2 h at different temperatures of 800, 100 and 1200 ℃ respectively (Magnification of all SEM micrographs is 200X) **138**

Figure 9: SEM surface micrographs (a-d), SEM cross-sectional micrographs (e-h), and EDX spectra (i-k) of ceramic membranes fabricated from 0%, 10%, 20%, and 30% natural sand and sintered at 1000 °C for 2 h. (magnification of all SEM micrographs is 200X) **140**

Chapter 5

Figure 1: Schematic diagram of the fabrication process of TiO_2-ZnO functionalized coal fly ash based ceramic membranes by the co-pressing and co-sintering technique **153**

Figure 2: Schematic representation of the three-point bending test **156**

Figure 3: Schematic representation of the filtration and photocatalytic set-up. **157**

Figure 4: Pristine and functionalized ceramic membrane before and after sintering. Pristine coal fly ash based ceramic membrane (a & e) and TiO_2-ZnO functionalized coal fly ash based ceramic membranes at different photocatalyst loading of (b & f) 0.25 g, (c & g) 0.50 g, and (d & h) 0.75 g. **158**

Figure 5:(a) Chemical stability and (b) Flexural strength of coal fly ash based ceramic membrane (PM) and functionalized ceramic membranes at different photocatalyst loading of 0.25g (PCM 0.25), 0.50g (PCM 0.50) and 0.75g (PCM 0.75) sintered at 850 °C for 2 h **160**

Figure 6: The FTIR spectra of TiO2-ZnO (black), pristine coal fly ash ceramic membrane (red) and functionalized ceramic membranes at different photocatalyst loading of 0.25 g (blue), 0.50 g (green) and 0.75 g (pink) **161**

Figure 7: X-ray diffraction spectra of TiO_2-ZnO (black), pristine coal fly ash ceramic membrane (green) and functionalized ceramic membranes at different photocatalyst loading of 0.25g (red), 0.50g (blue) and 0.75g (purple). (TiO_2 rutile (♥), ZnTiO3 (♦), Zincite ZnO (♣), mullite (●), cristobalite (©) and α-quartz (♠) **163**

Figure 8: Thermogravimetric (TG) and (b) Differential scanning calometry (DSC) graphs of ceramic membrane raw material mixture **164**

Figure 9: SEM surface micrographs of (a) pristine coal fly ash ceramic membrane and functionalized ceramic membranes at different photocatalyst loading of (b) 0.25g (c) 0.50g and (d) 0.75g and EDX spectra (e) of pristine coal fly ash ceramic membrane and functionalized ceramic membranes at different photocatalyst loading of (f) 0.25g (g) 0.50g and (h) 0.75g **165**

Figure 10: Photocatalytic degradation profile of Tetracycline by TiO_2-ZnO functionalized coal fly ash based ceramic membranes at different pH (a) 4, (b) 7, (c) 9, (d) Percentage degradation of TC under visible light (TC initial concentration: 25 mg/L) **167**

Figure 11: Effect of Tetracycline concentration at (a) 10 mg/L, (b) 25 mg/L and (c) 50 mg/L on the photocatalytic degradation of Tetracycline by TiO_2-ZnO functionalized coal fly ash based ceramic membranes and (d) the kinetic plots for the effect of antibiotic concentration on the photocatalytic degradation of Tetracycline. **168**

Figure 12: Degradation profile of (a) Pristine coal fly ash based ceramic membrane, (b) TiO_2-ZnO functionalized coal fly ash based ceramic membrane, (c) Photolysis of Tetracycline and (d) Percentage degradation of TC under visible light **170**

Figure 13: Rate of TC removal with varying TiO_2-ZnO loadings on coal fly ash based ceramic membranes (b). Reusability of TiO_2-ZnO functionalized coal fly ash based ceramic membrane for tetracycline degradation (c) Tetracycline removal efficiency by pristine coal fly ash based ceramic membrane and TiO_2-ZnO (0.5g) functionalized coal fly ash-based ceramic membrane through adsorption and filtration (TC concentration 25 mg/L, solution pH= 9, time 100 min) **171**

Figure 14: Photocatalytic degradation mechanism of Tetracycline by TiO_2-ZnO functionalized coal fly ash-based ceramic membrane. **172**

LIST OF TABLES

Chapter 2

Table 1: Variety of pharmaceutically active compounds detected in different environmental matrices in various countries with their classes and detected concentration **8**

Table 2: Toxic effects of tetracycline on different plants **12**

Table 3: Methods of removing tetracyclines from water **14**

Table 4: Advantages and disadvantages of ceramic and polymeric membranes **18**

Table 5: Mineralogical composition of kaolin, bentonite clay and coal fly ash **20**

Table 6: Techniques used in the manufacturing of coal fly ash-based ceramics and the properties of the resulting membranes **28**

Table 7: Advantages and disadvantages of ceramic membrane synthesis methods **31**

Table 8: Cost of different coal fly ash based ceramic membranes **34**

Table 9: Application of CFA-based membranes in the treatment of different effluent **37**

Table 10: Photocatalytic degradation of pharmaceuticals by metal oxide functionalized membranes **53**

Chapter 3

Table 1: Crystallite size and lattice microstrain of synthesized materials **91**

Table 2: Mulliken's electronegativity (χ), band gap energy (Eg), valence band (EVB) and conduction band (ECB) for the pristine nanoparticles and the nanocomposite. **93**

Table 3: Comparison of TC degradation using the prepared $BTiO_2$–ZnO with other different TiO_2 or ZnO based advanced oxidation process catalysts earlier reported **107**

Chapter 4

Table 1: Formulation of the raw materials and fabrication parameters. **122**

Table 2: Chemical composition of coal fly ash and natural sand expressed as percent by weight. **126**

Table 3: Heavy metal concentrations in coal fly ash both before and after leaching studies (unit: ppb). **127**

Table 4: Properties of the fabricated ceramic membranes **129**

Table 5: Comparative study of the properties of the fabricated ceramic membrane utilizing coal fly ash and natural sand against sustainable ceramic membranes reported in earlier studies **141**

Chapter 5

Table 1: Materials used to fabricate the photocatalytic ceramic membranes **153**

Table 2: A summary of pristine and functionalized ceramic membrane properties **159**

CHAPTER ONE

Introduction and general background

1.0 Problem statement

The continuous increase in production and consumption of pharmaceutical products without proper disposal procedures as well as the lack of efficient wastewater treatment methods has contributed to the emergence of new contaminants of concern in portable water. Tetracycline, an antibiotic, is a representative of widely used pharmaceuticals and is reported to be the world's second most often used antibiotic (Wang *et al.*, 2024). Its overindulgence and uncontrolled use contaminate the environment thereby disturbing the food chains, promoting risks of diseases, and depriving society of clean water. Furthermore, the presence of pharmaceuticals in wastewater has been red flagged as a major barrier for the attainment of sustainable development goal 6 (SDG6). Tetracycline is regarded as highly emerging persistent contaminant because of its low environmental degradation rate (Ahmad et al 2021). Tetracycline is detected at varying concentrations across different environmental matrices, including soil and aquatic systems. It is released into these environmental matrices through a wide range of sources which include pharmaceutical plants, wastewater treatment plants, sewage treatment plants, pharmaceutical improper disposal, human and animal excretion and aquafarming (Xu *et al.*, 2021). Trace levels of tetracycline in drinking water can cause significant unpleasant effects on human health and aquatic life over a more extended period (Daghrir & Drogui, 2013). The problem with the presence of pharmaceutical pollutants in municipal wastewater is that they are not effectively removed by conventional wastewater treatment techniques such as filtration, adsorption and coagulation-flocculation processes which are employed by most water treatment plants. These conventional wastewater treatment techniques have also been reported to transform targeted pollutants to secondary pollutants. For instance, the addition of chlorine to wastewater containing tetracycline can result in the transformation of tetracycline to toxic secondary pollutants such as chlorinated organic compounds and trihalomethanes (THMs) instead of being mineralized. The chlorinated by-products can be carcinogenic and mutagenic to human health as well as ecotoxic to the environment (Postigo *et al.*, 2021).

Recently, more advanced technologies such as membrane technology, bioremediation and advanced oxygen processes (ozonation, electrochemical oxidation, fenton process, and photocatalysis) have been reported to completely mineralize tetracycline from wastewater (Pelosato *et al.*, 2022). However, most of these techniques have some drawbacks that affects their application at large scale. For instance, using electrochemical treatment methods in water purification has multiple disadvantages, such as its need of high energy, high cost of operation and instability towards wide range of organic and inorganic contaminants (Radjenovic & Sedlak, 2015). Photocatalysis in pollutant degradation is rarely utilized at

large scale because of the expensive production cost of the photocatalyst and the difficult recovery process. Additionally, the limited light absorption of most photocatalysts further restricts the possibilities of photocatalysis. Ceramic membrane technology does not entirely mineralize contaminants; therefore, its effectiveness and lifespan are affected by its susceptibility to fouling. While bioremediation can be time-consuming, lead to the production of more toxic and mobile intermediates than the parent compound, demand high experimental costs, and not very proficient in pharmaceutical application (Priya *et al.*, 2024). Furthermore, various pharmaceuticals with different physicochemical properties are mixed in wastewater, which can complicate their removal efficiency. Consequently, the effort to increase the efficiency of wastewater treatment processes focuses on the development of new and effective treatment techniques that could provide a cost-effective, sustainable, and effective approach as part of the water management process.

As a result, this work focused on the removal of tetracycline from water utilizing a hybrid technique that combines photocatalysis via heterojunction of TiO_2 and ZnO with the technique of filtration that uses the ceramic membrane derived from waste coal fly ash and widely available natural sand.

1.1 Motivation and rationale

The large-scale application of pure advanced wastewater treatment techniques such as photocatalysis and membrane technology is limited due to the technical constraints posed by the different methods. For instance, in photocatalysis, post-recovery of the used photocatalyst is complex, and most of the widely explored photocatalysts at laboratory scale have shown poor pollutant adsorption capabilities, poor light absorption, and high recombination rates, which are critical processes in achieving effective photocatalysis (Dong *et al.*, 2015). The utilization of multiphase photocatalysts, doping with non-metals or metals, composite material synthesis, defect engineering, and heterojunction formation with other low-band gap photocatalyst are some of the methods that have been used to overcome these limitations (Scarpelli *et al.*, 2018). On the other hand, ceramic membrane technology is hindered by high fabrication costs resulting from high energy needs for sintering and the high cost of commercial starting materials (silicon nitride, titanium, alumina, zirconia oxide, silicon oxide and silicon carbide) as well as limited performance in pollutants mineralization, which give rise to membrane fouling (Molinari *et al.*, 2019). Fabrication of ceramic membranes from cheap materials like waste materials such as animal bones, coal fly ash, recycled glass, and paper mill sludge, as well as readily available materials such as clay, sand, bentonite, and kaoline, has recently been explored to overcome the production cost of ceramic membranes (Hubadillah *et al.*, 2022). The fabrication of ceramic membranes from such materials can also lower the sintering temperature of the membranes due to the formation of liquid phases at lower temperatures. The drawbacks of both photocatalysis and ceramic membrane technology

can be significantly mitigated by developing a hybrid technique with each other or with other wastewater treatment systems. Fabrication of a hybrid wastewater treatment technique from heterojunction photocatalyst and ceramic membranes fabricated from waste material coal fly ash and readily available material (natural sand) can exploit the combined advantages of photocatalysis and ceramic membrane technology, with the main goal of maximising their benefits while minimising their drawbacks. This approach seeks to minimize negative economic and environmental impacts while facilitating potential for commercialization. Moreover, repurposing coal fly ash for membrane fabrication contributes to sustainable waste management practices, reducing its environmental impact.

1.2 Research aim and objectives

The aim of this research was to develop cost-effective water treatment functionalized ceramic membrane that could efficiently remove pharmaceuticals (namely tetracycline) from wastewater.

The objectives are to:

- synthesize TiO_2-ZnO heterojunction photocatalyst for the light enhanced degradation process,
- synthesize coal fly ash-based ceramic membranes and characterize them using Fourier transform infrared spectroscopy (FTIR), Scanning electron microscope (SEM), X-ray diffraction (XRD), Energy-dispersive X-ray spectroscopy (EDS), and Thermogravimetric analysis (TGA) as well as evaluating its water flux, chemical stability and mechanical stability,
- functionalise the ceramic membrane with the synthesized TiO_2-ZnO nanoparticles and characterize it,
- evaluate the photocatalytic degradation and filtration efficiency of the synthesized TiO_2-ZnO functionalized ceramic membrane using tetracycline as model pollutant.

1.3 References

Daghrir, R., & Drogui, P. (2013). Tetracycline antibiotics in the environment: a review. *Environmental chemistry letters, 11*, 209-227.

Dong, H., Zeng, G., Tang, L., Fan, C., Zhang, C., He, X., & He, Y. (2015). An overview on limitations of TiO2-based particles for photocatalytic degradation of organic pollutants and the corresponding countermeasures. *Water research, 79*, 128-146.

Hubadillah, S. K., Jamalludin, M. R., Othman, M. H. D., & Iwamoto, Y. (2022). Recent progress on low-cost ceramic membrane for water and wastewater treatment. *Ceramics International, 48*(17), 24157-24191.

Molinari, R., Lavorato, C., Argurio, P., Szymański, K., Darowna, D., & Mozia, S. (2019). Overview of photocatalytic membrane reactors in organic synthesis, energy storage and environmental applications. *Catalysts, 9*(3), 239.

Pelosato, R., Bolognino, I., Fontana, F., & Sora, I. N. (2022). Applications of heterogeneous photocatalysis to the degradation of oxytetracycline in water: A review. *Molecules, 27*(9), 2743.

Postigo, C., Gil-Solsona, R., Herrera-Batista, M. F., Gago-Ferrero, P., Alygizakis, N., Ahrens, L., & Wiberg, K. (2021). A step forward in the detection of byproducts of anthropogenic organic micropollutants in chlorinated water. *Trends in Environmental Analytical Chemistry, 32*, e00148.

Priya, A., Muruganandam, M., Kumar, A., Senthilkumar, N., Shkir, M., Pandit, B., . . . Ubaidullah, M. (2024). Recent advances in microbial-assisted degradation and remediation of xenobiotic contaminants; challenges and future prospects. *Journal of Water Process Engineering, 60*, 105106.

Radjenovic, J., & Sedlak, D. L. (2015). Challenges and opportunities for electrochemical processes as next-generation technologies for the treatment of contaminated water. *Environmental science & technology, 49*(19), 11292-11302.

Scarpelli, F., Mastropietro, T. F., Poerio, T., & Godbert, N. (2018). Mesoporous TiO2 thin films: State of the art. *Titanium Dioxide-Material for a Sustainable Environment, 508*(1), 135-142.

Wang, F., Wang, Z., Zhao, Y., & Zhang, J. (2024). Performance of Traditional and Emerging Water-Treatment Technologies in the Removal of Tetracycline Antibiotics. *Catalysts, 14*(4), 269.

Xu, L., Zhang, H., Xiong, P., Zhu, Q., Liao, C., & Jiang, G. (2021). Occurrence, fate, and risk assessment of typical tetracycline antibiotics in the aquatic environment: A review. *Science of the total Environment, 753*, 141975.

CHAPTER TWO

Literature review

2.0 Pharmaceuticals as emerging contaminants in wastewater

The increasing world population, coupled with increasing water demand for agricultural, industrial, and domestic purposes, has led to the scarcity of clean water (Alatalo *et al.*, 2019). Pharmaceuticals and other emerging pollutants often pollute limited available water sources in many parts of the world. According to a UN report on world water development in 2020, about 4.2 billion people need access to adequately managed sanitation, and 2.2 billion people lack access to clean drinking water (Water & UNESCO: Paris, 2020). (Shi Y *et al.*, 2019), reported that the total amount of wastewater produced worldwide grew from 1500 km^3 in 1995 to 2212 km^3 in 2010. A worsening of the situation will only make it more difficult to fulfill Sustainable Development Goal (SDG) 6, which stipulates that everyone shall have access to clean water and adequate sanitation by 2030 (Griggs *et al.*, 2017). Although the use of pharmaceuticals in the treatment and prevention of diseases in both humans and animals has saved millions of lives, they have also caused unintended negative effects on the environment that have chronic and acute effects (Jelić *et al.*, 2012; Patel *et al.*, 2019). The presence of pharmaceuticals in the environment remains unregulated despite the significant negative effect on humans and the environment (Kumar *et al.*, 2022). They are thus categorized as emerging pollutants that require urgent attention. Emerging contaminants, according to (Dey *et al.*, 2019), are artificial or naturally occurring chemicals that are not regularly monitored in the environment but have a high risk of causing environmental harm. In addition, they are also responsible for some suspected adverse effects on human health and the ecological system. Given the accelerating rates of population expansion and the fast-increasing economic burden of human diseases, this group of emerging contaminants is anticipated to rise (Magagula *et al.*, 2022).

Pharmaceutical wastes include discarded health products, out-of-date medications, unused medications, unnecessary medications, waste produced at pharmacies, hospitals, and other healthcare facilities, and even medications that are no longer required because patients have either passed away or are no longer ill (Alnahas *et al.*, 2020). These pharmaceuticals pose a serious risk because the majority of their environmental and human toxicology has not been thoroughly investigated (Li Y *et al.*, 2020). Their environmental consequences have just recently been taken into consideration (Alazaiza *et al.*, 2022). Unfortunately, pharmaceutical pollutants have low biodegradability and high hydrophilicity, which means that present wastewater treatment technologies are not designed to degrade them (Mansouri *et al.*, 2021). According to a study conducted by Kooijman *et al*. (2020) (Kooijman *et al.*, 2020), about 16

pharmaceuticals that were studied could not be removed from wastewater using the traditional coagulation/flocculation wastewater treatment method. Pharmaceuticals and their metabolites are regularly dumped into wastewater as a result of how frequently they are used, manufactured and disposed (Wilkinson *et al.*, 2022). These active substances have been discovered in nearly all environmental matrices on every continent, according to recent global investigations (Bavumiragira *et al.*, 2022). Groundwater, drinking water, surface water, wastewater, sediments, and biota as well as wastewater treatment facilities, soils, and sludges have all been shown to have pharmaceutical pollutants (Dehkordi *et al.*, 2022). These pollutants include non-steroidal anti-inflammatory drugs (NSAIDs), blood lipid-lowering agents, beta-blockers (β-blockers), anti-retroviral treatments (ARVs), antipsychotics and antidepressants. All these are pharmaceuticals whose presence in the environment are of immense concern (Ahmed & Hameed, 2018; Madikizela *et al.*, 2017). Table 1 shows a wide variety of pharmaceutically active compounds detected in different environmental matrices in various countries with their classes and detected concentration.

Due to their availability over the counter and lack of a prescription, NSAIDs are the pharmaceuticals that are used most frequently among PPs (Manrique-Moreno *et al.*, 2016). Similarly, the consumption of antibiotics is on the high increase in many countries such as India, China, Brazil, Russia, and South Africa (Mendez *et al.*, 2017) owing to their effectiveness against harmful microorganisms and pathogens, as well as their increased use in food preservation (Varma *et al.*, 2020). Antimicrobial resistance in organisms like *Staphylococcus*, *Pseudomonas*, *Salmonella*, and *Escherichia coli* is increased when pharmaceutical compounds such as antibiotics are introduced into the wastewater system. Furthermore, disrupting the metabolism and biodegradation processes of organic matter in water bodies occurs when the enzymatic activity of microbiota present in the water is interrupted. In recent years, deaths due to antibiotic-resistant organisms have been reported to be higher than those due to diseases, such as HIV (Koch *et al.*, 2021). The death of oriented white-backed vultures has been linked to the consumption of water contaminated with commonly used pharmaceuticals (Oaks *et al.*, 2004). Different pharmaceutical pollution sources, routes, and receptors in the environment are shown in Figure 1. Emerging pollutants such as these PPs have recently sparked worries about water quality standards due to their rising prevalence in the environment. As a result, water quality has deteriorated, particularly in surface water (Oluwole & Olatunji, 2022). A large portion of the 1,000 water samples collected from 258 rivers in 104 countries contained concentrations of medicinal drugs that exceeded safe levels, according to a report from Global Agenda 2022, SDG 6 on clean water and sanitation (Broom, 2022).

Table 1: Variety of pharmaceutically active compounds detected in different environmental matrices in various countries with their classes and detected concentration.

Study Country	**Investigated source**	**Class of Pharmaceutical active compounds**	**Pharmaceutical active compounds**	**Concentration of the detected pharmaceuticals**
Brazil	Itaipu Lake reservoir in Brazil.	Nonsteroidal anti-inflammatory drugs (NSAID)	nimesulide	101.7 to 385.0 µg/L
South Africa	Umgeni estuary and seawater northern Durban in KwaZulu–Natal Province of South Africa	Non-steroidal anti-inflammatory drugs	naproxen,	0.36 µg/L
			ibuprofen	0.28 µg/L
Brazil	Urban wastewater of Rio de Janeiro affluent effluent from WWTP Penha Ilha do Governador, Rio de Janeiro, Brazil	Nonsteroidal anti-inflammatory drugs (NSAID)	Ibuprofen	6.55 - 27.4 µg/L 4.66- 39.88 µg/L
Republic of Korea	Influent at Gyeongsan Public Wastewater Treatment Plants effluent at Gyeongsan Public Wastewater Treatment Plants Influent at Gyeongsan Public Wastewater Treatment Plants Influent at Gyeongsan Public Wastewater Treatment Plants Influent at Gyeongsan Public Wastewater Treatment Plants	Anti-inflammatory analgesic drug Anti-inflammatory analgesic drug Anti-inflammatory analgesic drug antibiotics antiepileptics	Acetaminophen diclofenac diclofenac sulfamethoxazole trimethoprim Carbamazepine	14.0–67.5 µg/L 0.13 µg/L 0.11 µg/L 0.013-0.610 µg/L 0.006−0.101 µg/L 0.056−0.176 µg/L

South Africa	River water of selected rivers in the Eastern Cape Province in South Africa	Antibiotics	erythromycin	11.2 to 11,800 ng/L
			clarithromycin	4.8 to 3280.4 ng/L
			sulfamethoxazole	6.6 to 6968 ng/L
		anti-epileptic	Carbamazepine	81.8 to 36,576.2 ng/L
Jordan	Assamra wastewater treatment plant (WWTP) is the largest treatment facility in Jordan water resources in the ZR basin Samples of WWTP influent and effluent and river water from four sites along ZR were collected.	atenolol	beta-blocker;	1723–1952 ng/L
		anti-epileptic	Carbamazepine	2365–3020 ng/L
		(anti-inflammatory	paracetamol	14,891–24,309 ng/L
Ghana	surface water used for vegetable irrigation	Analgesics	Ibuprofen	10.0–319.0 ng/L
			Paracetamol	27.8 ng/L
			diclofenac	8.0 ng/L
		antibiotics	amoxicillin	145.0–659.0
			trimethoprim	840.0 ng/L
			cefuroxime	n.d–68.0 ng/L
USA	sediments of an urban river in Florida	stimulants	caffeine	0.2 to 24.4 ng/g
		Antibiotic	trimethoprim	0.01 to 0.83 ng/g
		anticonvulsant and analgesic	carbamazepine	0.1 to 32.9 ng/g
Latvia	wastewater treatment plant in Riga	central nervous system stimulator	caffeine	12 μg/L
		analgesic	acetaminophen	4.2 μg /L
		antibiotic	ciprofloxacin	250–400 ng/L
		non-steroidal anti-inflammatory drug (NSAID)	ibuprofen	100–325 ng/L

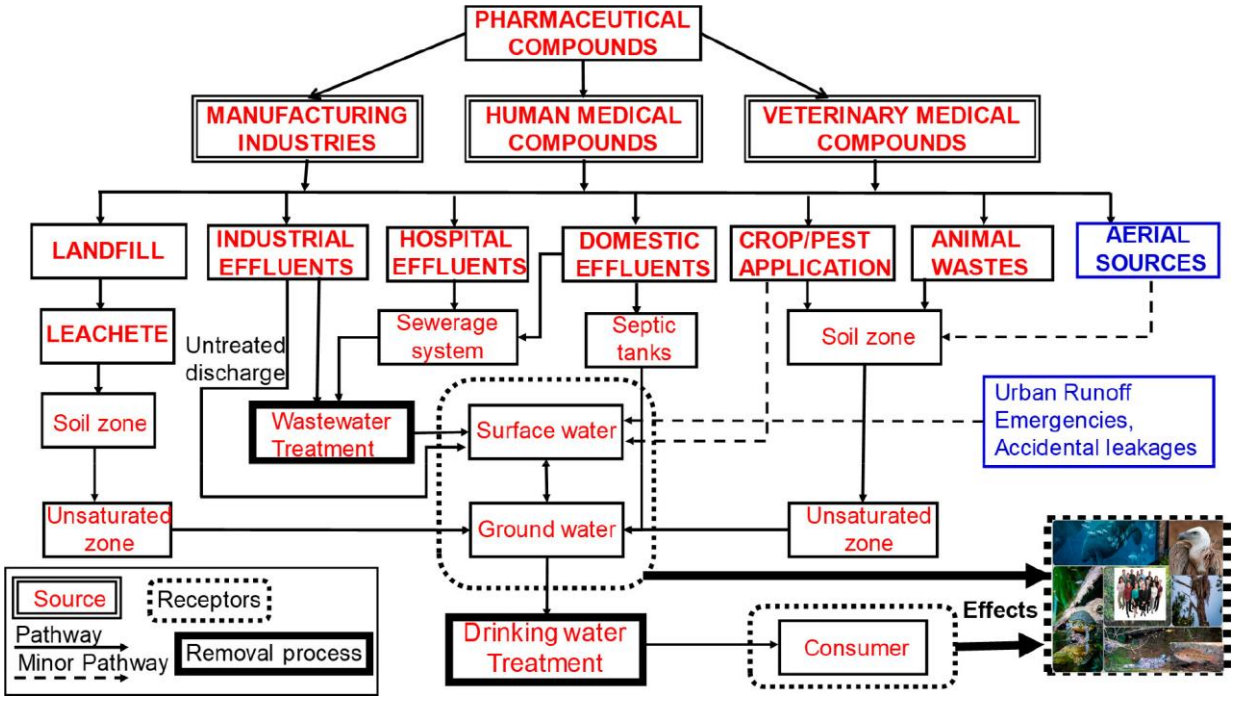


Figure 1: A schematic diagram showing possible pharmaceutical pollution sources, routes, and receptors in the environment (Patel et al., 2019).

The degradation of pharmaceutical waste has been studied using a variety of techniques. Example of these techniques includes bioremediation , adsorption, electrocoagulation , membrane, advanced oxidation processes (Lozano *et al.*, 2022; Pandis *et al.*, 2022), (UV/H_2O_2), Fenton and photo-Fenton, ozone-based (O_3) processes, photocatalysis, and sonolysis), as well as hybrid processes (Eniola *et al.*, 2022). Conventional wastewater treatment methods employ multiphase treatments such as clarity, filtration, coagulation, and flocculation. Conventional wastewater treatment methods cannot ensure the production of high-quality effluents, and even water that appears to be clean can contain pharmaceutical contaminants. In biodegradation techniques, plants and bacteria are used to treat wastewater (Xiong *et al.*, 2018). Wastewater from the pharmaceutical industry is completely mineralized as a result of biological treatment, leaving no waste behind. Moreover, great efficiency and cheap operation cost prove it to be a useful instrument. The breakdown of pharmaceutical wastewater by bioremediation currently has issues because a variety of chemical substances and functional groups of pharmaceutical substances hinder microbial activity (Alam *et al.*, 2021). Among these techniques, adsorption technique is the simplest, most affordable, and adaptable way for removing contaminants. However, it does not entirely break down the pollutants (Karimi-Maleh *et al.*, 2021). The employment of integrated technologies has recently garnered attention on a global scale due to its improved ability to eliminate contaminants. The use of combined technologies in the pharmaceutical wastewater treatment process has been reported by Masood *et al.* (Masood *et al.*, 2022), who investigated the degradation of

antibiotics namely Doxycycline, Tylosin Tartrate, and Timlicosin Phosphate from real veterinary pharmaceutical wastewater. The suggested method used multi-metal laden Zeolite 5A as a catalyst in a hybrid reactor system that combines electro flocculation and catalytic ozonation. A 55-99% breakdown of antibiotics was accomplished as a result of improved catalytic activity of metal-loaded zeolite. Sarkar *et al*. (2019), (Sarkar *et al.*, 2019) also studied an integrated treatment strategy for the removal of pharmaceutical waste. *A. faecalis* JF339228 and *E. aurantiacum* were used in the study of biological treatment after chemical treatment with ozone and adsorption by activated carbon made from the coffee husk. The combined approach demonstrated a synergistic effect in the breakdown of ondansetron with the least amount of chemicals and time needed. The observed elimination percentage ranged from 71 to 90%. The integrated treatment system was effective, affordable, and partially eco-friendly.

2.1 Tetracycline as emerging contaminant

Among the common pharmaceuticals found in water are antibiotics, particularly the tetracycline family. Tetracyclines are the second most widely used antibiotics worldwide due to their potency against numerous disease-causing bacteria in humans and animals (Adeyemi *et al.*, 2021). Moreover, tetracyclines are known to have specific characteristics not shared by other antibiotics. These characteristics include the ability to inhibit inflammation, anticancer potential, metabolism of bones, chelation of metal ions, apoptosis, angiogenesis, and proteolysis (Priya & Radha, 2017). Oxytetracycline and chlortetracycline are two of ten licensed growth promoters and antimicrobial agents registered in the United States (Daghrir & Drogui, 2013). Tetracycline is commonly used in veterinary medicine and aquaculture. Other pharmaceuticals in this category are doxycycline, demeclocycline, minocycline, methacycline, sancycline and chelocardin. Cyclic and aromatic rings are present in their structure (Figure 2). Despite their high consumption rate, many of these antibiotics are reported not to be entirely used by the living organisms' system. Instead, unutilized antibiotics are released into the environment as urine and faeces (Heilig *et al.*, 2002). Through these media, by leaching and surface runoff, antibiotics gain access to the ground and surface water (Zhang *et al.*, 2011). The continuous presence of these antibiotics in water leads to detrimental effects on both the environment and the organisms. For instance, the permeability of algae cells in freshwater has been reported to be negatively impacted by the presence of tetracyclines in water (Xu *et al.*, 2013). Similarly, the population of organisms such as fish, zooplankton, macrophytes, and microphytes has been negatively impacted due to the presence of tetracyclines in water (Kovalakova *et al.*, 2020). Due to tetracycline's low metabolism, around 60-90%, it is discharged into the environment in its original form or metabolized (Guo *et al.*, 2017). Several studies have shown that long-term exposure to antibiotics has harmful consequences, including acute or chronic disease, further endangering the ecosystem and humans (Jang *et al.*, 2018) .

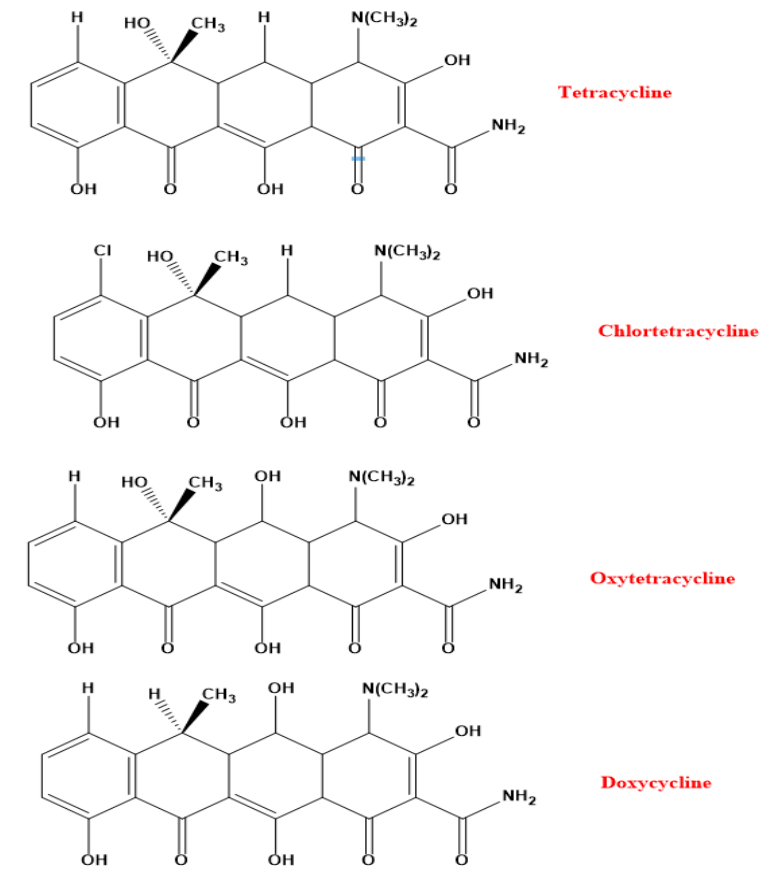


Figure 2: Structures of representative members of the tetracycline family**.**

2.1.2 Toxicity of tetracycline on plants and animals

The presence of tetracycline in various environments leads to different toxic effects on plants, humans, and the environment (Balakrishnan *et al.*, 2023). The effects of high volume of tetracycline in the environment on different plants have been investigated. Accumulation of tetracycline was detected in the root and stems of *Ipomoea aquatic* and *Brassica rapachinensis*. The concentration was found to be higher in the field that was polluted with tetracycline (Chen *et al.*, 2017). There is a risk of transferring tetracycline into the plants and animals that consume these vegetables. In a different research, it was discovered that the accumulation of tetracycline in the plant, up to 5 mg/L, negatively impacted the content of malondialdehyde in the plants. It also affected the frequency of chromosome aberration in plants (Xie *et al.*, 2011). Other plants that have been investigated for the impact of tetracyclines are shown in Table 2.

Table 2: Toxic effects of tetracycline on different plants

Plant investigated	**Plant part with tetracycline accumulation**	**Type of tetracycline and concentration**	**Effects of tetracycline on plants**	**Ref.**
Cucumber, tomato, and lettuce	Roots and leaves	Tetracycline, oxytetracycline, chlortetracycline (5-20 mg kg^{-1} soil)	Negative impacts on the growth of the plants	(Ahmed *et al.*, 2015)
Ryegrass	Roots	Tetracycline (0-100 mg L^{-1})	Stunted growth and decrease in the concentration of chlorophyll and carotene with increasing tetracycline concentration. It equally affected amino acid metabolism and biosynthesis of aminoacyl-tRNA	(Han *et al.*, 2019)
Rice	Roots	Zwitterionic tetracyclines (50 mg L^{-1})	Maximum Root Concentration Factors of the order of 2000 L kg^{-1} (d.w.) and concentrations in root tissue of greater than 1000 mg kg^{-1} (d.w.)	(Boonsaner & Hawker, 2012)
Pea seedlings	Roots	Tetracycline (150 mg kg^{-1} of soil)	Modification of biochemical processes connected with protein	(Margas *et al.*, 2016)
Peanuts	Leaves, stems, kernels, roots and shells	Tetracycline	Translocation as a result of tetracycline accumulation in the tissue	(Zhao *et al.*, 2019)
Iberis semperviren s L.	Leave and shoot	Tetracycline	Inhibition of photosynthetic activity, oxidative stress in plants as well as large reduction in plant growth and development	(Di Marco *et al.*, 2014)
Zea mays	Roots, stalks, and leave	Oxy- (15 mg L^{-1}) and Chlor-tetracycline (5 mg L^{-1}) while the residue is 1–50 ng g^{-1}	Inhibit the growth of the plants	(Migliore *et al.*, 2010)

In terrestrial animals, tetracycline has been found to have negative effects on the traits of the animals. For instance, in the studies conducted on *Cordylochernes scorpioides,* the sperm number, female reproduction, and body sizes of both male and female species were found not to be affected by tetracycline. However, the sperm viability of the male species exposed to tetracycline was reduced significantly compared to the male species without tetracycline treatment. This trait was passed to the male offspring that were not treated with tetracycline, but the effect was not noticed in the F_2 grandson of *Cordylochernes scorpioides* (Zeh *et al.*, 2012). The impact of tetracycline on aquatic animals has also been observed to be significant. Zhang et. al., discovered that exposure to 20 μg/L tetracycline in zebrafish resulted in oxidative stress-induced apoptosis and oxidative damage. The effects of these were

an uninflated swim bladder, increased yolk sac area, shorter body length, and delay in hatching (Zhang *et al.*, 2015). *Gambusia holbrooki,* which is a freshwater fish species experienced histological changes in the liver and gills when exposed to tetracycline. Also, there was observed pro-oxidative activity in the fish due to tetracycline exposure (Nunes *et al.*, 2015).

2.1.1 Removal methods for tetracycline in water

The toxicity of tetracyclines in water has led to their removal using various conventional methods (Table 3). Apart from these examples, other methods that have been used for removing pharmaceuticals and other organic pollutants in water are: thermal desorption, air stripping, settling, solvent extraction, solar destruction, vitrification, zero-valence iron, Fenton oxidation, molten salt oxidation, molten metal pyrolysis, ultrasonic technology, reduction processes, plasma systems, and bioremediation. All these methods have their own advantages but also have several limitations (Ajiboye *et al.*, 2021a; Taoufik *et al.*, 2021). The need to overcome these limitations led to the use of membrane technology. Studies have been carried out to enhance the properties of the membrane. One of the efforts towards achieving a more efficient membrane is the use of biocompatible ionic liquid for the synthesis of membranes (Khalid *et al.*, 2023). The use of membrane technology with photocatalysis has also been reported, thus leading to the synthesis of photocatalytic membranes. Photocatalysis is advantageous because it is carried out by using cheaply available light and a photocatalyst. Also, the pollutants are degraded rather than being transferred from one medium to another. Among the common photocatalyst materials used are photocatalytic membranes. The advantages of photocatalytic membranes are their reusability, good separation efficiency, easy recovery, and reduced membrane fouling (Balakrishnan *et al.*, 2022). The ceramic membranes are thermally stable, resistance to solvents and chemicals, durable, and possess high mechanical strength (Nabila *et al.*, 2023).The photocatalytic properties of the membranes are also enhanced when the ceramic membranes are functionalized with other photocatalytic materials (He Z *et al.*, 2019). As a result, the use of their composite for the removal of pollutants in water is desirable.

Table 3: Methods of removing tetracyclines from water

Removal method	**Tetracycline removed**	**Performance**	**Ref.**
Membrane filtration	Tetracycline hydrochloride	98.9% of antibiotic removed	(Liu *et al.*, 2017)
Hydrolysis	4-epitetracycline hydrochloride and anhydrotetracycline	0.3–97.8% of its antibacterial activity was lost after 6 h hydrolysis at 85 °C	(Kang *et al.*, 2012; Yi *et al.*, 2016)
Reverse osmosis	Tetracycline and oxytetracycline	More than 90% removal efficiencies	(Li *et al.*, 2009)
Electrochemical oxidation	Oxytetracycline hydrochloride	Removal of 87.75% and 93.2% when aluminium and iron were respectively used as the anodes with optimum current density of 20 mA/cm^2 for both anodes	(Nariyan *et al.*, 2017)
Supercritical oxidation	Tetracycline hydrochloride	Removal rate of 100% at 1000 mg/L, 400 °C and 100 s	(Gong *et al.*, 2022)
Ozonation	Tetracycline	89.1% of the COD removal in the presence of catalyst	(Hou *et al.*, 2013)
Electrochemical Incineration	Tetracycline	90% and 84% degradation was achieved after 30 min at 30 and 20 $mAcm^{-2}$ respectively	(Gul *et al.*, 2013)
Phytoremediation	Hydrochloride salt of tetracycline	99% and 54% of the total amount of tetracycline were removed within 2 h and 5 days, respectively by using *Myriophyllum aquaticum*	(Guo *et al.*, 2019)
Sludge digestion	Tetracycline	The maximum adsorption capacities were 2.984, 4.108 and 4.618 mg/g at 25, 35 and 45 °C, respectively and maximum adsorption of 93.0%.	(Li *et al.*, 2013)

2.2 Membrane technology

Membrane technology has recently become one of the most popular methods for treating wastewater because of its environmental friendliness, ease of use, simple upscaling and downscaling processes, and seamless integration into other wastewater treatment methods. In addition to providing effective treatment of wastewater, membranes can be recycled and used to generate significant economic, social, and environmental benefits. A membrane is a porous layer that allows fluid to flow through it while restricting contaminants based on their physicochemical properties (Chadha *et al.*, 2022; Obotey Ezugbe & Rathilal, 2020). It serves as a barrier in the treatment of wastewater by allowing water to pass through while trapping undesirable pollutants (Capodaglio, 2021). Membranes are categorized according to their type, structure, material composition, and charge as illustrated in Figure 3. The fundamental separation principles employed in the membrane process to remove contaminants from wastewater are based on their size or charge which includes adsorption, sieving, and electrostatic phenomena (Arola *et al.*, 2019). As a result, four membrane processes namely microfiltration,

ultrafiltration, nanofiltration, and reverse osmosis are used in the removal of pollutants (Loganathan *et al.*, 2022) and they differ based on the size of their pores. The most common pressure-driven membrane processes used in the removal of dissolved contaminants with very small molecular weight, such as pharmaceutical compounds and organic dyes are reverse osmosis and nanofiltration. Due to the ease with which these contaminants pass through the membrane, other filtration techniques like microfiltration and ultrafiltration hardly ever remove them. The only way these techniques can be employed in the removal of these contaminants is to act as pre-treatment steps that remove other pollutants such as organic matter (Ganiyu *et al.*, 2015).

Membranes are primarily categorized into organic (polymeric) and inorganic (ceramic) types (Kotobuki *et al.*, 2021). Organic membranes are those that are made up of nonporous polymeric materials, such as cellulose acetate, polyethersulfone, polyimide, polysulfone, polymethylpentene, polycarbonate, polydimethylsiloxane, and polyphenylene oxide (Binazadeh *et al.*, 2023). Ceramic membranes are fine artificial porous membranes made from sintering inorganic materials, such as alumina, zirconia oxide, titanium, silicon oxide, silicon carbide, and silicon nitride or a combination of these materials under high temperatures (Zhang Y *et al.*, 2023). At the moment, large-scale polymeric membrane systems are widely used over inorganic membranes due to good selectivity, ease of controlling pore size during formation, high flexibility, and cost-effectiveness (Sonawane *et al.*, 2021). Most applications of polymeric membranes are in gas separation and desalination due to high permeation and selectivity. They are, however, under-utilized in areas such as wastewater treatment due to low stability towards high temperatures, chemicals and harsh conditions (Ismail *et al.*, 2010)**.** Consequently, inorganic membranes have rapidly received global attention in being considered as one of the potential candidates to replace available polymeric membranes (Salleh *et al.*, 2011) due to several characteristics such as high stability under a variety of operating conditions such as temperature, and toxic chemicals, high eco-compatibility and scalability (Shehata *et al.*, 2023).

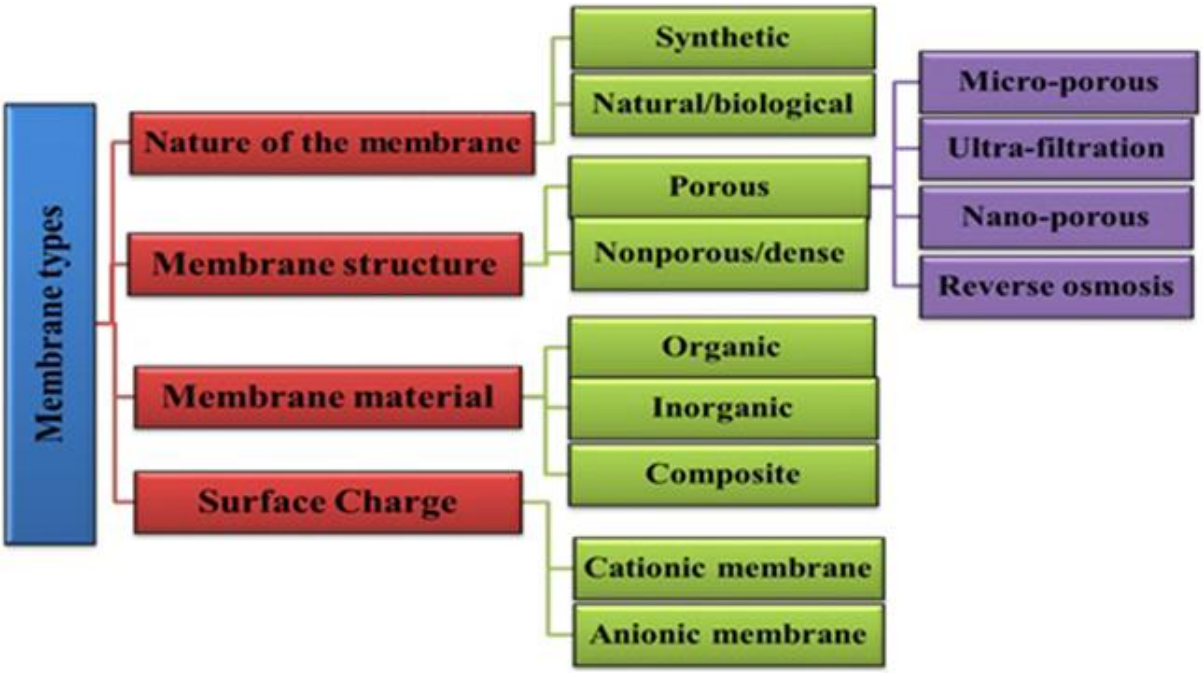


Figure 3:Types of membrane employed in the wastewater treatment sectors (Bera *et al.*, 2022)

2.2.1 Ceramic membrane technology in wastewater

Ceramic membranes can be classified as either symmetric or asymmetric based on their structural properties (Figure 4) (Sarp & Hilal, 2018). Symmetrical structured ceramic membranes have pores that are uniform in size across the membrane's thickness as shown in Figure 4(a). Conversely, asymmetric ceramic membranes feature three layers with pore patterns that are greatest on one surface and smallest near the other surface Figure 4(b) (Goh & Ismail, 2018). The membrane relies on a macroporous support that offers robustness due to its larger pores. Additionally, an intermediate layer with smaller pores compared to the support layer safeguards against material intrusion during fabrication. Lastly, the selective active layer, featuring even smaller pores than the intermediate layer, effectively rejects pollutants (Samadi *et al.*, 2022)**.** The efficiency of separating pollutants in wastewater using ceramic membranes depends on factors such as the membrane's pore volume, pore size, size distribution, and surface chemistry (Zhang Z *et al.*, 2023).

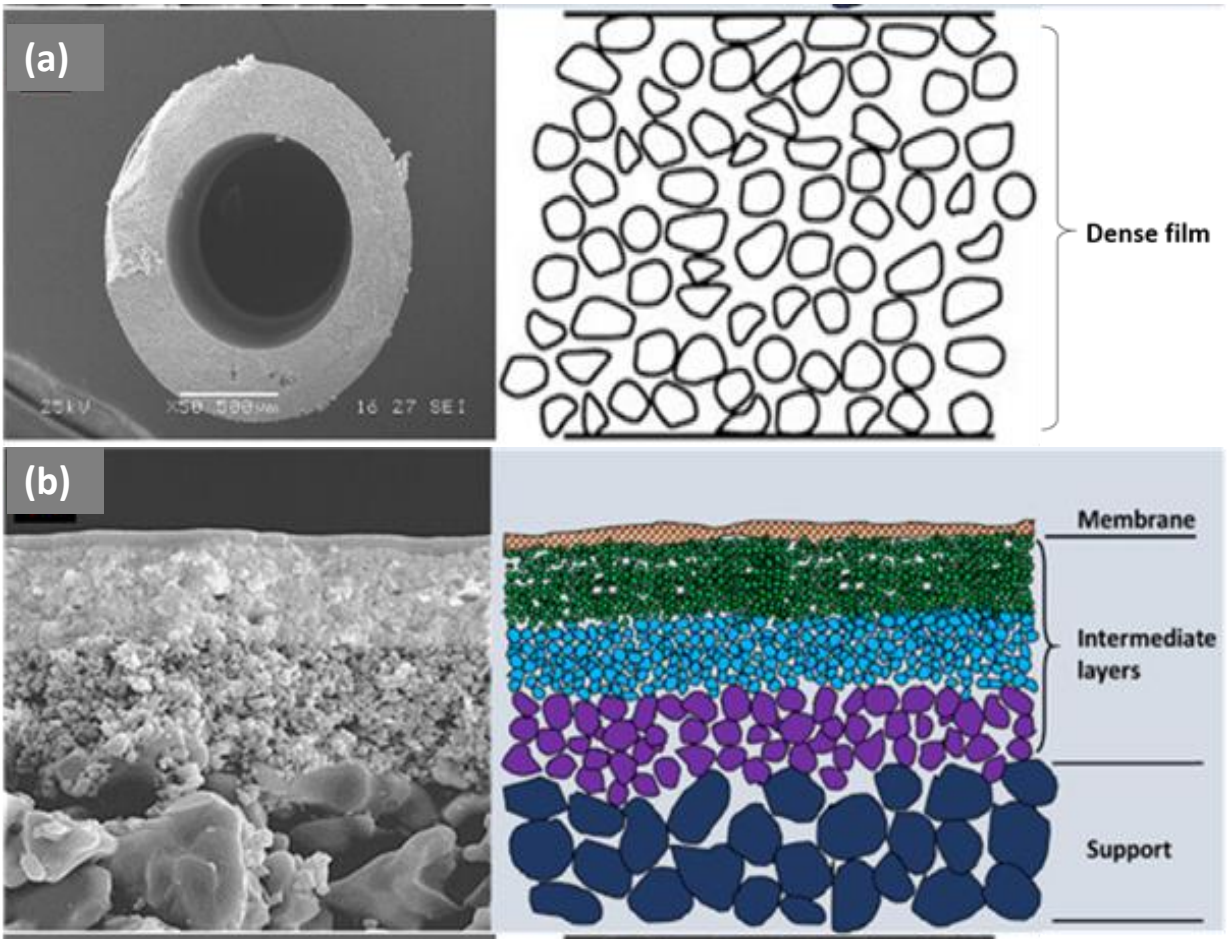


Figure 4:The typical cross-section of (a) symmetrical ceramic membrane (Drioli *et al.*, 2017) and (b) an asymmetrical ceramic membrane (Lee *et al.*, 2015).

2.2.2 Advantages and disadvantages of ceramic and polymeric membranes

As shown in Table 4, both ceramic and polymeric membranes are associated with some advantages and disadvantages. Some of these drawbacks make it challenging for pristine membranes to fully satisfy the fundamental property requirements for large-scale applications. For instance, the large-scale use of ceramic membranes has been adversely impacted by reversible membrane fouling and expensive production costs. On the other hand, the primary disadvantages of polymeric membranes for widespread applications are irreversible fouling, biodegradation, and instability in harsh conditions.

Table 2: Advantages and disadvantages of ceramic and polymeric membranes

	Ceramic membranes	Polymeric membranes
Advantages	Experience fewer failures in terms of breaches to the filtration barrier	Easily modifiable and accessible
	Tolerance of ceramic membranes to a wider variety of chemicals and chemical concentrations	Lower production cost
	Endure higher pressures	Ease of fabrication
	Water recovery of a ceramic membrane system exceeds 98%	Can be sintered at lower temperatures
	The rejection layer is thicker	
	Longer service life	
Disadvantages	Higher capital cost	Polymeric membranes have a defined range of allowable chemical types and concentrations for cleaning.
	The difficulty of achieving high selectivities in large-scale microporous membranes.	Doesn't endure higher pressures
	Difficult membrane to module sealing at high temperature	Water recoveries in the 93–96% range
		Suffer from biofouling and biodegradation
	Low membrane surface per module volume	The rejection layer is thinner

2.2.3 Challenges facing ceramic membrane technology and the remedial actions

The large-scale water treatment by ceramic membranes is limited due to high membrane fouling, concentration polarization, high cost of commercially available porous ceramic membrane raw materials and relatively high firing temperatures (Chaari *et al.*, 2021). These challenges tend to reduce the effectiveness of membrane separation in wastewater treatment (Obotey Ezugbe & Rathilal, 2020).

2.2.3.1 Ceramic membrane cost

Alumina, zirconia, silicon oxide, titanium oxide, and their composites are among the ceramic oxides that are frequently utilized for commercial ceramic membranes, along with non-oxide ceramics (silicon carbide and silicon nitride) (Dong Y. *et al.*, 2022). These raw materials are expensive, their cost price range from \$500–3000/m^2. The preparation of membranes from these materials requires high firing temperatures (1300–1500 °C) (Chaari et al., 2021). Hence, the large-scale application of ceramic membranes in wastewater treatment is very limited due to their high production cost. Many efforts have been made to reduce the fabrication cost of ceramic membranes to promote their widespread use. The utilization of commonly available and affordable materials such as ceramic membrane raw materials is drawing a lot of attention in these initiatives. These materials include natural kaolin, phosphate , coal fly ash, clay and rice husk (Hubadillah *et al.*, 2020). Clay, kaolin, and coal fly ash shown in Figure 5 are the most often utilized low-cost materials for the fabrication of ceramic membranes, according to a literature review by Abdullayev *et al*. (Abdullayev *et al.*, 2019). These materials can replace industrial-grade materials used in the fabrication of membranes because they have considerable amounts of SiO_2 and Al_2O_3 in their mineralogical compositions as shown in Table 5. Insignificant amounts of metal oxides like Fe_2O_3, TiO_2, and others contribute to the membrane's strength and function as catalytic modifiers in ceramic membranes.

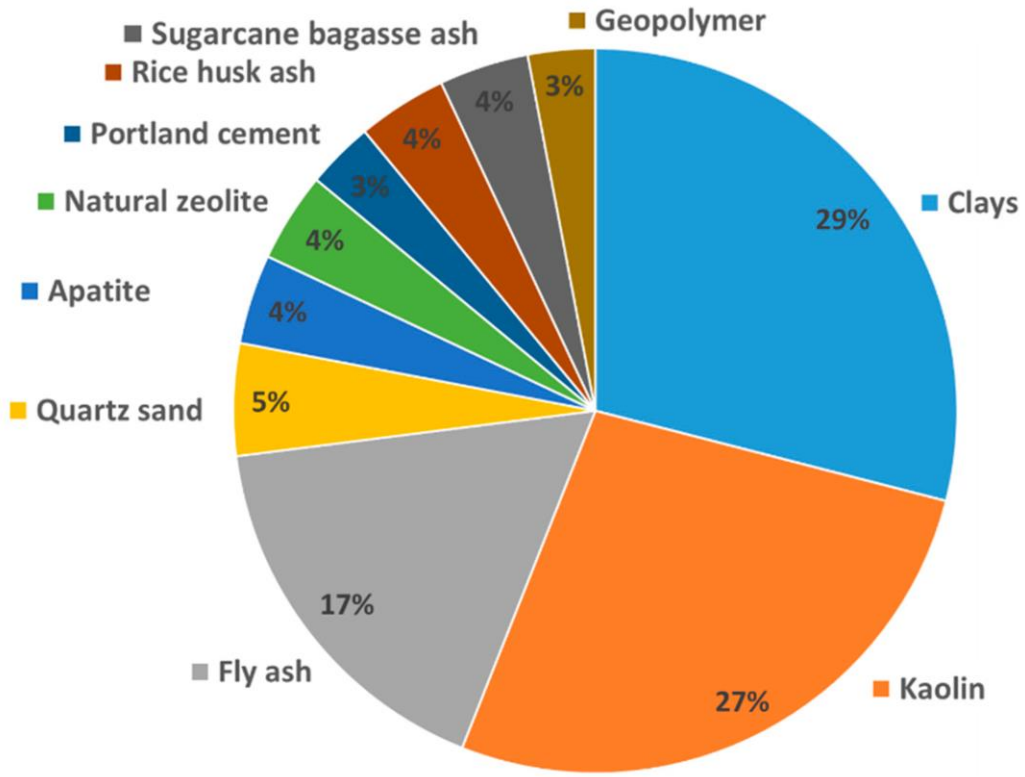


Figure 5:Representation of different raw materials in studies of low-cost ceramic membranes (Abdullayev et al., 2019).

Table 3: Mineralogical composition of kaolin, bentonite clay and coal fly ash

Material	Country	Percentage mineralogical composition									Ref
		SiO_2	Al_2O_3	Fe_2O_3	MgO	CaO	K_2O	TiO_2	P_2O_5	Others	
Kaolin	Malaysia	57.1	37.8	0.9	0.6	0.3	1.8	0.6	0.3	0.7	(Yahaya *et al.*, 2017)
	Uganda	49.2	35.9	0.5	0.1	-	1.0	0.1	0.1	13.1	(Nyakairu *et al.*, 2001)
	Egypt	41.0	36.1	5.3	0.1	-	1.0	3.2	0.1	13.2	(Saber *et al.*, 2018)
Coal fly ash	Canada	54.7	21.1	4.4	1.6	8.0	1.8	0.7	0.3	7.4	(Goodarzi, 2006)
	Poland	50.4	26.3	5.4	2.6	3.5	2.8	1.1	0.5	7.4	(Strzałkowska, 2021)
	South Africa	51.43	30.93	2.3	2.0	6.8	0.8	1.7	1.1	2.9	(Ayanda *et al.*, 2012)
Bentonite clay	Morocco	56.6	17.9	2.0	0.1	1.2	1.5	0.3	0.1	20.3	(Ddani *et al.*, 2005)
	China	48.7	29.1	2.3	1.7	0.2	3.3	4.4	0.1	10.2	(Hong *et al.*, 2019)
	Portugal	67.7	16	2.3	4.5	2.1	0.1	0.1	-	7.2	(da Silva Favero *et al.*, 2019)

2.2.3.2 Fouling and concentration polarization

Increased concentration of the rejected suspended or dispersed materials close to the membrane surface leads to concentration polarization. Membrane fouling occurs when suspended or dissolved materials are irreversibly deposited on the exterior membrane surface or membrane pores, impairing the membrane's overall functionality (Kuvarega & Mamba, 2016). Membrane fouling causes the holes of the membrane to keep contracting, which lowers the water quality and flow. It may be necessary to replace the membrane to prevent this kind of extreme fouling, in addition to using intensive chemical cleaning techniques (Ahmed *et al.*, 2022). If a strong casting of the fouling stratum is generated with the solution during the filtration operation, contradictory fouling could transform into an irreversible fouling layer (Liu *et al.*, 2019). When a membrane filter becomes fouled, it affects the performance of the membrane and frequently requires expensive cleaning processes that interfere with the membrane filtration process, such as back permeation, flushing, backwashing and air scouring (Gul *et al.*, 2021). To improve the reduction of membrane fouling, which is a significant problem for membrane processes, membrane modules and membrane elements are continuously modified. In several wastewater treatment plants, the potential for merging two or more membrane processes or with different technologies like coagulation or adsorption is also continuously being studied, developed, and implemented (Obotey Ezugbe & Rathilal, 2020).

Coagulation is one of the best pre-treatment methods for reducing membrane pore blockage and cake layer resistance because of its excellent performance, low cost, and capacity to remove naturally occurring organic waste (Zhang *et al.*, 2022). Due to their high coagulation efficacy and economical nature, Al- and Fe-based salts are the most widely used coagulants (Chekli *et al.*, 2017). Liu et al. (Liu *et al.*, 2022), studied the influence of titanium-based coagulant (poly titanium chloride) on controlling membrane fouling on the ceramic membrane. According to the results, 78.0% of organic particles were removed. The permeate flow through the ceramic membrane was higher than that of the traditional poly aluminium chloride case. For poly titanium chloride, the formation of a cake layer caused fouling of the ceramic membrane, whereas for poly aluminium chloride, clogging of the membrane pores was the major cause of fouling.

2.2.4 Coal fly ash as a sustainable alternative to commercial materials in membrane fabrication

Application of ceramic membranes is mainly at the laboratory scale due to the high cost of raw materials, multi-manufacturing steps and high sintering temperatures (Drioli *et al.*; Lorente-Ayza *et al.*, 2016). The estimated cost price of ceramic membranes ranges from $500 to $1000 per square meter, with the price of polymeric membranes accounting for 25% of that price (Li C *et al.*, 2020). In order to enhance the price competitiveness of ceramic membranes for large-scale applications, it is imperative to lower the fabrication costs associated with them (He Z et al., 2019)**.** The use of improved ceramic membranes for wastewater treatment appears to hold a significant prospect for future advancement in water treatment and sanitation. Several studies have employed ceramic membranes in wastewater treatment and the search for low-cost and environmentally friendly starting materials has continued to engender research interests. Therefore, solid wastes and readily available materials rich in Al_2O_3 and SiO_2 such as coal fly ash can be used as starting material for ceramic. It has been demonstrated in numerous studies that it is possible to fabricate ceramic membranes from coal fly ash. The utilization of these affordable starting materials in large-scale membrane processes presents sustainability, environmental benefits and potential high removal efficiencies for pollutants (Samadi et al., 2022; Zhou *et al.*, 2022)**.** In addition to resolving the problem of poor water quality, the use of coal fly ash in ceramic membranes in wastewater treatment represents a milestone in waste management because coal fly ash has detrimental environmental consequences (Mushtaq *et al.*, 2019).

2.2.4.1 Coal fly ash

Coal fly ash is a residue that is generated through the combustion of pulverized coal in thermal power plants (Ghazali *et al.*, 2019). It is an extremely fine, heterogeneous powder mixture of crystalline and

amorphous phases with spherical geometry, and particle sizes between 10 and 100 microns (Dwivedi & Jain, 2014). Oxides of silicon, aluminium, calcium, iron, and calcium are the main components of coal fly ash. There are also little amounts of magnesium, calcium, potassium, sodium, titanium, and sulphur as shown in Figure 5. Significant levels of hazardous metals such As, Ba, Hg, Cr, Ni, V, Pb, Zn, and Se are also present in the coal fly ash (Labidi *et al.*, 2023). These toxic substances may seep out of it and pollute the environment. Additionally, they may cause cancer, skin and lung infections, nausea, vomiting, and organ dysfunction in people(Jaishankar *et al.*, 2014). Coal fly ash can be further divided into two classes: Class C and Class F, depending on where the coal came from. Class F is from bituminous and anthracite coals, which have a lower calcium concentration than Class C's high calcium content (above 20%) lignite and sub-bituminous coals (Wang *et al.*, 2021). Compared to Class C, Class F contains a higher percentage of alumina, silica, and iron (around 70%) (Adewuyi, 2021). High calcium content in class C results in the production of a greater amount of calcium-aluminate-silicate hydrate, whereas Class F's higher silicon content produces a greater amount of sodium-aluminate-silicate-hydrate (Gollakota *et al.*, 2019; Vassilev & Vassileva, 2007). The source of the coal, the amount of ash in the coal, the degree of coal mining and preparation, the conditions during combustion and mining, the current climate, and other pertinent aspects all affect the properties (physical and chemical) and composition of coal fly ash (Openshaw, 1992).

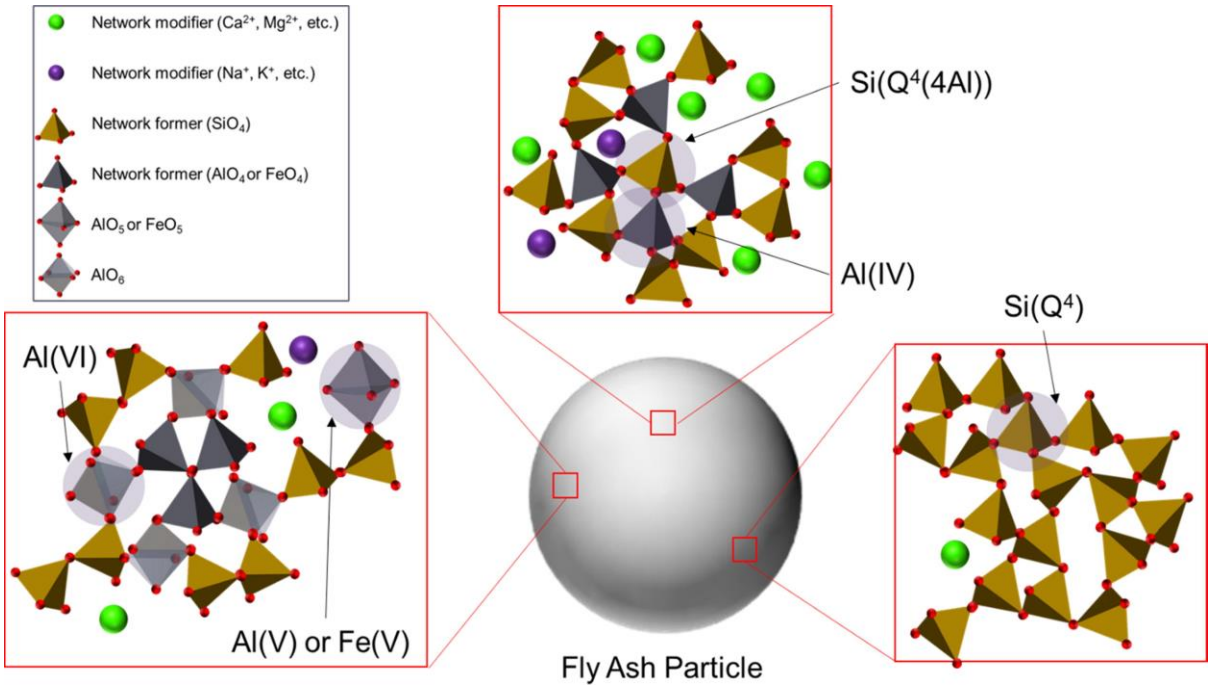


Figure 6:Schematic Illustration of the structure of coal fly ash (Jin *et al.*, 2020).

Around 8,025 Mt of coal were used worldwide in 2022 (Fig 7a) by several industries, including cement manufacturing, iron and steel production, and power generation. As a result, a lot of coal fly ash is being produced, but less than 30% of them are being recycled. Consequently, disposal takes up a lot of space, which is a significant problem. Transporting the coal fly ash for disposal also comes at a considerable expense. Coal fly ash is also harmful to the environment since it can contaminate the air, water, and soil and leach hazardous compounds (Feuerborn *et al.*, 2019; Jayaranjan *et al.*, 2014). Because of this, experts are now concerned about how to properly manage, dispose of, and use coal fly ash. Even though there has been a lot of research done on the global usage of coal fly ash (Fig (7a)), the building industry as shown in Fig (7b) is currently where it is most frequently used. These applications are ascribed to shape, surface area, high strength, lightweight, and non-toxic and porosity, among other physical characteristics (Nsiah-Gyambibi *et al.*, 2023). The most lucrative application of coal fly ash in terms of volume is as a raw material for ceramic membranes, yet little study has been done in this field.

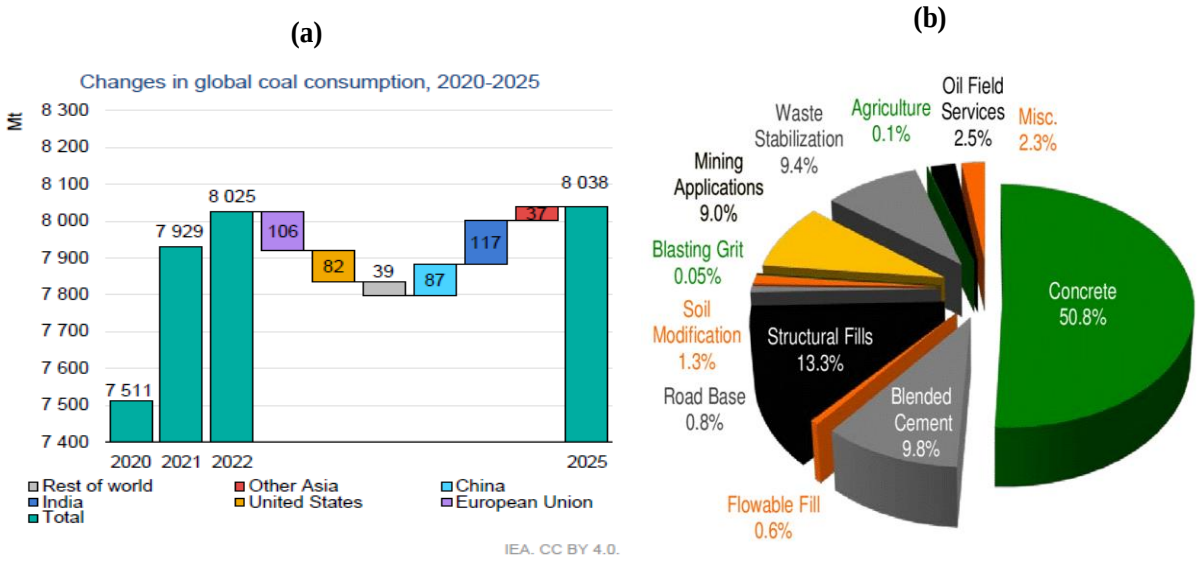


Figure 7: (a) Changes in global coal consumption (b) various uses of coal fly ash (IEA, 2020; Shearer, 2014).

2.2.4.2 Synthesis of coal fly ash-based ceramic membranes

The fundamental components required for the manufacture of ceramic membranes include inorganic precursors, and additives such as solvents, dispersants, pore formers, binders, and plasticizers. The fabrication process involves three primary steps which are: (1) preparation of suspension or paste from precursor material and additives, (2) shaping the suspension/paste into a desired geometry such as tubular, plate or disc configuration and (3) drying, and sintering of the resultant ceramic membrane (Ajiboye *et al.*, 2023). An optional step, which involves the leaching of undesired elements in the coal fly ash before the mixing of raw materials and additives is determined by the analysis of the elemental

composition of the coal fly ash. The allowable concentrations of these elements are guided by the thresholds indicated in the national guidelines for heavy metal release. This is due to the possible presence of large levels of toxic metals such as Ba, As, Hg, Cr, Ni, V, Pb, Zn, and Se in coal fly ash (Dan *et al.*, 2021; Peng *et al.*, 2022). The most common manufacturing techniques for ceramic membranes are freeze casting, slip casting, tape casting, pressing and extrusion. The choice of a ceramic membrane fabrication technique depends on application requirements, the desired membrane geometry, and the specific starting materials (Issaoui & Limousy, 2019). In the fabrication of ceramic membranes, the additives have a variety of important functions. The viscosity of the slurry is controlled using solvents like water and those with organic bases, such as acetone, to make it easier to spread over the carrier film and to increase the uniformity of the additives in the ceramic powder. Ceramic particles can be held together using binders such as polyvinyl alcohol, sodium metasilicate, carboxymethyl cellulose (CMC), and others. The settling of the powder particles is prevented by the use of dispersants like sodium hexametaphosphate (Zhang Z et al., 2023), sodium carbonate, and boric acid (Singh & Bulasara, 2015). In order to make synthetic membranes more flexible, glycerine is mostly utilized as a plasticizer. The porous ceramic membrane's porosity is increased using pore-forming materials including dextrin(Huang *et al.*, 2022), calcium carbonate(Jiang *et al.*, 2018; Singh & Bulasara, 2015; Wei *et al.*, 2016), and spherical graphite (Cui *et al.*, 2023; Das & Kayal, 2023) which decompose completely during the sintering process. Table 6 gives the properties, configurations, and fabrication techniques of some coal fly ash based ceramic membranes.

2.2.4.3 Synthesis of coal fly ash ceramic membranes by pressing method

Axial pressing and isostatic pressing are the two pressing techniques used in the fabrication of ceramic membrane supports. Axial pressing is classified as dry or wet, with dry pressing involving dry powders without water and wet pressing involving the addition of water to ceramic raw materials. The two types of isostatic pressing are cold pressing and hot pressing. Cold isostatic pressing creates membrane support using external pressure, but hot isostatic pressing creates the desired shape using heating. While isostatic pressing applies pressure from various directions to boost shape capabilities, axial pressing is more affordable and appropriate for high volume manufacture of simple geometrical ceramic membranes (Monash *et al.*, 2013)**.** Apriyanti et al (Apriyanti *et al.*, 2021) used the dry pressing method to fabricate flat ceramic membrane from coal fly ash. When a pressure of 1 bar and calcination temperature of 1100 °C for 7 h was applied, the resulting membrane was more durable and had a homogeneous surface free of any cracks. The coal ash membrane's major crystal structure morphology was Al_2O_3, according to XRD analysis. Due to the formation of a robust and porous ceramic membrane, the findings from the study demonstrated that coal fly ash can be used as a raw material for ceramic membranes. Liu et al (Liu *et al.*, 2016) fabricated a cylindrical-shaped porous ceramic membrane using wet ball milling and uniaxial pressing. Dolomite was employed as a pore-forming agent, sintering

inhibitor, and reactant in addition to coal fly ash as the starting material. The findings demonstrated that the addition of dolomite effectively modified the support pore structure by increasing pores through the release of CO_2 and preventing coal fly ash from sintering while supplying sufficient mechanical strength and good thermal characteristics in the finished porous ceramic membrane. In a similar study, Chathurappan et al reported the suitability and effectiveness of dry pressing method in the fabrication of coal fly ash based ceramic membranes. The main raw materials used in the synthesis process were coal fly ash and fuller clay. The procedure involved in the fabrication is shown in Figure 8 (Chathurappan & Jayapal, 2022).

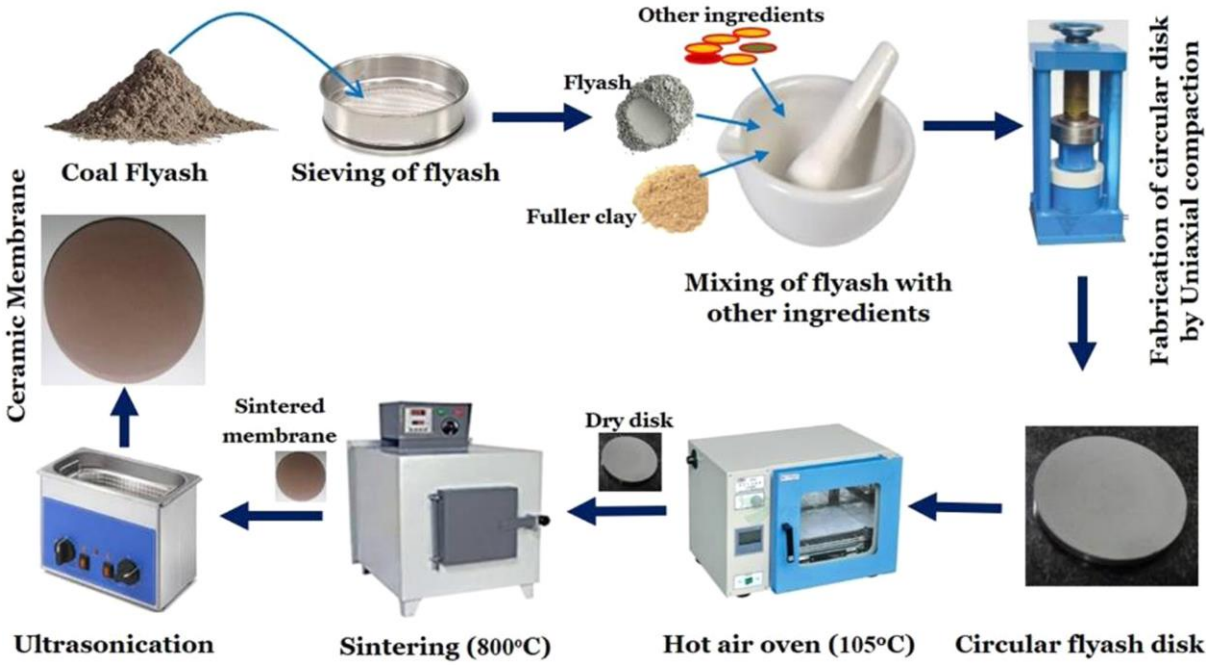


Figure 8:Schematic illustration for the preparation of coal fly ash based ceramic fabrication by dry pressing method (Chathurappan & Jayapal, 2022).

2.2.4.4 Synthesis of coal fly ash ceramic membranes by extrusion method

One of the often-employed conventional methods for fabricating multi-channel ceramic membranes that may be produced on an industrial scale is extrusion. The homogeneous, high-viscosity paste created by combining aggregate powder with additives is vacuum melted and aged. The additives form the required plastic properties for effective shape-forming without losing cohesiveness. The uniform high viscosity paste is then extruded into tubular supports by a nozzle after entering the vacuum extruder. To preserve the synthetic membrane's final structure, the remaining chemicals are evaporated. The most significant factors for process control are the applied pressure in extrusion and the rate of extrusion. The diameter of the raw material, the amount of binder, and the sintering temperature on the support affect the qualities and performance of the synthesized membrane (Ağtaş *et al.*, 2021; Fan *et al.*, 2016). Huang et al synthesized coal fly ash based ceramic membrane with high efficiency for water and heat

recovery. Dextrin was utilised as a binder, while carboxymethyl cellulose was used as a pore-forming agent. The procedure involved in the fabrication is shown in Figure 9 (Huang et al., 2022). In another study, Jedidi *et al.* (2011) reported the fabrication of porous tubular coal fly ash based ceramic membrane using extrusion method. At a constant sintering temperature of 1125 ℃, it was demonstrated that the ceramic membrane synthesized exhibited favourable mechanical and chemical resistances. Additionally, it possessed a significant average porosity of 51% and a mean pore diameter of 4.5 μm. The membrane's permeability was measured at 475 L h^{-1} m^{-2}bar.

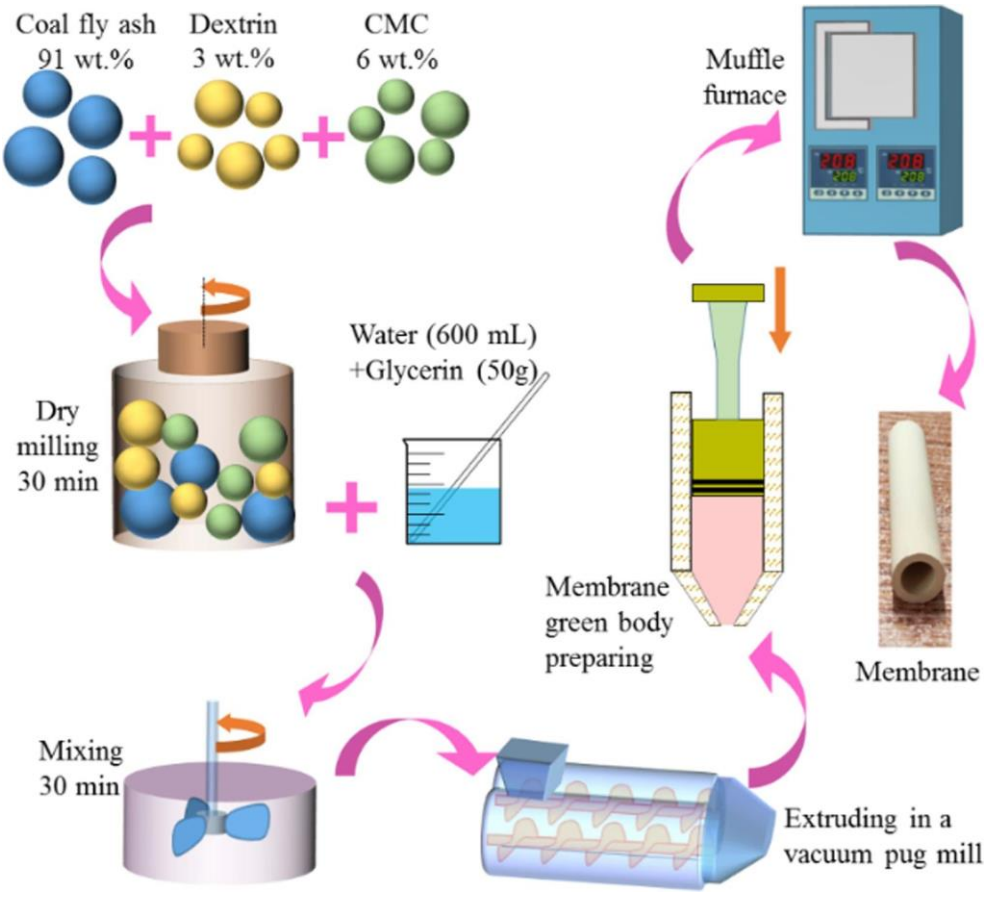


Figure 9:Fabrication of coal fly ash based ceramic membrane via extrusion method (Huang et al., 2022).

2.2.4.5 Synthesis of coal fly ash ceramic membranes by slip casting method

Slip casting is an easy, affordable, and adaptable technique. It is used to fabricate ceramic membranes with complicated shapes that are non-concentric and uneven. In slip casting technique high solid content suspensions are poured into porous cast molds, allowing the solvents to seep through the pores and precipitate the particles into a layer as illustrated in Figure 10. The resultant material is sintered after de-moulding, which is the final step in producing the desired ceramic membrane. The fabrication of

ceramic membranes from coal fly ash using the slip casting method was first reported by Jedidi *et al.* (2009). The primary chemical components of the coal fly ash employed in the study are mainly comprised of SiO_2, Al_2O_3, and Fe_2O_3. The minor components were made up of a variety of alkali metals. Fly ash powder, distilled water, and polyvinyl alcohol (PVA) were mixed to create the slurry. The final membrane was subjected to a thermal process that involves 24 hours of room temperature drying followed by 800 °C sintering. SEM images showed that the membrane surface was uniform and free of cracks. The results showed that the active layer's average pore diameter was 0.25 μm and its thickness was close to 20 μm. The fabricated ceramic membrane had a 475 L/h/m^2 bar permeability. A number of factors, such as sintering temperature, casting time, suspension pH, particle size, etc., have an impact on the properties of slip casted ceramic membranes (Kim *et al.*, 2015). Fang *et al.* (2011) investigated the effect of slip concentration, withdrawal speed and casting time on the preparation of coal fly ash ceramic membrane fabricated using the slip casting technique. The findings showed that an increase in slip concentration causes a significant increase in membrane thickness as well as an increase in porosity because more particles adhere to one another. Additionally, it was reported that the optimum slip concentration should be utilized to prevent the development of surface flaws like cracks. The average pore size distribution and pore diameters were observed to be unaffected by casting time and pull-out speed, while the thickness of the membrane was found to be affected.

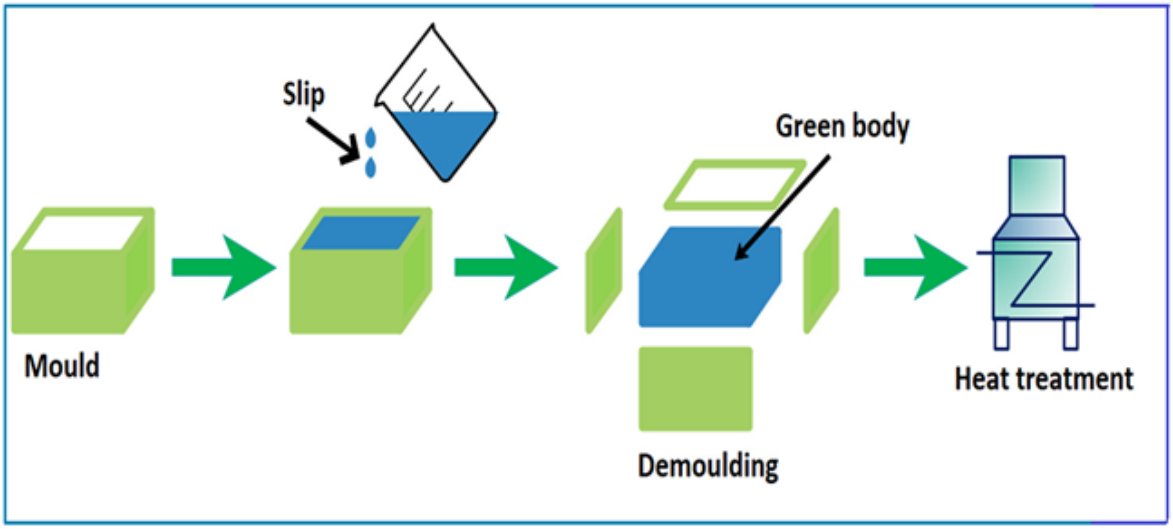


Figure 10:Schematic illustrations of the slip casting technique for fabricating ceramic membranes (Goswami *et al.*, 2022).

2.2.4.6 Synthesis of coal fly ash ceramic membranes by Tape casting method

Thin, flat dense ceramic membranes made of ceramic slurry are fabricated using tape casting technique. The steps in the tape casting method are as follows: A slurry made of inorganic powder and additives

such as binders, dispersants, and plasticizers are continually dispensed onto a moving substrate while a doctor blade could be adjusting the thickness (Figure 11). Then, the cast film is dried and sintered to form the resultant ceramic membrane. The benefit of tape casting is that ceramic sheets can be configured into any desired shapes, including circular, square, and rectangular shapes and also allows adjustment of the thickness of the ceramic membrane (Nishihora *et al.*, 2018). However, the main problem with tape casting is the loss of shape accuracy caused by the deterioration of the plaster mould. Tape casting also takes a very long time when a slurry of small granules is cast (Hubadillah *et al.*, 2018). Several factors, including the viscosity of the slip, the distance between the knife blade and the moving carrier, the depth of the reservoir, and the speed of the carrier, can affect the tape casting process used to fabricate the ceramic membranes (Mistler & Twiname, 2000).

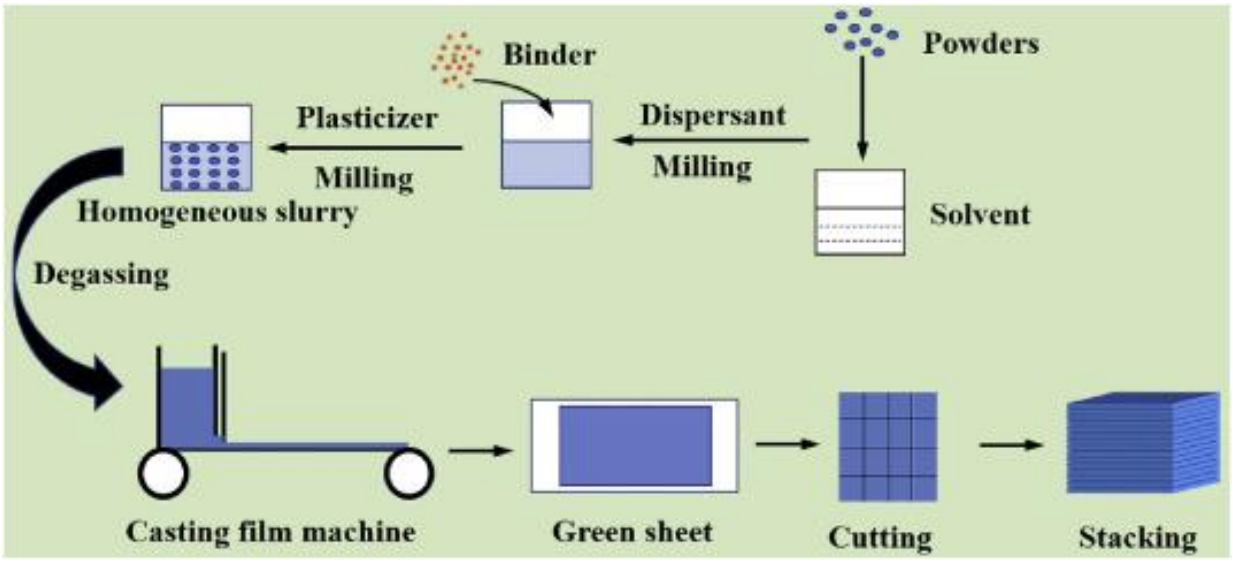


Figure 11:Schematic illustrations of the tape casting technique for fabricating ceramic membranes (Cheng *et al.*, 2018).

Table 4: Techniques used in the manufacturing of coal fly ash-based ceramics and the properties of the resulting membranes

Ceramic membrane	Fabrication method	Additives	Characteristic of the synthesized material	Ref.
Hydrophobic Coal-Fly-Ash-Based Ceramic Membrane	Extrusion	sodium hexametaphosphate of the suspension served as a dispersant and the PVA acted as a binder	Increased pore size from 0.15 μm to 1.57 μm, the water flux rose	(Zhang Z et al., 2023)
Highly porous whisker-structured	Uniaxial pressing	MoO_3 as a single sintering additive	Open porosity showed a significant increase from $41.65 \pm 0.13\%$ to	(Fu *et al.*, 2019)

mullite ceramic membranes		Organic binder polyvinyl alcohol	58.14 ± 0.15% as the MoO3 content increased from 0 to 20 wt.%, accompanied by a decrease in shrinkage and pore size in the absence of any pore-forming agent	
Coal fly ash based multipurpose ultrafiltration membrane	Uniaxial pressing	-	The membrane porosity-39.8% hydraulic pore radius - 41 nm. The membrane pure water flux increased from 2.09 to 11.31 m^3/m^2 sec as the applied pressure increased from 69 to 483 kPa.	(Chathurappan & Jayapal, 2022)
Low-cost microfiltration membranes from fly ash	Paste-casting	Sodium carbonate and boric acid act as dispersant Sodium metasilicate acts as binder Calcium carbonate act as pore forming agent	The membranes, which were defect-free, possessed an average pore size ranging from 1.2 to 2.3 μm and displayed excellent chemical stability in both acidic and basic solutions. Furthermore, they had a porosity level of 35-40%.	(Singh & Bulasara, 2015).
Porous mullite ceramic supports from high alumina fly ash	Dry pressing method	Spherical graphite as pore-forming agent. Polyvinyl alcohol (PVA) as a binder	Whose apparent porosity 55.7%, Flexural strength 8.5 MPa and	(Cui et al., 2023)
Kaolin-fly ash-based membranes	Paste-casting method	H_3BO_3 and na_2co_3 were used to provide homogeneity Calcium carbonate defines the pore morphology Sodium metasilicate ($na_2sio_3.9h_2o$) acts as a binder.	Porosity (~34.36–39.0%), pore size (~0.65–1.81 μm) flexural strength (~10–30 mpa)	(Agarwal *et al.*, 2020)
SiC-Coal fly ash ceramic membranes	dry pressing method	Polyvinyl alcohol Graphite- pore former	Porosity 54.46 % exhibited good, mechanical properties	(Das & Kayal, 2023)
Coal fly ash ceramic membrane	extrusion method	Dolomite used as a pore-forming Carboxymethyl cellulose (cmc) used as a binder	Large particles reduced mechanical strength of fly ash based membranes while increasing porosity.	(HuangChenYang *et al.*, 2023)

		Glycerin used as a plasticizer,		
Lumina based tubular asymmetric membranes incorporated with coal fly ash	Centrifugalcasting technique	-	Increased porosity and enhanced water permeability coincide with reduced mechanical strength and diminished linear shrinkage	(de la Rocha *et al.*, 2021)
High-aluminum coal fly ash ceramic membrane supports	Uniaxial cold-pressing	PVA solution as organic binder $CaCO_3$ pore forming agent	Mechanical strengths 34 - 90 MPa	(Wei et al., 2016)
Coal fly ash-based tubular ceramic membrane	Extrusion	Dextrin as pore-forming agent CMC, as organic binder Glycerin, to improve the plasticity	Porosity 38.9−45.9% Mechanical strength 14.8−36.0 MPa	(Liang *et al.*, 2021)
Fly ash cenosphere ceramic membrane	uniaxial pressing	organic binder PVA- $CaCO_3$- pore forming agent	Porosity 59.25% Mechanical strength 70 ± 2.58 MPa	(Jiang et al., 2018)
Tubular supported ceramic microfiltration membranes from fly ash	Slip- casting	Dispersant lomar-d Binder dsx 3290	Average pore diameter 0.77 μm. Pure water permeability- 1.56×10^4 l m^{-2} h^{-1} bar^{-1}, respectively, Transmembrane- 0.1 MPa at room temperature.	(Fang et al., 2011)
Mullite-whisker-structured porous ceramic membrane	Uniaxial pressing	Binder- PVA-1750 AlF_3 as crystallization catalyst MoO_3 as mineralizer	A porosity of 45.4 ± 0.9% was obtained.	(Zhu *et al.*, 2015)
Fly ash ceramic membrane	Slip casting method	Polyvinyl alcohol	Pore size- 1.47 (μm Porosity- 39(%) Mechanical strength 1.98 (MPa)	(Suresh, 2021)
Tubular coal fly ash based	Extrusion method	Dextrin as pore-forming agent	Porosity- 44.76–47.30 %	(Huang et al., 2022)

ceramic membranes.		CMC, as organic binder Glycerin, to improve the plasticity	Mechanical strength 15.16–29.11 (MPa)	

As shown in Table 7, each technique has distinct benefits and drawbacks. The process chosen for fabrication affects the structure and characteristics of produced membranes. A study by (Lorente-Ayza *et al.*, 2015) compared the microstructure and properties of ceramic membranes of the same composition obtained by pressing and extrusion. It was observed that the extruded supports displayed lower porosity and smaller pore size than the pressed supports. The higher the clay content in the starting composition, the clearer this tendency became.

Table 5: Advantages and disadvantages of ceramic membrane synthesis methods

	Ceramic membrane synthesis method	Examples of Synthesized ceramic membranes	Advantage of the synthesis method	Disadvantage of the synthesis method.	Ref.
1	Slip casting	Tubular ultrafiltration ceramic membrane based on titania nanoparticles immobilized on macroporous clay-alumina support. Microfiltration and ultrafiltration ceramic membranes prepared with Tunisian silty marls.	Simple method Cost effective method. Produce high stable membrane	Long casting time. Controlling the wall thickness is difficult. Produced walls are usually thick. weak ceramic membrane strength	(Oun *et al.*, 2017) (Khemakhem *et al.*, 2004).
2	Pressing	Flat ceramic membrane supports prepared from Moroccan Rif clay. Ceramic membranes derived from inexpensive raw material fuller's earth clay. Zirconia and alumina based UF and MF	Inexpensive technique. Applied for large production volumes. simplest method for the fabrication of ceramic membranes,	Difficulty to fine-tune the microstructures and control the membrane thickness to diameter ratio. Mainly used for laboratory scale Results into defects and cracks formation	(Tahiri *et al.*, 2021) (Rani *et al.*, 2022) (Del Colle *et al.*, 2011)

		porous ceramic membrane.			
3	Tap casting	Si_3N_4 ceramic planar membrane. Chitosan based ceramic ultrafiltration membrane.	Enables adjusting the thickness of the product. The process of tap casting can be automated at cheap price. low production cost and high production efficiency.	Membrane prone to cracking. Production of irregular shaped membranes.	(Tao *et al.*, 2018) (Jana *et al.*, 2011)
4	Extrusion	Tubular ceramic microfiltration membrane prepared from inexpensive clay mixtures namely. Mullite and mullite–alumina ceramic membranes.	high production efficiency wide application range higher mechanical strength good product uniformity	Size variances and configuration limitations Costly Time consuming	(Kumar *et al.*, 2015) (Abbasi & Mowla, 2014)
5	Freeze casting	Reticulated skeleton ceramic (RSC) membrane. Alumina ultra-filtration ceramic membrane.	Simple and inexpensive process. Less shrinkage on manufactured material.	Have low mechanical properties. Conditions for nucleation is difficult to modulate and control.	(Zhou *et al.*, 2021) (Liu *et al.*, 2018)

2.2.5 Coal fly ash based ceramic membrane cost analysis

Ceramic membrane fabrication by commercial starting materials such as silicon carbide, stainless steel, aluminium, zirconium oxide and silicon nitride are very expensive. Their cost price ranges from \$500–3000/m^2 with the price of polymeric membranes ranging from \$20–200/m^2 (Vasanth *et al.*, 2011). The preparation of ceramic membranes from these materials also requires high sintering temperatures (1300–1700 °C) which also makes the production process costly (Sarkar *et al.*, 2012). Ceramic

membranes offer lower operating costs than polymeric membranes due to their longer lifespan, simplicity of cleaning by high-temperature steam sterilization, and capacity to restore initial permeability and water flux by reverse flushing and proper cleaning (Samaei *et al.*, 2018). One of the main factors that have made the use of coal fly ash in the production of ceramic membranes popular is their low production cost as shown in Table 8. The inexpensive production costs of coal fly ash based ceramic membranes is one of the paramount reasons why it is so common to use it in the fabrication of ceramic membranes. Therefore, the use of coal fly ash as a ceramic membrane starting material is considered a viable solution. Coal fly ash cost price ranges from \$25 to \$250/m^2. The six ceramic membranes shown in Table 8 have significantly variable production cost prices because various expenses during the fabrication of the coal fly ash-based ceramic membrane were taken into account. The most complete production cost pricing should include the cost of starting materials, processing costs, maintenance expenses, labour costs, and electricity expenses (Dong Yingchao *et al.*, 2022). The estimated production cost of a coal fly ash-based ceramic membrane fabricated by Suresh et al (Suresh *et al.*, 2016) was USD225 /m^2. In their cost analysis studies, they factored in various parameters associated with the cost of coal fly ash, cost of additives, manpower, electricity and equipment. In another similar study, Goswami et al (Goswami & Pugazhenthi, 2022b) fabricated a coal fly ash ceramic membrane and the cost price of a unit membrane was estimated by considering several expenses as shown in Figure 12. The estimated unit cost price established was USD 250/m^2. Lower sintering temperatures and coal fly ash pricing are the two main factors that dramatically lower production costs (Chen *et al.*, 2019).

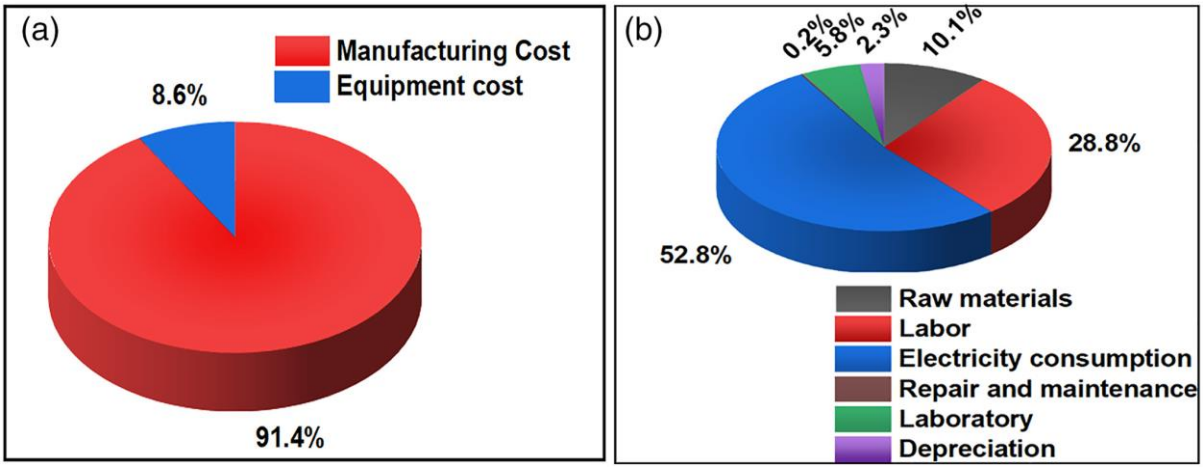


Figure 12:(a) Fabrication cost of coal fly ash based ceramic membrane as percentages of manufacturing cost and equipment cost and (b) factored in manufacturing expenses (Goswami & Pugazhenthi, 2022b).

Table 6: Cost of different coal fly ash based ceramic membranes

Coal fly based ceramic membrane	**Production cost price (USD/m^2)**	**Reference**
Novel fly ash blended ceramic membrane in MFC	35.76	(Rao *et al.*, 2023)
Coal fly ash ceramic membrane	25	(Samaei et al., 2018)
Defective analcime/geopolymer composite membrane derived from fly ash	31.8	(Shao *et al.*, 2020)
Fly ash-based low-cost tubular ceramic membrane	250	(Goswami & Pugazhenthi, 2022b)
Low-cost microfiltration membranes from fly ash	17	(Singh & Bulasara, 2015)
Fly ash based ceramic microfiltration membranes for oil-water emulsion treatment	225	(Suresh et al., 2016)

2.2.6 Application of coal fly ash in ceramic membrane for wastewater treatment

The increasing demand for environmental protection and the reuse of waste materials, implies that the utilization of CFA in different aspects of membrane development is being continually sought. The presence of heavy metals such as chromium, vanadium and antimony in CFA is a factor that has limited its application due to the possibility of long-term leaching. This has necessitated the pre-treatment of the CFA prior to its use in ceramic membranes. Nugteren *et al.* (2002) reported a forced leaching process using water, citrate, EDTA, oxalate and carbonate solutions. The use of cation exchange membrane assisted electro kinetic method for the removal of heavy metals from CFA has been reported by Peng *et al.* (2011). After the removal of heavy metals, CFA can serve the following five major purposes in the development of membranes for wastewater treatment:

2.2.6.1 Membrane precursor

The large amount of CFA being generated as waste in coal-fired electrical power stations, means it can be a readily available raw material for several industrial processes. Due to its high composition of SiO_2 and Al_2O_3, CFA can serve as an economical precursor for the synthesis of ceramic membranes for wastewater purification.

CFA has been significantly explored as raw material for the synthesis of mullite-based ceramics. Mullite is a solid solution with several unique properties, such as, low thermal conductivity, high chemical resistance and temperature stability, low thermal expansion coefficient and high flexural strength (Guo

et al., 2016). CFA pickling could be an important pre-treatment process in enhancing the flexural strength of mullite ceramics Li Chaoxin *et al.* (2019). Also, the sintering temperature and the addition of AlF_3 as a whisker promoter could influence the final property of the obtained ceramic. AlF_3 was observed to influence properties such as phase composition, porosity, bulk density, and aspect ratio of the obtained whiskers. Mullite obtained from CFA was employed together with multiwalled carbon nanotubes (MWCNT) to form a hierarchically structured membrane, the membrane achieved complete retention of *E. coli* and *S. Aureus* (Zhu *et al.*, 2019). Interestingly, no pore blockage was reported for the material and fouling only occurred due to the bacterial cell deposition of the surface.

Tobermorite, a crystalline calcium silicate hydrate, is another ceramic material that has been obtained using CFA as a raw material(Luo *et al.*, 2017). The excellent mechanical properties and durability of tobermorite, makes it a potential material in various structural application. The high reaction activity of tobermorite has been reported to allow for a lower sintering temperature compared to traditional ceramics Luo et al. (2017),. Aluminum substitution and morphology were also observed to be two factors that influenced the mechanical property of the membrane. Tobermorite from waste materials such as newsprint recycling residue and, paper recycling ash have been reported as efficient adsorbent and cation exchanger in a few studies (Hurt *et al.*, 2022).

In another study, the synthesis of Al_2O_3-NaA zeolite hollow fibre membranes from CFA with high efficiency for Pb(II) ions removal in low concentration has been reported Zhu *et al.* (2018) reported. The membrane displayed a pore diameter of 0.41 nm, permeation flux of 670 ± 20.6 L/h/m^2 and Pb(II) ion removal reached 99.9% at 0.1 MPa. The high membrane area per volume and thin thickness of the Al_2O_3 support was important in enhancing the permeation flux of the composite membrane.

2.2.6.2 Sintering additive

The presence of additives often influences shrinkage, dimensional changes, grain growth and homogenization during sintering of ceramics. With the aid of appropriate additives, the sintering temperature of ceramics can be reduced through the formation of eutectic composition (Janani *et al.*, 2014; Li *et al.*, 2023). The sintering additive should enhance densification without decomposing the base materials, while also introducing a weak interface. Das *et al.* (2021) reported the use of CFA as sintering additive in the synthesis of a mullite bonded porous SiC ceramic membrane. The obtained membrane exhibited high water flux of 5261 L/m/h bar, mean pore size of 3. 7 µm open porosity of 44.4%. The membrane was able to achieve 91% removal of oil from a kitchen wastewater with initial oil concentration of 1657 mg/L. The presence of CFA as a sintering additive, allowed for the processing of the membrane at a lower temperature, without comprising its mechanical and permeability characteristics.

2.2.6.3 Membrane filler

To improve the hydrophilicity and stability of polymeric membranes, inorganic fillers have become very important in forming mixed matrix membranes. These membranes possess numerous advantages arising from the synergy between the organic and inorganic phases (Saranya *et al.*, 2017). Several studies have explored the incorporation of ceramic metal oxides such as cerium oxide (CeO_2), zirconium dioxide (ZrO_2) and aluminium oxide (Al_2O_3) as nano-fillers for ceramic membranes in wastewater treatment because of their potential to enhance the selectivity, surface area, hydrophilicity and stability of polymeric membranes (Lavanya *et al.*, 2021). Because of the large amounts of fly ash being produced by power stations and the similarity between the chemical composition of fly ash and traditional raw materials, the use of fly ash in membrane fillers as high economic and environmental value(Jha *et al.*, 2008). The mechanical properties of ceramics obtained using fly ash fillers, generally depends on the quantity of the reinforcing materials, component of ceramic, porosity, shape, interfacial interaction between filler and composite matrix and the presence of other reinforcements(Manocha *et al.*, 2012). As observed by Manocha et al. (2012), the porosity of a carbon-fly ash-ceramic composite was observed to increase with higher fly ash composition. This improved porosity, however, implies that the membrane suffers from reduced coefficient of friction. This limitation could be mitigated by adding silicon carbide into the mixture, which led to an improvement in the coefficient of friction of the membrane.

The use of CFA-modified ceramics has been explored in various wastewater treatment processes because of their unique advantages. Recently, Rao et al. (2023), reported the application of a novel fly ash blended/potter clay ceramic membrane in microbial fuel cell (MFC) technology for COD removal from wastewater. The hydration property of the membrane showed CFA concentration dependency, resulting from the variation in the concentration of SiO_2 and Al_2O_3 in the composite as the quantity of CFA is varied. This is significant for the ceramic membrane's proton conduction efficiency and their optimal composition is highly important for improved membrane performance. The introduction of CFA as fillers for the membrane reportedly improved the thermal stability, optimized the pore size distribution and heterogeneity, enhanced water uptake, improved proton conductivity, and decreased oxygen mass transport coefficient. This improved property of the CFA-modified membranes was important in the wastewater treatment efficiency of the ceramic membrane. CFA-filled ceramic membranes were also reported as micro-electrolysis ceramic media for the pre-treatment of tetracycline wastewater. Two novel ceramics: sintering ferric-carbon (SFC) and sintering-free ferric-carbon ceramics (SFFC) based on coal ash, and scrap iron were used in tetracycline wastewater pre-treatment to improve biodegradability, removal efficiency and inhibit antibiotic-resistant bacteria growth(Yang *et al.*, 2017).

2.2.6.4 Membrane filters

Microfiltration membranes comprising of CFA active layer is another well explored application of CFA in wastewater treatment. Most fly ash membranes developed till date have been focused on the treatment of oily wastewater. However, the numerous advantages of the materials mean it is being explored also in the removal of other organic and inorganic pollutants from water. Recently, CFA-based membranes have been utilized in the treatment of effluents from textile and tin industries, domestic households, and poultry slaughterhouses. Table 9, shows the application of CFA-based membranes in the treatment of different industry generated effluents. CFA-based membranes have also been found to be effective for the removal of bacteria, phenol, and humic acid from wastewater.

Table 7: Application of CFA-based membranes in the treatment of different effluent

Description	Fabrication technique	Composition	Membrane characteristic	Wastewater type	Efficiency	Reference
Tubular microfiltration membrane	Extrusion	75% CFA, 20% quartz; 5% calcium carbonate	Pore size: 0.133 µm Porosity: 40.17%; Water permeability17.75 x10^5($Lm^{-2}h^{-1}bar^{-1}$)	Poultry slaughterhouse wastewater	COD removal: 100%; TSS: 100%	(Goswami & Pugazhenthi, 2020)
Tubular membrane	Extrusion	75% CFA, 20% quartz; 5% calcium carbonate	Pore size:0.133 µm; Water permeability:4.93x10^{14} $Lm^{-2}h^{-1}bar^{-1}$ Tortuosity:1.68	Starch-rich wastewater	COD: 100% TOC:100% Turbidity:100%	(Goswami & Pugazhenthi, 2022a)
Fly ash/alumina composite membrane	Thermal spraying	Mullite whiskers/fly ash/polyviny	Pore size: 0.1 um	Oily emulsion and stannic acid rejection	TOC: 99% Tin rejection: 99.9	(Zou *et al.*, 2019)

		l alcohol /glycerol	Permeability: 445 $Lm^{-2}h$-1bar^{-1}			
TiO_2-fly ash membrane	Hydraulic press and hydrothermal synthesis	Fly ash:80%; Quartz:10%: Calcium carbonate:10 %	Porosity:35% Pore size: 1.32 um; Permeability: 6.135 $Lm^{-2}h^{-1}bar^{-1}$	Oil-in-water emulsion	Oil rejection: 98.7%	(Suresh *et al.*, 2017)
Kaolin/fly ash composite membrane	Sintering	AFA/kaolin/ fly ash	Pore diameter: 0.32 um; Permeability: 3650 $Lm^{-2}h^{-1}bar^{-1}$	Distillery wastewater	Oil rejection: 98.05%	(Zou *et al.*, 2021)

The synthesis of microfiltration membranes with CFA as both microporous support and active layer has been reported Jedidi et al. (2011). The active layer obtained by slip-casting and sintering yielded a pore size of 0.25 µm and possess a water permeability of 475 L/h m^2 bar. The membrane showed high efficiency in the treatment of dyeing effluents from the textile industry. The stabilised permeate flux was 100 L/h/m^2, the COD and color removal were 75 and 90% respectively, with the permeate turbidity reduced to 0.5 NTU from the initial 45.5 NTU.

Modification of CFA membranes with nanostructured materials is a potential route to obtaining highly efficient filters for wastewater treatment. The incorporation of nanoparticles could influence the properties of CFA-membranes such as hydrophilicity, permeation flux, and their adsorption property (Zhang J *et al.*, 2021a). Zhang J et al. (2021a) synthesized Fe_3O_4@CFAS with high efficiency for Cu(II) ion removal. The incorporation of Fe_3O_4 resulted in an enhancement of the hydrophilicity of the membrane, with no significant alteration in the permeation flux of the composite membrane observed. The improved hydrophilicity played a significant role in enhancing the adsorption property of the composite as it promotes contact and chelation of active sites with Cu(II) ion.

The use of CFA as membrane support have also reported in literatures. The synthesis of a porous mullite-whisker-structured ceramic membrane supported with CFA and bauxite as starting materials has been reported Zhu et al. (2015) reported , while AlF_3 and MoO_3 acted as crystallization catalyst and mineralizer, respectively. The introduction of MoO_3 was observed to lead to a reduction of the high temperature viscosity of liquid melts which promoted the growth of elongated mullite crystallites. The open porosity of the membrane was observed to be enhanced by the introduction of AlF_3. At the optimal

weight composition of MoO_3 and AlF3 (5 and 4 wt% respectively), the open porosity of the membrane was 47.3 ± 0.6%. The study further affirmed that despite the enhancement of the membrane's porosity, the mechanical strength was not compromised even though the membrane was prepared at a relatively low temperature of 1200 ^oC. The membrane achieved a total organic carbon removal of over 90% at 0.2 MPa for oil-in-water emulsion.

Recently, the synthesis of TiO_2 nanofiber membrane loaded on porous fly ash ceramic support was reported by Zhang J *et al.* (2021b). The novel composite membrane obtained from fly ash, graphite and industrial rutile was fabricated using a semi-dry press and hydrothermal process. The composite membrane showed excellent activity for the simultaneous removal of heavy metal ions and rhodamine B. The capacity of the membrane for dual functionality as both adsorbent and photocatalyst makes it a potential cost effective material for wastewater treatment.

The solute rejection efficiency at a constant flux of a choline chloride blended cellulose acetate membrane, used in CFA support, demonstrated dependence on pH. When the pH was basic, both the membrane and solute had negative charges, resulting in an increased ability to retain phenol. On the other hand, when the support membrane was coated with formaldehyde-cross-linked polyvinyl alcohol, the correlation of the rejection pattern changed considerably, leading to high rejection rates at acidic pH levels (Gupta & Anandkumar, 2019; Gupta *et al.*, 2020)

2.2.7 Factors affecting the physical properties and performance of coal fly ash based ceramic membranes

The mean pore size, porosity, flexural strength, and permeability of coal fly ash based ceramic membrane can be affected significantly by several factors such as sintering temperature, dosage of the pore-forming agent, particle size of coal fly ash, and dosage of binding additives, as indicated by several studies. In contrast, numerous experiments have shown that when operating conditions change, ceramic membranes made of coal fly ash does not crack. However, the precise trend of variation of these factors with properties and performance could not be established, as a result of the involvement of other factors that influence both the performance and properties of coal fly ash based ceramic membrane (Goswami et al., 2022). Therefore, major factors that need optimization in the fabrication of coal fly ash ceramic membrane are highlighted in this section.

2.2.7.1 Effect of sintering temperature on the properties of coal fly ash ceramic membranes

The properties of coal fly ash ceramic membranes are affected by the sintering temperature. Singh and Bulasara (2015) examined how the sintering temperature affects the properties of a ceramic membrane made from coal fly ash. The membranes were sintered at 800, 850, 900, and 1,000 ℃. The physical characteristics of the coal fly ash ceramic membrane, including color, tensile strength, crystal phase, pore size, and porosity, were observed to be impacted by changes in the sintering temperature. The results showed that the average pore size only increased for the membrane sintered at 1,000 ℃ whereas it decreased for sintering temperatures up to 900 ℃ (Fig. 13a). Except for those sintered at 1,000 ℃, as shown in Fig. 13b, the sintered membranes all had similar colors. Fig. 13c shows that when sintering temperature increased, mechanical strength also increased. Continuous phase transitions occur during the sintering process, as shown by a comparison of the XRD patterns of various samples (Fig. 13d). The membrane sintered at 1,000 °C lost anorthite, which was a significant component in the other four samples. Throughout the sintering process, other phases underwent changes and their contents changed as well. The membranes' porosity dropped from 38.1 to 34.8% when the sintering temperature rose from 800 to 900 ºC. However, the porosity of the membranes increased significantly to 39.7% when sintered at 1,000 °C Fig. 13e. As the sintering temperature rises, the material's thermal properties cause the membrane structure to alter significantly in terms of porosity and mechanical strength. Up to a certain point, high sintering temperatures improve structural integrity, but they may also cause thermal stress-induced cracking in the long run. Further increase in sintering temperature may cause porosity to decrease as particles fuse, resulting in a denser structure and less permeability.

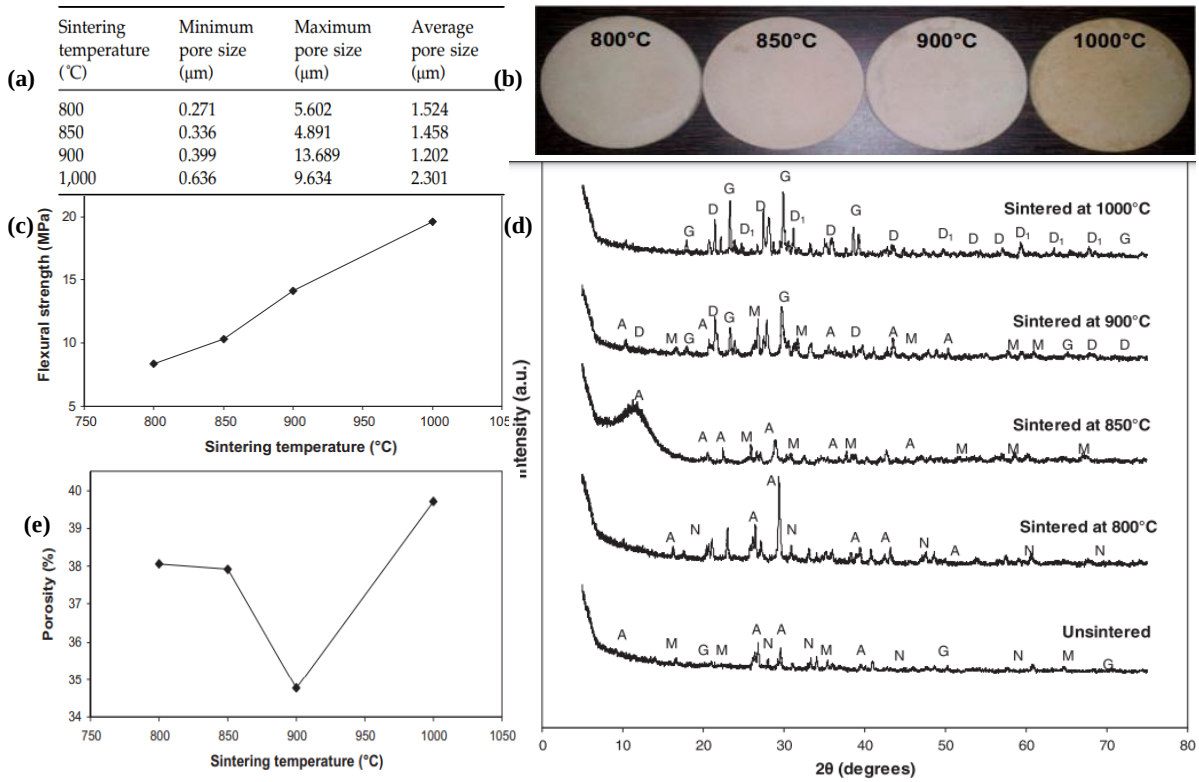


Figure 13:(a)Variation of average pore size with sintering temperature, (b) picture of membranes sintered at four different temperatures, (c) variation of flexural strength with sintering temperature (d) XRD spectra at different sintering temperatures, XRD spectra of membranes sintered at different temperatures. A: Anorthite; D: Dickite; D_1: Dmisteinbergite; G: Gehlenite; M: Mullite; and N: Nacrite and (e) variation of porosity with sintering temperature (Singh & Bulasara, 2015).

2.2.7.2 Effect of pore forming agent dosage on the properties of coal fly ash ceramic membrane

Pore-forming agents are essential in improving the permeability of ceramic membranes by changing the morphology and porosity of the pores. These pore-forming agents can be either inorganic or organic compounds that decompose at high temperatures. Cui et al. (2023) studied the effect of pore-forming agent dosage on the characteristics of coal fly ash ceramic membrane. Spherical graphite was used as a pore-forming agent in their investigation, and the dosage was altered as wt%. The results demonstrated that as the dosage increased, many pores developed and were linked together to generate holes. As a result, water absorption and permeability flow improved. Liang et al. (2021) also investigated the effect of pore forming agent dosage on the properties of coal fly ash ceramic membrane. They used dextrin as the pore-forming agent, with compositions of 0, 3, 6 and 9 wt% (D_{50} = 7 μm, $C_{6n}H_{10n}O_{5n}xH_2O$, and ρ= 1.8 g/cm^3). The experimental results indicated that the pore-forming agent content and mechanical strength of the samples are essentially inversely correlated (Fig. 14a). Additionally, the results demonstrated that when the dextrin concentration increases, more pores appear in the ceramic

membranes made of tubular coal fly ash, resulting in a more porous structure, as seen in the SEM micrograph in Fig. 14b. The average pore size showed a trend of initially increasing and then decreasing with increasing pore-forming agent content, reaching its maximum value when the quantity is 6 wt%. The decrease of average pore size when the pore-forming agent level reaches 9 wt% was attributed to the strong binding action of dextrin. All the aforementioned studies revealed that altering the dosage of the pore-forming agent does not affect the development of cracks in the ceramic membrane made of coal fly ash. Suresh et al (Suresh et al., 2016) also investigated the effect of pore-forming agents on mechanical strength and porosity of the fabricated membrane. In their study, coal fly ash was used as the main precursor and a mixture of corn oil, waste cooking oil and starch solution as the pore forming agent. The results showed that porosity increased with increasing dosage of the pore-forming agent which corresponded to a decrease in mechanical strength.

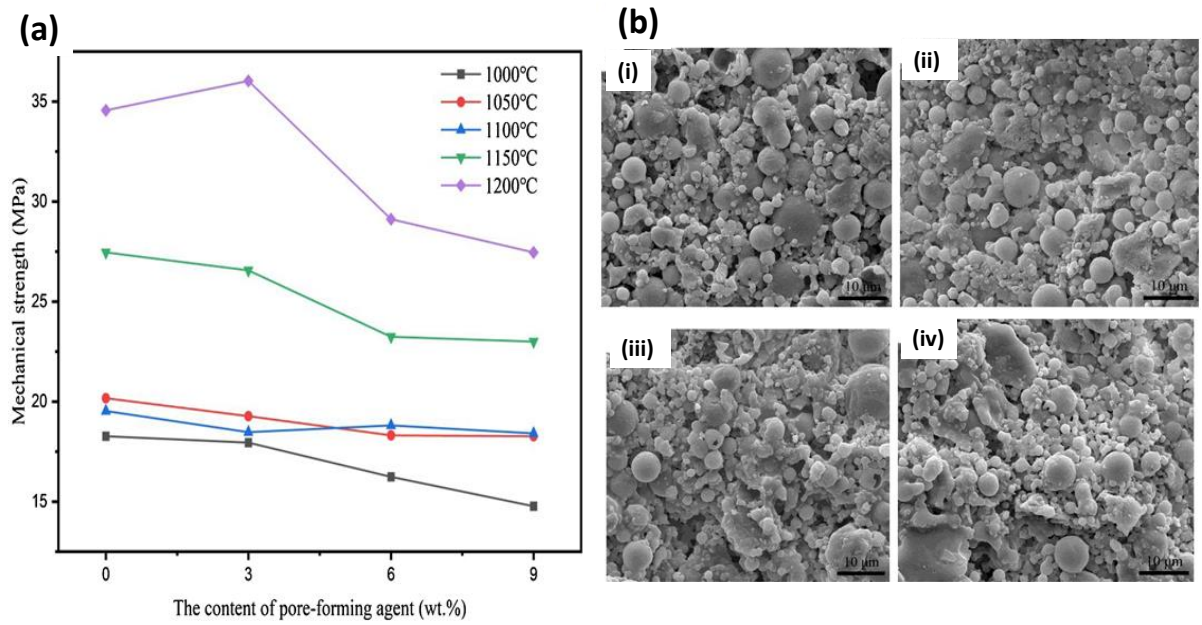


Figure 14:(a) Relationship between the mechanical strength of the membrane and the content of the pore-forming agent as well as the temperature of sintering. (b) SEM images of Coal fly ash ceramic membrane with Wt% of dextrin (i) 0, (ii) 3, (iii) 6, and (iv) 9 sintered at 1150 °C (Liang et al., 2021).

2.2.7.3 Effect of particle size of coal fly ash on the properties of coal fly ash ceramic membrane

Particle size optimization of starting materials is key in the manufacturing of ceramic membrane as it helps maintain material consistency. Particle size has a significant influence on the mechanical and physical properties of ceramic membrane such as pore size, post-sintering shrinkage, bending strength, microstructural morphology, and porosity (Qian *et al.*, 2022; Xu *et al.*, 2022). The effect of coal fly ash particle size on the porosity, pore size, microstructure and mechanical strength of synthesized coal fly

ash based ceramic membrane has been investigated (HuangChenYang et al., 2023). The experimental results showed that, a membrane with a denser structure and less porosity is produced when coal fly ash has a wider particle size distribution. As particle size increases, the membrane's pores get bigger while mechanical strength gets weaker. Large particles in the fly ash play a significant role in the mechanical strength of the ceramic membrane because they produce cracks in the membrane.

2.2.7.4 Effect of binder dosage on the properties of coal fly ash ceramic membrane

Binders are used to hold ceramic particles together. Goswami et al (Goswami & Pugazhenthi, 2021) investigated how the amount of binder affected the characteristics of a ceramic membrane made from coal fly ash by extrusion technique. Fly ash was used as the basic material (75%), together with the necessary amounts of quartz (20%), calcium carbonate (5%), and sodium salts of carboxymethyl cellulose acting as binders, to create tubular ceramic membranes. The results revelled that, a higher binder concentration causes agglomeration in the membrane matrix, which results in the creation of big, irregular holes. With a rise in binder concentration, the membranes' mechanical strength considerably decreased. In addition, the results showed that an increase in binder concentration had a detrimental effect on the membrane's chemical stability.

2.2.8 Factors that affect separation efficiency of coal fly ash-based ceramic membranes

The surface characteristics of the ceramic membrane (surface wettability and surface charge), the solution properties (pH, temperature, viscosity), and the operation parameters (pressure difference, flow rate, and time) are key variables that determine the separation effectiveness of ceramic membranes (Katibi *et al.*, 2023). Surface charge of coal fly ash based ceramic membranes have an impact on how pollutants interact with the membrane surface, which has an influence on the ceramic membrane's permeability and rejection capabilities (Arumugham *et al.*, 2021; Radeva *et al.*, 2021). Higher membrane flux and improved antifouling properties occur when membrane surface charge is similar to contaminants charge due to the repulsive effect of similar charge (Du *et al.*, 2020). Contrarily, opposing charges cause electrostatic interactions between contaminants and membranes, which have a major negative impact on the effectiveness of separation and on membrane anti-fouling properties (Ahmad *et al.*, 2022). The pH of the filtration feed has a significant impact on the surface charge of the membranes.

The separation effectiveness of coal fly ash based ceramic membrane is also impacted by the presence of inorganic ions in the contaminants matrices. This results from these ions' ability to alter the surface charge of membrane surfaces and contaminants (Tufail *et al.*, 2020). (Alventosa-deLara *et al.*, 2014) studied the effects of the feed salt concentration on the removal of organic dyes by ultrafiltration

ceramic membranes. The results showed increased overall resistance and decreased dye rejection by the ceramic membrane in the presence of NaCl. This occurred as a result of the Na^+ ion neutralization of the membrane surface charge and allowing more dye particles to pass through.

Hydrophobicity and hydrophilicity of coal fly ash based ceramic membrane surfaces affect separation effectiveness of the membrane (Zou et al., 2021). This is due to the correlation between contact angle values and ceramic membrane morphology and pore size (Melo *et al.*, 2021). Surface wettability has an impact on how membranes are utilised, with hydrophilic membranes frequently employed in water filtration and hydrophobic membranes excellent for membrane distillation (Chang *et al.*, 2020). For instance, Zhang et al (Zhang Z et al., 2023) fabricated hydrophobic coal fly ash based ceramic membrane for desalination. The membrane showed excellent water flux and higher salt rejection compared to aluminium based ceramic membranes. Surface geometrical structure or surface free energy can be modified to alter the wettability of membrane surfaces (Usman *et al.*, 2021; Zhang Z et al., 2023). Zhang et al (Fu *et al.*, 2022) studied the effect of changing wettability of the surface of a coal fly ash based ceramic membrane. In their study the ceramic membrane was modified from hydrophilic to hydrophobic through immersion of 1H,1H,2H,2H-perfluorodecyltriethoxysilane (FC8) on the surface of the membrane. The results demonstrated that the final super hydrophobic membrane outperformed hydrophilic ones in terms of self-cleaning. The physical and chemical characteristics of the materials being separated, such as viscosity, charge, stability, and solubility, can be influenced by temperature and pH (Simonič, 2019). This could impact on the diffusion rate across the membrane pores. The fouling behaviour of the contaminants was also influenced by temperature (Alresheedi & Basu, 2020).

2.2.9 Management of fouling on coal fly ash based ceramic membranes

There have been numerous investigations on the physical and chemical deposition or adsorption of microbiological, organic, and inorganic compounds onto membrane pores or onto the membrane surface. This causes the membrane pores to contract or clog thereby reducing permeability and raising the flow resistance, which has an impact on the quantity and quality of treated effluent (Warsinger *et al.*, 2015). This dramatically lowers the lifespan and separation effectiveness of these membranes (Cai *et al.*, 2023; Luo & Deng, 2018).

Reversible fouling, which often forms on the membrane surface, and irreversible fouling, which refers to internal fouling in the membrane pores, are the two subgroups of membrane fouling (Basile *et al.*, 2015). Ceramic membrane fouling is primarily a function of the properties and performance of ceramic membranes, operational conditions as well as the characteristics and nature of the filtering feed. These membrane properties include roughness, wettability, surface charge, and membrane pore size (Bai *et al.*, 2021). Foulant type (inorganic salts, metal oxides, natural organic matter, manufactured organic

matter, and microbiological contaminants), concentration, pH, charge, and ionic strength are some of the properties of the feed. Fouling of ceramic membranes is influenced by a number of operating factors, including flow rate, temperature, and pressure. Coal fly ash is less likely to get irreversible fouling than organic membranes because it is predominantly composed of metallic oxides, which have strong hydrophilicity and chemical stability (Bai et al., 2021; HuangChenQi *et al.*, 2023)**.** However, reversible fouling of coal fly ash or other ceramic based membranes are major obstacles to their use in wastewater treatment.

Fouling raises operational costs because it necessitates higher pressures to maintain permeate flux, uses more energy, requires more time to clean, and costs more to replace the membrane (Gruskevica & Mezule, 2021; Nthunya *et al.*, 2022). Therefore, specific steps must be taken to either prevent fouling or clean the fouled membrane in order to restore and maintain membrane flux, extend the cleaning cycle, and prolong the lifespan of ceramic membranes (Sakamoto *et al.,* 2022). Pre-treating influents with sacrificial membranes or another type of treatment method before ceramic membrane filtration, optimizing operational parameters, controlling the feed solution's properties, and using a pre-coat layer on the membrane are all actions that reduce fouling (Baker, 2002; Basile et al., 2015). Combining different processes, such as advanced oxidation with ceramic membrane technology can also lessen fouling through changing properties of ceramic membranes and enhancing separation efficiency. Ceramic membrane surfaces that have been dip-coated with nanoparticles are an example of how the surfaces are modified (Li C et al., 2020). Bao Y *et al.* (2019) studied how to get rid of fouling by coating the ceramic membrane with cobalt oxide. The cobalt oxide was ensured not to leak into the pores of the ceramic membrane by the development of the Co-O-Al bond on its surface. The results of the study showed that ceramic membrane functionalized with cobalt oxide have antifouling properties. The pollutant's intrinsic catalytic decomposition by the metal oxide may be the cause of the antifouling qualities since it keeps the pollutant from passing untreated through the ceramic barrier.

Ceramic membrane fouling can be eliminated through cleaning procedures such as chemical, physical, electrical, and vibration. All these methods do not guarantee the complete regeneration of ceramic membranes. Chemical cleaning uses chemicals such as acids, surfactants, oxidizing agents, chelating agents, and alkali to clean ceramic membrane pores and surfaces (Ahmed *et al.*, 2023; Cai et al., 2023)**.** This approach can be used to independently or in conjunction with physical cleaning techniques. Although chemical cleaning is a common cleaning approach, it has a number of negative aspects, including harm to the environment, membrane degradation, cost due to the high cost of cleaning chemicals, and the tendency to alter the nature of the foulants (Basile et al., 2015; Johns, 2000). Back washing and mechanical scraping of contaminants on the membrane surface and pores are examples of physical cleaning methods. The most common of these techniques is back washing. It entails washing

the membrane against the direction of the typical flux of membrane penetrates. However, according to Zielińska (2018)**,** this method can harm the ceramic membrane structure. The ideal strategy for cleaning ceramic membranes is combining cleaning techniques that work in conjunction. This is due to the fact that different ceramic membranes foulants, such as inorganic salts, metal oxides, naturally occurring organic matter, synthetically produced organic matter, and microbiological contaminants have distinct properties (Zuo *et al.*, 2020).

2.3. Metal oxide functionalized ceramic membranes

Surface modification, a novel and evolving technique, can be used to change the hydrophilicity, surface roughness, and pore size of ceramic membranes. This improves the membranes' capacity to resist fouling while also enhancing their filtering efficiency, robustness, anti-abrasion, and self-cleaning properties (Asif & Zhang, 2021). Numerous surface modification methods, such as integrating materials or chemicals with the ceramic support layer could be used to reconfigure and modify the surface of the membrane (Ewis *et al.*, 2021). Global attention is being drawn to the use of metal oxide functionalized membranes in energy-efficient wastewater treatment and water purification.

The mechanism combines photocatalysis by semiconductors and the membrane separation process in a single component (Leong *et al.*, 2014). Semiconductors, specifically metal oxide nanoparticles such as ZnO, ZrO_2, TiO_2, WO_3, and Fe_2O_3, are frequently used in the photocatalysis process (Park *et al.*, 2022). Since the valence band of the semiconductors is rich in electrons, the electrons are excited to the vacant conduction band in the presence whose energy is equal to or greater than the bandgap energy of the semiconductors. This excitation results in the formation of positively charged holes in the valence band. Hence, electron-hole pairs are formed. The holes (positively charged) attack the water molecules to generate highly oxidizing hydroxyl radicals. Both the holes and hydroxyl ions in the system attack the tetracyclines and convert them into non-toxic or less toxic products. At the conduction band, the photogenerated electrons attack the molecular oxygen that dissolves in the water and give superoxide anion radicals. These superoxide radicals also cause the degradation of tetracyclines and other organic pollutants (Ajiboye et al., 2021a; Fauzi *et al.*, 2022). The whole photocatalytic process is summarized in Figure 15 and Equations (1-8)

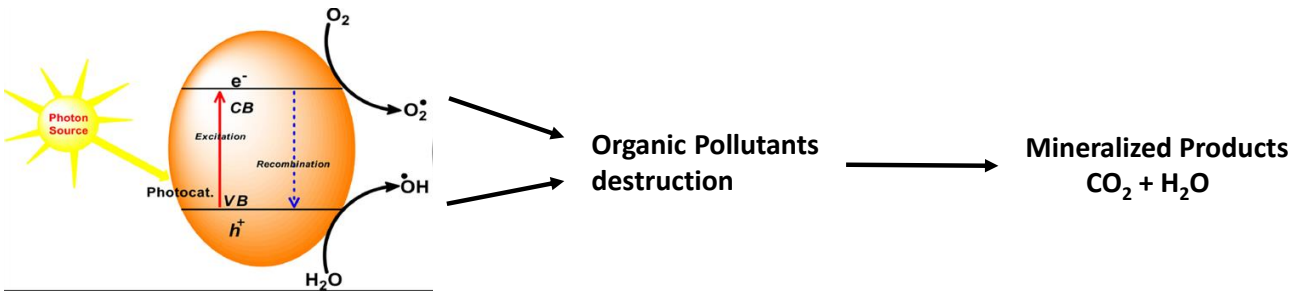


Figure 15:Mechanism of photocatalysis (Ajiboye *et al.*, 2021b).

Photocatalytic ceramic membrane (CCC) + Tetracycline (TC) → CCC (TC adsorption) (1)

$CCC + hv \rightarrow CCC\ (e^{-} + h^{+})$ (2)

$O_2 + e^{-} \rightarrow O_2^{\bullet -}$ (3)

$2O_2^{\bullet -} + 2H_2O \rightarrow H_2O_2 + 2OH^{-} + O_2$ (4)

$H_2O_2 + e^{-} \rightarrow {}^{\bullet}OH + OH^{-}$ (5)

$O_2^{\bullet -} + TC \rightarrow CO_2 + H_2O + NH_3$ (6)

$h^{+} + TC \rightarrow CO_2 + H_2O + NH_3$ (7)

$^{\bullet}OH + TC \rightarrow CO_2 + H_2O + NH_3$ (8)

The rate of photocatalysis is dependent on the effectiveness of the adsorption process. This is because the organic pollutants to be degraded first adsorb to the surface of the photocatalyst before the photocatalytic degradation takes place. The adsorption process involves the movement and accumulation of substances at the junction of two phases (liquid/liquid, solid/gas, or liquid/solid). The properties of the adsorbent/photocatalyst and that of the pollutants being adsorbed (adsorbate) in water significantly influence the process of pollutants removal (Ajiboye *et al.*, 2021c). In particular, the presence of a ceramic membrane in the nanocomposite increases the rate at which the composite adsorbs the tetracycline. This is because ceramic membranes have sharply distributed nanosized pores, which make it easy for water to penetrate at low pressure. Apart from this, the relatively long service life, good mechanical strength, good corrosion resistance, high thermal resistance, and inert character of the ceramic membrane contribute to their usage as adsorbent under extreme environmental conditions (Pagana *et al.*, 2008). The functionalization of ceramic membranes by these nanomaterials has the potential to improve water treatment processes by enhancing the membrane's hydrophilicity, stability, and porosity. In addition, the incorporation of metal oxide nanoparticles into a membrane has the potential to improve membrane performance by boosting the photoactivity functionality as well as reducing foulants under oxidizing conditions (Ewis et al., 2021). While metal oxide nanomaterials

destroy pollutants and have antibacterial characteristics, membranes play a role in the physical separation of contaminants (Shi Y et al., 2019).

The catalytic components are either integrated into the membrane matrix or on the membrane surface, and light illumination can be inside the reactor, outside the reactor, or vertical to the reactor as shown in Figure 16. When photocatalysts are immobilized on a membrane surface, the photoactive layer must be exposed to radiation while in contact with the feed solution (Gu *et al.*, 2022). The distinctiveness of these oxide materials lies in their biological immunity, the relative simplicity of synthesis, ability to harness energy in the UV/Vis range, environmental friendliness, low cost, ease of handling, resistance to photo-corrosion, and general high surface ratio to mass, among other things (Singh *et al.*, 2022; Velempini *et al.*, 2021).

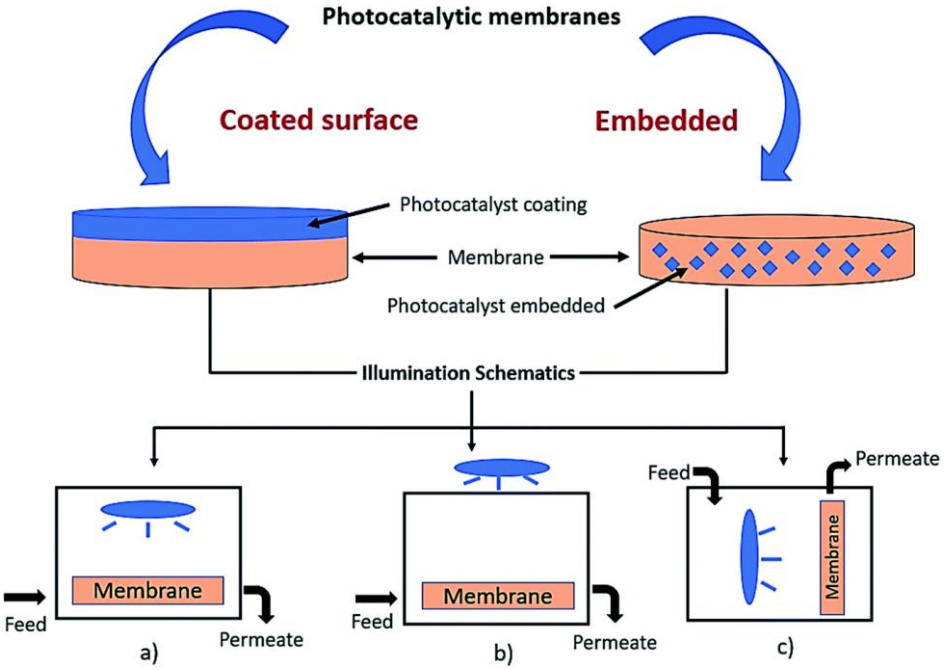


Figure 16: Illustration of the integrated photocatalyst on the surface and embedded membrane. Orientation of light source: (a) inside the reactor, (b) outside the reactor, and (c) vertical inside the reactor (Zakria *et al.*, 2021).

For maximizing photocatalytic activity, metal oxides are typically used in their modified form rather than their naïve structure (Saravanan *et al.*, 2022). The amount of metal oxide nanomaterial must be carefully chosen, as a deficit of nanomaterial won't be enough to noticeably alter the performance of the membrane (Desa *et al.*, 2019). Due to their inherent hydrophilicity, metal oxides attracts water molecules to membrane pores by their surface hydroxyls, which is useful for water and wastewater treatment because it increases water flux (Xu *et al.*, 2019). These metal oxides can be employed independently, as heterojunctions, or as part of composites with other components. It has been demonstrated that some heterojunction structures, such as $TiO_2/Al_2O_3/WO_3$, can store photogenerated electrons for a long time (Djurišić *et al.*, 2014).

2.3.1 Synthesis of metal oxide functionalized ceramic membranes

Ceramic membrane surfaces are typically modified by depositing or grafting specific elements or chemically desired groups onto the membrane surface. Inorganic and organic surface modifications are the two different types of surface modification. Catalytic membranes have been prepared using one of two major methods: either covering the membrane surface with catalysts or integrating the catalysts into the membrane matrix (Gu et al., 2022). Despite the simplicity of the second technique, its membranes' overall catalytic activity is limited since the embedded catalysts are only partially accessible (Qing *et al.*, 2019). As a result, surface coating for catalysts is frequently a preferred method for creating catalytic membranes since it not only allows for direct catalyst exposure to the reactants but also can increase mass transfer and reaction rates through forced convection (Qing *et al.*, 2020).

The functionalization of ceramic membranes with metal oxide nanomaterials is a method of inorganic surface modification. Numerous methods, including dip-coating, phase inversion, sol-gel, electrospinning, hydrothermal reaction inversion, physical deposition, atomic layer deposition, simple spray-deposition, and others, can be used to accomplish this (Deepracha *et al.*, 2021). One of the preparation processes (spin coating) is illustrated in Fig. 17. The most well-known technique for depositing a photocatalyst layer onto the membrane is the dip-coating method. Inorganic and polymer membranes can both be modified using this technique (Molinari *et al.*, 2017). This method creates microporous top layers using polymeric sols and mesoporous intermediate layers with colloidal sols. Metal salts or metal organic precursors are used to create the sols. By dip coating, the layers are applied to the membrane structure. The supports' or the prior multilayer structure's porosity is what causes the sols to gel. The final membrane layers are created by further drying and thermally treating these gel layers. The crystallographic and morphological structure of the dried material is stabilized by a final heating process known as "calcination" or "sintering" (Buekenhoudt & technology, 2008).

Using titanium dioxide (TiO_2) nanocomposites that were made using a sol-gel process, Mohamed and Co-workers (Mohamad Esham *et al.*, 2021) successfully functionalize the bentonite membrane. The performance of the pure water flux of the functionalized bentonite membranes increased from that of pristine bentonite membranes. In another study, the dip-coating method was used to synthesize TiO_2 functionalized ceramic hollow fiber membrane. The prepared photocatalytic ceramic membrane exhibited a strong penetration flux and excellent porosity of around 80% as compared to the non-functionalized membrane (Zhang *et al.*, 2016). Wu and co-workers (Wu *et al.*, 2019) functionalized a ceramic membrane with manganese oxide using a one-step ball-milling procedure. The results showed that MnO_2 nanocatalysts were equally dispersed around the Al_2O_3 particles, which consequently supplied a significant number of active sites for the activation of peroxymonosulphate to produce

sulphate radicals. A study by Marzouk and co-workers (Marzouk *et al.*, 2021) evaluated the effects of inhomogeneity of metal oxide functionalized ceramic membrane. TiO_2/SiO_2 functionalized ceramic membrane's water flux and photocatalytic degradation of organic contaminants were unaffected by the coatings' inhomogeneity.

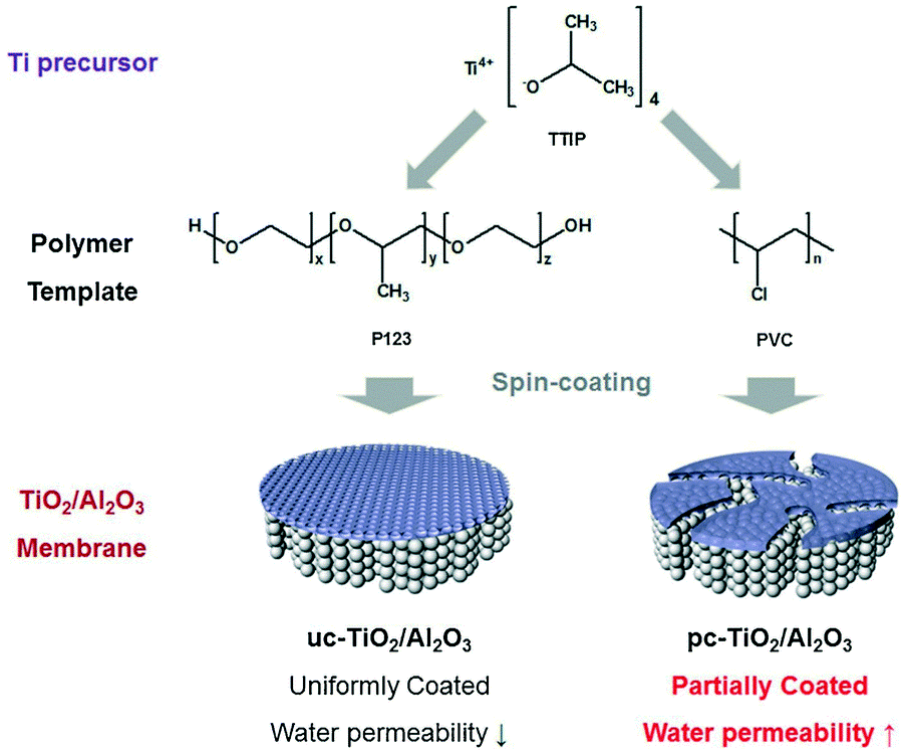


Figure 17: Scheme of the preparation of TiO_2 functionalized Al_2O_3 porous ceramic membrane (Ashley *et al.*, 2022)

2.3.2 Application of metal oxide functionalized ceramic membranes in the degradation of pharmaceuticals in wastewater

The use of metal oxide functionalized membranes demonstrates a synergistic impact of the coupled catalytic membrane-AOPs, which increases pollutants' breakdown and provides efficient fouling management and disinfection (Asif & Zhang, 2021). Pollutants are concurrently broken down by photocatalysis, and the by-products of that degradation are separated and filtered out by photocatalytic membranes. The key to the breakdown of organics is the generation of reactive oxygen species with high oxidizing power, such as $^{\bullet}O^{-}_{2}$ and $^{\bullet}OH$, by photocatalysts under visible light (Zhang ML *et al.*, 2021). Table 10 shows metal oxide functionalized ceramic membranes that have been investigated for their possible use in the breakdown of pharmaceuticals. The rate at which pharmaceutical contaminants degrade using a metal oxide factionalized membrane varies according to several operational factors and the efficiency of the metal oxide and membrane that are being employed. In most reported studies, the first 60 min of the investigation demonstrated 99% pharmaceutical degradation. Most of the research

showed that several reaction factors, including pH and temperature, have a significant impact on the degradation rate, according to the presented data. For instance, the metal oxide functionalized membranes reported in different studies (Anucha *et al.*, 2022; Li M *et al.*, 2022) have demonstrated good efficiency in the removal of pharmaceuticals in a neutral environment. This parameter is crucial because it affects how catalysts aggregate and how charged their surfaces are, which in turn regulates how effectively pollutants are removed (Sakarkar *et al.*, 2020). Optimization of pH improves flow rate which subsequently reduces membrane fouling. The rate of the photocatalytic reaction is affected by the presence of ions (Borthakur *et al.*, 2018). According to a study by Luster *et al*. (Luster *et al.*, 2017), the addition of Ca^{2+} had a detrimental effect on the degradation of Carbamazepine (CBZ) photocatalysts, which was only observed when phosphate buffer was utilized. This effect was most likely brought by the deposition of $CaHPO_4$ or $CaHPO_4{\bullet}2H_2O$ on the catalyst surface. Inorganic ions present in water scavenge holes in the valence band and hydroxyl radicals (•OH), which consequently reduces the photocatalytic activity.

2.3.3 Photodegradation mechanism and products

The complete mineralization of pharmaceuticals is one of the main obstacles to photocatalytic breakdown. Under ideal conditions, a high and rapid degradation of the target pollutants can be achieved, while the mineralization rate can be lower than the removal rate, which results in the presence of degradation intermediates and/or products whose toxicity may be higher than that of the parent compound (Mestre & Carvalho, 2019). It is crucial to comprehend the various degradation products from the system, the routes by which they are produced, and the toxicity of the products relative to the target pollutant to build a safe and efficient photodegradation system.

The ultimate goal of any photodegradation process is to degrade pollutants without producing any hazardous by-products. It is thought that the mineralization of contaminants throughout the degradation process will improve the waste water's ability to biodegrade after photodegradation treatment (Olatunde *et al.*, 2020). In monitoring photodegradation investigations, hyphenated techniques are the most effective analytical method (Nagajyothi *et al.*, 2017). UPLC-Q-TOF/MS analysis, HPLC MS Q-TOF, Q-TOF LC/MS, HPLC-MS, and LC-MS are a few of these methods. An ultra-high-performance chromatography, a diode array detector, and a high-resolution mass spectrometer are the three major tools that are utilized to identify the key transformation products of the photodegradation pathway (Trawinski & Skibinski, 2017).

Li and co-workers (Li QL *et al.*, 2019) investigated and proposed mechanisms for the mineralization and degradation of amoxicillin (AMX) using TiO_2 functionalized porous ceramic membranes. Degradation intermediates were studied using Q-TOF LC/MS. It was reported that the UV

photocatalytic degradation of the AMX process used hydroxyl radicals as the active species. Five degradation intermediates were produced by the two AMX degradation pathways suggested in Figure 7. The hydroxylation process produces the intermediates B1 and B2. The release of NH_4^+ species in conjunction with oxidation processes resulted in the formation of further intermediaries. Another method of degradation involved the creation of intermediate A, which was broken down at the secondary amine and carbonyl groups after hydroxyl radicals attacked the primary amino group. Wang and co-workers (Wang *et al.*, 2020) also studied the degradation pattern of ibuprofen by $CoFe_2O_4$ functionalized α-Al_2O_3 ceramic membranes. By using LC-MS, the permeation solutions were examined. The m/z values attributed to the various compounds are shown in Figure 8 and they were discussed in relation to the ESI-MS spectra that were produced. Sulphate radicles were the most prevalent radical during the catalytic degradation process. According to the suggested mechanism, organic intermediates, carbon dioxide, and water were produced.

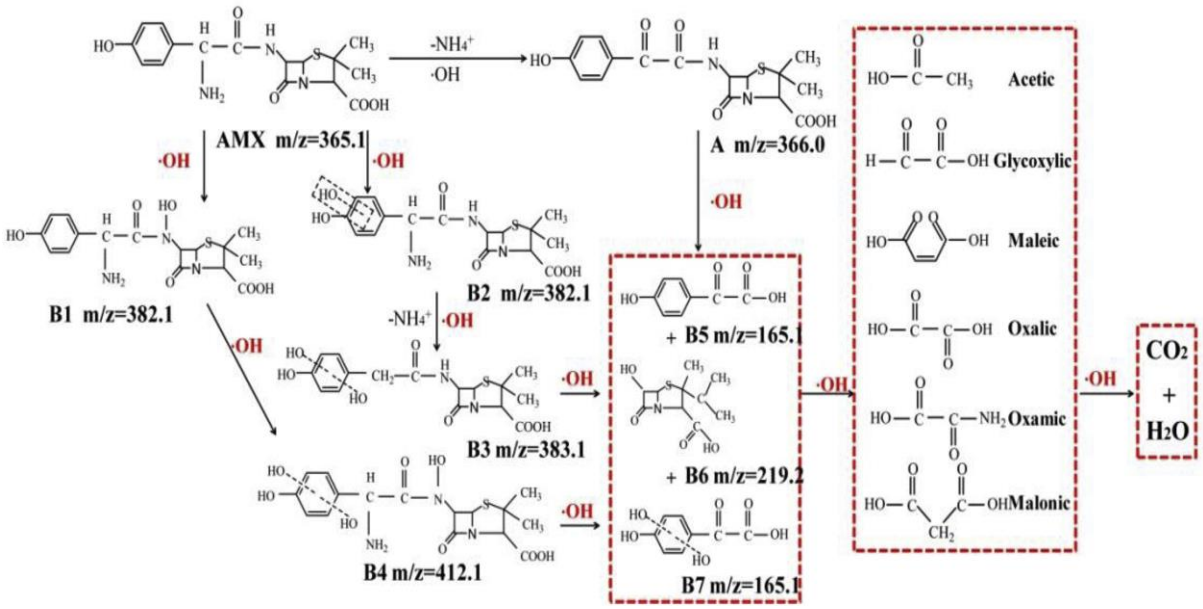


Figure 18: Photodegradation mechanism and products for amoxicillin using TiO_2 nanoparticles coupled with a novel submerged porous ceramic membrane reactor (Li QL et al., 2019).

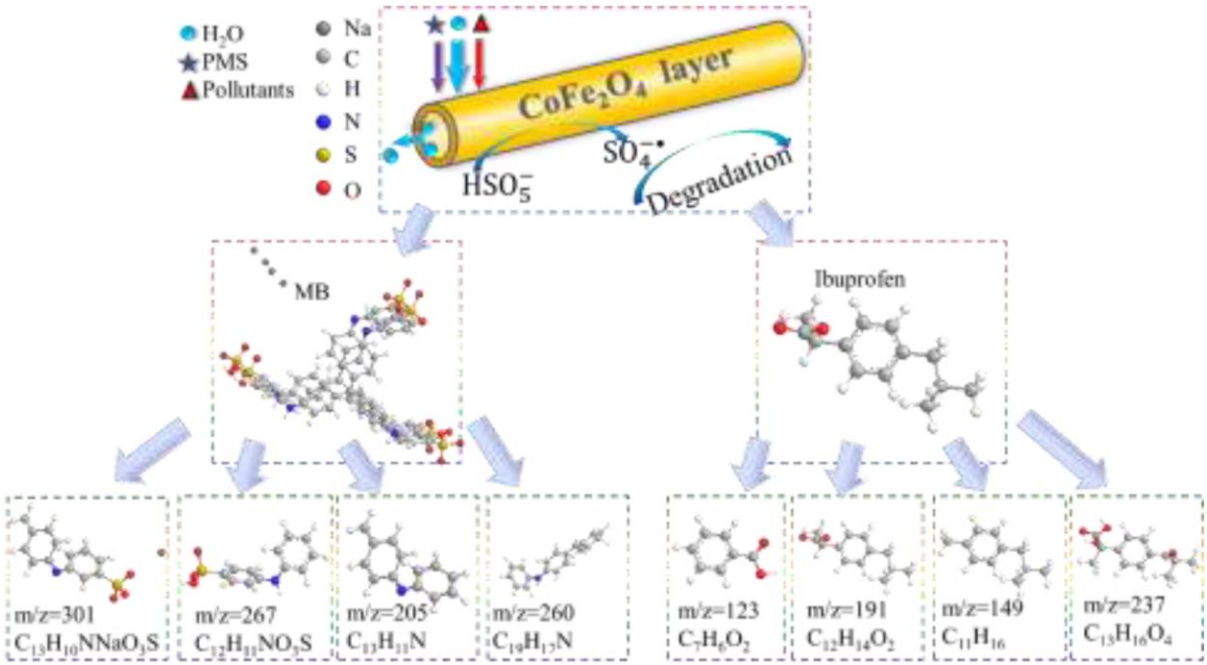


Figure 19: Photodegradation mechanism and products for ibuprofen via α-Al_2O_3/$CoFe_2O_4$ catalytic membrane (Wang et al., 2020)

Table 8: Photocatalytic degradation of pharmaceuticals by metal oxide functionalized membranes

Metal oxide functionalized ceramic membrane	**Fabrication method**	**Pharmaceutical pollutants and their concentration**	**Optimization of metal oxide functionalized membrane/reaction conditions**	**Performance of metal oxide functionalized membrane**	**Ref.**
Graphene oxide-titanium dioxide (GO-TiO_2) photocatalytic ceramic membranes	hydrothermal method	naproxen (NAP) diclofenac (DCF) carbamazepine (CBZ)	-	100% 100% 90%	(Li C *et al.*, 2022)
Molybdenum Doped TiO_2 on α-Al_2O_3 Ceramic membrane	Sonochemical method	Ibuprofen (IBU)- 50 mg/L	1 g/L Mo/HRTiO_2 photocatalyst, 365 nm UV light irradiation and under natural pH conditions	98%	(Anucha et al., 2022)
Tubular ceramic membrane coated with TiO_2-P25	dip-coating	Amoxicillin (AMX) 2.0 mg/L	UVC/H_2O_2/TiO_2 system with radial addition of H_2O_2 (20 mg/L) and with a UV fluence of 45 mJ cm^{-2}	72.2 ± 0.5%	(Diorio *et al.*, 2022)
N-doped TiO_2-coated Al_2O_3 photocatalytic membrane	sol-gel method	carbamazepine (CBZ)- 1 mg/L	highest degradation rate of CBZ was observed at a neutral pH	efficiently degraded	(Luster et al., 2017)

Pore-functionalized ceramic membrane with isotropically impregnated cobalt oxide (CoCM)	in-situ self-sacrificed template	Sulfamethoxazole (SMX)-0.08mM		59%	(Bao YP *et al.*, 2019)
Mn-Fe binary oxides (Mn/FeOx)-modified ceramic membrane	wet impregnation	Trimethoprim-5.0 mg/L	0.5 mg/L, membrane flux was controlled to be 10 L/m^2, temperature was about 25 ± 0.5 °C and the initial pH was about 7.1 ± 0.1	98.6%	(Liu et al., 2022)
$CoFe_2O_4$-decorated flat-sheet Al_2O_3 ceramic membrane	hydrothermal method	Ofloxacin (OFX)-40 μM	OFX was completely decomposed under optimal conditions (pH 6.0, [PMS] = 2 mM and TMP = 100 kPa)	100%	(Fan *et al.*, 2020)
ceramic membranes functionalized with titanium dioxide (TiO_2) graphene oxide (GO)	simple vacuum filtration	Ibuprofen (IBU)-100 ppb	Membrane operating condition was at a pH range of 6–7	73%	(Li C. *et al.*, 2019)
		Diclofenac (DCF)-100 ppb		78%	
		Carbamazepine (CBZ)- 100 ppb		20%	
		Naproxen (NAP)-100 ppb		73%	
TiO_2 nanoparticle coupling with a novel submerged porous ceramic membrane		Amoxicillin (AMX)- 10 mg/L	high removal capacity and stability for amoxicillin (AMX) degradation over a wide pH range, i.e., 6.5 to 9.0.	83.3%	(Li QL et al., 2019)
Tubular porous alumina (α-Al_2O_3) membrane, as support material, with embedded iron oxide		Diclofenac (DCF)-1000 μg/L	pH 3 and 42.9 mg/L H_2O_2 feed volumetric rate 0.5 L/min, TMP 0.5 bar	65%	(Plakas *et al.*, 2019)
CuO/TiO_2 ceramic ultrafiltration membrane	dip coating	Ciprofloxacin 500 μgL^{-1}	2.0 bar TMP and 2 $Lmin^{-1}$ of CFV	99%	(Bhattacharya *et al.*, 2019)
α-Al_2O_3/$CoFe_2O_4$ catalytic ceramic membrane	Dip coating	Ibuprofen (IBU)-2.0 mg/ L	T = 22 °C, water column height = 30.0 cm, membrane length = 8.0 ± 0.1 cm, without adjustment of pH	99.5%	(Wang et al., 2020)
Nano-MgO/diatomite ceramic membrane	Facile method	Tetracycline (TC) 10 mg/L	flow rate= 120.5 L m^{-2} h^{-1}	99.7%	(Meng *et al.*, 2016)

N-doped TiO_2 coated photocatalytic membrane	a sol-gel technique	Carbamazepine (CBZ)- 1 mg/L			(Horovitz *et al.*, 2016)

2.3.4 Strategies for improving the efficiency of metal oxides in functionalized ceramic membranes

The maximum light absorption and charge transfer at the surface can theoretically increase photocatalytic activity. Recombination can be decreased by achieving effective charge separation and maximizing surface redox processes aiding in increased photocatalytic activity (Homocianu & Pascariu, 2022). Heterojunction fabrications, sensitization with various sensitizers, defect engineering, doping with various elements, etc. are a few alternative methods for improving photocatalytic activity (Djurišić et al., 2014). Semiconductor-based modified composite materials with high photocatalyst performance efficiency were produced by utilizing one of these modification strategies, or even more than one in a combination a of mixed-methods approach, for environmental remediation and other related energy sustainable applications (Anucha et al., 2022).

2.3.4.1 Doping

Doping is the injection of extra energy levels into the band structure of a semiconductor. Non-metals and metals (as shown in Figure 20), rare earth metals, and many other forms of dopants are among the various types that are frequently utilized (Nasirian *et al.*, 2018; Raj *et al.*, 2018; Tang *et al.*, 2022). Doping alters the band gap energy, electrical structure, and crystal structure of the semiconductor. As a result, optical properties are improved for maximum light absorption, surface properties are improved, and the rate at which photogenerated carriers recombine is drastically decreased and subsequently improves the photocatalytic performance. Doping can impair photocatalytic performance by aggregating photocatalysts, altering their structural characteristics, and enlarging the bandgap energy via Moss-Burstein transfer. Optimizing the amount of the dopant is, therefore, crucial (Huang *et al.*, 2016; Yang *et al.*, 2022). Horovitz and co-workers (Horovitz et al., 2016) studied the degradation of carbamazepine using doped and undoped TiO_2 functionalized Al_2O_3 microfiltration membranes. The investigation results revealed rate constants of 0.0085 ±0.0004 min^{-1} and 0.0040 ±0.0007 min^{-1} for doped and undoped membranes respectively. The results also showed that the N-doped TiO_2-coated membranes generated a much higher (by > 100%) degradation rate than the undoped TiO_2-coated. The enhanced photocatalytic activity of the doped photocatalytic membrane was a result of the introduced narrow isolated N band that formed above the TiO_2 valence band which served as an important level for excited electrons thereby promoting visible light absorption. Elhalil *et al.*, (Elhalil *et al.*, 2018), examined the photocatalytic degradation of caffeine using a Mg-doped ZnO-Al_2O_3 heterostructure.

Results showed that 1% Mg-ZnO-Al_2O_3 catalyst had a greater photocatalytic degradation of caffeine than pure ZnO, ZnO-Al_2O_3, and Degussa P-25 TiO_2 catalysts. It was anticipated that 1% Mg-ZnO-Al_2O_3 would have outstanding photocatalytic activity because two metal oxides create novel interfacial active sites that boost catalytic activity. Particle size, adsorption process, and crystallinity also improved the catalytic activity.

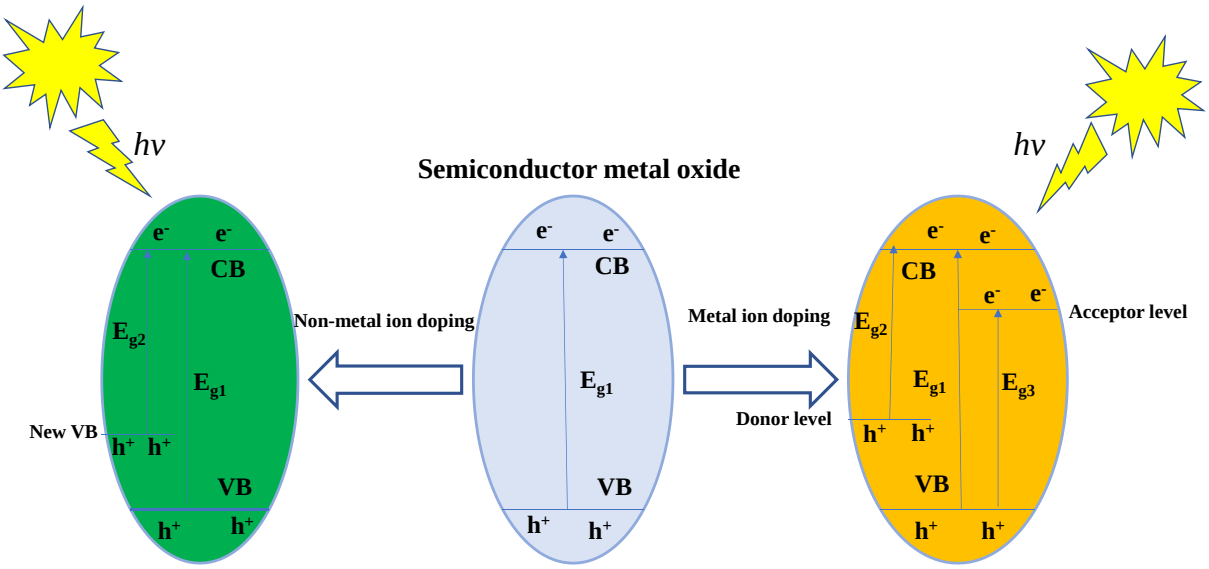


Figure 20: The mechanism of non-metal and metal ion doping on metal oxide semiconductor.

2.3.4.1 Heterojunction fabrications

Coupling of two different semiconductors results in the formation of heterojunctions. Differentiation of heterojunctions is centred on type 1, type 2, and type 3 photocatalysts as shown in Figure 21. The fermi energy level of the coupled semiconductor should be different so that electrons can move from a region of high fermi energy level to a lower fermi energy level. The importance of heterojunction is to enhance photocatalytic efficiency through achieving partial separation of electron-hole pairs and broadening the absorption wavelength. Charge carriers by hetero junction type 1 and type 3 are not favourable due to the gathering of electrons and holes within single semiconductors and the inability of semiconductor bands to overlap respectively. Type 2 or the Z-scheme exhibit efficient electron-hole separation because of the staggered band structure of semiconductor 1 and 2, which results in electron and hole sinks (Arora *et al.*, 2022; Yang, 2021). Li et al. (Li *et al.*, 2021), investigated the effectiveness of heterogeneous catalytic oxidation of pollutants in wastewater treatment using bi-metallic oxide-modified flat-sheet ceramic membranes. In this study, Mg, Ce, and Mn oxides were coated onto a flat-sheet ceramic membrane by co-precipitation. Membrane catalytic ozonation resulted in the effective removal of organic pollutants as well as effective membrane fouling control. The efficiency of bi-metallic oxide-modified flat-sheet ceramic membranes could be attributed to one of the metal oxides acting as an active site and reacting with the other metal oxides to affect the intermediate state of the reactions.

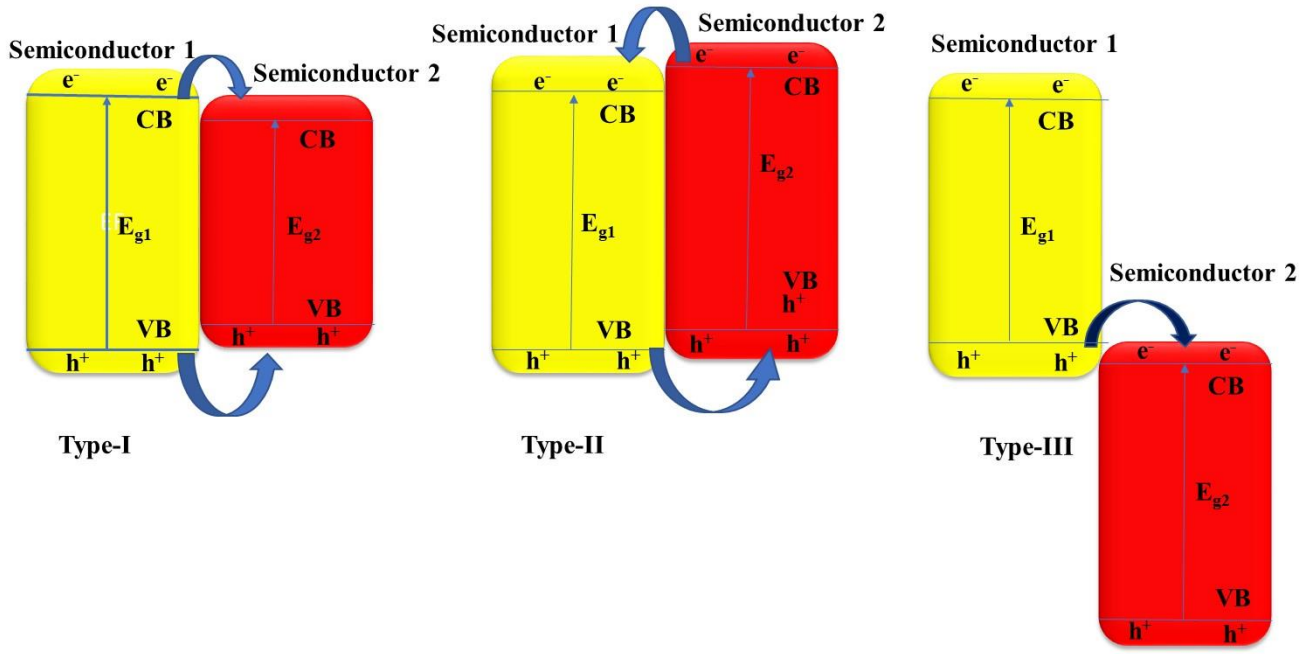


Figure 21: Classification of semiconductor heterostructures, their configurations, and electron migration: type I heterojunction, type II heterojunction, and type III heterojunction.

2.3.4.2 Defect engineering

Defects in photocatalysts (Figure 22) arise due to the inclusion of disorder inside the lattice pattern of the photocatalyst. Of these disorders, oxygen vacancies are the most widely investigated type of photocatalyst defect. These defects can cause distorted bond lengths and bond angles, increase surface area as well as induce donor levels on the structure of the photocatalyst thereby enhancing photocatalysis and suppressing the recombination rate of photo-excited carriers (Shi R *et al.*, 2019; Su *et al.*, 2022). Tetracycline (TC) was photodegraded by black-TiO_2, nitrogen-doped-TiO_2, and white-TiO_2 (Wu *et al.*, 2021). The results showed that, under visible light illumination, black TiO_2 (66.2%) had the best TC removal efficiency, followed by n-doped TiO_2 (59.6%), and white TiO_2 (43.3%). The increased photocatalytic degradation by black TiO_2 was a result of improved optical visible light absorption, decreased photogenerated charge carrier recombination, and the development of mid-gap energy levels between the valence and conduction bands (Andronic *et al.*, 2021). The main defect capable of modifying band structure, optical, electrical, and surface properties is recognized as the controlled insertion of oxygen vacancies (VO) (Wang *et al.*, 2018).

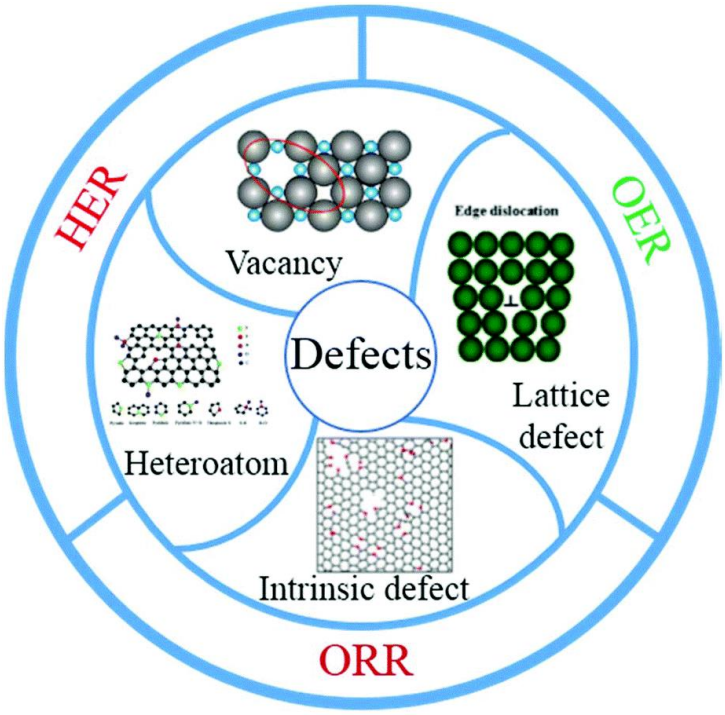


Figure 22: Schematic illustration of the different types of photocatalyst defects (He J *et al.*, 2019).

2.3.5 Factors that affect pharmaceutical removal by metal oxide functionalized membranes

Operating and process parameters determine whether a hybrid method using photocatalysis and membrane technology for contaminants' degradation is successful. These variables include pH, pharmaceutical characteristics, membrane characteristics, loaded catalyst concentration, light source and intensity, and temperature. Therefore, to prevent a decrease in process efficiency, an optimal set of these operational parameters should be employed.

2.3.5.1 Loaded catalyst concentration

The increase of loaded catalyst on the membrane surface increases the surface area for adsorption and photocatalysis and subsequently increases the number of reactive radical species. An increase of the catalyst beyond certain concentration levels results in decreased removal efficiency because of increased agglomeration of surface particles as well as reduced light penetration to the target contaminants (Riaz & Park, 2020). Berger et al. (Berger *et al.*, 2020), reported that the removal of methyl blue by TiO_2 functionalized ceramic membrane increased up to 50% when catalyst coating thickness was increased up to 6 nm. This provides further evidence that the catalyst had penetrated the pore structure and indeed yielded strong absorption of UV light.

2.3.5.2 Membrane properties

Membrane characteristics that affect pollutant degradation include thickness, shape, porosity, roughness and zeta potential. These membrane properties are also critical in determining cleaning efficiency and clogging susceptibility (Marcucci *et al.*, 2003). Membranes with widely distributed large pores show enhanced pollutants removal due to increased access to active sites that allow more pollutants to be adsorbed on the pores since the adsorption of pollutants are not restricted to the membrane surface (Rani *et al.*, 2021). Li and co-workers (Li C et al., 2022) reported the enhancement in the removal of naproxen, diclofenac and carbamazepine when membrane separation was used simultaneously with graphene oxide-titanium dioxide photocatalyst as a single unit. Results showed that membrane filtration increased the mass transfer effect in membrane pores, which in turn increases the efficiency of pharmaceutical contaminants degradation by a factor of four.

2.3.5.3 Pharmaceutical pollutant characteristics

Pharmaceutical pollutants' concentration and charge are critical in their removal efficiency and kinetics by photocatalytic membranes. At low pharmaceutical concentrations, the rate of degradation is increased with increasing the photocatalyst. This is because of sufficient active sites for adsorption and photocatalysis (Mirzaei *et al.*, 2016). Whereas at higher pollutant concentrations, degradation efficiency is reduced because more pollutants are adsorbed on the surface of the membrane thereby reducing the generation of radicles as well as absorbing light. According to Song (Song *et al.*, 2019), the kinetic constant dropped with the rising humic acid constant, whereas the rate of humic acid degradation by TiO_2-functionalized ceramic membrane rose with decreasing humic acid concentration.

2.3.5.4 pH

The effect of pH is well-reported to play an integral role in the processes that leads to the degradation of pollutants. One of its critical effects is its ability to control the surface charge properties of the photocatalytic membrane therefore it must be optimized accordingly. The effect of pH on the removal of contaminants in water by photocatalytic membranes depends on: surface particle agglomeration, the position of the valence band and conduction band on the photocatalyst and many others. At a pH value equal to the point of zero charge (pH_{pzc}) of the catalyst, the surface charge is usually zero, while pH values lower or higher than the pH_{pzc} leave a net positive or negative charge on the catalyst. Neutral contaminants dissociate to charged species so that they can be adsorbed (Kaur *et al.*, 2020; Olatunde et al., 2020). Urase *et al*., (Urase *et al.*, 2005) observed higher degradation of acid pharmaceuticals when

the operation pH was lowered. The increase in degradation was attributed to the increased tendency of adsorption to the sludge particles.

2.4 References

Abbasi, M., & Mowla, D. (2014). Analysis of membrane pore-blocking models applied to the MF of real oily wastewaters treatment using mullite and mullite–alumina ceramic membranes. *Desalination and Water Treatment, 52*(13-15), 2481-2493.

Abdullayev, A., Bekheet, M. F., Hanaor, D. A. H., & Gurlo, A. (2019). Materials and Applications for Low-Cost Ceramic Membranes. *Membranes (Basel), 9*(9), 105. doi:10.3390/membranes9090105

Adewuyi, Y. G. (2021). Recent advances in fly-ash-based geopolymers: Potential on the utilization for sustainable environmental remediation. *ACS omega, 6*(24), 15532-15542.

Adeyemi, J. O., Ajiboye, T., & Onwudiwe, D. C. (2021). Mineralization of Antibiotics in Wastewater Via Photocatalysis. *Water, Air, & Soil Pollution, 232*(5), 219. doi:10.1007/s11270-021-05167-3

Agarwal, A., Samanta, A., Nandi, B. K., & Mandal, A. (2020). Synthesis, characterization and performance studies of kaolin-fly ash-based membranes for microfiltration of oily waste water. *Journal of Petroleum Science and Engineering, 194*, 107475.

Ağtaş, M., Dilaver, M., & Koyuncu, İ. (2021). Ceramic membrane overview and applications in textile industry: A review. *Water Science and Technology, 84*(5), 1059-1078.

Ahmad, N. N. R., Mohammad, A. W., Mahmoudi, E., Ang, W. L., Leo, C. P., & Teow, Y. H. (2022). An Overview of the Modification Strategies in Developing Antifouling Nanofiltration Membranes. *Membranes, 12*(12), 1276.

Ahmed, M. A., Amin, S., & Mohamed, A. A. (2023). Fouling in reverse osmosis membranes: monitoring, characterization, mitigation strategies and future directions. *Heliyon*.

Ahmed, M. B. M., Rajapaksha, A. U., Lim, J. E., Vu, N. T., Kim, I. S., Kang, H. M., . . . Ok, Y. S. (2015). Distribution and accumulative pattern of tetracyclines and sulfonamides in edible vegetables of cucumber, tomato, and lettuce. *Journal of Agricultural and Food Chemistry, 63*(2), 398-405.

Ahmed, M. J., & Hameed, B. H. (2018). Removal of emerging pharmaceutical contaminants by adsorption in a fixed-bed column: A review. *Ecotoxicol Environ Saf, 149*, 257-266. doi:10.1016/j.ecoenv.2017.12.012

Ahmed, S. F., Mehejabin, F., Momtahin, A., Tasannum, N., Faria, N. T., Mofijur, M., . . . Mahlia, T. M. I. (2022). Strategies to improve membrane performance in wastewater treatment. *Chemosphere, 306*, 135527. doi:10.1016/j.chemosphere.2022.135527

Ajiboye, T. O., Oyewo, O. A., & Onwudiwe, D. C. (2021a). Adsorption and photocatalytic removal of Rhodamine B from wastewater using carbon-based materials. *FlatChem, 29*, 100277. doi:https://doi.org/10.1016/j.flatc.2021.100277

Ajiboye, T. O., Oyewo, O. A., & Onwudiwe, D. C. (2021b). The performance of bismuth-based compounds in photocatalytic applications. *Surfaces and Interfaces, 23*, 100927. doi:https://doi.org/10.1016/j.surfin.2021.100927

Ajiboye, T. O., Oyewo, O. A., & Onwudiwe, D. C. (2021c). Simultaneous removal of organics and heavy metals from industrial wastewater: A review. *Chemosphere, 262*, 128379. doi:https://doi.org/10.1016/j.chemosphere.2020.128379

Ajiboye, T. O., Saunyama, L., Ravele, M., Rasheed-Adeleke, A. A., Seheri, N., Onwudiwe, D. C., & Mhlanga, S. D. (2023). Synthesis approaches to ceramic membranes, their composites, and application in the removal of tetracycline from water. *Environmental Advances*, 100371.

Alam, R., Sheob, M., Saeed, B., Khan, S. U., Shirinkar, M., Frontistis, Z., . . . Farooqi, I. H. (2021). Use of Electrocoagulation for Treatment of Pharmaceutical Compounds in Water/Wastewater: A Review Exploring Opportunities and Challenges. *Water, 13*(15), 2105. doi:ARTN 2105 10.3390/w13152105

Alatalo, S.-M., Daneshvar, E., Kinnunen, N., Meščeriakovas, A., Thangaraj, S. K., Jänis, J., . . . Lähde, A. (2019). Mechanistic insight into efficient removal of tetracycline from water by Fe/graphene. *Chemical Engineering Journal, 373*, 821-830. doi:https://doi.org/10.1016/j.cej.2019.05.118

Alazaiza, M. Y. D., Albahnasawi, A., Ali, G. A. M., Bashir, M. J. K., Nassani, D. E., Al Maskari, T., . . . Abujazar, M. S. S. (2022). Application of Natural Coagulants for Pharmaceutical Removal from Water and Wastewater: A Review. *Water, 14*(2), 140. doi:ARTN 140 10.3390/w14020140

Alnahas, F., Yeboah, P., Fliedel, L., Abdin, A. Y., & Alhareth, K. (2020). Expired Medication: Societal, Regulatory and Ethical Aspects of a Wasted Opportunity. *Int J Environ Res Public Health, 17*(3), 787. doi:10.3390/ijerph17030787

Alresheedi, M. T., & Basu, O. D. (2020). Interplay of water temperature and fouling during ceramic ultrafiltration for drinking water production. *Journal of Environmental Chemical Engineering, 8*(5), 104354.

Alventosa-deLara, E., Barredo-Damas, S., Zuriaga-Agustí, E., Alcaina-Miranda, M. I., & Iborra-Clar, M. I. (2014). Ultrafiltration ceramic membrane performance during the treatment of model solutions containing dye and salt. *Separation and Purification Technology, 129*, 96-105.

Andronic, L., Enesca, A. J. C., & Pick, P. E. s. (2021). Black Reduction TiO2 Methods Synthesis for by Chemical Photocatalysis Applications.

Anucha, C. B., Bacaksiz, E., Stathopoulos, V. N., Pandis, P. K., Argirusis, C., Andreouli, C.-D., . . . Altin, I. J. C. (2022). Preparation and Characterization of Supported Molybdenum Doped TiO2 on α-Al2O3 Ceramic Substrate for the Photocatalytic Degradation of Ibuprofen (IBU) under UV Irradiation. *https://doi.org/10.3390/catal12050562*, *12*(5), 562.

Apriyanti, E., Susanto, H., & Widiasa, I. N. (2021). *Development of Fly Ash Coal/TiO2 Pored Composite Materials in The Making of Ceramic Membrane for Water Treatment Process.* Paper presented at the IOP Conference Series: Materials Science and Engineering.

Arola, K., Van der Bruggen, B., Manttari, M., & Kallioinen, M. (2019). Treatment options for nanofiltration and reverse osmosis concentrates from municipal wastewater treatment: A review. *Critical Reviews in Environmental Science and Technology, 49*(22), 2049-2116. doi:10.1080/10643389.2019.1594519

Arora, I., Chawla, H., Chandra, A., Sagadevan, S., & Garg, S. (2022). Advances in the strategies for enhancing the photocatalytic activity of TiO2: Conversion from UV-light active to visible-light

active photocatalyst. *Inorganic Chemistry Communications, 143*, 109700. doi:ARTN 109700 10.1016/j.inoche.2022.109700

Arumugham, T., Kaleekkal, N. J., Gopal, S., Nambikkattu, J., Rambabu, K., Aboulella, A. M., . . . Banat, F. (2021). Recent developments in porous ceramic membranes for wastewater treatment and desalination: A review. *Journal of environmental management, 293*, 112925.

Ashley, A., Thrope, B., Choudhury, M. R., & Pinto, A. H. (2022). Emerging investigator series: photocatalytic membrane reactors: fundamentals and advances in preparation and application in wastewater treatment. *Environmental Science: Water Research & Technology, 8*(1), 22-46. doi:10.1039/d1ew00513h

Asif, M. B., & Zhang, Z. H. (2021). Ceramic membrane technology for water and wastewater treatment: A critical review of performance, full-scale applications, membrane fouling and prospects. *Chemical Engineering Journal, 418*, 129481. doi:ARTN 129481 10.1016/j.cej.2021.129481

Ayanda, O. S., Fatoki, O. S., Adekola, F. A., & Ximba, B. J. (2012). Characterization of Fly Ash Generated from Matla Power Station in Mpumalanga, South Africa. *E-Journal of Chemistry, 9*(4), 1788-1795. doi:Doi 10.1155/2012/451801

Bai, Z., Zhang, R., Wang, S., Gao, S., & Tian, J. (2021). Membrane fouling behaviors of ceramic hollow fiber microfiltration (MF) membranes by typical organic matters. *Separation and Purification Technology, 274*, 118951.

Baker, R. W. (2002). Membrane technology. *Encyclopedia of polymer science and technology, 3*.

Balakrishnan, A., Chinthala, M., Polagani, R. K., & Vo, D.-V. N. (2022). Removal of tetracycline from wastewater using g-C3N4 based photocatalysts: A review. *Environmental Research*, 114660.

Balakrishnan, A., Chinthala, M., Polagani, R. K., & Vo, D.-V. N. (2023). Removal of tetracycline from wastewater using g-C3N4 based photocatalysts: A review. *Environmental Research, 216*, 114660. doi:https://doi.org/10.1016/j.envres.2022.114660

Bao, Y., Lee, W. J., Lim, T.-T., Wang, R., & Hu, X. (2019). Pore-functionalized ceramic membrane with isotropically impregnated cobalt oxide for sulfamethoxazole degradation and membrane fouling elimination: Synergistic effect between catalytic oxidation and membrane separation. *Applied Catalysis B: Environmental, 254*, 37-46.

Bao, Y. P., Lee, W. J., Lim, T. T., Wang, R., & Hu, X. (2019). Pore-functionalized ceramic membrane with isotropically impregnated cobalt oxide for sulfamethoxazole degradation and membrane fouling elimination: Synergistic effect between catalytic oxidation and membrane separation. *Applied Catalysis B-Environmental, 254*, 37-46. doi:10.1016/j.apcatb.2019.04.081

Basile, A., Cassano, A., & Rastogi, N. K. (2015). *Advances in membrane technologies for water treatment: materials, processes and applications*: Elsevier.

Bavumiragira, J. P., Ge, J., & Yin, H. (2022). Fate and transport of pharmaceuticals in water systems: A processes review. *Sci Total Environ, 823*, 153635. doi:10.1016/j.scitotenv.2022.153635

Bera, S. P., Godhaniya, M., & Kothari, C. (2022). Emerging and advanced membrane technology for wastewater treatment: A review. *J Basic Microbiol, 62*(3-4), 245-259. doi:10.1002/jobm.202100259

Berger, T. E., Regmi, C., Schafer, A. I., & Richards, B. S. (2020). Photocatalytic degradation of organic dye via atomic layer deposited TiO2 on ceramic membranes in single-pass flow-through

operation. *Journal of Membrane Science, 604*, 118015. doi:ARTN 118015 10.1016/j.memsci.2020.118015

Bhattacharya, P., Mukherjee, D., Dey, S., Ghosh, S., & Banerjee, S. (2019). Development and performance evaluation of a novel CuO/TiO2 ceramic ultrafiltration membrane for ciprofloxacin removal. *Materials Chemistry and Physics, 229*, 106-116. doi:10.1016/j.matchemphys.2019.02.094

Binazadeh, M., Rasouli, J., Sabbaghi, S., Mousavi, S. M., Hashemi, S. A., & Lai, C. W. (2023). An Overview of Photocatalytic Membrane Degradation Development. *Materials, 16*(9), 3526.

Boonsaner, M., & Hawker, D. W. (2012). Investigation of the mechanism of uptake and accumulation of zwitterionic tetracyclines by rice (Oryza sativa L.). *Ecotoxicology and Environmental Safety, 78*, 142-147. doi:https://doi.org/10.1016/j.ecoenv.2011.11.023

Borthakur, P., Das, M. R. J. J. o. c., & science, i. (2018). Hydrothermal assisted decoration of NiS2 and CoS nanoparticles on the reduced graphene oxide nanosheets for sunlight driven photocatalytic degradation of azo dye: Effect of background electrolyte and surface charge. *516*, 342-354.

Broom, D. (2022). Pharmaceuticals are present in almost all the world's rivers, study finds. Retrieved from https://www.weforum.org/agenda/2022/02/pharmaceutical-pollution-health-drugs-rivers/

Buekenhoudt, A. J. M. s., & technology. (2008). Stability of porous ceramic membranes. *13*, 1-31. doi:https://doi.org/10.1016/S0927-5193(07)13001-1

Cai, C., Sun, W., He, S., Zhang, Y., & Wang, X. (2023). Ceramic membrane fouling mechanisms and control for water treatment. *Frontiers of Environmental Science & Engineering, 17*(10), 126.

Capodaglio, A. G. (2021). Fit-for-purpose urban wastewater reuse: Analysis of issues and available technologies for sustainable multiple barrier approaches. *Critical Reviews in Environmental Science and Technology, 51*(15), 1619-1666. doi:10.1080/10643389.2020.1763231

Chaari, I., Medhioub, M., Jamoussi, F., & Hamzaoui, A. H. (2021). Acid-treated clay materials (Southwestern Tunisia) for removing sodium leuco-vat dye : Characterization, adsorption study and activation mechanism. *Journal of Molecular Structure, 1223*, 128944. doi:ARTN 128944 10.1016/j.molstruc.2020.128944

Chadha, U., Selvaraj, S. K., Thanu, S. V., Cholapadath, V., Abraham, A. M., Zaiyan, M. M., . . . Paramsivam, V. (2022). A review of the function of using carbon nanomaterials in membrane filtration for contaminant removal from wastewater. *Materials Research Express, 9*(1). doi:ARTN 012003 10.1088/2053-1591/ac48b8

Chang, H., Liu, B., Zhang, Z., Pawar, R., Yan, Z., Crittenden, J. C., & Vidic, R. D. (2020). A critical review of membrane wettability in membrane distillation from the perspective of interfacial interactions. *Environmental Science & Technology, 55*(3), 1395-1418.

Chathurappan, R., & Jayapal, A. (2022). Synthesis and characterization of coal fly ash based multipurpose ultrafiltration membrane. *Materialia, 25*, 101548.

Chekli, L., Eripret, C., Park, S. H., Tabatabai, S. A. A., Vronska, O., Tamburic, B., . . . Shon, H. K. (2017). Coagulation performance and floc characteristics of polytitanium tetrachloride (PTC) compared with titanium tetrachloride (TiCl4) and ferric chloride (FeCl3) in algal turbid water. *Separation and Purification Technology, 175*, 99-106. doi:10.1016/j.seppur.2016.11.019

Chen, H.-R., Rairat, T., Loh, S.-H., Wu, Y.-C., Vickroy, T. W., & Chou, C.-C. (2017). Assessment of veterinary drugs in plants using pharmacokinetic approaches: The absorption, distribution and elimination of tetracycline and sulfamethoxazole in ephemeral vegetables. *PLoS One, 12*(8), e0183087.

Chen, H., Li, X., Wei, J., Feng, Y., & Gao, D. (2019). Preparation and properties of coal ash ceramic membranes for water and heat recovery from flue gas. *Journal of Chemistry, 2019*, 1-10.

Cheng, L., Sun, M., Ye, F., Bai, Y., Li, M., Fan, S., & Zhang, L. (2018). Structure design, fabrication, properties of laminated ceramics: a review. *International Journal of Lightweight Materials and Manufacture, 1*(3), 126-141.

Cui, Z., Hao, T., Yao, S., & Xu, H. (2023). Preparation of porous mullite ceramic supports from high alumina fly ash. *Journal of Material Cycles and Waste Management, 25*(2), 1120-1129.

da Silva Favero, J., dos Santos, V., Weiss-Angeli, V., Gomes, L. B., Veras, D. G., Dani, N., . . . Bergmann, C. P. (2019). Evaluation and characterization of Melo Bentonite clay for cosmetic applications. *Applied Clay Science, 175*, 40-46. doi:10.1016/j.clay.2019.04.004

Daghrir, R., & Drogui, P. (2013). Tetracycline antibiotics in the environment: a review. *Environmental Chemistry Letters, 11*(3), 209-227. doi:10.1007/s10311-013-0404-8

Dan, A. K., Bhattacharjee, D., Ghosh, S., Behera, S. S., Bindhani, B. K., Das, D., & Parhi, P. K. (2021). Prospective utilization of coal fly ash for making advanced materials. In *Clean Coal Technologies: Beneficiation, Utilization, Transport Phenomena and Prospective* (pp. 511-531): Springer.

Das, D., & Kayal, N. (2023). Influence of additive contents on the properties of SiC ceramic membranes and their performance in oil-water separation. *International Journal of Applied Ceramic Technology, 20*(3), 1715-1729.

Das, D., Kayal, N., & Innocentini, M. D. d. M. (2021). Permeability Behavior and Wastewater Filtration Performance of Mullite Bonded Porous SiC Ceramic Membrane Prepared Using Coal Fly Ash as Sintering Additive. *Transactions of the Indian Ceramic Society, 80*(3), 186-192. doi:10.1080/0371750X.2021.1934122

Ddani, M., Meunier, A., Zahraoui, M., Beaufort, D., El Wartiti, M., Fontaine, C., . . . El Mahi, B. (2005). Clay mineralogy and chemical composition of bentonites from the Gourougou volcanic massif (northeast Morocco). *Clays and Clay Minerals, 53*(3), 250-267. doi:10.1346/Ccmn.2005.0530305

de la Rocha, M. R., Virginie, M., Khodakov, A., Pollo, L. D., Marcílio, N. R., & Tessaro, I. C. (2021). Preparation of alumina based tubular asymmetric membranes incorporated with coal fly ash by centrifugal casting. *Ceramics International, 47*(3), 4187-4196.

Deepracha, S., Atfane, L., Ayral, A., & Ogawa, M. (2021). Simple and efficient method for functionalizing photocatalytic ceramic membranes and assessment of its applicability for wastewater treatment in up-scalable membrane reactors. *Separation and Purification Technology, 262*, 118307. doi:10.1016/j.seppur.2021.118307

Dehkordi, S. K., Paknejad, H., Blaha, L., Svecova, H., Grabic, R., Simek, Z., . . . Bittner, M. (2022). Instrumental and bioanalytical assessment of pharmaceuticals and hormone-like compounds in a major drinking water source-wastewater receiving Zayandeh Rood river, Iran. *Environ Sci Pollut Res Int, 29*(6), 9023-9037. doi:10.1007/s11356-021-15943-7

Del Colle, R., Fortulan, C. A., & Fontes, S. R. (2011). Manufacture and characterization of ultra and microfiltration ceramic membranes by isostatic pressing. *Ceramics International, 37*(4), 1161-1168.

Desa, A. L., Hairom, N. H. H., Sidik, D. A., Misdan, N., Yusof, N., Ahmad, M. K., & Mohammad, A. W. (2019). A comparative study of ZnO-PVP and ZnO-PEG nanoparticles activity in membrane photocatalytic reactor (MPR) for industrial dye wastewater treatment under different membranes. *Journal of Environmental Chemical Engineering, 7*(3), 103143. doi:ARTN 103143 10.1016/j.jece.2019.103143

Dey, S., Bano, F., & Malik, A. (2019). Pharmaceuticals and personal care product (PPCP) contamination—a global discharge inventory. In *Pharmaceuticals and personal care products: waste management and treatment technology* (pp. 1-26): Elsevier.

Di Marco, G., Gismondi, A., Canuti, L., Scimeca, M., Volpe, A., & Canini, A. (2014). Tetracycline accumulates in Iberis sempervirens L. through apoplastic transport inducing oxidative stress and growth inhibition. *Plant Biology, 16*(4), 792-800. doi:https://doi.org/10.1111/plb.12102

Diorio, A., Diaz-Angulo, J., Castellanos, R. M., Gomes, A. I., Bergamasco, R., Vieira, M. F., . . . Vilar, V. J. P. (2022). A tubular ceramic membrane coated with TiO2-P25 for radial addition of H2O2 towards AMX removal from synthetic solutions and secondary urban wastewater. *Environ Sci Pollut Res Int, 29*(28), 42120-42129. doi:10.1007/s11356-021-14297-4

Djurišić, A. B., Leung, Y. H., & Ching Ng, A. M. (2014). Strategies for improving the efficiency of semiconductor metal oxide photocatalysis. *Materials Horizons, 1*(4), 400-410. doi:10.1039/c4mh00031e

Dong, Y., Wu, H., Yang, F., & Gray, S. (2022). Cost and efficiency perspectives of ceramic membranes for water treatment. *Water research, 220*, 118629.

Dong, Y., Wu, H., Yang, F., & Gray, S. (2022). Cost and efficiency perspectives of ceramic membranes for water treatment. *Water Res, 220*, 118629. doi:10.1016/j.watres.2022.118629

Drioli, E., Giorno, L., & Fontananova, E. Membrane operations in advanced molecular separations. *(No Title)*.

Drioli, E., Giorno, L., & Fontananova, E. (2017). *Comprehensive membrane science and engineering*: Elsevier.

Du, X., Shi, Y., Jegatheesan, V., & Haq, I. U. (2020). A review on the mechanism, impacts and control methods of membrane fouling in MBR system. *Membranes, 10*(2), 24.

Dwivedi, A., & Jain, M. K. (2014). Fly ash–waste management and overview: A Review. *Recent Research in Science and Technology, 6*(1).

Elhalil, A., Elmoubarki, R., Farnane, M., Machrouhi, A., Sadiq, M., Mahjoubi, F. Z., . . . Barka, N. (2018). Photocatalytic degradation of caffeine as a model pharmaceutical pollutant on Mg doped ZnO-Al2O3 heterostructure. *Environmental Nanotechnology, Monitoring & Management, 10*, 63-72. doi:10.1016/j.enmm.2018.02.002

Eniola, J. O., Kumar, R., Barakat, M. A., & Rashid, J. (2022). A review on conventional and advanced hybrid technologies for pharmaceutical wastewater treatment. *Journal of Cleaner Production, 356*, 131826. doi:ARTN 131826 10.1016/j.jclepro.2022.131826

Ewis, D., Ismail, N. A., Hafiz, M., Benamor, A., & Hawari, A. H. (2021). Nanoparticles functionalized ceramic membranes: fabrication, surface modification, and performance. *Environ Sci Pollut Res Int, 28*(10), 12256-12281. doi:10.1007/s11356-020-11847-0

Fan, P., Zhen, K., Zan, Z., Chao, Z., Jian, Z., & Yun, J. (2016). Preparation and development of porous ceramic membrane supports fabricated by extrusion technique. *Chemical Engineering Transactions, 55*, 277-282.

Fan, Y., Zhou, Y., Feng, Y., Wang, P., Li, X. Y., & Shih, K. M. (2020). Fabrication of reactive flat-sheet ceramic membranes for oxidative degradation of ofloxacin by peroxymonosulfate. *Journal of Membrane Science, 611*, 118302. doi:ARTN 118302 10.1016/j.memsci.2020.118302

Fang, J., Qin, G., Wei, W., & Zhao, X. (2011). Preparation and characterization of tubular supported ceramic microfiltration membranes from fly ash. *Separation and Purification Technology, 80*(3), 585-591.

Fauzi, A. A., Jalil, A. A., Hassan, N. S., Aziz, F. F. A., Azami, M. S., Hussain, I., . . . Vo, D. V. N. (2022). A critical review on relationship of CeO2-based photocatalyst towards mechanistic degradation of organic pollutant. *Chemosphere, 286*, 131651. doi:https://doi.org/10.1016/j.chemosphere.2021.131651

Feuerborn, H., Harris, D., & Heidrich, C. (2019). *Global aspects on coal combustion products.* Paper presented at the Proc. Eurocoalash Conf. Univ. DundeeScotl. Great Br.

Fu, H., Li, Z., Zhang, Y., Zhang, H., & Chen, H. (2022). Preparation, characterization and properties study of a superhydrophobic ceramic membrane based on fly ash. *Ceramics International, 48*(8), 11573-11587.

Fu, M., Liu, J., Dong, X., Zhu, L., Dong, Y., & Hampshire, S. (2019). Waste recycling of coal fly ash for design of highly porous whisker-structured mullite ceramic membranes. *Journal of the European Ceramic Society, 39*(16), 5320-5331.

Ganiyu, S. O., van Hullebusch, E. D., Cretin, M., Esposito, G., & Oturan, M. A. (2015). Coupling of membrane filtration and advanced oxidation processes for removal of pharmaceutical residues: A critical review. *Separation and Purification Technology, 156*, 891-914. doi:10.1016/j.seppur.2015.09.059

Ghazali, N., Muthusamy, K., & Wan Ahmad, S. (2019). *Utilization of fly ash in construction.* Paper presented at the IOP conference series: materials science and engineering.

Goh, P., & Ismail, A. (2018). A review on inorganic membranes for desalination and wastewater treatment. *Desalination, 434*, 60-80.

Gollakota, A. R., Volli, V., & Shu, C.-M. (2019). Progressive utilisation prospects of coal fly ash: A review. *Science of the Total Environment, 672*, 951-989.

Gong, M., Wang, M., Wang, L., Feng, A., & Hu, J. (2022). Degradation of tetracycline hydrochloride in sub- and supercritical water with and without oxidation. *Process Safety and Environmental Protection, 162*, 373-383. doi:https://doi.org/10.1016/j.psep.2022.04.030

Goodarzi, F. (2006). Characteristics and composition of fly ash from Canadian coal-fired power plants. *Fuel, 85*(10-11), 1418-1427. doi:10.1016/j.fuel.2005.11.022

Goswami, K. P., Pakshirajan, K., & Pugazhenthi, G. (2022). Process intensification through waste fly ash conversion and application as ceramic membranes: A review. *Science of the Total Environment, 808*, 151968.

Goswami, K. P., & Pugazhenthi, G. (2020). Treatment of poultry slaughterhouse wastewater using tubular microfiltration membrane with fly ash as key precursor. *Journal of Water Process Engineering, 37*, 101361. doi:https://doi.org/10.1016/j.jwpe.2020.101361

Goswami, K. P., & Pugazhenthi, G. (2021). Effect of binder concentration on properties of low-cost fly ash-based tubular ceramic membrane and its application in separation of glycerol from biodiesel. *Journal of Cleaner Production, 319*, 128679.

Goswami, K. P., & Pugazhenthi, G. (2022a). Treatment of starch-rich wastewater using fly ash-based low-cost tubular ceramic membrane. *Environmental Progress & Sustainable Energy, 41*(6), e13906. doi:https://doi.org/10.1002/ep.13906

Goswami, K. P., & Pugazhenthi, G. (2022b). Treatment of starch-rich wastewater using fly ash-based low-cost tubular ceramic membrane. *Environmental Progress & Sustainable Energy, 41*(6), e13906.

Griggs, D., Nilsson, M., Stevance, A., & McCollum, D. (2017). *A guide to SDG interactions: from science to implementation*: International Council for Science, Paris.

Gruskevica, K., & Mezule, L. (2021). Cleaning methods for ceramic ultrafiltration membranes affected by organic fouling. *Membranes, 11*(2), 131.

Gu, Q., Ng, T. C. A., Bao, Y., Ng, H. Y., Tan, S. C., & Wang, J. (2022). Developing better ceramic membranes for water and wastewater Treatment: Where microstructure integrates with chemistry and functionalities. *Chemical Engineering Journal, 428*, 130456. doi:10.1016/j.cej.2021.130456

Gul, A., Hruza, J., & Yalcinkaya, F. (2021). Fouling and Chemical Cleaning of Microfiltration Membranes: A Mini-Review. *Polymers (Basel), 13*(6), 846. doi:10.3390/polym13060846

Gul, S., Parra, K. N., Miwa, D. W., & Motheo, A. d. J. (2013). *Electrochemical Incineration of Tetracycline Hydrochloride Using Titanium Based Anode in Saline Medium: Kinetic and Energy Consumption Evolution.* Paper presented at the Electrochemical Society Meeting Abstracts 224.

Guo, H., Li, W., & Ye, F. (2016). Low-cost porous mullite ceramic membrane supports fabricated from kyanite by casting and reaction sintering. *Ceramics International, 42*(4), 4819-4826.

Guo, X., Mu, Q., Zhong, H., Li, P., Zhang, C., Wei, D., & Zhao, T. (2019). Rapid removal of tetracycline by Myriophyllum aquaticum: Evaluation of the role and mechanisms of adsorption. *Environmental Pollution, 254*, 113101. doi:https://doi.org/10.1016/j.envpol.2019.113101

Guo, Y., Huang, W., Chen, B., Zhao, Y., Liu, D., Sun, Y., & Gong, B. (2017). Removal of tetracycline from aqueous solution by MCM-41-zeolite A loaded nano zero valent iron: synthesis, characteristic, adsorption performance and mechanism. *Journal of hazardous materials, 339*, 22-32.

Gupta, V., & Anandkumar, J. (2019). Synthesis of crosslinked PVA-ceramic composite membrane for phenol removal from aqueous solution. *Journal of the Serbian Chemical Society, 84*(2), 211-224.

Gupta, V., Raja, C., & Anandkumar, J. (2020). Phenol removal by novel choline chloride blended cellulose acetate-fly ash composite membrane. *Periodica Polytechnica Chemical Engineering, 64*(1), 116-123.

Han, T., Liang, Y., Wu, Z., Zhang, L., Liu, Z., Li, Q., . . . Wu, M. (2019). Effects of tetracycline on growth, oxidative stress response, and metabolite pattern of ryegrass. *Journal of Hazardous Materials, 380*, 120885. doi:https://doi.org/10.1016/j.jhazmat.2019.120885

He, J., Zou, Y., & Wang, S. J. D. T. (2019). Defect engineering on electrocatalysts for gas-evolving reactions. *48*(1), 15-20.

He, Z., Lyu, Z., Gu, Q., Zhang, L., & Wang, J. (2019). Ceramic-based membranes for water and wastewater treatment. *Colloids and Surfaces A: Physicochemical and Engineering Aspects, 578*, 123513.

Heilig, S., Lee, P., & Breslow, L. (2002). Curtailing antibiotic use in agriculture: it is time for action: this use contributes to bacterial resistance in humans. *Western journal of medicine, 176*(1), 9.

Homocianu, M., & Pascariu, P. (2022). High-performance photocatalytic membranes for water purification in relation to environmental and operational parameters. *Journal of Environmental Management, 311*, 114817. doi:10.1016/j.jenvman.2022.114817

Hong, H. L., Zhao, L. L., Fang, Q., Algeo, T. J., Wang, C. W., Yu, J. X., . . . Ji, K. P. (2019). Volcanic sources and diagenetic alteration of Permian-Triassic boundary K-bentonites in Guizhou Province, South China. *Palaeogeography Palaeoclimatology Palaeoecology, 519*, 141-153. doi:10.1016/j.palaeo.2018.01.019

Horovitz, I., Avisar, D., Baker, M. A., Grilli, R., Lozzi, L., Di Camillo, D., & Mamane, H. (2016). Carbamazepine degradation using a N-doped TiO2 coated photocatalytic membrane reactor: Influence of physical parameters. *J Hazard Mater, 310*, 98-107. doi:10.1016/j.jhazmat.2016.02.008

Hou, L., Zhang, H., Wang, L., & Chen, L. (2013). Ultrasound-enhanced magnetite catalytic ozonation of tetracycline in water. *Chemical Engineering Journal, 229*, 577-584. doi:https://doi.org/10.1016/j.cej.2013.06.013

Huang, F., Yan, A., Zhao, H. J. S. p.-m., mechanisms, & applications. (2016). Influences of doping on photocatalytic properties of TiO2 photocatalyst. 31-80.

Huang, J., Chen, H., Qi, R., Yang, J., Li, Z., & Zhang, H. (2023). Porous ceramic membranes from coal fly ash with addition of various pore-forming agents for oil-in-water emulsion separation. *Journal of Environmental Chemical Engineering, 11*(3), 109929.

Huang, J., Chen, H., Yang, J., Zhou, T., & Zhang, H. (2023). Effects of particle size on microstructure and mechanical strength of a fly ash based ceramic membrane. *Ceramics International*.

Huang, J., Zhang, H., Zhang, Y., Liang, D., & Chen, H. (2022). Recycle coal fly ash for preparing tubular ceramic membranes applied in transport membrane condenser. *Separation and Purification Technology, 282*, 119972.

Hubadillah, S. K., Othman, M. H. D., Matsuura, T., Ismail, A., Rahman, M. A., Harun, Z., . . . Nomura, M. (2018). Fabrications and applications of low cost ceramic membrane from kaolin: A comprehensive review. *Ceramics International, 44*(5), 4538-4560.

Hubadillah, S. K., Othman, M. H. D., Tai, Z. S., Jamalludin, M. R., Yusuf, N. K., Ahmad, A., . . . Harun, Z. (2020). Novel hydroxyapatite-based bio-ceramic hollow fiber membrane derived from waste cow bone for textile wastewater treatment. *Chemical Engineering Journal, 379*, 122396. doi:ARTN 122396 10.1016/j.cej.2019.122396

Hurt, A. P., Coleman, A. A., Ma, H., Li, Q., & Coleman, N. J. (2022). Calcium Silicate Hydrate Cation-Exchanger from Paper Recycling Ash and Waste Container Glass. *Ceramics, 5*(3), 301-317. doi:10.3390/ceramics5030024

IEA. (2020). Coal 2020. Retrieved from https://iea.blob.core.windows.net/assets/00abf3d2-4599-4353-977c-8f80e9085420/Coal_2020.pdf

Ismail, S., de La Parra, C., Temmink, H., & Van Lier, J. (2010). Extracellular polymeric substances (EPS) in upflow anaerobic sludge blanket (UASB) reactors operated under high salinity conditions. *Water research, 44*(6), 1909-1917.

Issaoui, M., & Limousy, L. (2019). Low-cost ceramic membranes: Synthesis, classifications, and applications. *Comptes Rendus Chimie, 22*(2-3), 175-187.

Jaishankar, M., Tseten, T., Anbalagan, N., Mathew, B. B., & Beeregowda, K. N. (2014). Toxicity, mechanism and health effects of some heavy metals. *Interdisciplinary toxicology, 7*(2), 60.

Jana, S., Saikia, A., Purkait, M., & Mohanty, K. (2011). Chitosan based ceramic ultrafiltration membrane: Preparation, characterization and application to remove Hg (II) and As (III) using polymer enhanced ultrafiltration. *Chemical Engineering Journal, 170*(1), 209-219.

Janani, N., Deviannapoorani, C., Dhivya, L., & Murugan, R. (2014). Influence of sintering additives on densification and Li+ conductivity of Al doped Li7La3Zr2O12 lithium garnet. *RSC advances, 4*(93), 51228-51238. doi:10.1039/C4RA08674K

Jang, H. M., Yoo, S., Choi, Y.-K., Park, S., & Kan, E. (2018). Adsorption isotherm, kinetic modeling and mechanism of tetracycline on Pinus taeda-derived activated biochar. *Bioresource Technology, 259*, 24-31.

Jayaranjan, M. L. D., Van Hullebusch, E. D., & Annachhatre, A. P. (2014). Reuse options for coal fired power plant bottom ash and fly ash. *Reviews in Environmental Science and Bio/Technology, 13*, 467-486.

Jedidi, I., Khemakhem, S., Saïdi, S., Larbot, A., Elloumi-Ammar, N., Fourati, A., . . . Amar, R. B. (2011). Preparation of a new ceramic microfiltration membrane from mineral coal fly ash: Application to the treatment of the textile dying effluents. *Powder Technology, 208*(2), 427-432. doi:https://doi.org/10.1016/j.powtec.2010.08.039

Jedidi, I., Saïdi, S., Khemakhem, S., Larbot, A., Elloumi-Ammar, N., Fourati, A., . . . Amar, R. B. (2009). Elaboration of new ceramic microfiltration membranes from mineral coal fly ash applied to waste water treatment. *Journal of hazardous materials, 172*(1), 152-158.

Jelić, A., Gros, M., Petrović, M., Ginebreda, A., Barceló, D. J. E., & rivers, p. p. i. (2012). Occurrence and elimination of pharmaceuticals during conventional wastewater treatment. 1-23.

Jha, V. K., Matsuda, M., & Miyake, M. (2008). Resource recovery from coal fly ash waste: an overview study. *Journal of the Ceramic Society of Japan, 116*(1350), 167-175. doi:10.2109/jcersj2.116.167

Jiang, F., Zhang, L., Mukiza, E., Qi, Z., & Cang, D. (2018). Formation mechanism of high apparent porosity ceramics prepared from fly ash cenosphere. *Journal of Alloys and Compounds, 749*, 750-757.

Jin, Y., Feng, W., Zheng, D., Dong, Z., & Cui, H. (2020). Structure refinement of fly ash in connection with its reactivity in geopolymerization. *Waste Management, 118*, 350-359.

Johns, W. (2000). Computer-Aided Chemical Engineering. *Kirk-Othmer Encyclopedia of Chemical Technology*.

Kang, H.-J., Lim, M.-Y., & Kwon, J.-H. (2012). Effects of adsorption onto silica sand particles on the hydrolysis of tetracycline antibiotics. *Journal of Environmental Monitoring, 14*(7), 1853-1859. doi:10.1039/C2EM10961A

Karimi-Maleh, H., Ayati, A., Davoodi, R., Tanhaei, B., Karimi, F., Malekmohammadi, S., . . . Sillanpaa, M. (2021). Recent advances in using of chitosan-based adsorbents for removal of pharmaceutical contaminants: A review. *Journal of Cleaner Production, 291*, 125880. doi:ARTN 125880 10.1016/j.jclepro.2021.125880

Katibi, K. K., Mohd Nor, M. Z., Yunos, K. F. M., Jaafar, J., & Show, P. L. (2023). Strategies to Enhance the Membrane-Based Processing Performance for Fruit Juice Production: A Review. *Membranes, 13*(7), 679.

Kaur, H., Dahake, R., Maddigapu, P. R., Hippargi, G., Pophali, G. R., & Bansiwal, A. (2020). Enhanced photocatalytic degradation of antimicrobial triclosan using rGO-TiO2 composite under natural solar illumination. *Journal of Materials Science-Materials in Electronics, 31*(8), 6045-6058. doi:10.1007/s10854-020-03156-6

Khalid, A., Zulfiqar, S., Tabassum, N., Khan, A. S., Abid, M. A., Akhtar, M. S., . . . Asif, S. (2023). Biocompatible cellulose acetate supported ammonium based ionic liquid membranes; way forward to remediate water pollution. *Chemosphere, 322*, 138151. doi:https://doi.org/10.1016/j.chemosphere.2023.138151

Khemakhem, S., Amar, R. B., Hassen, R. B., Larbot, A., Medhioub, M., Salah, A. B., & Cot, L. (2004). New ceramic membranes for tangential waste-water filtration. *Desalination, 167*, 19-22.

Kim, J.-M., Kim, H.-N., Park, Y.-J., Ko, J.-W., Lee, J.-W., & Kim, H.-D. (2015). Fabrication of transparent MgAl2O4 spinel through homogenous green compaction by microfluidization and slip casting. *Ceramics International, 41*(10), 13354-13360.

Koch, N., Islam, N. F., Sonowal, S., Prasad, R., & Sarma, H. (2021). Environmental antibiotics and resistance genes as emerging contaminants: Methods of detection and bioremediation. *Curr Res Microb Sci, 2*, 100027. doi:10.1016/j.crmicr.2021.100027

Kooijman, G., de Kreuk, M. K., Houtman, C., & van Lier, J. B. (2020). Perspectives of coagulation/flocculation for the removal of pharmaceuticals from domestic wastewater: A critical view at experimental procedures. *Journal of Water Process Engineering, 34*, 101161. doi:ARTN 101161 10.1016/j.jwpe.2020.101161

Kotobuki, M., Gu, Q., Zhang, L., & Wang, J. (2021). Ceramic-polymer composite membranes for water and wastewater treatment: Bridging the big gap between ceramics and polymers. *Molecules, 26*(11), 3331.

Kovalakova, P., Cizmas, L., McDonald, T. J., Marsalek, B., Feng, M., & Sharma, V. K. (2020). Occurrence and toxicity of antibiotics in the aquatic environment: A review. *Chemosphere, 251*, 126351. doi:https://doi.org/10.1016/j.chemosphere.2020.126351

Kumar, B., Rai, P., & Chakraborty, P. (2022). Pharmaceuticals in Indian Aquatic Environment: Risk and Implications for Management. In *Legacy and Emerging Contaminants in Water and Wastewater* (pp. 47-76): Springer.

Kumar, R. V., Ghoshal, A. K., & Pugazhenthi, G. (2015). Elaboration of novel tubular ceramic membrane from inexpensive raw materials by extrusion method and its performance in microfiltration of synthetic oily wastewater treatment. *Journal of Membrane Science, 490*, 92-102.

Kuvarega, A. T., & Mamba, B. B. (2016). Photocatalytic membranes for efficient water treatment. In *Semiconductor photocatalysis-materials, mechanisms and applications*: IntechOpen.

Labidi, A., Ren, H., Sial, A., Wang, H., Lichtfouse, E., & Wang, C. (2023). Coal ash for removing toxic metals and phenolic contaminants from wastewater: A brief review. *Critical Reviews in Environmental Science and Technology*, 1-24.

Lavanya, C., Kusuma, J., & Geetha Balakrishna, R. (2021). Pyrochlores: oxygen-rich moieties as ceramic fillers in uplifting the antifouling property and dye removal capacity of polymeric membranes. *Separation and Purification Technology, 272*, 118946. doi:https://doi.org/10.1016/j.seppur.2021.118946

Lee, M., Wu, Z., & Li, K. (2015). Advances in ceramic membranes for water treatment. In *Advances in membrane technologies for water treatment* (pp. 43-82): Elsevier.

Leong, S. W., Razmjou, A., Wang, K., Hapgood, K., Zhang, X. W., & Wang, H. T. (2014). TiO2 based photocatalytic membranes: A review. *Journal of Membrane Science, 472*, 167-184. doi:10.1016/j.memsci.2014.08.016

Li, C., Lu, Z., Ao, X., Sun, W., & Huang, X. (2022). Degradation kinetics and removal efficiencies of pharmaceuticals by photocatalytic ceramic membranes using ultraviolet light-emitting diodes. *Chemical Engineering Journal, 427*, 130828.

Li, C., Sun, W., Lu, Z., Ao, X., & Li, S. (2020). Ceramic nanocomposite membranes and membrane fouling: A review. *Water research, 175*, 115674.

Li, C., Sun, W. J., Lu, Z. D., Ao, X. W., Yang, C., & Li, S. M. (2019). Systematic evaluation of TiO2-GO-modified ceramic membranes for water treatment: Retention properties and fouling mechanisms. *Chemical Engineering Journal, 378*, 122138. doi:ARTN 122138 10.1016/j.cej.2019.122138

Li, C., Zhou, Y., Tian, Y., Zhao, Y., Wang, K., Li, G., & Chai, Y. (2019). Preparation and characterization of mullite whisker reinforced ceramics made from coal fly ash. *Ceramics International, 45*(5), 5613-5616. doi:https://doi.org/10.1016/j.ceramint.2018.12.021

Li, K., Ji, F., Liu, Y., Tong, Z., Zhan, X., & Hu, Z. (2013). Adsorption removal of tetracycline from aqueous solution by anaerobic granular sludge: equilibrium and kinetic studies. *Water Science and technology, 67*(7), 1490-1496. doi:10.2166/wst.2013.016

Li, M., Yang, K., Huang, X., Liu, S., Jia, Y., Gu, P., & Miao, H. (2022). Efficient degradation of trimethoprim by catalytic ozonation coupled with Mn/FeOx-functionalized ceramic membrane:

Synergic catalytic effect and enhanced anti-fouling performance. *J Colloid Interface Sci, 616*, 440-452. doi:10.1016/j.jcis.2022.02.061

Li, P., Miao, R., Wang, P., Sun, F. Y., & Li, X. Y. (2021). Bi-metal oxide-modified flat-sheet ceramic membranes for catalytic ozonation of organic pollutants in wastewater treatment. *Chemical Engineering Journal, 426*, 131263. doi:ARTN 131263 10.1016/j.cej.2021.131263

Li, Q. L., Jia, R. R., Shao, J. H., & He, Y. L. (2019). Photocatalytic degradation of amoxicillin via TiO2 nanoparticle coupling with a novel submerged porous ceramic membrane reactor. *Journal of Cleaner Production, 209*, 755-761. doi:10.1016/j.jclepro.2018.10.183

Li, W. Y., Wang, Q., Xiao, Q. F., & Dong, B. Z. (2009, 11-13 June 2009). *Removal of Tetracycline and Oxytetracycline in Water by a Reverse Osmosis Membrane.* Paper presented at the 2009 3rd International Conference on Bioinformatics and Biomedical Engineering.

Li, Y., Zhang, L., Ding, J., & Liu, X. (2020). Prioritization of pharmaceuticals in water environment in China based on environmental criteria and risk analysis of top-priority pharmaceuticals. *Journal of Environmental Management, 253*, 109732. doi:10.1016/j.jenvman.2019.109732

Li, Z., Molin, C., & Gebhardt, S. E. (2023). Influence of Sintering Additives on Modified (Ba,Sr)(Sn,Ti)O3 for Electrocaloric Application. *Inorganics, 11*(4). doi:10.3390/inorganics11040151

Liang, D., Huang, J., Zhang, Y., Zhang, Z., Chen, H., & Zhang, H. (2021). Influence of dextrin content and sintering temperature on the properties of coal fly ash-based tubular ceramic membrane for flue gas moisture recovery. *Journal of the European Ceramic Society, 41*(11), 5696-5710.

Liu, C., Wang, C., Guo, Y. Q., Zhang, J. M., Cao, Y. Y., Liu, H. P., . . . Zhang, C. H. (2019). High-performance polyamide membrane with tailored water channel prepared via bionic neural networks for textile wastewater treatment. *Journal of Materials Chemistry A, 7*(12), 6695-6707. doi:10.1039/c9ta00031c

Liu, J., Dong, Y., Dong, X., Hampshire, S., Zhu, L., Zhu, Z., & Li, L. (2016). Feasible recycling of industrial waste coal fly ash for preparation of anorthite-cordierite based porous ceramic membrane supports with addition of dolomite. *Journal of the European Ceramic Society, 36*(4), 1059-1071.

Liu, M.-k., Liu, Y.-y., Bao, D.-d., Zhu, G., Yang, G.-h., Geng, J.-f., & Li, H.-t. (2017). Effective Removal of Tetracycline Antibiotics from Water using Hybrid Carbon Membranes. *Scientific Reports, 7*(1), 43717. doi:10.1038/srep43717

Liu, X. M., Tian, C., Zhao, Y. X., Xu, W. Y., Dong, D. H., Shih, K. M., . . . Song, W. (2022). Enhanced cross-flow filtration with flat-sheet ceramic membranes by titanium-based coagulation for membrane fouling control. *Frontiers of Environmental Science & Engineering, 16*(8), 1-16. doi:ARTN 110 10.1007/s11783-022-1531-x

Liu, Y., Zhu, W., Guan, K., Peng, C., & Wu, J. (2018). Freeze-casting of alumina ultra-filtration membranes with good performance for anionic dye separation. *Ceramics International, 44*(10), 11901-11904.

Loganathan, P., Kandasamy, J., Ratnaweera, H., Vigneswaran, S. J. E. S., & Research, P. (2022). Submerged membrane/adsorption hybrid process in water reclamation and concentrate management—a mini review. 1-15.

Lorente-Ayza, M.-M., Mestre, S., Sanz, V., & Sánchez, E. (2016). On the underestimated effect of the starch ash on the characteristics of low cost ceramic membranes. *Ceramics International, 42*(16), 18944-18954.

Lorente-Ayza, M. M., Mestre, S., Menendez, M., & Sanchez, E. (2015). Comparison of extruded and pressed low cost ceramic supports for microfiltration membranes. *Journal of the European Ceramic Society, 35*(13), 3681-3691. doi:10.1016/j.jeurceramsoc.2015.06.010

Lozano, I., Perez-Guzman, C. J., Mora, A., Mahlknecht, J., Aguilar, C. L., & Cervantes-Aviles, P. (2022). Pharmaceuticals and personal care products in water streams: Occurrence, detection, and removal by electrochemical advanced oxidation processes. *Sci Total Environ, 827*, 154348. doi:10.1016/j.scitotenv.2022.154348

Luo, X., & Deng, F. (2018). *Nanomaterials for the removal of Pollutants and Resource reutilization*: Elsevier.

Luo, Y., Ma, S., Zhao, Z., Wang, Z., Zheng, S., & Wang, X. (2017). Preparation and characterization of whisker-reinforced ceramics from coal fly ash. *Ceramics International, 43*(1, Part A), 1-11. doi:https://doi.org/10.1016/j.ceramint.2016.09.211

Luster, E., Avisar, D., Horovitz, I., Lozzi, L., Baker, M. A., Grilli, R., & Mamane, H. (2017). N-Doped TiO(2)-Coated Ceramic Membrane for Carbamazepine Degradation in Different Water Qualities. *Nanomaterials (Basel), 7*(8), 206. doi:10.3390/nano7080206

Madikizela, L. M., Tavengwa, N. T., & Chimuka, L. (2017). Status of pharmaceuticals in African water bodies: Occurrence, removal and analytical methods. *Journal of Environmental Management, 193*, 211-220. doi:10.1016/j.jenvman.2017.02.022

Magagula, B. K., Rampedi, I. T., & Yessoufou, K. (2022). Household Pharmaceutical Waste Management Practices in the Johannesburg Area, South Africa. *Int J Environ Res Public Health, 19*(12), 7484. doi:10.3390/ijerph19127484

Manocha, L. M., Prasad, G., & Manocha, S. (2012). Structural, Mechanical and Frictional Studies on Carbon-Fly ash-Ceramic Composites. *Transactions of the Indian Ceramic Society, 71*(2), 86-94. doi:10.1080/0371750X.2012.716232

Manrique-Moreno, M., Heinbockel, L., Suwalsky, M., Garidel, P., & Brandenburg, K. (2016). Biophysical study of the non-steroidal anti-inflammatory drugs (NSAID) ibuprofen, naproxen and diclofenac with phosphatidylserine bilayer membranes. *Biochim Biophys Acta, 1858*(9), 2123-2131. doi:10.1016/j.bbamem.2016.06.009

Mansouri, F., Chouchene, K., Roche, N., & Ksibi, M. (2021). Removal of Pharmaceuticals from Water by Adsorption and Advanced Oxidation Processes: State of the Art and Trends. *Applied Sciences-Basel, 11*(14), 6659. doi:ARTN 6659 10.3390/app11146659

Marcucci, M., Ciabatti, I., Matteucci, A., & Vernaglione, G. (2003). Membrane technologies applied to textile wastewater treatment. *Ann N Y Acad Sci, 984*(1), 53-64. doi:10.1111/j.1749-6632.2003.tb05992.x

Margas, M., Piotrowicz-Cieślak, A. I., Ziółkowska, A., & Adomas, B. (2016). Tetracycline Accumulation in Pea Seedlings and its Effects on Proteome and Enzyme Activities. *International Journal of Agriculture & Biology, 18*(4).

Marzouk, S. S., Naddeo, V., Banat, F., & Hasan, S. W. (2021). Preparation of TiO2/SiO2 ceramic membranes via dip coating for the treatment of produced water. *Chemosphere, 273*, 129684. doi:10.1016/j.chemosphere.2021.129684

Masood, Z., Ikhlaq, A., Farooq, U., Qi, F., Javed, F., & Aziz, H. A. (2022). Removal of anti-biotics from veterinary pharmaceutical wastewater using combined Electroflocculation and Fe-Zn loaded zeolite 5A based catalytic ozonation process br. *Journal of Water Process Engineering, 49*, 103039. doi:ARTN 103039 10.1016/j.jwpe.2022.103039

Melo, W. d., Lesak, G. V. G., Oliveira, T. V. d., Voll, F. A. P., Santos, A. F., & Vieira, R. B. (2021). Microfiltration of oil-in-water emulsion using modified ceramic membrane: surface properties, membrane resistance, critical flux, and cake behavior. *Materials Research, 25*, e20210365.

Mendez, E., Gonzalez-Fuentes, M. A., Rebollar-Perez, G., Mendez-Albores, A., & Torres, E. (2017). Emerging pollutant treatments in wastewater: Cases of antibiotics and hormones. *J Environ Sci Health A Tox Hazard Subst Environ Eng, 52*(3), 235-253. doi:10.1080/10934529.2016.1253391

Meng, X., Liu, Z., Deng, C., Zhu, M., Wang, D., Li, K., . . . Jiang, M. (2016). Microporous nano-MgO/diatomite ceramic membrane with high positive surface charge for tetracycline removal. *J Hazard Mater, 320*, 495-503. doi:10.1016/j.jhazmat.2016.08.068

Mestre, A. S., & Carvalho, A. P. (2019). Photocatalytic Degradation of Pharmaceuticals Carbamazepine, Diclofenac, and Sulfamethoxazole by Semiconductor and Carbon Materials: A Review. *Molecules, 24*(20), 3702. doi:10.3390/molecules24203702

Migliore, L., Godeas, F., De Filippis, S. P., Mantovi, P., Barchi, D., Testa, C., . . . Brambilla, G. (2010). Hormetic effect(s) of tetracyclines as environmental contaminant on Zea mays. *Environmental Pollution, 158*(1), 129-134. doi:https://doi.org/10.1016/j.envpol.2009.07.039

Mirzaei, A., Chen, Z., Haghighat, F., & Yerushalmi, L. (2016). Removal of pharmaceuticals and endocrine disrupting compounds from water by zinc oxide-based photocatalytic degradation: A review. *Sustainable Cities and Society, 27*, 407-418. doi:10.1016/j.scs.2016.08.004

Mistler, R. E., & Twiname, E. R. (2000). *Tape casting: theory and practice*: American ceramic society.

Mohamad Esham, M. I., Ahmad, A. L., & Othman, M. H. D. (2021). Fabrication, Optimization, and Performance of a TiO2 Coated Bentonite Membrane for Produced Water Treatment: Effect of Grafting Time. *Membranes (Basel), 11*(10), 739. doi:10.3390/membranes11100739

Molinari, R., Lavorato, C., & Argurio, P. (2017). Recent progress of photocatalytic membrane reactors in water treatment and in synthesis of organic compounds. A review. *Catalysis Today, 281*, 144-164. doi:10.1016/j.cattod.2016.06.047

Monash, P., Pugazhenthi, G., & Saravanan, P. (2013). Various fabrication methods of porous ceramic supports for membrane applications. *Reviews in Chemical Engineering, 29*(5), 357-383.

Mushtaq, F., Zahid, M., Bhatti, I. A., Nasir, S., & Hussain, T. (2019). Possible applications of coal fly ash in wastewater treatment. *Journal of environmental management, 240*, 27-46.

Nabila, Ahmad, M., Althobaiti, A. T., Ali, W., Masood, K., Ramadan, M. F., . . . Asif, S. (2023). Membrane-processed honey samples for pollen characterization with health benefits. *Chemosphere, 319*, 137994. doi:https://doi.org/10.1016/j.chemosphere.2023.137994

Nagajyothi, S., Swetha, Y., Neeharika, J., Suresh, P., Ramarao, N. J. I. J. f. A. R., & Development. (2017). Hyphenated techniques-a comprehensive review. *2*(4).

Nariyan, E., Aghababaei, A., & Sillanpää, M. (2017). Removal of pharmaceutical from water with an electrocoagulation process; effect of various parameters and studies of isotherm and kinetic. *Separation and Purification Technology, 188*, 266-281. doi:https://doi.org/10.1016/j.seppur.2017.07.031

Nasirian, M., Lin, Y. P., Bustillo-Lecompte, C. F., & Mehrvar, M. (2018). Enhancement of photocatalytic activity of titanium dioxide using non-metal doping methods under visible light: a review. *International Journal of Environmental Science and Technology, 15*(9), 2009-2032. doi:10.1007/s13762-017-1618-2

Nishihora, R. K., Rachadel, P. L., Quadri, M. G. N., & Hotza, D. (2018). Manufacturing porous ceramic materials by tape casting—A review. *Journal of the European Ceramic Society, 38*(4), 988-1001.

Nsiah-Gyambibi, R., Sokama-Neuyam, Y., Boakye, P., Ampomah, W., Aggrey, W., & Wang, S. (2023). Valorization of coal fly ash (CFA): a multi-industry review. *International Journal of Environmental Science and Technology*, 1-16.

Nthunya, L. N., Bopape, M. F., Mahlangu, O. T., Mamba, B. B., Van der Bruggen, B., Quist-Jensen, C. A., & Richards, H. (2022). Fouling, performance and cost analysis of membrane-based water desalination technologies: A critical review. *Journal of environmental management, 301*, 113922.

Nugteren, H. W., Janssen-Jurkovícová, M., & Scarlett, B. (2002). Removal of heavy metals from fly ash and the impact on its quality. *Journal of Chemical Technology & Biotechnology, 77*(3), 389-395. doi:https://doi.org/10.1002/jctb.600

Nunes, B., Antunes, S. C., Gomes, R., Campos, J. C., Braga, M. R., Ramos, A. S., & Correia, A. T. (2015). Acute Effects of Tetracycline Exposure in the Freshwater Fish Gambusia holbrooki: Antioxidant Effects, Neurotoxicity and Histological Alterations. *Archives of Environmental Contamination and Toxicology, 68*(2), 371-381. doi:10.1007/s00244-014-0101-z

Nyakairu, G. W. A., Koeberl, C., & Kurzweil, H. (2001). The Buwambo kaolin deposit in central Uganda: Mineralogical and chemical composition. *Geochemical Journal, 35*(4), 245-256. doi:DOI 10.2343/geochemj.35.245

Oaks, J. L., Gilbert, M., Virani, M. Z., Watson, R. T., Meteyer, C. U., Rideout, B. A., . . . Khan, A. A. (2004). Diclofenac residues as the cause of vulture population decline in Pakistan. *Nature, 427*(6975), 630-633. doi:10.1038/nature02317

Obotey Ezugbe, E., & Rathilal, S. (2020). Membrane Technologies in Wastewater Treatment: A Review. *Membranes (Basel), 10*(5), 89. doi:10.3390/membranes10050089

Olatunde, O. C., Kuvarega, A. T., & Onwudiwe, D. C. (2020). Photo enhanced degradation of contaminants of emerging concern in waste water. *Emerging Contaminants, 6*, 283-302. doi:10.1016/j.emcon.2020.07.006

Oluwole, A. O., & Olatunji, O. S. (2022). Photocatalytic degradation of tetracycline in aqueous systems under visible light irridiation using needle-like SnO2 nanoparticles anchored on exfoliated g-C3N4. *Environmental Sciences Europe, 34*(1), 1-14. doi:ARTN 5 10.1186/s12302-021-00588-7

Openshaw, S. C. (1992). *Utilization of coal fly ash*. Retrieved from

Oun, A., Tahri, N., Mahouche-Chergui, S., Carbonnier, B., Majumdar, S., Sarkar, S., . . . Amar, R. B. (2017). Tubular ultrafiltration ceramic membrane based on titania nanoparticles immobilized

on macroporous clay-alumina support: elaboration, characterization and application to dye removal. *Separation and Purification Technology, 188*, 126-133.

Pagana, A. E., Sklari, S. D., Kikkinides, E. S., & Zaspalis, V. T. (2008). Microporous ceramic membrane technology for the removal of arsenic and chromium ions from contaminated water. *Microporous and Mesoporous Materials, 110*(1), 150-156. doi:https://doi.org/10.1016/j.micromeso.2007.10.013

Pandis, P. K., Kalogirou, C., Kanellou, E., Vaitsis, C., Savvidou, M. G., Sourkouni, G., . . . Argirusis, C. (2022). Key Points of Advanced Oxidation Processes (AOPs) for Wastewater, Organic Pollutants and Pharmaceutical Waste Treatment: A Mini Review. *Chemengineering, 6*(1), 8. doi:ARTN 8 10.3390/chemengineering6010008

Park, S. H., Kim, T., Kadam, A. N., Bathula, C., Ghfar, A. A., Kim, H., . . . Interfaces. (2022). Synergistic photocatalysis of Z-scheme type Fe2O3/g-C3N4 heterojunction coupled with reduced graphene oxide. *30*, 101910.

Patel, M., Kumar, R., Kishor, K., Mlsna, T., Pittman, C. U., Jr., & Mohan, D. (2019). Pharmaceuticals of Emerging Concern in Aquatic Systems: Chemistry, Occurrence, Effects, and Removal Methods. *Chem Rev, 119*(6), 3510-3673. doi:10.1021/acs.chemrev.8b00299

Peng, W., Liu, Y., Lin, M., Liu, Y., Zhu, C., Sun, L., & Gui, H. (2022). Toxicity of coal fly ash and coal gangue leachate to Daphnia magna: Focusing on typical heavy metals. *Journal of Cleaner Production, 330*, 129946.

Peng, X., Jiao, B., Yu, L., Li, D., & Yang, K. (2011). Enhanced Electrokinetic Removal of Heavy Metals in MSWI Fly Ash Assisted by Cation Exchange Membranes. *Applied Mechanics and Materials, 84-85*. doi:10.4028/www.scientific.net/AMM.84-85.626

Plakas, K. V., Mantza, A., Sklari, S. D., Zaspalis, V. T., & Karabelas, A. J. (2019). Heterogeneous Fenton-like oxidation of pharmaceutical diclofenac by a catalytic iron-oxide ceramic microfiltration membrane. *Chemical Engineering Journal, 373*, 700-708. doi:10.1016/j.cej.2019.05.092

Priya, S. S., & Radha, K. V. (2017). A Review on the Adsorption Studies of Tetracycline onto Various Types of Adsorbents. *Chemical Engineering Communications, 204*(8), 821-839. doi:10.1080/00986445.2015.1065820

Qian, C., Hu, K., Wang, H., Nie, L., Feng, Q., Lu, Z., . . . Lu, K. (2022). The effect of particle size distribution on the microstructure and properties of Al2O3 ceramics formed by stereolithography. *Ceramics International, 48*(15), 21641-21650.

Qing, W., Liu, F., Yao, H., Sun, S., Chen, C., & Zhang, W. (2020). Functional catalytic membrane development: A review of catalyst coating techniques. *Adv Colloid Interface Sci, 282*, 102207. doi:10.1016/j.cis.2020.102207

Qing, W. H., Li, X. H., Shao, S. L., Shi, X. N., Wang, J. Q., Feng, Y., . . . Zhang, W. D. (2019). Polymeric catalytically active membranes for reaction-separation coupling: A review. *Journal of Membrane Science, 583*, 118-138. doi:10.1016/j.memsci.2019.04.053

Radeva, J., Roth, A. G., Göbbert, C., Niestroj-Pahl, R., Dähne, L., Wolfram, A., & Wiese, J. (2021). Hybrid Ceramic Membranes for the Removal of Pharmaceuticals from Aqueous Solutions. *Membranes, 11*(4), 280.

Raj, K. P., Sadaiyandi, K., Kennedy, A., Sagadevan, S., Chowdhury, Z. Z., Bin Johan, M. R., . . . Bala, R. R. (2018). Influence of Mg Doping on ZnO Nanoparticles for Enhanced Photocatalytic Evaluation and Antibacterial Analysis. *Nanoscale Research Letters, 13*(1), 1-13. doi:ARTN 229 10.1186/s11671-018-2643-x

Rani, C. N., Karthikeyan, S., & Doss, S. P. A. (2021). Photocatalytic ultrafiltration membrane reactors in water and wastewater treatment-A review. *Chemical Engineering and Processing-Process Intensification, 165*, 108445. doi:ARTN 108445 10.1016/j.cep.2021.108445

Rani, P., Mishra, A. R., Deveci, M., & Antucheviciene, J. (2022). New complex proportional assessment approach using Einstein aggregation operators and improved score function for interval-valued Fermatean fuzzy sets. *Computers & Industrial Engineering, 169*, 108165.

Rao, A., Kaushik, A., Kuppurangan, G., & Selvaraj, G. (2023). Characterization and application of novel fly ash blended ceramic membrane in MFC for low-cost and sustainable wastewater treatment and power generation. *Environmental Science and Pollution Research, 30*(16), 45872-45887. doi:10.1007/s11356-023-25327-8

Riaz, S., & Park, S. J. (2020). An overview of TiO2-based photocatalytic membrane reactors for water and wastewater treatments. *Journal of Industrial and Engineering Chemistry, 84*, 23-41. doi:10.1016/j.jiec.2019.12.021

Saber, E., Ali, M., & El-Sheikh, A. (2018). Provenance studies of Kalabsha kaolin deposits, Egypt: a petrographical and geochemical approach. *Arabian Journal of Geosciences, 11*(13), 1-15. doi:ARTN 339 10.1007/s12517-018-3690-4

Sakamoto, H., Hafuka, A., Tsuchiya, T., & Kimura, K. (2022). Intensive routine cleaning for mitigation of fouling in flat-sheet ceramic membranes used for drinking water production: Unique characteristics of resulting foulants. *Separation and Purification Technology, 301*, 121950.

Sakarkar, S., Muthukumran, S., & Jegatheesan, V. (2020). Factors affecting the degradation of remazol turquoise blue (RTB) dye by titanium dioxide (TiO2) entrapped photocatalytic membrane. *Journal of Environmental Management, 272*, 111090. doi:10.1016/j.jenvman.2020.111090

Salleh, W. N. W., Ismail, A. F., Matsuura, T., & Abdullah, M. S. (2011). Precursor selection and process conditions in the preparation of carbon membrane for gas separation: a review. *Separation & Purification Reviews, 40*(4), 261-311.

Samadi, A., Gao, L., Kong, L., Orooji, Y., & Zhao, S. (2022). Waste-derived low-cost ceramic membranes for water treatment: Opportunities, challenges and future directions. *Resources, Conservation and Recycling, 185*, 106497.

Samaei, S. M., Gato-Trinidad, S., & Altaee, A. (2018). The application of pressure-driven ceramic membrane technology for the treatment of industrial wastewaters–A review. *Separation and Purification Technology, 200*, 198-220.

Saranya, R., Arthanareeswaran, G., Ismail, A., Reddy, N. L., Shankar, M., & Kweon, J. (2017). Efficient rejection of organic compounds using functionalized ZSM-5 incorporated PPSU mixed matrix membrane. *RSC advances, 7*(25), 15536-15552.

Saravanan, A., Kumar, P. S., Jeevanantham, S., Anubha, M., & Jayashree, S. (2022). Degradation of toxic agrochemicals and pharmaceutical pollutants: Effective and alternative approaches toward photocatalysis. *Environ Pollut, 298*, 118844. doi:10.1016/j.envpol.2022.118844

Sarkar, K. K., Majee, S., Pathak, U., Polepali, S., Haider, G., Mandal, D. D., & Mandal, T. (2019). Development of an integrated treatment strategy for removal of ondansetron using simultaneous adsorption, oxidation and bioremediation technique. *Journal of Environmental Chemical Engineering, 7*(2), 103020. doi:ARTN 103020 10.1016/j.jece.2019.103020

Sarkar, S., Bandyopadhyay, S., Larbot, A., & Cerneaux, S. (2012). New clay–alumina porous capillary supports for filtration application. *Journal of Membrane Science, 392*, 130-136.

Sarp, S., & Hilal, N. (2018). *Membrane-based salinity gradient processes for water treatment and power generation*: Elsevier.

Shao, N., Tang, S., Li, S., Chen, H., & Zhang, Z. (2020). Defective analcime/geopolymer composite membrane derived from fly ash for ultrafast and highly efficient filtration of organic pollutants. *Journal of hazardous materials, 388*, 121736.

Shearer, C. R. (2014). *The productive reuse of coal, biomass and co-fired fly ash.* Georgia Institute of Technology,

Shehata, N., Egirani, D., Olabi, A., Inayat, A., Abdelkareem, M. A., Chae, K.-J., & Sayed, E. T. (2023). Membrane-based water and wastewater treatment technologies: Issues, current trends, challenges, and role in achieving sustainable development goals, and circular economy. *Chemosphere, 320*, 137993.

Shi, R., Zhao, Y. X., Waterhouse, G. I. N., Zhang, S., & Zhang, T. R. (2019). Defect Engineering in Photocatalytic Nitrogen Fixation. *Acs Catalysis, 9*(11), 9739-9750. doi:10.1021/acscatal.9b03246

Shi, Y., Huang, J., Zeng, G., Cheng, W., & Hu, J. (2019). Photocatalytic membrane in water purification: is it stepping closer to be driven by visible light? *Journal of Membrane Science, 584*, 364-392. doi:10.1016/j.memsci.2019.04.078

Simonič, M. (2019). Membrane surface properties and their effects on real waste oil-in-water emulsion ultrafiltration. *Water SA, 45*(3), 367-373.

Singh, G., & Bulasara, V. K. (2015). Preparation of low-cost microfiltration membranes from fly ash. *Desalination and Water Treatment, 53*(5), 1204-1212.

Singh, S., Garg, R., Jana, A., Bathula, C., Naik, S., & Mittal, M. J. C. I. (2022). Current developments in nanostructurally engineered metal oxide for removal of contaminants in water.

Sonawane, S., Thakur, P., Sonawane, S. H., & Bhanvase, B. A. (2021). Nanomaterials for membrane synthesis: Introduction, mechanism, and challenges for wastewater treatment. In *Handbook of Nanomaterials for Wastewater Treatment* (pp. 537-553): Elsevier.

Song, L., Zhu, B., Jegatheesan, V., Gray, S. R., Duke, M. C., & Muthukumaran, S. (2019). Effect of hybrid photocatalysis and ceramic membrane filtration process for humic acid degradation. In *Water Scarcity and Ways to Reduce the Impact* (pp. 95-113): Springer.

Strzałkowska, E. (2021). Morphology, chemical and mineralogical composition of magnetic fraction of coal fly ash. *International Journal of Coal Geology, 240*, 103746. doi:10.1016/j.coal.2021.103746

Su, Z. Y., Fang, F., Li, X., Han, W. J., Liu, X. L., & Chang, K. (2022). Synergistic surface oxygen defect and bulk Ti3+ defect engineering on SrTiO3 for enhancing photocatalytic overall water

splitting. *Journal of Colloid and Interface Science, 626*, 662-673. doi:10.1016/j.jcis.2022.06.109

Suresh, K. (2021). Recycling of fly ash for development of value added products. *Materials Today: Proceedings, 46*, 5666-5674.

Suresh, K., Pugazhenthi, G., & Uppaluri, R. (2016). Fly ash based ceramic microfiltration membranes for oil-water emulsion treatment: Parametric optimization using response surface methodology. *Journal of Water Process Engineering, 13*, 27-43.

Suresh, K., Pugazhenthi, G., & Uppaluri, R. (2017). Preparation and characterization of hydrothermally engineered TiO2-fly ash composite membrane. *Frontiers of Chemical Science and Engineering, 11*(2), 266-279. doi:10.1007/s11705-017-1608-4

Tahiri, A., Messaoudi, L., Tijani, N., Zerrouk, M. H., & Messaoudi, M. (2021). Manufacture and characterization of flat membrane supports based on Moroccan Rif clay. *Materials Today: Proceedings, 43*, 209-215.

Tang, J., Chen, Z. L., Yu, X. L., & Tang, W. Z. (2022). Rare earth elements (lanthanum, cerium and erbium) doped black oxygen deficient Bi2O3-Bi2O3-x as novel photocatalysts enhanced photocatalytic performance. *Journal of Rare Earths, 40*(7), 1053-1062. doi:10.1016/j.jre.2021.07.008

Tao, S., Xu, Y.-D., Gu, J.-Q., Abadikhah, H., Wang, J.-W., & Xu, X. (2018). Preparation of high-efficiency ceramic planar membrane and its application for water desalination. *Journal of Advanced Ceramics, 7*, 117-123.

Taoufik, N., Boumya, W., Achak, M., Sillanpää, M., & Barka, N. (2021). Comparative overview of advanced oxidation processes and biological approaches for the removal pharmaceuticals. *Journal of Environmental Management, 288*, 112404. doi:https://doi.org/10.1016/j.jenvman.2021.112404

Trawinski, J., & Skibinski, R. (2017). Studies on photodegradation process of psychotropic drugs: a review. *Environ Sci Pollut Res Int, 24*(2), 1152-1199. doi:10.1007/s11356-016-7727-5

Tufail, A., Price, W. E., & Hai, F. I. (2020). Impact of Inorganic Ions and Organic Matter on the Removal of Trace Organic Contaminants by Combined Direct Contact Membrane Distillation–UV Photolysis. *Membranes*, *10*(12), 428.

Urase, T., Kagawa, C., & Kikuta, T. (2005). Factors affecting removal of pharmaceutical substances and estrogens in membrane separation bioreactors. *Desalination, 178*(1-3), 107-113. doi:10.1016/j.desal.2004.11.031

Usman, J., Othman, M. H. D., Ismail, A. F., Rahman, M. A., Jaafar, J., Raji, Y. O., . . . Said, K. A. M. (2021). An overview of superhydrophobic ceramic membrane surface modification for oil-water separation. *Journal of Materials Research and Technology, 12*, 643-667.

Varma, K. S., Tayade, R. J., Shah, K. J., Joshi, P. A., Shukla, A. D., & Gandhi, V. G. (2020). Photocatalytic degradation of pharmaceutical and pesticide compounds (PPCs) using doped TiO2 nanomaterials: A review. *Water-Energy Nexus, 3*, 46-61. doi:10.1016/j.wen.2020.03.008

Vasanth, D., Uppaluri, R., & Pugazhenthi, G. (2011). Influence of sintering temperature on the properties of porous ceramic support prepared by uniaxial dry compaction method using low-cost raw materials for membrane applications. *Separation Science and Technology, 46*(8), 1241-1249.

Vassilev, S. V., & Vassileva, C. G. (2007). A new approach for the classification of coal fly ashes based on their origin, composition, properties, and behaviour. *Fuel, 86*(10-11), 1490-1512.

Velempini, T., Prabakaran, E., & Pillay, K. (2021). Recent developments in the use of metal oxides for photocatalytic degradation of pharmaceutical pollutants in water-a review. *Materials Today Chemistry, 19*, 100380. doi:ARTN 100380 10.1016/j.mtchem.2020.100380

Wang, C., Xu, G., Gu, X., Gao, Y., & Zhao, P. (2021). High value-added applications of coal fly ash in the form of porous materials: A review. *Ceramics International, 47*(16), 22302-22315.

Wang, J., Chen, R. S., Xiang, L., & Komarneni, S. (2018). Synthesis, properties and applications of ZnO nanomaterials with oxygen vacancies: A review. *Ceramics International, 44*(7), 7357-7377. doi:10.1016/j.ceramint.2018.02.013

Wang, X. L., Li, Y. L., Yu, H. T., Yang, F. L., Tang, C. Y. Y., Quan, X., & Dong, Y. C. (2020). High-flux robust ceramic membranes functionally decorated with nano-catalyst for emerging micro-pollutant removal from water. *Journal of Membrane Science, 611*, 118281. doi:ARTN 118281 10.1016/j.memsci.2020.118281

Warsinger, D. M., Swaminathan, J., Guillen-Burrieza, E., & Arafat, H. A. (2015). Scaling and fouling in membrane distillation for desalination applications: A review. *Desalination, 356*, 294-313.

Water, U. J. T. U. N. W. W. D. R., & UNESCO: Paris, F. (2020). Water and climate change.

Wei, Z., Hou, J., & Zhu, Z. (2016). High-aluminum fly ash recycling for fabrication of cost-effective ceramic membrane supports. *Journal of Alloys and Compounds, 683*, 474-480.

Wilkinson, J. L., Boxall, A. B. A., Kolpin, D. W., Leung, K. M. Y., Lai, R. W. S., Galban-Malagon, C., . . . Teta, C. (2022). Pharmaceutical pollution of the world's rivers. *Proc Natl Acad Sci U S A, 119*(8), e2113947119. doi:10.1073/pnas.2113947119

Wu, H., Xu, X., Shi, L., Yin, Y., Zhang, L. C., Wu, Z., . . . Sun, H. (2019). Manganese oxide integrated catalytic ceramic membrane for degradation of organic pollutants using sulfate radicals. *Water Res, 167*, 115110. doi:10.1016/j.watres.2019.115110

Wu, S. Q., Li, X. Y., Tian, Y. Q., Lin, Y., & Hu, Y. H. (2021). Excellent photocatalytic degradation of tetracycline over black anatase-TiO2 under visible light. *Chemical Engineering Journal, 406*, 126747. doi:ARTN 126747 10.1016/j.cej.2020.126747

Xie, X., Zhou, Q., Lin, D., Guo, J., & Bao, Y. (2011). Toxic effect of tetracycline exposure on growth, antioxidative and genetic indices of wheat (Triticum aestivum L.). *Environmental Science and Pollution Research, 18*(4), 566-575.

Xiong, J.-Q., Kurade, M. B., & Jeon, B.-H. J. T. i. b. (2018). Can microalgae remove pharmaceutical contaminants from water? , *36*(1), 30-44.

Xu, D.-m., Wang, Y.-h., & Rao, G.-w. (2013). [Cellular response of freshwater green algae to the toxicity of tetracycline antibiotics]. *Huan jing ke xue= Huanjing kexue, 34*(9), 3386-3390. Retrieved from http://europepmc.org/abstract/MED/24288980

Xu, F., Wei, M., Zhang, X., Song, Y., Zhou, W., & Wang, Y. J. R. (2019). How pore hydrophilicity influences water permeability? , *2019*.

Xu, X., Liu, X., Wua, J., Ma, S., Liu, S., & Chen, T. (2022). Effect of SiC Particle Size on Properties of SiC Porous Ceramics. *Journal of Wuhan University of Technology-Mater. Sci. Ed., 37*(1), 13-22.

Yahaya, S., Jikan, S. S., Badarulzaman, N. A., & Adamu, A. D. J. T. N. P. o. S. (2017). Chemical composition and particle size analysis of kaolin. *3*(10), 1001-1004.

Yang, H. (2021). A short review on heterojunction photocatalysts: Carrier transfer behavior and photocatalytic mechanisms. *Materials Research Bulletin, 142*, 111406. doi:ARTN 111406 10.1016/j.materresbull.2021.111406

Yang, H., Yang, B., Chen, W., & Yang, J. J. C. (2022). Preparation and Photocatalytic Activities of TiO2-Based Composite Catalysts. *12*(10), 1263.

Yang, K., Jin, Y., Yue, Q., Zhao, P., Gao, Y., Wu, S., & Gao, B. (2017). Comparison of two modified coal ash ferric-carbon micro-electrolysis ceramic media for pretreatment of tetracycline wastewater. *Environmental Science and Pollution Research, 24*(13), 12462-12473. doi:10.1007/s11356-017-8841-8

Yi, Q., Gao, Y., Zhang, H., Zhang, H., Zhang, Y., & Yang, M. (2016). Establishment of a pretreatment method for tetracycline production wastewater using enhanced hydrolysis. *Chemical Engineering Journal*, *300*, 139-145. doi:https://doi.org/10.1016/j.cej.2016.04.120

Zakria, H. S., Othman, M. H. D., Kamaludin, R., Sheikh Abdul Kadir, S. H., Kurniawan, T. A., & Jilani, A. (2021). Immobilization techniques of a photocatalyst into and onto a polymer membrane for photocatalytic activity. *RSC Adv*, *11*(12), 6985-7014. doi:10.1039/d0ra10964a

Zeh, J. A., Bonilla, M. M., Adrian, A. J., Mesfin, S., & Zeh, D. W. (2012). From father to son: transgenerational effect of tetracycline on sperm viability. *Scientific Reports, 2*(1), 375. doi:10.1038/srep00375

Zhang, B., Mao, X., Tang, X. M., Tang, H. L., Zhang, B., Shen, Y., & Shi, W. X. (2022). Pre-coagulation for membrane fouling mitigation in an aerobic granular sludge membrane bioreactor: A comparative study of modified microbial and organic flocculants. *Journal of Membrane Science, 644*, 120129. doi:ARTN 120129 10.1016/j.memsci.2021.120129

Zhang, J., Yan, M., Sun, G., & Liu, K. (2021a). An environment-friendly Fe3O4@CFAS porous ceramic: Adsorption of Cu(II) ions and process optimisation using response surface methodology. *Ceramics International, 47*(6), 8256-8264. doi:https://doi.org/10.1016/j.ceramint.2020.11.185

Zhang, J., Yan, M., Sun, G., & Liu, K. (2021b). Simultaneous removal of Cu(II), Cd(II), Cr(VI), and rhodamine B in wastewater using TiO2 nanofibers membrane loaded on porous fly ash ceramic support. *Separation and Purification Technology, 272*, 118888. doi:https://doi.org/10.1016/j.seppur.2021.118888

Zhang, L., Song, X., Liu, X., Yang, L., Pan, F., & Lv, J. (2011). Studies on the removal of tetracycline by multi-walled carbon nanotubes. *Chemical Engineering Journal*, *178*, 26-33.

Zhang, M. L., Yang, Y., An, X. Q., & Hou, L. A. (2021). A critical review of g-C3N4-based photocatalytic membrane for water purification. *Chemical Engineering Journal*, *412*, 128663. doi:ARTN 128663 10.1016/j.cej.2021.128663

Zhang, Q., Cheng, J., & Xin, Q. (2015). Effects of tetracycline on developmental toxicity and molecular responses in zebrafish (Danio rerio) embryos. *Ecotoxicology, 24*(4), 707-719. doi:10.1007/s10646-015-1417-9

Zhang, Q., Wang, H., Fan, X. F., Lv, F. H., Chen, S., & Quan, X. (2016). Fabrication of TiO2 nanofiber membranes by a simple dip-coating technique for water treatment. *Surface & Coatings Technology*, *298*, 45-52. doi:10.1016/j.surfcoat.2016.04.054

Zhang, Y., Tan, Y., Sun, R., & Zhang, W. (2023). Preparation of Ceramic Membranes and Their Application in Wastewater and Water Treatment. *Water*, *15*(19), 3344.

Zhang, Z., Yang, J., Qi, R., Huang, J., Chen, H., & Zhang, H. (2023). Development of Hydrophobic Coal-Fly-Ash-Based Ceramic Membrane for Vacuum Membrane Distillation. *Materials*, *16*(8), 3153.

Zhao, F., Yang, L., Chen, L., Li, S., & Sun, L. (2019). Bioaccumulation of antibiotics in crops under long-term manure application: Occurrence, biomass response and human exposure. *Chemosphere*, *219*, 882-895. doi:https://doi.org/10.1016/j.chemosphere.2018.12.076

Zhou, H., Bhattarai, R., Li, Y., Si, B., Dong, X., Wang, T., & Yao, Z. (2022). Towards sustainable coal industry: Turning coal bottom ash into wealth. *Science of the Total Environment*, *804*, 149985.

Zhou, W., Wu, P., Zhang, L., Zhu, D., Zhao, X., & Cai, Y. (2021). Fabrication and performance of reticular ceramic fiber membranes by freeze casting using a gel network. *Journal of the European Ceramic Society*, *41*(13), 6586-6595.

Zhu, L., Dong, Y., Li, L., Liu, J., & You, S.-J. (2015). Coal fly ash industrial waste recycling for fabrication of mullite-whisker-structured porous ceramic membrane supports. *RSC advances*, *5*(15), 11163-11174.

Zhu, L., Ji, J., Wang, S., Xu, C., Yang, K., & Xu, M. (2018). Removal of Pb(II) from wastewater using Al2O3-NaA zeolite composite hollow fiber membranes synthesized from solid waste coal fly ash. *Chemosphere*, *206*, 278-284. doi:https://doi.org/10.1016/j.chemosphere.2018.05.001

Zhu, L., Rakesh, K. P., Xu, M., & Dong, Y. (2019). Ceramic-based composite membrane with a porous network surface featuring a highly stable flux for drinking water purification. *Membranes*, *9*(1), 5.

Zielińska, A. (2018). Methods for regeneration and storage of ceramic membranes. *Acta Innovations*(28), 72-81.

Zou, D., Fan, W., Xu, J., Drioli, E., Chen, X., Qiu, M., & Fan, Y. (2021). One-step engineering of low-cost kaolin/fly ash ceramic membranes for efficient separation of oil-water emulsions. *Journal of Membrane Science*, *621*, 118954. doi:https://doi.org/10.1016/j.memsci.2020.118954

Zou, D., Xu, J., Chen, X., Drioli, E., Qiu, M., & Fan, Y. (2019). A novel thermal spraying technique to fabricate fly ash/alumina composite membranes for oily emulsion and spent tin wastewater treatment. *Separation and Purification Technology*, *219*, 127-136. doi:https://doi.org/10.1016/j.seppur.2019.02.051

Zuo, X., Zhang, S., Ma, G., Lv, Y., & Li, P. (2020). *Analysis of ceramic membrane fouling behavior and cleaning technology*. Paper presented at the E3S Web of Conferences.

CHAPTER 3

Photocatalytic degradation of tetracycline using surface defective black TiO_2-ZnO heterojunction photocatalyst under visible light

3.0 Introduction

The rising global population, increasing outbreaks of diseases, and high demand for food production have resulted in the increased usage of pharmaceutical products (Rohr *et al.*, 2019). These products include antibiotics, and among them, tetracycline is one of the most used. Its wide consumption compared to other antibiotics used by humans and animals is attributed to its benefit, for example, tetracycline improves the growth rate in aquaculture and poultry industries (Andronic & Enesca, 2020; Daghrir & Drogui, 2013; Lyu *et al.*, 2020). Despite its huge benefits, the discharge of tetracycline-contaminated effluents into the aquatic environment has given rise to persistent ecological contamination, antibiotic resistance, and eco-toxicological effects on plants and aquatic life (Bilal *et al.*, 2020; Polianciuc *et al.*, 2020). The consequence of these is the upsetting of the food chain. In humans, the effects of excess consumption of tetracycline include teeth staining, skin side effects, oesophagus damage, and gastrointestinal disturbances (Amangelsin *et al.*, 2023; Faus-Matoses *et al.*, 2017).

Generally, pharmaceutical contaminants in the environment are a challenge to manage because (1) conventional wastewater remediation methods are unable to remove them completely, (2) they have detrimental effects even at low concentrations, and (3) their rate of discharge into the environment exceeds their rates of degradation. This is because they are poorly absorbed by humans, livestock, and poultry; thus discharged as unmetabolized active substances, (4) most pharmaceutical pollutants such as unused drugs, expired drugs, agricultural and aquaculture pharmaceuticals can easily enter water bodies directly (Ajiboye *et al.*, 2023; OECD, 2019; Phoon *et al.*, 2020). Therefore, it is important to come up with feasible, very effective, environmental-friendly, and affordable methods that can mineralize tetracycline from wastewater to conserve water resources and achieve the sustainable development goal 6.

Several methods such as membrane technology (Heberer *et al.*, 2008),(Li *et al.*, 2009), bioremediation (Nguyen *et al.*, 2019), advanced oxidation processes (AOPs), electrocoagulation (Paredes *et al.*, 2019), adsorption (Ouyang *et al.*, 2020), and hybrid techniques (Sawunyama *et al.*, 2023) have been used for the removal of pharmaceuticals from wastewaters. However, they all have different drawbacks and advantages. One of the most convenient methods for the complete removal of these pharmaceuticals is

the advanced oxidation process, due to its high oxidation effectiveness and no generation of secondary pollutants. The advanced oxidation process is applicable in different processes including photocatalysis, photolysis, fenton oxidation, electrochemical, ozone, sonolysis, etc (Saravanan *et al.*, 2022). Photocatalysis by metal oxide nanoparticles, zeolites, metal-organic frameworks and nanorods has since attracted much interest due to their great potential to utilize the complete solar spectrum in photocatalytic reactions. Among them, metal oxide nanoparticles are one of the most efficient and effective AOP that is effective for the removal of tetracycline from wastewater. Examples of metal oxide nanoparticles that have been reported include ZnO, Fe_2O_3, TiO_2, CuO, MgO, SiO_2, and SnO_2. Out of the several metal oxides nanoparticles, ZnO and TiO_2 have been mostly reported due to their ease of synthesis, chemical stability, cost-effectiveness, long-standing photostability, non-corrosive property, and non-toxicity (Goncalves *et al.*, 2021). However, these nanomaterials utilize visible light inefficiently because of their wide band gap energies and fast recombination process of the photogenerated electron/hole pairs, which subsequently affects photocatalytic efficiency(Cao *et al.*, 2023). Therefore, several studies have been carried out to improve the photocatalytic efficiency of metal oxide nanoparticles such as ZnO and TiO_2 through the reduction of recombination rate and shifting of the optical response from UV to the visible spectral range because visible light accounts for 45% of the solar energy (Han *et al.*, 2019)**.** These strategies include (1) heterojunction fabrications, (2) defect engineering, (3) doping with various elements and (4) co-catalyst loading (Apostolescu *et al.*, 2023; Arora *et al.*, 2022). Most published research papers on ZnO and TiO_2 technologies in recent years, focused on single photocatalytic enhancement technique. For example, Apostolescu *et al.*(Apostolescu et al., 2023) studied the degradation of chlortetracycline and ceftriaxone using heterojunction of CeO_2/ZnO. The results showed an increase in the degradation efficiency of the antibiotics by the heterojunction system compared to the CeO_2 and ZnO tested separately. Andronic *et al.*(Andronic & Enesca, 2020) reported the synthesis of black TiO_2 with Ti^{3+} defects and oxygen vacancies via defect engineering. The synthesized nanomaterial exhibited very good photocatalytic degradation of organic pollutants compared to pristine TiO_2. However, very few studies reported the combination of photocatalytic enhancement techniques of both materials in single system. Therefore, in this current study, the formation of heterojunction of TiO_2 and ZnO nanoparticles together with the engineering of their surface defects have been synergistically employed to enhance the photocatalytic degradation of tetracycline (TC).

The surface defected heterostructure was obtained by the conventional sol-gel approach coupled with aluminium foil assisted $NaBH_4$ reduction. The performance of the Black ZnO, Black TiO_2, and Black TiO_2-ZnO samples was studied under direct light. The process variables such as the initial concentration of tetracycline and the catalyst loading were explored to establish the performance of the nanocomposite in the TC degradation process. The surface defected heterojunction photocatalytic nanomaterial is expected to have low bandgap energy and thus high degradation rate in direct sunlight.

This study is relevant with respect to the development of enhanced novel photocatalysts for the degradation of antibiotics.

3.1 Experimental

3.1.1 Materials

Titanium tetra-isopropoxide [$Ti(OCH(CH_3)_2)_4$, 98%], zinc acetate [$Zn(CH_3COO)_2{\cdot}2H_2O$, ≥98%,], sodium hydroxide [NaOH, 98%], absolute ethanol [CH_3CH_2OH, >99%], sodium borohydride, [$NaBH_4$, >98%], and hydrochloric acid [HCl, 28%] were purchased from Merck, South Africa. All the chemicals were of analytical grade. The nanomaterials were prepared by following already reported procedures (Ali *et al.*, 2021; Rajaraman *et al.*, 2022).

3.1.2 Synthesis of ZnO nanoparticles

A conventional sol-gel approach was used to synthesize ZnO nanoparticles from zinc acetate dihydrate and sodium hydroxide. Briefly, about 10 g of $Zn(CH_3COO)_2{\cdot}2H_2O$ was mixed with 200 mL of distilled water and stirred continuously for 20 min at 35℃. Thereafter, 0.8 M NaOH was added in dropwise to the mixture to adjust the pH. The resultant mixture was then stirred for 2 h, giving rise to a white sol. After that the sol was aged for 24 h to convert it to a white gel, which was centrifuged, and then washed several times with distilled water. The obtained powder was dried for 12 h at 150 ℃ and finally calcinated at 400 ℃ in the muffle furnace for 3 h.

3.1.3 Synthesis of TiO_2 nanoparticles

A conventional sol-gel approach was used to synthesize TiO_2 nanoparticles from titanium tetra-isopropoxide and absolute ethanol. About 30 mL of [$Ti(OCH(CH_3)_2)_4$, 98%] was mixed with 75 mL of CH_3CH_2OH and stirred well for 45 min. Then, 30 mL of distilled water was introduced in dropwise to initiate the ionization process. The resultant mixture was stirred for 45 min, to afford a white sol, which was aged for 24 h to form a white gel. The gel product was centrifuged and washed several times with distilled water. The obtained powder was dried for 12 h at 150 ℃ and finally calcinated at 500 ℃ in the muffle furnace for 3 h.

3.1.4 Synthesis of TiO_2-ZnO heterojunction nanoparticles

The synthesized ZnO and TiO_2 sol were mixed and thoroughly stirred on a magnetic stirrer plate for 4 h at 25 ℃. The formed TiO_2-ZnO precipitate was aged for 24 h, then centrifuged and washed with distilled water. The obtained powder was dried for 12 h at 150 ℃ and followed by calcination at 500 ℃ for 3 h.

3.1.5 Synthesis of $BTiO_2$, BZnO and $BTiO_2$-ZnO nanoparticles

Firstly, 2 g of each as-prepared material (pristine ZnO, pristine TiO_2 and TiO_2-ZnO nanoparticles) was mixed with about 0.4 g of $NaBH_4$ powder, and the mixture was tightly wrapped in an aluminium foil. The resultant aluminium foils were calcinated in a muffle furnace at three different temperatures of 300, 350 and 400 ºC for 1 h. The enclosed samples were cooled down to room temperature, washed with methanol, and several times with deionized water to remove any sodium and borate impurities. The washed samples were then dried at 100 ℃ overnight.

3.1.6 Characterization of synthesized nanocomposites

Functional groups of the synthesized materials were analysed on a Bruker alpha-P FTIR spectrophotometer. The XRD analysis was carried out on a Bruker D8 Advance X-ray diffractometer (Karlsruhe, Germany). The diffractometer has single-wavelength Cu Kα radiation (λ = 1.546060 Å). JEOL 2100 JEM Transmission electron microscopy (TEM) was used to evaluate the surface morphology of the synthesized materials. Surface morphology, composition and sizes of the nanoparticles were evaluated using a Quanta FEG 250 Environmental scanning electron microscope (ESEM) coupled with EDX. PerkinElmer λ20 UV–vis spectrophotometer was used to obtain the absorption spectra, and Malvern Zetasizer Nanoseries was used for the measurement of the Zeta potential.

3.1.7 Photocatalytic degradation of tetracycline in water

The photocatalytic performance of the synthesized materials was evaluated on the degradation of tetracycline in water. The photocatalyst was first submerged in a photocatalytic reactor system kept at a constant temperature of 25 ℃. A 250 mL tetracycline solution with a starting concentration of 50 mg/ L was placed in the reactor system. The system was agitated for 30 min in complete darkness, to achieve

steady-state adsorption-desorption equilibrium. The suspension was continuously stirred while exposed to 300W of Xe lamp light. At intervals of 20 min, 5 mL of aliquots were taken from the suspension and immediately filtered through a 0.22 μm microporous membrane to obtain the solutions. TC degradation was measured at 200-900 nm wavelength using a UV-visible spectrophotometer. The effect of process variables such photocatalyst loading, tetracycline concentration, and pH were assessed. The percentage of tetracycline that has been photocatalytically degraded was obtained by using Equation 1.

$$\text{Percentage removal of Tetracycline} = \frac{Co-C}{Co} \text{x } 100 \qquad (1)$$

Where C_o is the concentration of tetracycline before photocatalysis and C is the concentration of tetracycline after the photocatalytic process.

3.2 Results and discussion

3.2.1 Fourier transforms infra-Red (FT-IR) spectroscopy

FTIR spectra is of the pristine TiO_2, $BTiO_2$, pristine ZnO, BZnO, TiO_2-ZnO and $BTiO_2$-ZnO are presented in Figure 1 (a -f) respectively. The spectrum of pristine TiO_2 and $BTiO_2$ showed all the characteristic bands of TiO_2, with the vibrational bands of Ti-O observed around 470 and 590 cm^{-1} (Rajakumar *et al.,* 2012; Sunaryono *et al.,* 2021). The peak observed at 1630 cm^{-1} corresponds to the deformative vibration of Ti-OH stretching mode(Al-Taweel & Saud, 2016; Chougala *et al.*, 2017). The peak at 760 cm^{-1} is related to Ti-O stretching band, which is the characteristic peak of TiO_2 (Ba-Abbad *et al.,* 2012; Praveen *et al.,* 2014). FTIR spectra of the pristine ZnO and BZnO nanoparticles display vibrational band attributed to the Zn–O vibrations of ZnO around 400–600 cm^{-1} (Sharwani *et al.,* 2022). A band at 860 cm^{-1} could be ascribed to the stretching vibration of the Zn-O bond (Valerio *et al.,* 2019). A band at 860 cm^{-1} could be ascribed to the stretching vibration of the Zn-O bond (Valerio et al., 2019). The bands at 1440 cm^{-1} could be assigned to the asymmetric stretching modes of oxygen molecules present in the sample (Menazea & Awwad, 2020; Rajendran & Sengodan, 2017). The spectra of TiO_2-ZnO and $BTiO_2$-ZnO composites showed bands that are consistent with pristine TiO_2 and ZnO nanoparticles. The absorption peak at 675 cm^{-1} is due to the vibrational mode of −Zn–O–Ti group (Mousa H. M. *et al.*, 2021). During the compositing reaction, the interaction between these two metal oxides (TiO_2 and ZnO) broke the metal-oxygen bonds, facilitating the compositing of the complex metal oxides system that resulted in the desired TiO_2-ZnO and black TiO_2-ZnO. In the composite, the disappearance of peaks at 1630 cm^{-1} and 1440 cm^{-1} due to Ti-OH and symmetric stretching modes of the oxygen (O_2) molecules that were initially present in the pristine TiO_2 and ZnO respectively further supports the successful formation of the heterojunction materials.

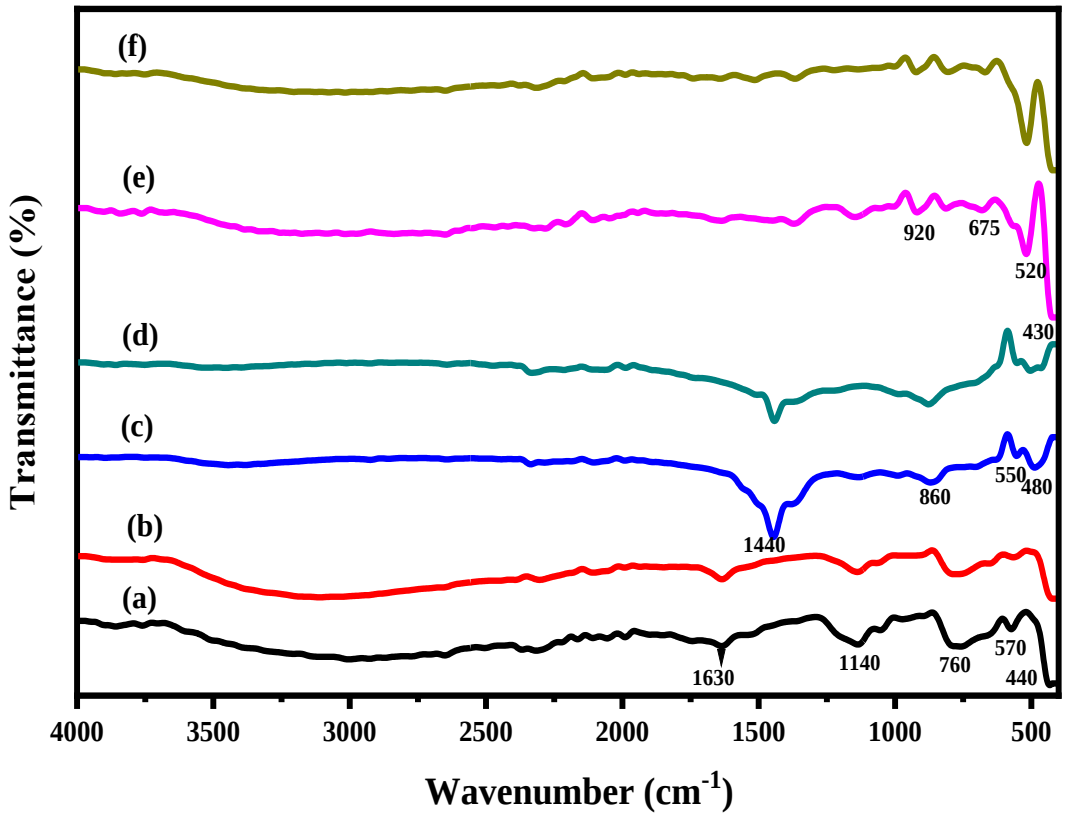


Figure 1: FTIR spectra of (a) pristine TiO_2, (b) $BTiO_2$, (c) pristine ZnO, (d) BZnO, (e) TiO_2-ZnO, and (f) $BTiO_2$-ZnO.

3.2.2 X-ray diffraction (XRD) analysis

XRD analysis was used to investigate the crystal structure and phase purity of the synthesized materials. Fig. 2 presents the X-ray diffraction spectra of pristine ZnO together with BZnO synthesized at 300 ℃, 350 ℃ and 400 ℃ (Fig. 2a), pristine TiO_2 and $BTiO_2$, synthesized at 300 ℃, 350 ℃ and 400 ℃ (Fig. 2b), and TiO_2-ZnO and $BTiO_2$-ZnO synthesized at 300 ℃, 350 ℃ and 400 ℃ (Fig. 2c). The diffraction patterns of the pristine ZnO and BZnO at different temperatures displayed six characteristics peaks of hexagonal wurtzite phase (JCPDS no 036-1451) at 2 theta values of 31.5, 34.1, 36.1, 56.6 and 64.0^o which can be indexed to the (100), (002), (101), (102), (110) and (200) planes respectively (Menazea & Awwad, 2020). This, thus, indicates that the pristine ZnO has the same crystal structure as BZnO, which suggest that the surface defective engineering does not affect the crystal structure but only altered the colour of pristine ZnO to black. The diffraction peaks for major anatase phase peaks are reported to appear at 25.4, 37.7, 47.8, and 54.8°, while the weaker rutile phases are located at 27.4 and 36°. The diffraction pattern of the pristine TiO_2 and $BTiO_2$ synthesized at different temperatures confirmed the presence of only the anatase phase with (JCPDS Card no. 21-1272) (Fig 2b). The reflection at 2θ angle

of 25.6, 37.9,48, 53.9, and 55.2° correspond to the (1 0 1), (0 0 4), (2 0 0), (1 0 5), and (2 1 1) planes respectively (Li *et al.*, 2014; Zhang *et al.*, 2016). The XRD patterns of the heterojunctions system are composed of TiO_2 (anatase) and ZnO (hexagonal) peaks at (25.6, 37.9,48, 53.9, and 55.2°) and (31.5, 34.1, 36.1, 56.6 and 64°) respectively, indicating that the introduction of surface defects did not alter the crystallographic structure. The most common possible defects that might have developed when TiO_2 and ZnO were reduced by $NaBH_4$ for 1 h at 350 ℃ are oxygen vacancies. There is also a noticeable slight increase in the peak intensities as reaction temperature increased, which proved that the induced oxygen vacancies and Ti^{3+} resulted to increased crystallinity in the synthesized composites.

Debye-Scherrer (equation 2) and Lattice micro strain (equation 3) were used to calculate the crystalline size and lattice micro strain (Al-Khalqi *et al.*, 2021) of each of the synthesized catalysts and the values are presented in Table 1. As the temperature increased, the crystallite size of each synthesized material marginally increased. Compared to other synthesized materials, $BTiO_2$-ZnO has the largest lattice micro strain, which could enhance the photocatalytic performance of the composite relative to the individual metal oxide since more hydroxyl radicals would be generated due to higher possibility of photocarrier transition and hole trapping (Cao *et al.*, 2022; Hu *et al.*, 2020). The dislocation density (δ) of the synthesized materials was calculated from the average particle size values, (equation 4) (Siregar *et al.*, 2021). The sample with the lowest dislocation density was $BTiO_2$-ZnO produced at 350 ℃ (Table 1). The lowest dislocation density value indicates that the $BTiO_2$-ZnO produced at 350 ℃ possess a high degree of crystallinity compared to other synthesized materials (Sutapa *et al.*, 2018).

Debye–Scherrer formulae: $$D = K\lambda / \beta \text{Cos}\,\theta \qquad (2)$$

Where D = Crystallites size (nm), K = Scherrer's constant (Shape factor) (Here, taken as 0.94), λ = Wavelength of X-rays (Å), β = F. W. H. M (Full Width at Half Maxima in degrees), θ = Peak position in XRD graph (that is 2θ in degrees).

$$Lattice\ strain\ (\varepsilon) = \frac{\beta Cos\theta}{4} \qquad (3)$$

Dislocation density $$\delta = \frac{1}{D^2} \qquad (4)$$

Table 1: Crystallite size and lattice microstrain of synthesized materials

Synthesized Nanomaterial	**Crystallite size (nm)**	**Lattice strain**	**Dislocation density (δ) (m^2)**
Pristine ZnO	26.15	6.64×10^{-2}	1.46×10^{-3}
BZnO@300°C	28.61	5.59×10^{-2}	1.22×10^{-3}
BZnO@350°C	31.47	5.08×10^{-2}	1.01×10^{-3}
BZnO@400°C	34.61	6.72×10^{-3}	8.34×10^{-4}
Pristine TiO_2	13.86	1.68×10^{-3}	5.21×10^{-3}
$BTiO_2$@300°C	13.41	1.73×10^{-3}	5.56×10^{-3}
$BTiO_2$@350°C	20.46	7.27×10^{-3}	2.39×10^{-3}
$BTiO_2$@400°C	21.20	8.12×10^{-3}	2.22×10^{-3}
TiO_2-ZnO	28.29	5.79×10^{-3}	1.25×10^{-3}
TiO_2-ZnO@300°C	31.55	1.521×10^{-2}	1.00×10^{-3}
TiO_2-ZnO@350°C	32.68	1.503×10^{-2}	9.36×10^{-4}
TiO_2-ZnO@400°C	37.81	1.32×10^{-3}	6.99×10^{-4}

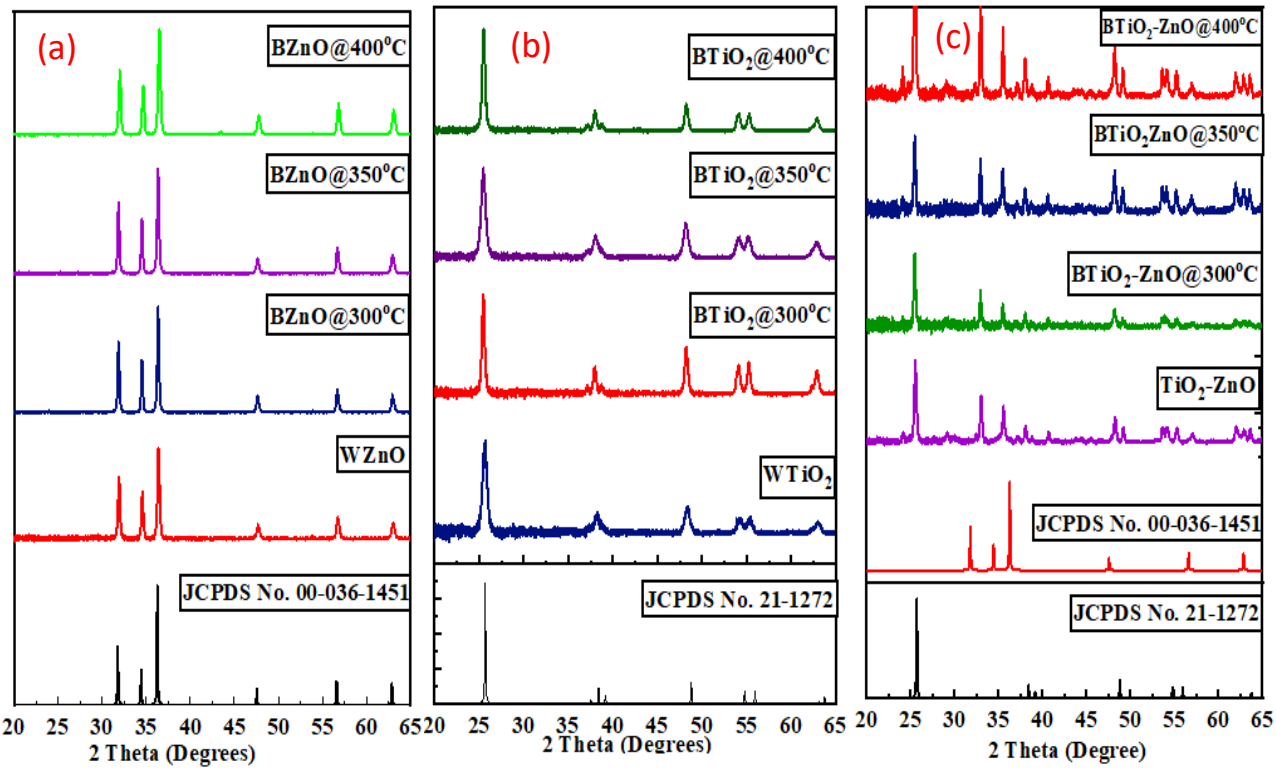


Figure 2: X-ray diffraction patterns of (a) overlaid pristine ZnO and BZnO synthesized at 300 °C, 350 °C and 400 °C, (b) overlaid pristine TiO_2 and $BTiO_2$ synthesized at 300 °C, 350 °C and 400 °C, and (c) TiO_2-ZnO and $BTiO_2$-ZnO synthesized at 300 °C, 350 °C and 400 °C.

3.2.3 Optical properties of the binary metal oxides and composite oxides

UV-vis spectrometer was used to determine the optical properties of the synthesized materials by measuring absorbance. Figure 3a-c presented the UV-absorption spectra of (a) pristine ZnO together with BZnO, (b) pristine TiO_2 and $BTiO_2$, and (c) TiO_2-ZnO and $BTiO_2$-ZnO synthesized at 300, 350. and 400 ℃ respectively. The absorption spectra of the pristine ZnO and BZnO synthesized at 300 and 350 ℃ exhibited a narrow peak in the UV region around 380 nm (Fig 3a). BZnO synthesized at 400 ℃ showed a peak near the band edge region (at about 400 nm) with a dramatic increase in the absorption intensity. Pristine TiO_2 and $BTiO_2$ (Fig 3b) also showed in the near-UV region with absorption edge at around 400 and 425 nm respectively. $BTiO_2$ synthesized at 350 and 400 ℃ absorbed in the near-UV to the visible region. The significant absorption of UV light was caused by the charge transfer from the 2p orbital of TiO_2 to 3d orbital of the Ti^{4+} which acts as the valence band and conduction band respectively (Momeni *et al.*, 2019). The spectrum of the heterojunction materials in Fig 3c showed that the absorption edge was red-shifted relevant to the position of absorption in the pristine ZnO and pristine TiO_2; hence, confirmed that the absorption edge of both ZnO and TiO_2 can be changed through the formation of a heterojunction. The absorption intensities significantly increased as the reduction temperature increased during the defective engineering, and a slight shift in the optical absorption edge towards the longer wavelength region occurred. This may be ascribed to an increase in particle size and the nano-confinement effect of oxygen vacancies, which changed the local electronic states (Abdissa *et al.*, 2018; Wang *et al.*, 2023) (Hidalgo-Jimenez *et al.*, 2020). The optical bandgap energies- of the materials were obtained using Tauc plots of $(hv)^{1/2}$ against Eg and are shown in Fig 3d-f. The optical bandgap energy became narrowed with the formation of oxygen vacancy in the heterojunction systems at different synthesis temperatures. The differences in band gap energy for the samples could be attributed to the formation of new electronic levels in the heterojunction. Therefore, more charge separation and increased lifetime of charge carriers in the material can be achieved (Hidalgo-Jimenez et al., 2020; Mousa Hamouda M *et al.*, 2021). Additionally, Equations (5) and (6) were used to calculate the conduction band potential (E_{CB}) and valence band potential (E_{VB}) of the composite nanomaterials.

$$E_{VB} = \chi - E_e - 0.5E_g \quad (5)$$

$$E_{CB} = E_{VB} - E_g \quad (6)$$

where Eg denotes the semiconductor's band gap energy, E_{VB} denotes the VB edge, E_{CB} denotes the CB edge, χ denotes the electronegativity of the semiconductor nanoparticles, and E_e denotes the energy of free electrons as measured on the hydrogen scale (4.5 eV). The values are 5.78 and 5.82 eV, respectively, for ZnO and TiO_2. Table 2 displays the calculated band alignments.

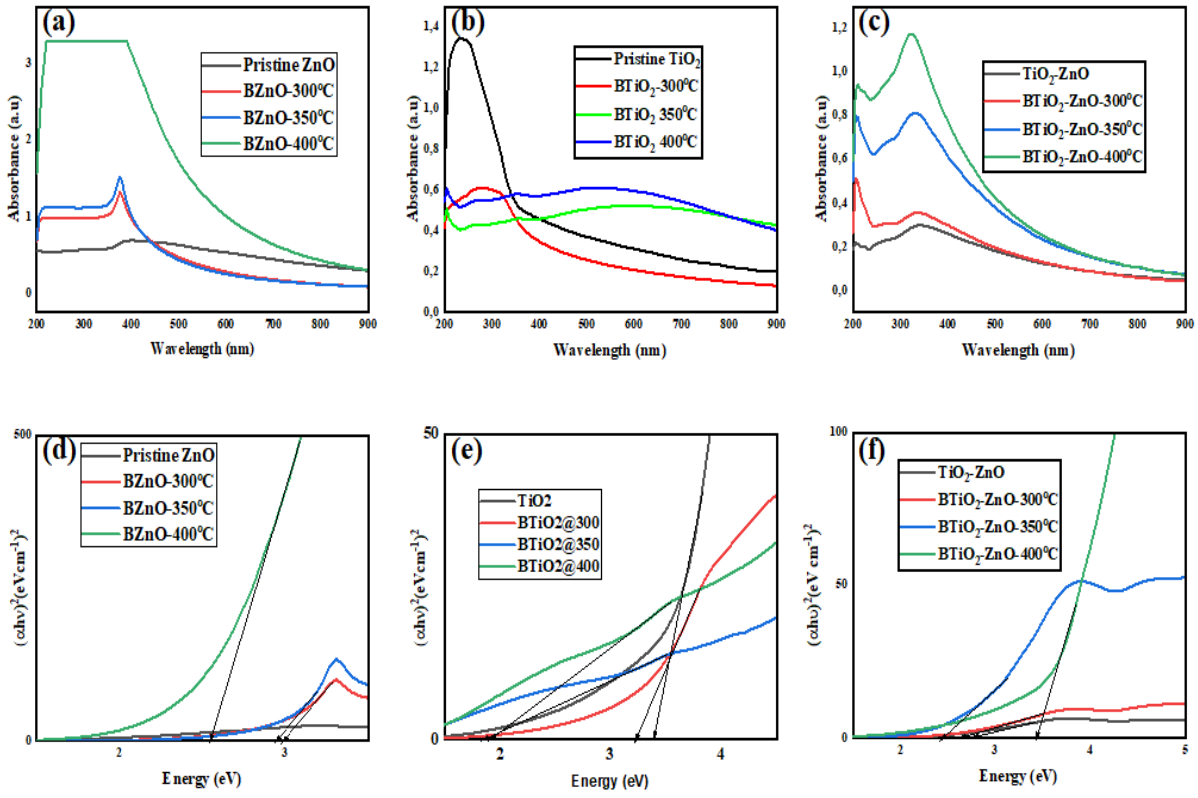


Figure 3: Optical spectra of overlapped (a) ZnO and BZnO synthesized at 300 ℃, 350 ℃ and 400 ℃, (b) pristine TiO_2 and $BTiO_2$, synthesized at 300 ℃, 350 ℃ and 400 ℃, and (c) TiO_2-ZnO and $BTiO_2$-ZnO synthesized at 300 ℃, 350 ℃ and 400 ℃ while d, e and f are the tauc plots respectively.

Table 2**:** Mulliken's electronegativity (χ), band gap energy (E_g), valence band (E_{VB}) and conduction band (E_{CB}) for the pristine nanoparticles and the nanocomposite.

Semiconductors utilized in photocatalytic studies.	χ (eV)	E_g (eV)	E_{CB} (eV)	E_{VB} (eV)
$BTiO_2$	5.82	1.8	0.42	+1.38
BZnO	5.78	3.8	-0.62	+4.42
$BTiO_2$-ZnO	5.82	2.5	0.07	-0.47

3.2.4 Morphological study

3.4.1 Scanning electron microscope (SEM) analysis

The surface morphologies of the synthesized materials were investigated and presented in Figs. 4a-f. The SEM micrographs of BZnO nanoparticles displayed small crystals with pseudo-spherical morphology aggregated on the surface. The micrograph of $BTiO_2$ nanoparticles, synthesized at 350 ℃ (presented in Fig. 3b) shows small spherical particles that formed into larger agglomerates. However, the $BTiO_2$-ZnO nanocomposite at different temperatures exhibited minimal agglomeration with a spherical shape. An increase in the synthesis temperature influenced both the size and shape of the nanocomposite (Fig. 3f). This increased the surface area of the nanocomposite, which could enhance the photocatalytic activities of these materials.

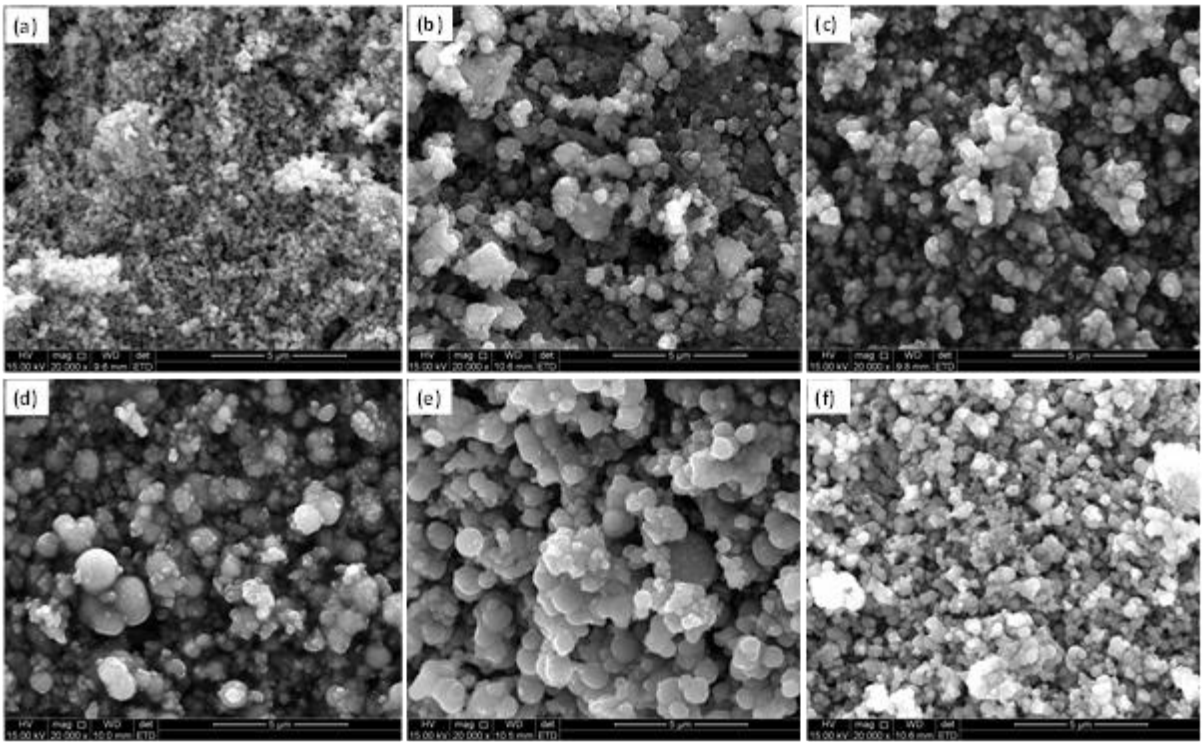


Figure 4: SEM micrographs of (a) $BTiO_2$, (b) BZnO, (c) TiO_2-ZnO, (d) $BtiO_2$-ZnO synthesized at 300 ℃, (e) $BTiO_2$-ZnO synthesized at 350 ℃, and (f) $BTiO_2$-ZnO synthesized at 400 ℃.

3.4.2 Transmission electron microscope (TEM), elemental mapping, and Energy Dispersive X-ray (EDX) analysis

Figs. 5 (a and b) show the TEM images and particle size histogram of BZnO nanoparticles respectively. The TEM images confirm that the nanomaterials are of spherical morphology which are visibly arranged in a chain-like configuration. The average particle size of the synthesized material was about

44.6 nm, which was close to the value obtained from the XRD pattern. The EDX spectrum of BZnO (Fig. 5c) shows the presence of only zinc and oxygen, and the even distribution of both elements (zinc and oxygen) within the modified binary metal oxide was confirmed by the elemental mapping images of Fig 5 (d-f).

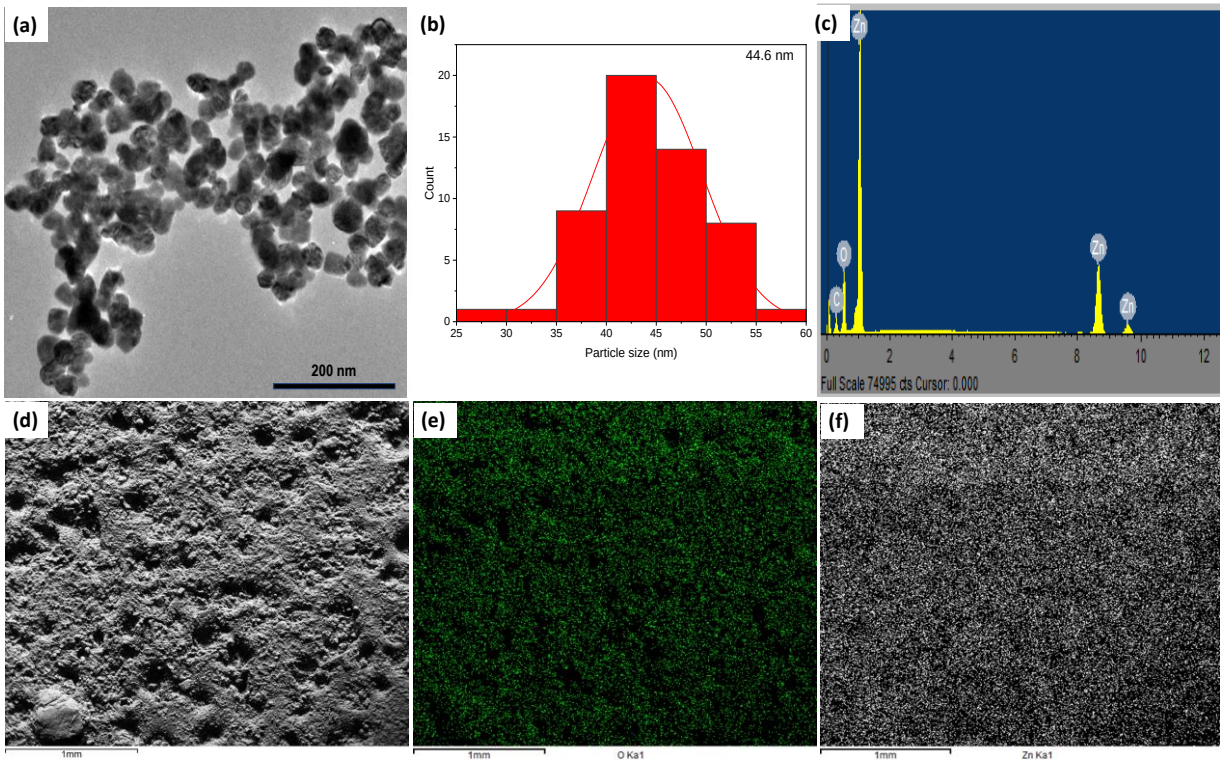


Figure 5 **:** (a) TEM image, (b) particle size distribution histogram, (c) EDX spectrum, and (d) elemental mapping showing (e) O, and (f) Zn elements of black ZnO.

The TEM images of $BTiO_2$ nanoparticles and the particle size distribution histogram are presented in (Figs. 6 a and b) respectively. The nanoparticles were of spherical morphology with slight agglomeration, and the average particle size was about 15.0 nm and agrees with the crystalline size obtained from the XRD pattern. The representative EDX spectrum presented in Figure 6c shows the distinct peaks corresponding to titanium and oxygen. The elemental mapping images in Fig. 6 e and f show that titanium and oxygen were homogeneously distributed across the $BTiO_2$ particles, suggesting a good dispersion of the elemental composition of the nanostructures.

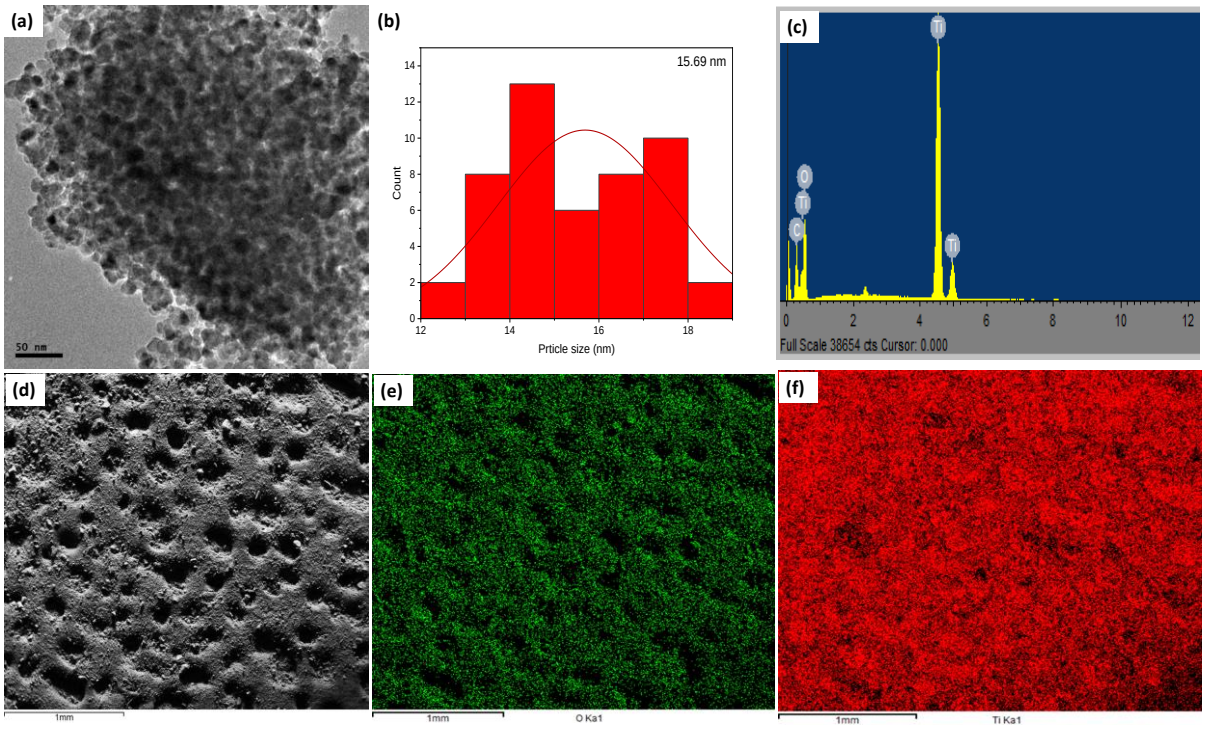


Figure 6: TEM image, (b) particle size distribution histogram, (c) EDX spectra, and (d) elemental mapping showing (e) O, and (f) Zn elements of black TiO_2.

A heterojunction of two binary components prepared via calcination process often have a high tendency to agglomerate. Figs (7a and 8a) and Figs (9a and 10a) show the TEM, EDX and elemental mapping images for the heterojunction compounds TiO_2-ZnO, $BTiO_2$-ZnO (300 °C), $BTiO_2$-ZnO (350 °C), and $BTiO_2$-ZnO (400 °C) respectively. All the TEM images show highly agglomerated spherical nanograins. TEM images for $BTiO_2$-ZnO synthesized at 350 °C showed the least agglomeration indicating that it could be the best catalyst since agglomeration influences the optical properties of materials and therefore their ability to absorb and scatter the incoming radiation thereby influencing the photocatalytic activity (Pellegrino *et al.*, 2017). The elemental composition of the nanocomposite is shown in the EDX spectrum presented in Figs (7b and 8b) and Figs (9b and 10b) confirms heterojunctions are primarily composed of titanium, zinc and oxygen with no impurity. The elemental mapping images of the composite prepared at 350 ºC (Figures 9c - f) and at 400 ºC (Figures 10c-f) confirmed the uniform distribution of the titanium, zinc, and oxygen across the synthesized heterojunctions.

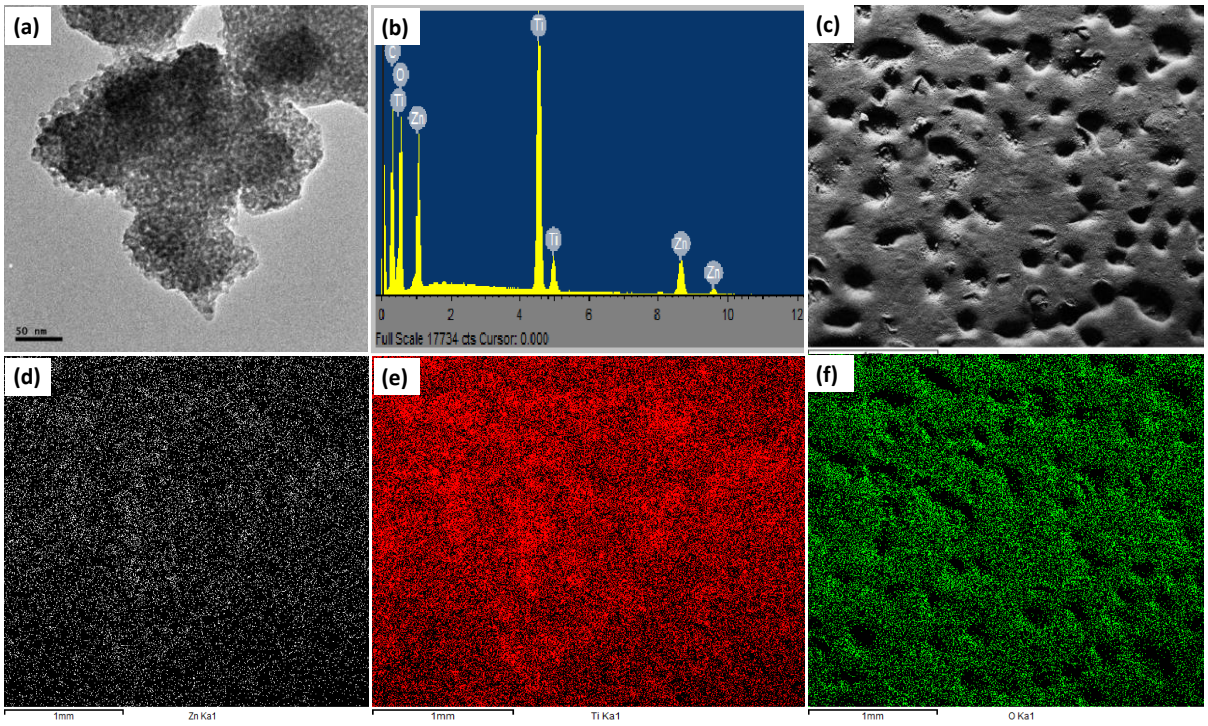


Figure 7: TEM image, (b) EDX spectrum, (c) elemental mapping showing (d) Zn, (e)Ti, and (f) O elements of the pristine TiO_2-ZnO.

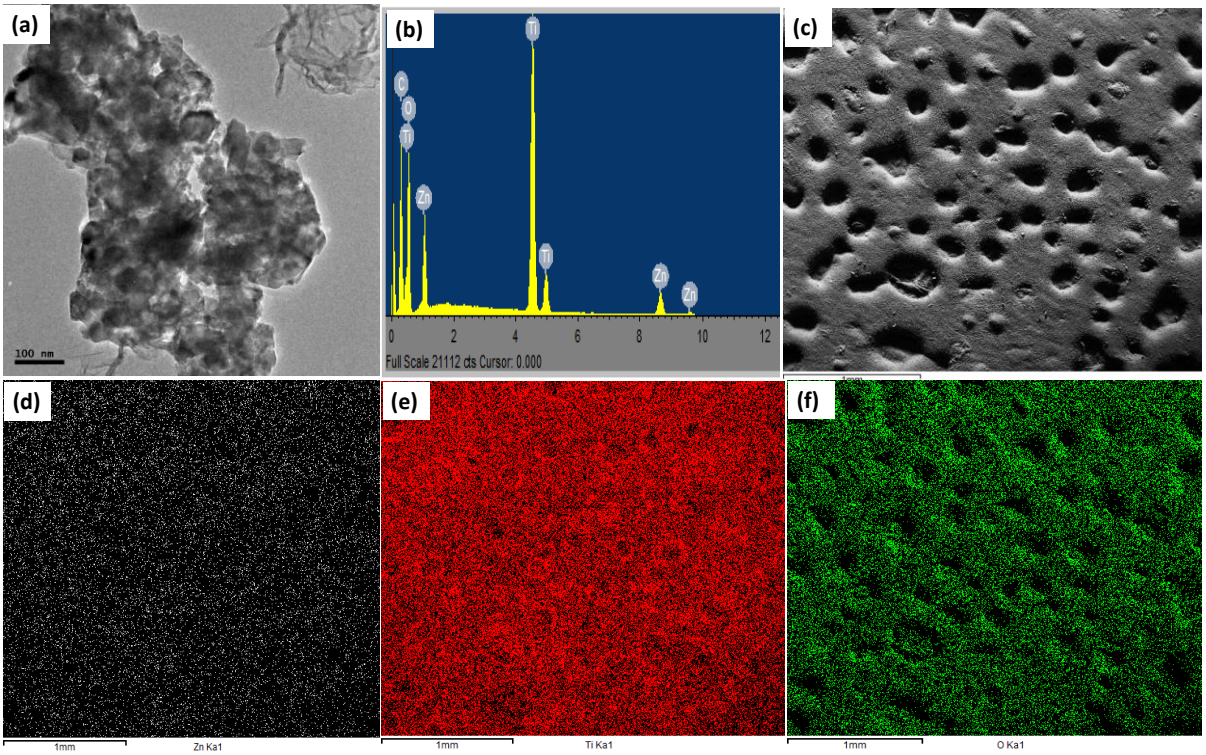


Figure 8: TEM image, (b) EDX spectrum, (c) elemental mapping showing (d) Zn, (e)Ti, and (f) O elements of Black TiO_2-ZnO prepared at 300 ℃ for 1 h.

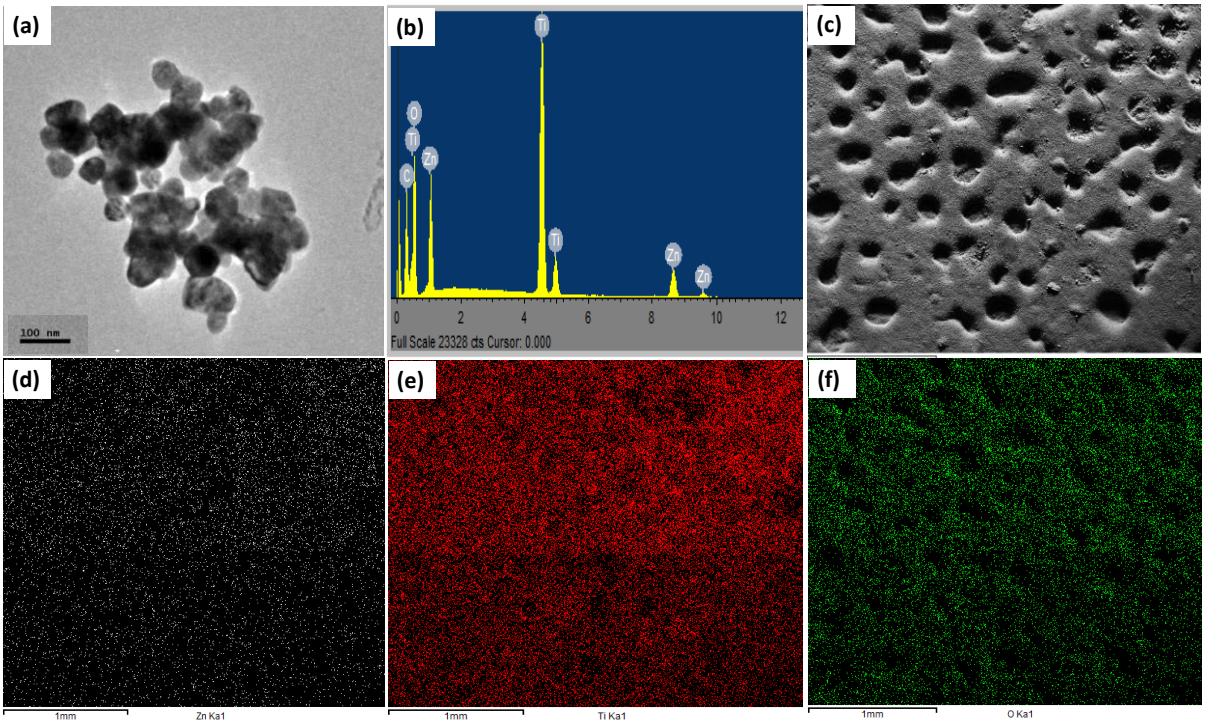


Figure 9:(a) TEM image, (b) EDX spectra, (c) elemental mapping showing (d) Zn, (e)Ti, and (f) O elements of Black TiO_2-ZnO prepared at 350 ℃ for 1 h.

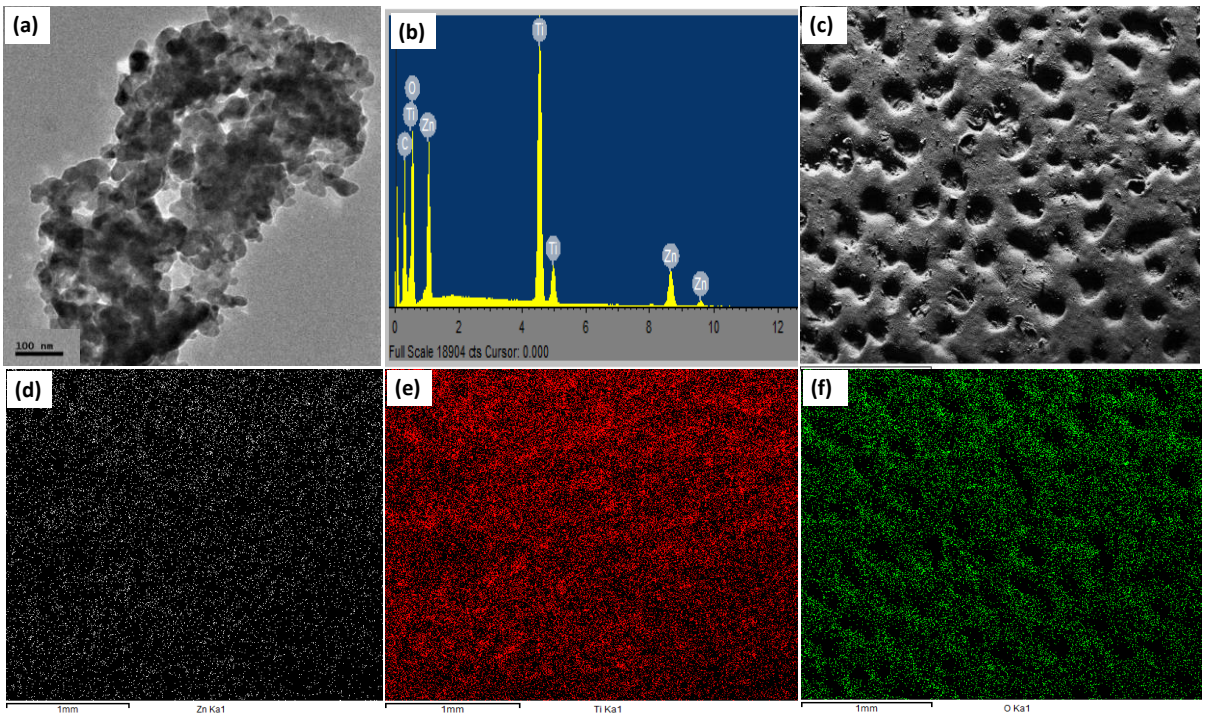


Figure 10: TEM image, (b) EDX spectra, (c) elemental mapping showing (d) Zn, (e)Ti, and (f) O elements of Black TiO_2-ZnO prepared at 400 ℃ for 1 h.

3.2.5 Photoluminescence (PL) study

The PL spectra of $BTiO_2$, BZnO, TiO_2-ZnO, and $BTiO_2$-ZnO with excitation wavelength of 325 nm are shown in Figure 11. The observed peak, exhibited by all samples around 360 nm, is due to photoinduced charges naturally recombining from the conduction band to the valence band (Liao *et al.*, 2012). The observed lower PL emission intensity of the $BTiO_2$-ZnO heterojunction composite is related to the improvement of the charge separation rate, which in turn reduces the radiative recombination of electron-hole pairs. Efficient charge separation, therefore, increases the lifetime of the charge carriers and subsequently enhances the photocatalytic activity of the synthesized nanomaterial.

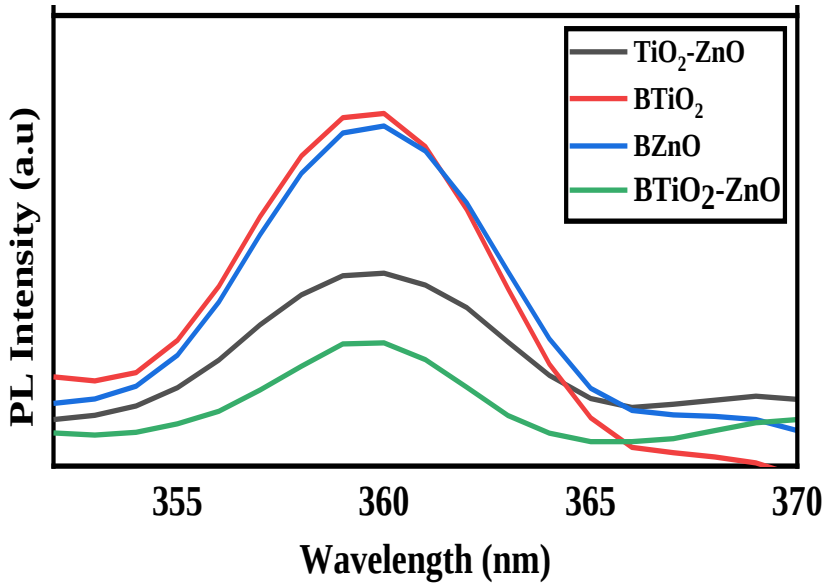


Figure 11: Photoluminescence spectra of $BTiO_2$, BZnO, TiO_2-ZnO and $BTiO_2$-ZnO.

3.2.6 Photodegradation of tetracycline

The photocatalytic efficiency of the nanocomposites prepared at different temperatures (300, 350, and 400 °C) was evaluated on a 50 mg/L tetracycline concentration, 100 mg of each catalyst, and a pH of 5.6. The degradation patterns at various reduction temperatures, presented in Fig. 12 a-c, were slightly different. Results of the preliminary study showed that the photocatalytic degradation efficiency of $BTiO_2$-ZnO at 350 °C was higher than in other nanocomposites. The smaller band gap energy of $BTiO_2$-ZnO (350 °C) might be responsible for the enhanced performance achieved. Therefore, the $BTiO_2$-ZnO at 350 °C was chosen for the subsequent evaluation of the photocatalytic degradation of TC in this study.

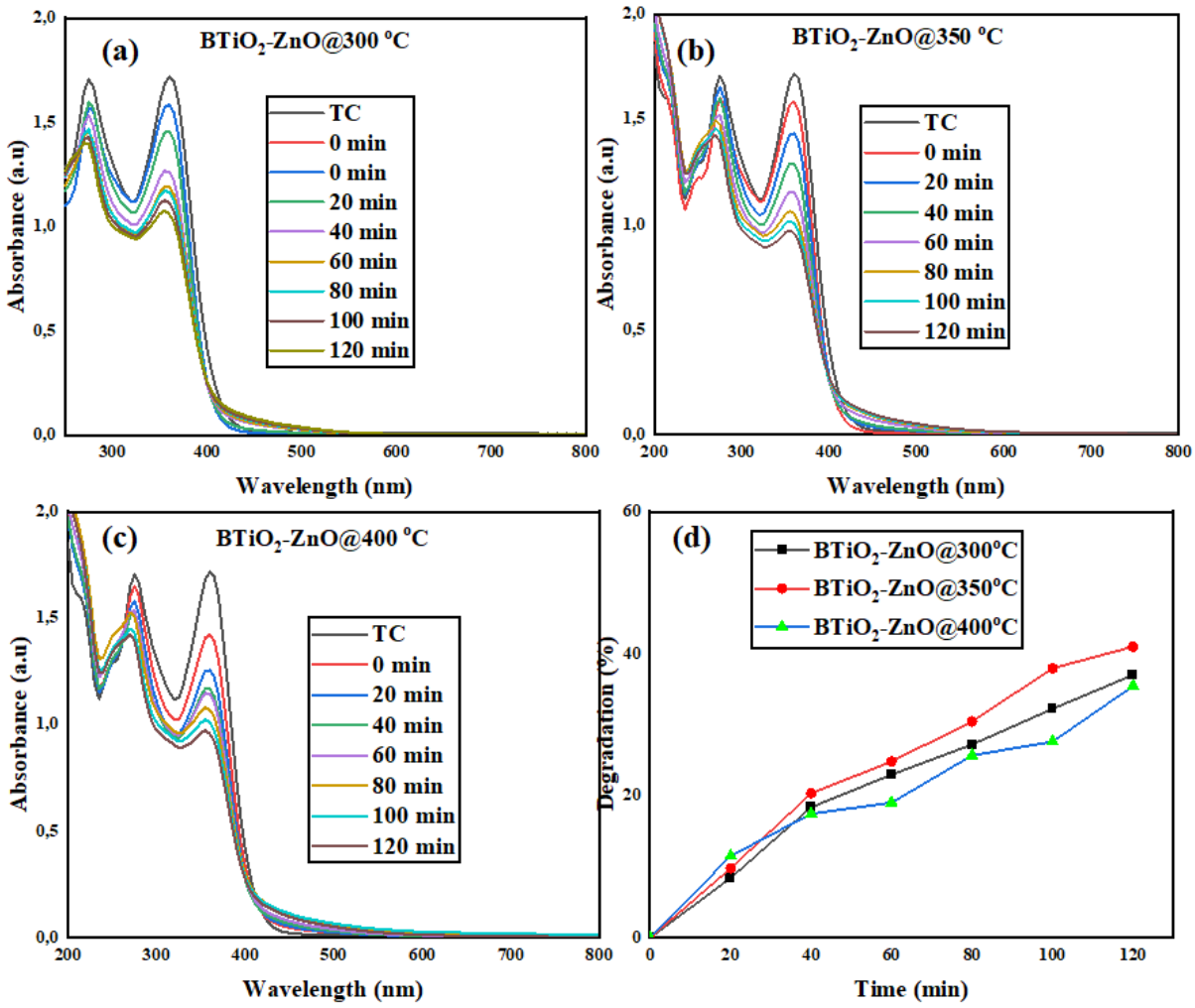


Figure 12**:** UV-vis absorption spectra of photocatalytic degradation of TC using $BTiO_2$-ZnO synthesized at (a) 300°C), (b) 350°C and (c) 400°C (d) percentage degradation of TC under visible light (50 mg/L dye concentration and catalysts dosage 100 mg/L.

3.2.7 Influence of TC Solution pH on the degradation efficiency

Solution pH is an important factor in the evaluation of photocatalytic degradation of tetracycline because pH affects the electrical charge properties of the photocatalyst's surface. The pH determines the ionization state of the photocatalyst surface, and then affects the adsorption and photocatalytic performance of any photocatalyst (Divakaran *et al.*, 2021; Saadati *et al.*, 2016). The photocatalytic degradation efficiencies of TC in the pH range of 4, 7 and 10 were evaluated using 50 mg/L tetracycline concentration and 100 mg of each catalyst and presented in Figures 13a, b, and c respectively. The photocatalytic degradation efficiencies of TC at different pH values followed the order of pH10 > pH7 > pH4. The results showed a similar trend with previously reported results (Zhu *et al.*, 2013), whereby the degradation of tetracycline in aqueous solution by nanosized TiO_2 was studied. The slow

degradation of TC under acidic conditions may be because ZnO, which is one of the component compounds, is not acid resistant. It can also be attributed to the repulsive force between protonated TC and the positively charged catalyst. Aggregation of nanoparticles under acidic conditions is reported to contribute to poor photocatalytic activity of some metal oxide nanoparticles due to the reduced surface area of the photocatalysts (Safari *et al.*, 2015). The faster degradation of TC at pH 10 may be due to the alkaline pH, and hydroxyl radicals were easier to form by the oxidization of more hydroxide ions available on the photocatalyst surface. Fig. 13c shows that as the photocatalytic degradation of TC progresses under alkaline pH, the maximum absorption peak at 350 nm gradually decreased, while the minimum absorption peak at 276 nm slightly increased. Hence, confirms the increase in the concentration of absorbing species at 276 nm. A new absorption peak appears at 550 nm which reveals the formation of by-products. Similar results on the emergence of new absorption peak under alkaline pH were previously reported (Jia *et al.*, 2022). The existence of by-products may be caused by the electrophilic attack on the TC ring structures that possess high electronic densities, such as aromatic rings and the keto-enol groups. Additionally, electronic density would alter the bond orbital energy of molecules, resulting in various rates of light absorption (Song *et al.*, 2020). Figures 13d and e show the rate of decomposition and the kinetics graph of the decomposition process respectively.

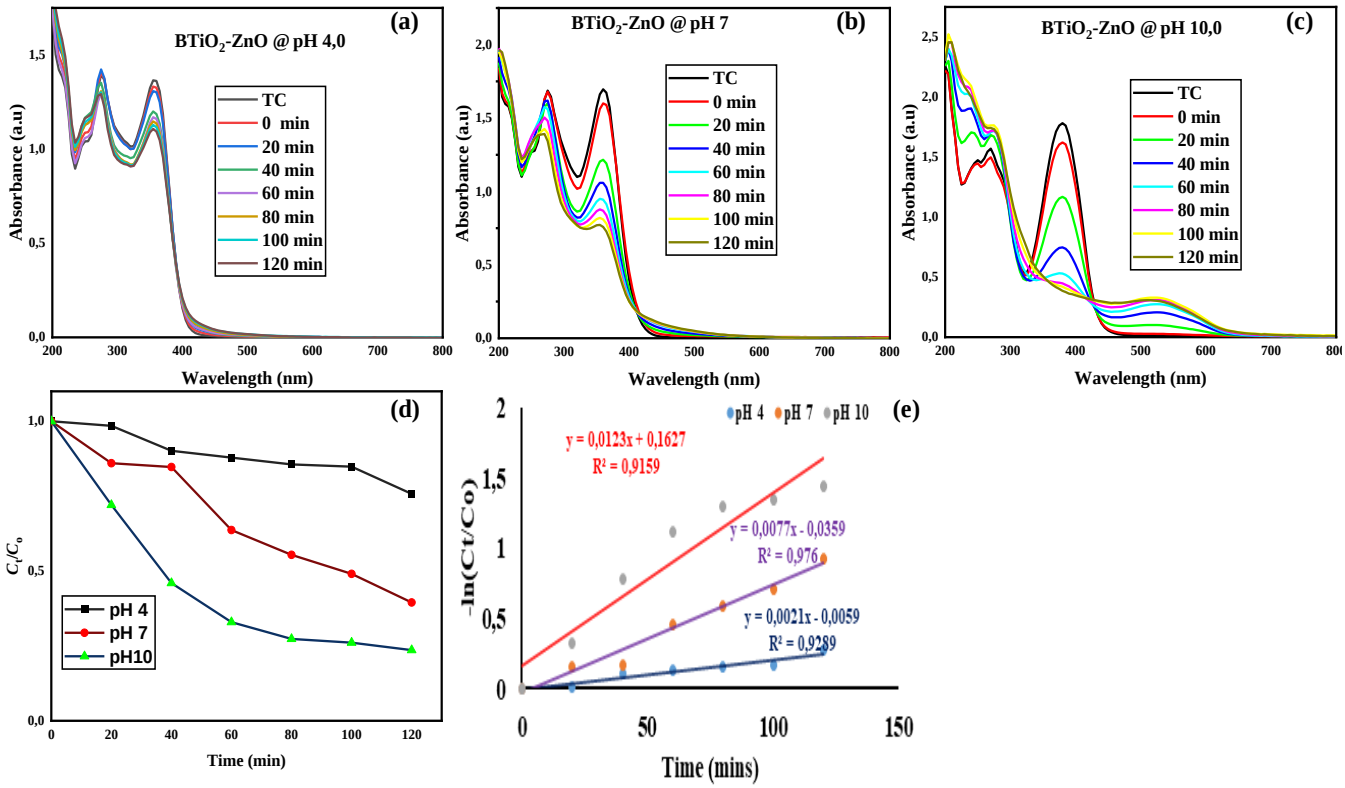


Figure 13: Absorption spectra of TC (50 mg/L) at different time using 100 mg/L of $BTiO_2$-ZnO at pH values of (a) pH 4, (b) pH 7 and (c) pH 10, (d) rate of decomposition, and (e) the kinetics graph of the decomposition process.

The zeta potential of the synthesized materials was found to be +26.1, -45.1, and -39.5 ± 5.64 mV for BZnO, $BTiO_2$ and $BTiO_2$-ZnO Figs 14a-c. The nanomaterials ($BTiO_2$-ZnO and $BTiO_2$) have negative zeta potential, which indicates strong stability and low agglomeration of the nanoparticles in solution because of stronger repelling forces (Chand *et al.*, 2021; Mbenga *et al.*, 2023; Raja *et al.*, 2017). Since both $BTiO_2$ and $BTiO_2$-ZnO have significantly charged surfaces, as shown by zeta potential studies, electrostatic interaction is unlikely to have an impact on tetracycline sorption on either material. This is because TC is an amphoteric molecule due to the presence of dimethylammonium, phenolic diketone moiety and the tricarbonyl system. As a result, at pH values of >3, 3.3–7.7, and <7.7, TC occurs as cationic, zwitterionic, and anionic species, respectively (Li *et al.*, 2010).

The zeta potential was also established for pH values of 4, 7, and 10 (Fig. 14) to assess the surface charges of $BTiO_2$-ZnO related to changes in pH. According to reported studies, neutral nanoparticles are those with a zeta potential between -10 and +10 mV, whereas strongly cationic and strongly anionic nanoparticles are those with a zeta potential of greater than +30 mV and less than -30 mV, respectively (Clogston & Patri, 2011). Thus, net surface charge of the $BTiO_2$-ZnO nanocomposite is highly negative under pH 10 and pH 7 and was expected to repel the anionic form of the TC molecule and form strong electrostatic interactions with the cationic form of TC (William IV *et al.*, 2008).

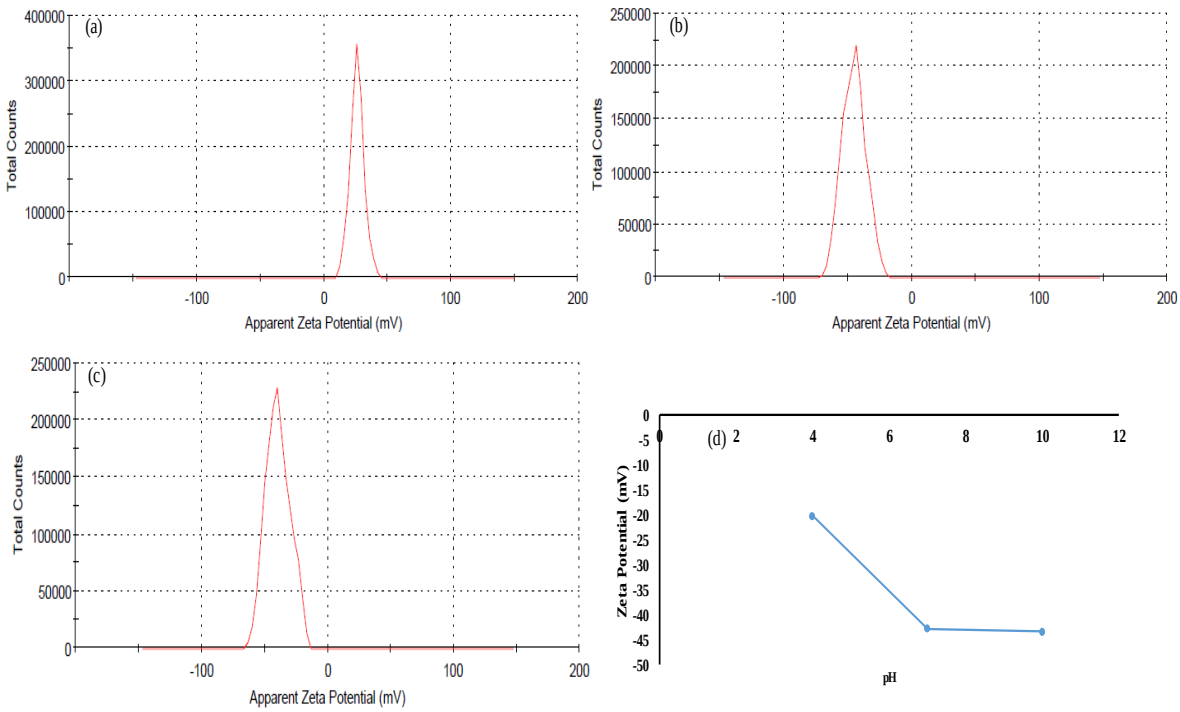


Figure 14**:** Zeta potential of (a) BZnO, (b) $BTiO_2$, (c) $BTiO_2$-ZnO (all under natural pH) and (d) $BTiO_2$-ZnO under acidic, neutral, and alkaline conditions

The photolysis of TC at different pH values of 4, 7 and 10 are shown in Figures 15a, b and c respectively. The results show a favourable photolysis of tetracycline at pH 10, which may contribute to the increased photocatalytic degradation of the TC by $BTiO_2$-ZnO at pH 10. Lower photolysis of TC at pH 4 and pH

7 indicates poor degradation of TC^+ and TC°, respectively. The attraction between TC^- and hydroxyl radicles caused by the high electronic density of the TC^- ring system could be responsible for the high photolysis rate at pH 10 (Jiao *et al.*, 2008). Since the bond orbital energy changes at high pH, TC tends to absorb more photons thereby enhancing photolysis (Song et al., 2020). Other studies has reported that tetracycline shows a favourable photolysis at alkaline pH (López-Peñalver *et al.*, 2010). A kinetics graph at different pH values, and percentage degradation of TC under visible light using an initial concentration of 50 mg/L and 100 mg/L catalyst dosage are shown in Figures 15d and e respectively.

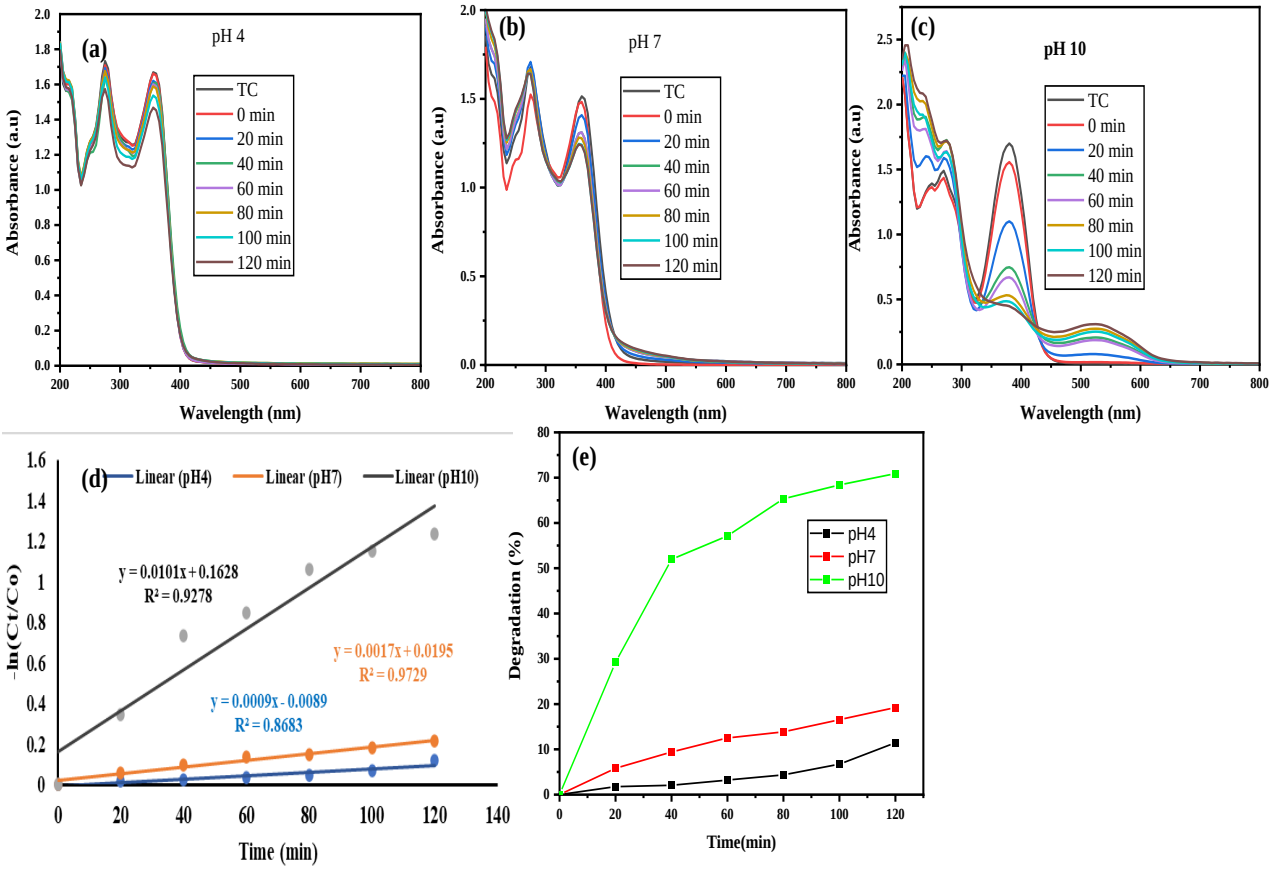


Figure 15: Absorption spectra of TC showing its photolysis at different pH (a) 4, (b) 7, (c) 10, (d) Kinetic graphs at different pH values, and (e) percentage degradation of TC under visible light (TC initial concentration: 50 mg/L, catalyst dosage 100 mg/L).

3.2.8 Influence of photocatalysts dose

The influence of photocatalyst dosage on the degradation of TC was evaluated in the absence of the photocatalyst (Fig 16a) and using 75, 100 and 125 mg/L of $BTiO_2$-ZnO at a constant TC concentration of 50 mg/L, while a constant pH of 7 was maintained and the reaction was monitored for120 min (Figs.16 b, c and d respectively). Photocatalytic degradation efficiency of TC was observed to increase

as the catalyst dosage increases (Fig. 16e). The kinetics graphs of the decomposition process at initial TC concentration of 50 mg/L and solution pH 7 is presented in Fig. 16 f. This could be attributed to an increase in the number of active sites on the surface of the photocatalysts, which subsequently increased the production of hydroxyl radicals responsible for photocatalysis process (Hunge *et al.*, 2022). Studies have shown that increase in the concentrations of catalyst has a direct effect on the photocatalytic activity, but only up to a certain level. This is because at a high catalyst loading, most of the catalysts may experience deactivation due to agglomeration and precipitation. This might reduce the amount of catalyst surface that is available for light absorption and, as a result, decreases the rate of pollutant degradation (Ravele *et al.*, 2021). The marginal degradation of TC in the absence of the photocatalyst could be attributed to photolysis.

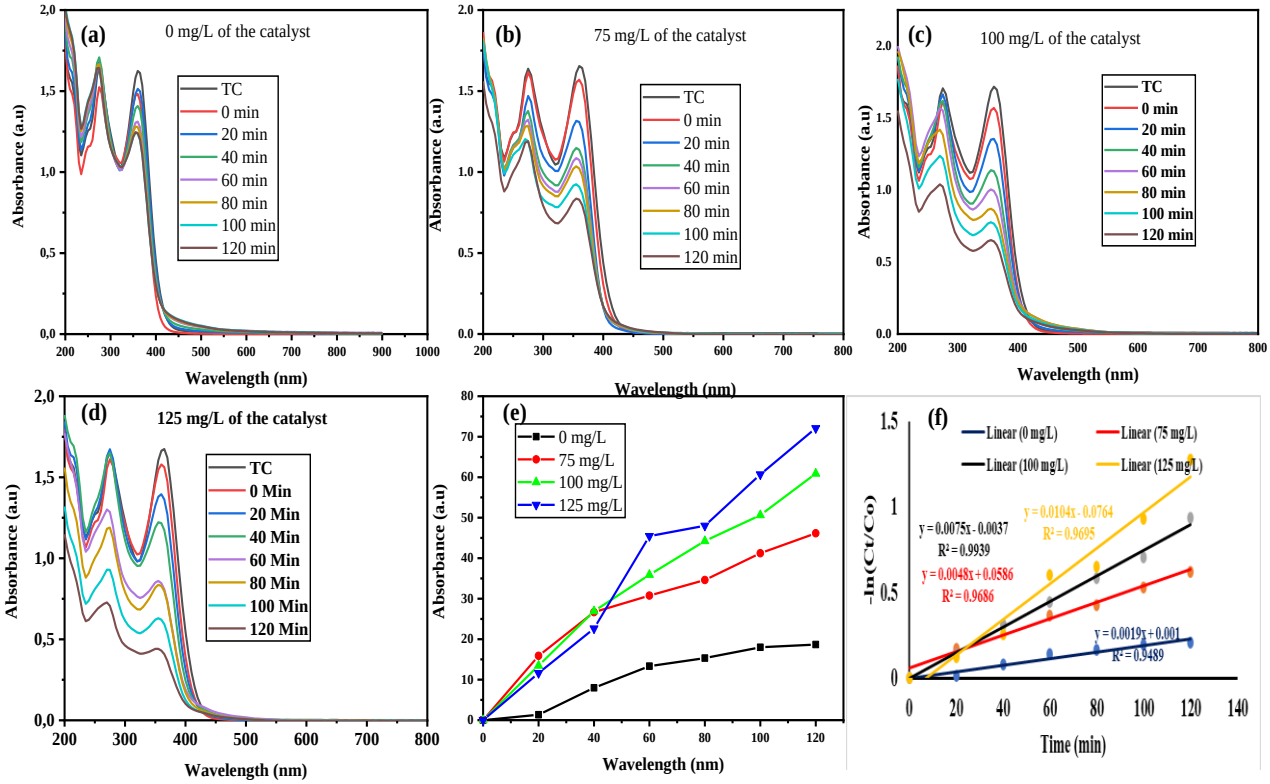


Figure 16: Absorption spectra of TC showing its photodegradation by BTiO$_2$-ZnO nanocomposite at catalyst loading concentrations of (a) 0, (b) 75, (c) 100, and (d) 125 mg/L, and (e) percentage degradation of TC under visible light (TC initial concentration: 50 mg/L, pH: 7), and (f) kinetics of graphs of the decomposition process.

3.2.9 Influence of initial concentration of tetracycline on the degradation process

The influence of TC concentration on the degradation process was evaluated by using 100 mg of $BTiO_2$-ZnO to 1 L of 25-75 mg/L TC solution while maintaining a constant pH of 7 and the duration of the reaction was 120 min. The result of the degradation process is presented in Figs. 17 (a-c). The photocatalytic degradation efficiency of TC decreased with an increase in the concentration of TC. Previous studies have reported that at higher concentrations of pollutants, more intermediates are produced, which enhances the adsorption competition between the pollutant and its degradation products (intermediates) on the catalyst surface (Chen *et al.*, 2016). Fig 17d shows the pseudo-first order rate constant of 0.0112 min^{-1} at a dose of 25 mg/L, which however decreased to 0.0075 min^{-1} and 0.0052 min^{-1} at 50 mg/L and 75 mg/L, respectively. This could be attributed to the increase in the path length of photons entering the reaction system, thereby reducing the photons on the surface of the catalyst (Wang *et al.*, 2021). In addition, as tetracycline ions dominate the photocatalyst's active site, it causes a reduction in the number of hydroxyl radicals formed on the surface of the catalyst thereby decreasing the photocatalytic activity.

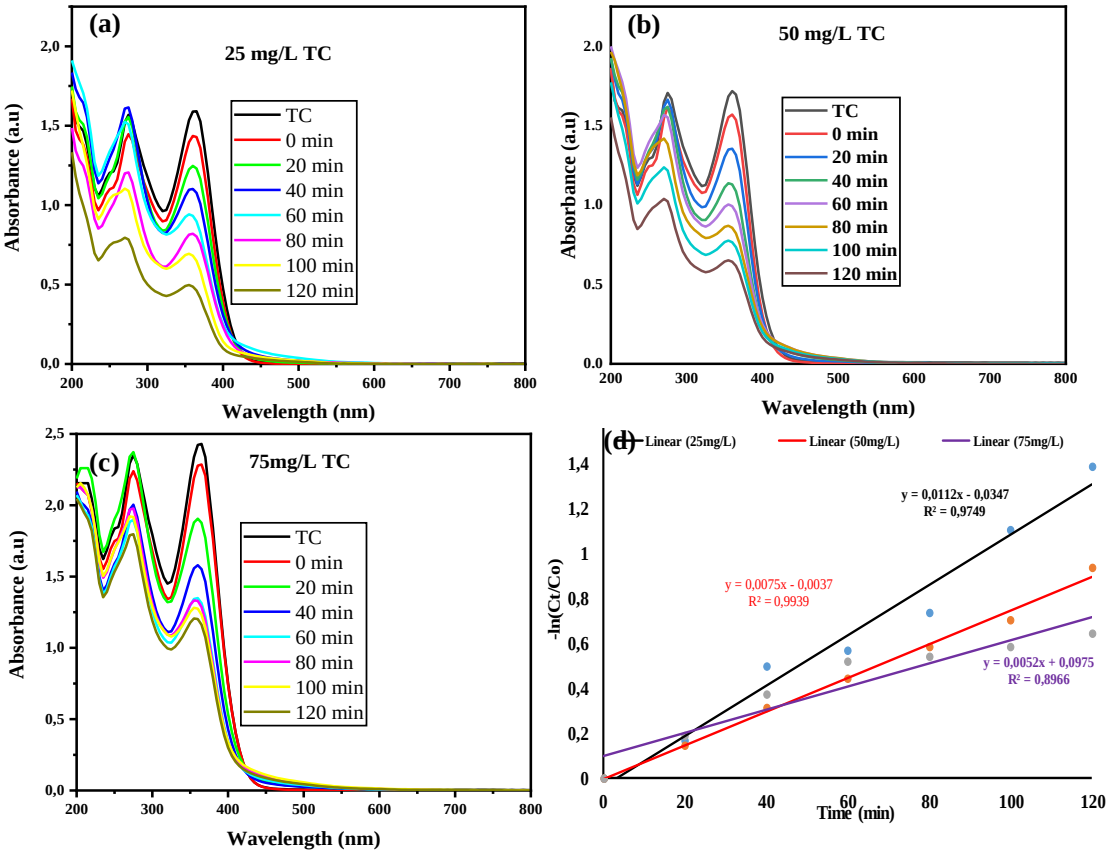


Figure 17: Absorption spectra of TC showing its photodegradation by $BTiO_2$-ZnO nanocomposite at initial TC concentrations of (a) 25, (b) 50, and (c) 75 mg/L. (d) the kinetics graph of the decomposition process.

3.2.10 Degradation efficiency and kinetics of the degradation process by $BTiO_2$-ZnO, $BTiO_2$ and BZnO

To fully evaluate the photocatalytic degradation efficiency of TC by the studied photocatalysts, the adsorptive ability of each catalyst was assessed by first equilibrating the suspension in the dark for 30 min without light irradiation. Figs 18 (a-c) show the photocatalytic degradation graphs of TC by BZnO, $BTiO_2$ and $BTiO_2$-ZnO nanoparticles respectively under visible light illumination. The graphs are presented for the sake of comparison at the same experimental conditions of 50 mg/L concentration of TC at pH 7 and 100 mg/L of each catalyst was used. After 120 min of irradiation, 56, 58, and 63% of TC was degraded with BZnO, $BTiO_2$ and $BTiO_2$-ZnO nanoparticles respectively (Fig 18d). The rate of photocatalytic degradation of TC by BZnO, $BTiO_2$ and $BTiO_2$-ZnO nanoparticles are 0.0050 min^{-1}, 0.0056 min^{-1} and 0.0077 min^{-1} respectively Fig. 18(e-g). Photocatalytic degradation efficiency of the synthesized photocatalysts on TC obtained in this current study and other related studies have been compared in Table 3. Variable amounts of the catalyst and TC concentration were used, which led to a considerable difference in the degradation efficiency. The improved photocatalytic activity of heterojunction composite of $BTiO_2$ and BZnO compared to the individual materials can be attributed to the transfer of electrons and holes, which takes place in $BTiO_2$ and BZnO as they possess different redox energy levels for their corresponding conduction and valence bands. Efficient charge separation increases the lifetime of the charge carriers and enhances the efficiency of the interfacial charge transfer to adsorbed substrates (Liao *et al.*, 2008; Qin *et al.*, 2019; Tian *et al.*, 2015). Increased oxygen vacancies on the surface of both BZnO and $BTiO_2$ in the heterostructure could have also contributed in the effective degradation efficiency of TC by acting as electron acceptors, thereby decreasing the surface recombination centers. Oxygen vacancies can also facilitate the adsorbed O_2 to capture photo-induced electrons, synchronously generating superoxide radical anions, thereby greatly enhancing the photocatalytic properties (Ullattil *et al.*, 2018; Wang *et al.*, 2015).

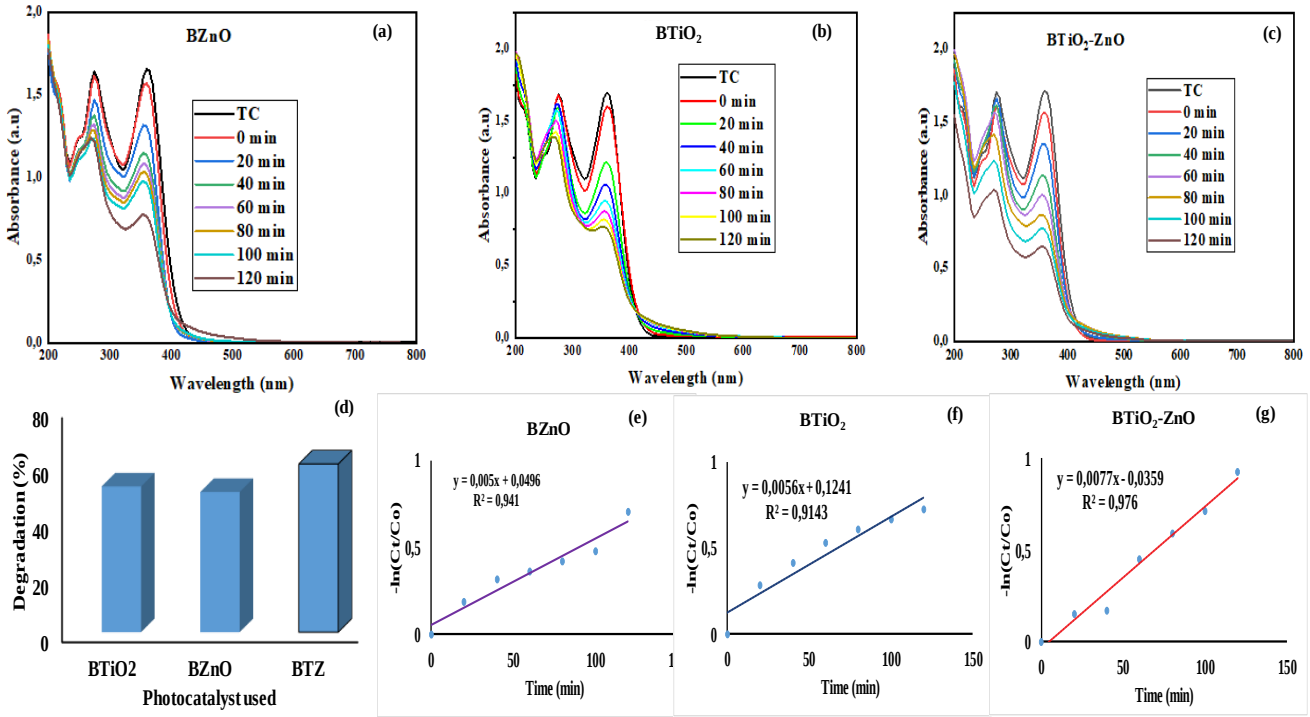


Figure 18:(a-c) Absorption profile, (d) percentage degradation, and (e-g) kinetics graphs of BZnO, $BTiO_2$, and $BTiO_2$-ZnO, respectively and (100 mg/L photocatalyst, 50 mg/L TC and pH = 7

Table 3: Comparison of TC degradation using the prepared $BTiO_2$–ZnO with other different TiO_2 or ZnO based advanced oxidation process catalysts earlier reported

Nanomaterial	Catalyst (mg/L)	TC (mg/L)	pH	K (min^{-1})	Time (min)	Efficiency (%)	Ref.
TiO_2@ZnO	2500	10	11	0.0296	180	99.11	(Heris *et al.*)
TiO_2–ZnO/CS–Gr	500	20	4	-	180	97.2	(Asadzadeh Patehkhor *et al.*, 2021)
ZnO/TiO_2 NBT	10	10	-	0.314	20	100	(Jiang *et al.*, 2022)

Black anatase-TiO_2	200	10	7.2	0.0045	270	66.2	(Wu *et al.*, 2021)
ZnO/γ-Fe_2O_3	10	30	-	0.01321	160	83	(Semeraro *et al.*, 2020)
TiO_2	1000	40	9.0	-	60	95	(Zhu et al., 2013)
Ag/ZnO@Biochar	10	50	6.0	-	60	70.3	(Hosny *et al.*, 2022)
TiO_2	200	10	-	-	120	56.7	(Wu et al., 2021)
MWCNT/TiO_2	200	10	5.2	-	300	83	(Wang *et al.*, 2011)
SDS/ZnO	20	40	7	-	150	49.0	(Jia et al., 2022)
TiO_2/activated carbon	1000	50	-	0.0029	75	100	(Martins *et al.*, 2017)
$BTiO_2$-ZnO	100	50	7.0	0.0077	120	63	Present study
	125	50	7.0	-	120	74	

3.2.11 Photocatalytic Mechanism

Figure 13 illustrates the photocatalytic mechanism leading to the degradation of tetracycline using $BTiO_2$-ZnO heterojunction photocatalyst under visible light. The TiO_2-ZnO heterojunction photocatalyst formed electron-hole pairs upon irradiation by UV light with energy exceeding its band gap energy. The photoactive centre $BTiO_2$ and the electron trapping BZnO process contributed to the lowering of the rate of recombination of the electron-hole pairs that have strong reducing and oxidizing powers, respectively (Haghighizadeh *et al.*, 2023). The efficient separation of photo-generated electrons

is facilitated by the transfer of electrons from TiO_2 to ZnO and holes from ZnO to TiO_2. This minimizes charge carrier recombination during the electron transfer process, thereby improving the photocatalytic reaction. By generating a second electron trap site and facilitating electron transport from TiO_2 to ZnO, oxygen vacancies in the photocatalyst further increase the photocatalytic activity and lower the rate of electron-hole recombination. The oxygen vacancies also serve as a source of reactive species, such as hydroxyl and superoxide radicals, which aid the breakdown of tetracycline. Due to electrostatic attraction and Van der Waals forces, the active antibiotic Tetracycline gets adsorbed onto the surface of the photocatalyst. The adsorbed antibiotics are attacked by the hydroxyl radicals (•OH) produced when water molecules on the surface of the photocatalyst react with photogenerated holes (h+). The •OH radicals attack the C-N-C fragment of TC, leading to the detachment of the N-methyl group (Wu et al., 2021). The photocatalytic breakdown intermediates are further oxidized by hydroxyl radicals, which causes the tetracycline to completely mineralize into carbon dioxide, water, and inorganic ions by ring-opening processes.

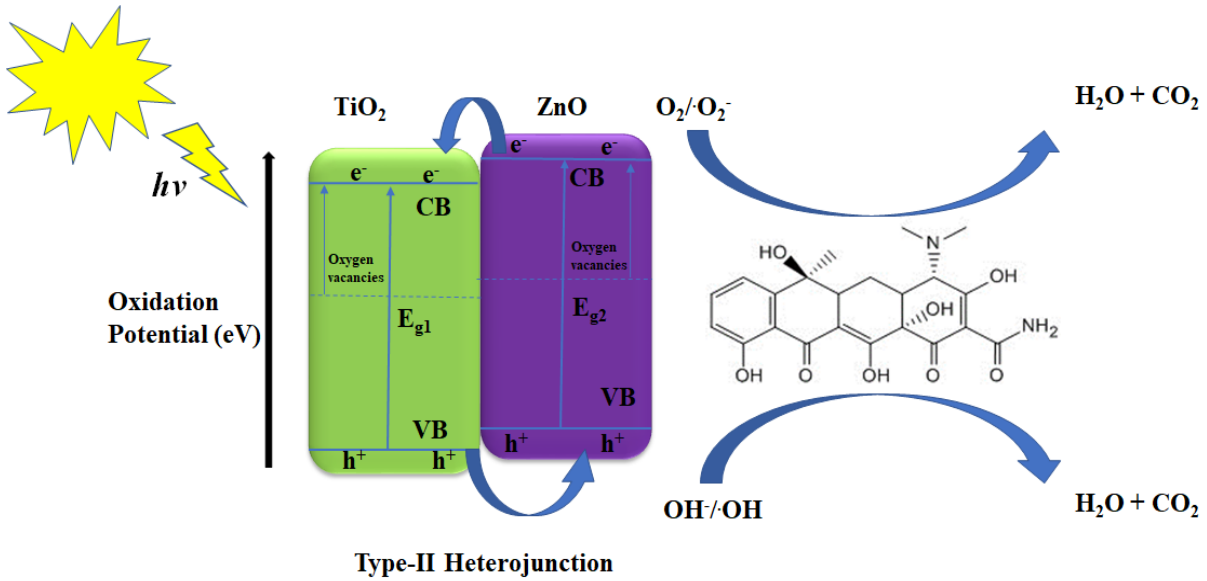


Figure 19: Proposed mechanism for the photocatalytic degradation of Tetracycline with $BTiO_2$-ZnO.

3.3 Conclusion

The fabrication of a highly photocatalytically active surface defective heterojunction semiconductor system composed of TiO_2 and ZnO was successfully achieved through a two-step method. The method of synthesis facilitated the formation of oxygen vacancies through surface engineering. The $BTiO_2$-ZnO heterostructure was able to degrade 64% of tetracycline, and it performed better as a photocatalyst than $BTiO_2$ and BZnO. The enhanced light absorption properties and improved charge separation of the photocatalyst due to the formation of heterojunction and oxygen vacancies might be attributed to the enhanced photocatalytic activity of $BTiO_2$-ZnO. The percentage degradation improved with increase in

photocatalyst dosage, a decrease in the concentration of tetracycline concentration and a neutral condition. The study also confirmed that the solution pH plays a critical role in the degradation process. The outcomes of the study showed that the use of $BTiO_2$-ZnO heterostructure in the photocatalytic degradation of tetracycline in water may guide the development of novel future semiconductor photocatalysts in water treatment that utilizes cheap and effective multi-photocatalytic enhancement techniques.

3.5 References

Abdissa, Y., Siraj, K., & Selale, G. (2018). Effect of Mg^{2+}, Ca^{2+} and Sr^{2+} ions doping on the band gap energy of ZnO nanoparticle. *Juniper Online Journal Material Science, 3*(4), 1-6.

Ajiboye, T. O., Saunyama, L., Ravele, M., Rasheed-Adeleke, A. A., Seheri, N., Onwudiwe, D. C., & Mhlanga, S. D. (2023). Synthesis approaches to ceramic membranes, their composites, and application in the removal of tetracycline from water. *Environmental Advances*, 100371.

Al-Khalqi, E. M., Abdul Hamid, M. A., Al-Hardan, N. H., & Keng, L. K. (2021). Highly sensitive magnesium-doped ZnO nanorod pH sensors based on electrolyte–insulator–semiconductor (EIS) Sensors. *Sensors, 21*(6), 2110.

Al-Taweel, S. S., & Saud, H. R. (2016). New route for synthesis of pure anatase TiO2 nanoparticles via utrasound-assisted sol-gel method. *J. Chem. Pharm. Res, 8*(2), 620-626.

Ali, M. M., Haque, M. J., Kabir, M. H., Kaiyum, M. A., & Rahman, M. (2021). Nano synthesis of ZnO–TiO2 composites by sol-gel method and evaluation of their antibacterial, optical and photocatalytic activities. *Results in Materials, 11*, 100199.

Amangelsin, Y., Semenova, Y., Dadar, M., Aljofan, M., & Bjørklund, G. (2023). The Impact of Tetracycline Pollution on the Aquatic Environment and Removal Strategies. *Antibiotics, 12*(3), 440.

Andronic, L., & Enesca, A. J. F. i. C. (2020). Black TiO2 synthesis by chemical reduction methods for photocatalysis applications. *8*, 565489.

Apostolescu, N., Farmus, R. E. T., Harja, M., Vizitiu, M. A., Cernatescu, C., Cobzaru, C., & Apostolescu, G. A. (2023). Photocatalytic Removal of Antibiotics from Wastewater Using the CeO2/ZnO Heterojunction. *Materials, 16*(2), 850. doi:ARTN 850 10.3390/ma16020850

Arora, I., Chawla, H., Chandra, A., Sagadevan, S., & Garg, S. (2022). Advances in the strategies for enhancing the photocatalytic activity of TiO2: Conversion from UV-light active to visible-light active photocatalyst. *Inorganic Chemistry Communications, 143*, 109700. doi:ARTN 109700 10.1016/j.inoche.2022.109700

Asadzadeh Patehkhor, H., Fattahi, M., & Khosravi-Nikou, M. (2021). Synthesis and characterization of ternary chitosan–TiO2–ZnO over graphene for photocatalytic degradation of tetracycline from pharmaceutical wastewater. *Scientific reports, 11*(1), 1-17.

Ba-Abbad, M. M., Kadhum, A. A. H., Mohamad, A. B., Takriff, M. S., & Sopian, K. (2012). Synthesis and catalytic activity of TiO2 nanoparticles for photochemical oxidation of concentrated chlorophenols under direct solar radiation. *Int. J. Electrochem. Sci, 7*(6), 4871-4888.

Bilal, M., Mehmood, S., Rasheed, T., & Iqbal, H. M. N. (2020). Antibiotics traces in the aquatic environment: persistence and adverse environmental impact. *Current Opinion in Environmental Science & Health, 13*, 68-74. doi:10.1016/j.coesh.2019.11.005

Cao, X., Chen, Y., Tang, J., Zhang, H., & Tang, X. (2023). Mechanistic study of Nitrogen-Modified Titanium Dioxide Nanoparticles for Enhancing the Degradation of Organic Dyes and Antibacterial Properties under Visible-Light Irradiation. *Materials Today Communications*, 106166.

Cao, X., Huang, A., Liang, C., Chen, H. C., Han, T., Lin, R., . . . Li, Y. (2022). Engineering Lattice Disorder on a Photocatalyst: Photochromic BiOBr Nanosheets Enhance Activation of Aromatic C-H Bonds via Water Oxidation. *J Am Chem Soc, 144*(8), 3386-3397. doi:10.1021/jacs.1c10112

Chand, K., Jiao, C., Lakhan, M. N., Shah, A. H., Kumar, V., Fouad, D. E., . . . Cao, D. (2021). Green synthesis, characterization and photocatalytic activity of silver nanoparticles synthesized with Nigella Sativa seed extract. *Chemical Physics Letters, 763*, 138218.

Chen, F., Yang, Q., Zhong, Y., An, H., Zhao, J., Xie, T., . . . Zeng, G. (2016). Photo-reduction of bromate in drinking water by metallic Ag and reduced graphene oxide (RGO) jointly modified BiVO4 under visible light irradiation. *Water Res, 101*, 555-563. doi:10.1016/j.watres.2016.06.006

Chougala, L., Yatnatti, M., Linganagoudar, R., Kamble, R., & Kadadevarmath, J. (2017). A simple approach on synthesis of TiO2 nanoparticles and its application in dye sensitized solar cells.

Clogston, J. D., & Patri, A. K. (2011). Zeta potential measurement. *Methods Mol Biol, 697*, 63-70. doi:10.1007/978-1-60327-198-1_6

Daghrir, R., & Drogui, P. (2013). Tetracycline antibiotics in the environment: a review. *Environmental Chemistry Letters, 11*(3), 209-227. doi:10.1007/s10311-013-0404-8

Divakaran, K., Baishnisha, A., Balakumar, V., Perumal, K. N., Meenakshi, C., & Kannan, R. S. (2021). Photocatalytic degradation of tetracycline under visible light using TiO2@sulfur doped carbon nitride nanocomposite synthesized via in-situ method. *Journal of Environmental Chemical Engineering, 9*(4), 105560. doi:ARTN 105560 10.1016/j.jece.2021.105560

Faus-Matoses, V., Faus-Matoses, I., Ruiz-Bell, E., & Faus-Llácer, V. J. (2017). Severe tetracycline dental discoloration: Restoration with conventional feldspathic ceramic veneers. A clinical report. *Journal of clinical and experimental dentistry, 9*(11), e1379.

Goncalves, R. A., Toledo, R. P., Joshi, N., & Berengue, O. M. (2021). Green Synthesis and Applications of ZnO and TiO(2) Nanostructures. *Molecules, 26*(8), 2236. doi:10.3390/molecules26082236

Haghighizadeh, A., Aghababai Beni, A., Haghmohammadi, M., Adel, M. S. S., & Farshad, S. (2023). Green Synthesis of ZnO-TiO2 Nano-Photocatalyst Doped with Fe (III) Ions Using Bitter Olive Extract to Treat Textile Wastewater Containing Reactive Dyes. *Water, Air, & Soil Pollution, 234*(6), 1-17.

Han, B., Wei, W., Li, M., Sun, K., & Hu, Y. H. (2019). A thermo-photo hybrid process for steam reforming of methane: highly efficient visible light photocatalysis. *Chem Commun (Camb), 55*(54), 7816-7819. doi:10.1039/c9cc04193a

Heberer, T., Feldmann, D. J. P. i. t. E. S., Fate, Effects, & Risks. (2008). Removal of pharmaceutical residues from contaminated raw water sources by membrane filtration. 427-453.

Heris, S. Z., Etemadi, M., Mousavi, S., Mohammadpourfard, M., & Ramavandi, B. Preparation and characterizations of TiO2/ZnO nanohybrid and its application in photocatalytic degradation of tetracycline in wastewater. *Available at SSRN*.

Hidalgo-Jimenez, J., Wang, Q., Edalati, K., Cubero-Sesin, J. M., Razavi-Khosroshahi, H., Ikoma, Y., . . . Horita, Z. (2020). Phase transformations, vacancy formation and variations of optical and photocatalytic properties in TiO2-ZnO composites by high-pressure torsion. *International Journal of Plasticity, 124*, 170-185. doi:10.1016/j.ijplas.2019.08.010

Hosny, M., Fawzy, M., & Eltaweil, A. S. (2022). Green synthesis of bimetallic Ag/ZnO@ Biohar nanocomposite for photocatalytic degradation of tetracycline, antibacterial and antioxidant activities. *Scientific Reports, 12*(1), 7316.

Hu, Y., Pan, Y., Wang, Z., Lin, T., Gao, Y., Luo, B., . . . Wang, L. (2020). Lattice distortion induced internal electric field in TiO2 photoelectrode for efficient charge separation and transfer. *Nature Communications, 11*(1), 2129.

Hunge, Y. M., Yadav, A., Kang, S.-W., & Kim, H. (2022). Photocatalytic degradation of tetracycline antibiotics using hydrothermally synthesized two-dimensional molybdenum disulfide/titanium dioxide composites. *Journal of Colloid and Interface Science, 606*, 454-463.

Jia, K., Liu, G., Lang, D. N., Chen, S. F., Yang, C., Wu, R. L., . . . Wang, J. D. (2022). Degradation of tetracycline by visible light over ZnO nanophotocatalyst. *Journal of the Taiwan Institute of Chemical Engineers, 136*, 104422. doi:ARTN 104422 10.1016/j.jtice.2022.104422

Jiang, Q., Han, Z., Qian, Y., Yuan, Y., Ren, Y., Wang, M., & Cheng, Z. (2022). Enhanced visible-light photocatalytic performance of ZIF-8-derived ZnO/TiO2 nano-burst-tube by solvothermal system adjustment. *Journal of Water Process Engineering, 47*, 102768.

Jiao, S., Zheng, S., Yin, D., Wang, L., & Chen, L. (2008). Aqueous photolysis of tetracycline and toxicity of photolytic products to luminescent bacteria. *Chemosphere, 73*(3), 377-382.

Li, W.-Y., Wang, Q., Xiao, Q.-F., & Dong, B.-Z. (2009). *Removal of tetracycline and oxytetracycline in water by a reverse osmosis membrane.* Paper presented at the 2009 3rd International Conference on Bioinformatics and Biomedical Engineering.

Li, W., Liang, R., Hu, A., Huang, Z., & Zhou, Y. N. J. R. a. (2014). Generation of oxygen vacancies in visible light activated one-dimensional iodine TiO 2 photocatalysts. *4*(70), 36959-36966.

Li, Z., Schulz, L., Ackley, C., & Fenske, N. (2010). Adsorption of tetracycline on kaolinite with pH-dependent surface charges. *Journal of colloid and interface science, 351*(1), 254-260.

Liao, D. L., Badour, C. A., & Liao, B. Q. (2008). Preparation of nanosized TiO2/ZnO composite catalyst and its photocatalytic activity for degradation of methyl orange. *Journal of Photochemistry and Photobiology a-Chemistry, 194*(1), 11-19. doi:10.1016/j.jphotochem.2007.07.008

Liao, Y., Xie, C., Liu, Y., Chen, H., Li, H., & Wu, J. (2012). Comparison on photocatalytic degradation of gaseous formaldehyde by TiO2, ZnO and their composite. *Ceramics International, 38*(6), 4437-4444.

López-Peñalver, J. J., Sánchez-Polo, M., Gómez-Pacheco, C. V., Rivera-Utrilla, J. J. J. o. C. T., & Biotechnology. (2010). Photodegradation of tetracyclines in aqueous solution by using UV and UV/H2O2 oxidation processes. *85*(10), 1325-1333.

Lyu, J., Yang, L., Zhang, L., Ye, B., & Wang, L. (2020). Antibiotics in soil and water in China-a systematic review and source analysis. *Environ Pollut, 266*(Pt 1), 115147. doi:10.1016/j.envpol.2020.115147

Martins, A. C., Cazetta, A. L., Pezoti, O., Souza, J. R., Zhang, T., Pilau, E. J., . . . Almeida, V. C. (2017). Sol-gel synthesis of new TiO2/activated carbon photocatalyst and its application for degradation of tetracycline. *Ceramics International, 43*(5), 4411-4418.

Mbenga, Y., Mthana, M. S., Mthiyane, D. M., Ogunjinmi, O. E., Singh, M., & Onwudiwe, D. C. (2023). Facile biosynthesis of CaO nanoparticles using extract of Tulbaghia violacea and evaluation of

their antibacterial and cytotoxicity activity. *Inorganic Chemistry Communications, 151*, 110581.

Menazea, A. A., & Awwad, N. S. (2020). Antibacterial activity of TiO2 doped ZnO composite synthesized via laser ablation route for antimicrobial application. *Journal of Materials Research and Technology-Jmr&T, 9*(4), 9434-9441. doi:10.1016/j.jmrt.2020.05.103

Momeni, M. M., Taghinejad, M., Ghayeb, Y., Bagheri, R., & Song, Z. (2019). Preparation of various boron-doped TiO 2 nanostructures by in situ anodizing method and investigation of their photoelectrochemical and photocathodic protection properties. *Journal of the Iranian Chemical Society, 16*, 1839-1851.

Mousa, H. M., Alenezi, J. F., Mohamed, I. M., Yasin, A. S., Hashem, A.-F. M., & Abdal-Hay, A. (2021). Synthesis of TiO2@ ZnO heterojunction for dye photodegradation and wastewater treatment. *Journal of Alloys and Compounds, 886*, 161169.

Mousa, H. M., Alenezi, J. F., Mohamed, I. M. A., Yasin, A. S., Hashem, A. F. M., & Abdal-hay, A. (2021). Synthesis of TiO2@ZnO heterojunction for dye photodegradation and wastewater treatment. *Journal of Alloys and Compounds, 886*, 161169. doi:ARTN 161169 10.1016/j.jallcom.2021.161169

Nguyen, P. M., Afzal, M., Ullah, I., Shahid, N., Baqar, M., & Arslan, M. (2019). Removal of pharmaceuticals and personal care products using constructed wetlands: effective plant-bacteria synergism may enhance degradation efficiency. *Environ Sci Pollut Res Int, 26*(21), 21109-21126. doi:10.1007/s11356-019-05320-w

OECD. (2019). Pharmaceutical Residues in Freshwater: Hazards and Policy Responses. *Hazards and Policy Responses.* Retrieved from https://www.oecd.org/environment/resources/Pharmaceuticals-residues-in-freshwater-policy-highlights-preliminary-version.pdf

Ouyang, J. B., Zhou, L. M., Liu, Z. R., Heng, J. Y. Y., & Chen, W. Q. (2020). Biomass-derived activated carbons for the removal of pharmaceutical mircopollutants from wastewater: A review. *Separation and Purification Technology, 253*, 117536. doi:ARTN 117536 10.1016/j.seppur.2020.117536

Paredes, L., Murgolo, S., Dzinun, H., Othman, M. H. D., Ismail, A. F., Carballa, M., & Mascolo, G. (2019). Application of immobilized TiO2 on PVDF dual layer hollow fibre membrane to improve the photocatalytic removal of pharmaceuticals in different water matrices. *Applied Catalysis B-Environmental, 240*, 9-18. doi:10.1016/j.apcatb.2018.08.067

Pellegrino, F., Pellutie, L., Sordello, F., Minero, C., Ortel, E., Hodoroaba, V. D., & Maurino, V. (2017). Influence of agglomeration and aggregation on the photocatalytic activity of TiO2 nanoparticles. *Applied Catalysis B-Environmental, 216*, 80-87. doi:10.1016/j.apcatb.2017.05.046

Phoon, B. L., Ong, C. C., Mohamed Saheed, M. S., Show, P. L., Chang, J. S., Ling, T. C., . . . Juan, J. C. (2020). Conventional and emerging technologies for removal of antibiotics from wastewater. *J Hazard Mater, 400*, 122961. doi:10.1016/j.jhazmat.2020.122961

Polianciuc, S. I., Gurzau, A. E., Kiss, B., Stefan, M. G., & Loghin, F. (2020). Antibiotics in the environment: causes and consequences. *Med Pharm Rep, 93*(3), 231-240. doi:10.15386/mpr-1742

Praveen, P., Viruthagiri, G., Mugundan, S., & Shanmugam, N. (2014). Structural, optical and morphological analyses of pristine titanium di-oxide nanoparticles--synthesized via sol-gel route. *Spectrochim Acta A Mol Biomol Spectrosc, 117*, 622-629. doi:10.1016/j.saa.2013.09.037

Qin, R., Meng, F. M., Khan, M. W., Yu, B., Li, H. J., Fan, Z. H., & Gong, J. F. (2019). Fabrication and enhanced photocatalytic property of TiO2-ZnO composite photocatalysts. *Materials Letters, 240*, 84-87. doi:10.1016/j.matlet.2018.12.139

Raja, S., Ramesh, V., & Thivaharan, V. (2017). Green biosynthesis of silver nanoparticles using Calliandra haematocephala leaf extract, their antibacterial activity and hydrogen peroxide sensing capability. *Arabian journal of chemistry, 10*(2), 253-261.

Rajakumar, G., Rahuman, A. A., Roopan, S. M., Khanna, V. G., Elango, G., Kamaraj, C., . . . Velayutham, K. (2012). Fungus-mediated biosynthesis and characterization of TiO2 nanoparticles and their activity against pathogenic bacteria. *Spectrochimica Acta Part A: Molecular and Biomolecular Spectroscopy, 91*, 23-29.

Rajaraman, T. S., Gandhi, V. G., Nguyen, V. H., & Parikh, S. P. (2022). Aluminium foil-assisted NaBH4 reduced TiO2 with surface defects for photocatalytic degradation of toxic fuchsin basic dye. *Applied Nanoscience*, 1-20. doi:10.1007/s13204-022-02628-x

Rajendran, S. P., & Sengodan, K. (2017). Synthesis and characterization of zinc oxide and iron oxide nanoparticles using Sesbania grandiflora leaf extract as reducing agent. *Journal of Nanoscience, 2017*.

Ravele, M. P., Oyewo, O. A., Ramaila, S., Mavuru, L., & Onwudiwe, D. C. (2021). Photocatalytic Degradation of Tetracycline in Aqueous Solution Using Copper Sulfide Nanoparticles. *Catalysts, 11*(10), 1238.

Rohr, J. R., Barrett, C. B., Civitello, D. J., Craft, M. E., Delius, B., DeLeo, G. A., . . . Tilman, D. (2019). Emerging human infectious diseases and the links to global food production. *Nat Sustain, 2*(6), 445-456. doi:10.1038/s41893-019-0293-3

Saadati, F., Keramati, N., & Ghazi, M. M. (2016). Influence of parameters on the photocatalytic degradation of tetracycline in wastewater: A review. *Critical Reviews in Environmental Science and Technology, 46*(8), 757-782. doi:10.1080/10643389.2016.1159093

Safari, G. H., Hoseini, M., Seyedsalehi, M., Kamani, H., Jaafari, J., & Mahvi, A. H. (2015). Photocatalytic degradation of tetracycline using nanosized titanium dioxide in aqueous solution. *International Journal of Environmental Science and Technology, 12*(2), 603-616. doi:10.1007/s13762-014-0706-9

Saravanan, A., Deivayanai, V., Kumar, P. S., Rangasamy, G., Hemavathy, R., Harshana, T., . . . Krishnapandi, A. (2022). A detailed review on advanced oxidation process in treatment of wastewater: Mechanism, challenges and future outlook. *Chemosphere*, 136524.

Sawunyama, L., Oyewo, O. A., Seheri, N., Onjefu, S. A., & Onwudiwe, D. C. (2023). Metal oxide functionalized ceramic membranes for the removal of pharmaceuticals in wastewater. *Surfaces and Interfaces*, 102787.

Semeraro, P., Bettini, S., Sawalha, S., Pal, S., Licciulli, A., Marzo, F., . . . Giancane, G. (2020). Photocatalytic degradation of tetracycline by ZnO/γ-Fe2O3 paramagnetic nanocomposite material. *Nanomaterials, 10*(8), 1458.

Sharwani, A. A., Narayanan, K. B., Khan, M. E., & Han, S. S. (2022). Photocatalytic degradation activity of goji berry extract synthesized silver-loaded mesoporous zinc oxide (Ag@ZnO) nanocomposites under simulated solar light irradiation. *Sci Rep, 12*(1), 10017. doi:10.1038/s41598-022-14117-w

Siregar, N., Motlan, Panggabean, J. H., Sirait, M., Rajagukguk, J., Gultom, N. S., & Sabir, F. K. (2021). Fabrication of dye-sensitized solar cells (DSSC) using Mg-doped ZnO as photoanode and extract of rose myrtle (Rhodomyrtus tomentosa) as natural dye. *International Journal of Photoenergy, 2021*, 1-7.

Song, C., Liu, H. Y., Guo, S., & Wang, S. G. (2020). Photolysis mechanisms of tetracycline under UV irradiation in simulated aquatic environment surrounding limestone. *Chemosphere, 244*, 125582. doi:10.1016/j.chemosphere.2019.125582

Sunaryono, S., Halizah, S. N., Zulaikah, S., Susanto, H., Mufti, N., & Taufiq, A. (2021). *Contribution of ZnO/TiO2 nanocomposite particles towards bacterial growth inhibition.* Paper presented at the AIP Conference Proceedings.

Sutapa, I., Wahid Wahab, A., Taba, P., & Nafie, N. (2018). *Dislocation, crystallite size distribution and lattice strain of magnesium oxide nanoparticles.* Paper presented at the Journal of Physics: Conference Series.

Tian, M., Mahjouri-Samani, M., Eres, G., Sachan, R., Yoon, M., Chisholm, M. F., . . . Duscher, G. (2015). Structure and Formation Mechanism of Black TiO2 Nanoparticles. *ACS Nano, 9*(10), 10482-10488. doi:10.1021/acsnano.5b04712

Ullattil, S. G., Narendranath, S. B., Pillai, S. C., & Periyat, P. (2018). Black TiO2 Nanomaterials: A Review of Recent Advances. *Chemical Engineering Journal, 343*, 708-736. doi:10.1016/j.cej.2018.01.069

Valerio, T. L., Maia, G. A. R., Gonçalves, L. F., Viomar, A., Banczek, E. d. P., & Rodrigues, P. R. P. (2019). Study of the Nb 2 O 5 insertion in ZnO to dye-sensitized solar cells. *Materials Research, 22*.

Wang, C., Wu, D., Wang, P. F., Ao, Y. H., Hou, J., & Qian, J. (2015). Effect of oxygen vacancy on enhanced photocatalytic activity of reduced ZnO nanorod arrays. *Applied Surface Science, 325*, 112-116. doi:10.1016/j.apsusc.2014.11.003

Wang, P., Yap, P.-S., & Lim, T.-T. (2011). C–N–S tridoped TiO2 for photocatalytic degradation of tetracycline under visible-light irradiation. *Applied Catalysis A: General, 399*(1-2), 252-261.

Wang, Q., Qian, X., Xu, H., He, G., & Chen, H. (2023). Enriched surface oxygen vacancies of Bi2WO6/NH2-MIL-68 (In) Z-scheme heterojunction with boosted visible-light photocatalytic degradation for levofloxacin: Performance, degradation pathway and mechanism insight. *Separation and Purification Technology, 306*, 122577.

Wang, X., Zhu, G., Wang, C., & Niu, Y. (2021). Effective degradation of tetracycline by organic-inorganic hybrid materials induced by triethylenediamine. *Environ Res, 198*, 111253. doi:10.1016/j.envres.2021.111253

William IV, L., Kostedt, I., Ismail, A. A., & Mazyck, D. W. (2008). Impact of heat treatment and composition of ZnO− TiO2 nanoparticles for photocatalytic oxidation of an azo dye. *Industrial & engineering chemistry research, 47*(5), 1483-1487.

Wu, S., Li, X., Tian, Y., Lin, Y., & Hu, Y. H. (2021). Excellent photocatalytic degradation of tetracycline over black anatase-TiO2 under visible light. *Chemical Engineering Journal, 406*, 126747.

Zhang, L. L., Xing, Z. P., Zhang, H., Li, Z. Z., Wu, X. Y., Zhang, X. D., . . . Zhou, W. (2016). High thermostable ordered mesoporous SiO2-TiO2 coated circulating-bed biofilm reactor for unpredictable photocatalytic and biocatalytic performance. *Applied Catalysis B-Environmental, 180*, 521-529. doi:10.1016/j.apcatb.2015.07.002

Zhu, X. D., Wang, Y. J., Sun, R. J., & Zhou, D. M. (2013). Photocatalytic degradation of tetracycline in aqueous solution by nanosized TiO2. *Chemosphere, 92*(8), 925-932. doi:10.1016/j.chemosphere.2013.02.066

CHAPTER 4

Fabrication and Characterization of Low-Cost Ceramic Membranes from Coal Fly Ash and Natural Sand

4.0 Introduction

The interest on ceramic membranes has recently increased due to their versatility and effectiveness in addressing the expanding demands for cutting-edge separation technologies (Issaoui & Limousy, 2019; SawunyamaOlatunde *et al.*, 2024). Application in water treatment, gas separation, pervaporation, membrane reactors, and medicinal fields are some of the industrial relevance of ceramic membranes. The overall cost of ceramic membranes is mostly influenced by the price of their raw materials, the production time, and the amount of energy used during the sintering process All these make the wide deployment of ceramic membrane technology costly (Zou *et al.*, 2021). The price is further hiked by the incorporation of pore-forming substances, plasticizers, lubricants, and binding chemicals into the membrane (Rani & Kumar, 2021). The reported current cost price of commercially available ceramic membranes composed of alumina, silica, titania, zirconia, and their composites is above \$500 per m^2 (Sawunyama *et al.*, 2023). In addition, the fabrication process of ceramic membranes lasts for two to three days, requiring an inert environment, and high energy above 1500 °C (Liang *et al.*, 2021). The shift in environmental legislation on the use of chemicals, and the quest to drastically reduce the manufacturing costs of ceramic membranes have attracted research interest. It has inspired the fabrication of ceramic membranes from waste and low-cost natural raw materials. These natural resources and waste products are cheap, abundant, and readily available locally (Khedidja *et al.*, 2024; Xue *et al.*, 2024).

Natural materials used in the fabrication of ceramic membranes includes clay (Foorginezhad *et al.*, 2022), sand (Alftessi *et al.*, 2022), and bentonite (Satyannarayana *et al.*, 2022), while waste materials include coal fly ash (Chathurappan & Anandkumar, 2022; Huang *et al.*, 2022), volcanic ash, and rice husk ash (Raychaudhuri & Behera, 2020), among others. The functional characteristics of various raw materials used as precursors for ceramic membrane fabrication vary. The best starting material should yield a ceramic membrane with an ideal surface charge and hydrophilic-hydrophobic characteristics, superior mechanical strength, improved thermal and chemical stability, good pore size distribution, less energy use, and less environmental contamination (Arumugham *et al.*, 2021; SawunyamaAjiboye *et al.*, 2024; Zou et al., 2021). Different waste materials can also be combined in the fabrication of ceramic

membranes. This approach has proven to be effective in impacting a range of desirable properties on the ceramic membranes such as enhanced mechanical strength, improved thermal stability, and greater permeability (Wang *et al.*, 2021). Furthermore, the ability to blend various waste materials enables the tailoring of membrane functionality to fulfil certain application requirements. For example, Kouotou *et al.* (2024) successfully fabricated ceramic membrane by combining kaolinitic clay with waste from palm and mango fruits. The waste materials from the palm and mango acted as pore formers, adding to the porosity nature of the membrane. The resultant ceramic membrane showed very good physicochemical qualities.

The disposal of waste materials like coal fly ash is a huge environmental problem, particularly in developing countries. It results in significant human respiratory health issues and soil acidification. For instance, Zimbabwe produces about 136.6 t of fly ash from coal every day and they are not utilized in any way (Bobo *et al.*). In other parts of the world, several studies have been reported on the potential large-scale use of coal fly ash in ceramic membranes. Gradients in pressure, chemical concentration, temperature, and electric potential could all act as the driving forces of these membranes. Chathurappan and Anandkumar (2022) prepared a coal fly ash-based ceramic membrane with 39.8% membrane porosity and a hydraulic pore radius of 41nm. The prepared multipurpose ultrafiltration membrane was used to treat Rhodamine B, Bovine Serum Albumin and Vanillin, showing removal efficiency of 95.2%, 92.8% and 39.4% respectively. Zhang *et al.* (2023) fabricated a ceramic hydrophobic microfiltration membrane (0.18 μm pore size) from coal fly ash. It was utilized in water desalination with a water flux of 9.54 $L \cdot m^{-2} \cdot h^{-1}$ and a salt rejection of higher than 98.36%. Using coal fly ash as a raw material for ceramic membranes, as part of a waste-to-resource strategy, can not only reduce the improper disposal of large amounts of coal fly ash to the environment but also lower the cost of membrane production. In addition to serving as a main material, the presence of metal oxides with low melting points can cause coal fly ash to also act as a sintering agent. This lowers the sintering temperature and, consequently, lowers the cost of fabrication (Zou *et al.*, 2019). Additionally, due to its synergistic effect of filtration, adsorption, and catalytic properties, ceramic membranes have excellent pollutant removal performance (He *et al.*, 2022).

Ceramic membranes made from coal fly ash still face significant limitations, such as lower mechanical strengths caused by the presence of volatile and degradable materials in coal fly ash (Huang *et al.*, 2023; Samadi *et al.*, 2022). To improve the mechanical strength and stability of coal fly ash ceramic membranes, different inorganic compounds have been incorporated into the ceramic membrane (Liang et al., 2021). However, to reduce the production cost of ceramic membranes to a greater extend, such inorganic additives should be derived from locally available cheap natural materials that are rich in aluminium and silicon such as bauxite and natural sand respectively. Silica sand is a natural white ceramic material with a high melting point and high purity of silica. It is made up of silicon and oxygen, the two most abundant naturally occurring elements (Alftessi *et al.*, 2021). In addition to increasing the

mechanical strength of ceramic membranes, silica sand can also increase their stiffness, chemical resistance, and adsorption capabilities (Addich *et al.*, 2022). The silanol (Si-OH) and siloxane (Si-O-Si) groups in silica sand can make these properties easier to achieve (Meldha *et al.*, 2023). Other challenges associated with the fabrication of ceramic membranes from waste materials include inconsistent quality and properties of the fabricated ceramic membranes. This is due to the considerable regional variations in the elemental and phase composition of the waste materials. The existence of contaminants in the solid wastes such as heavy metals and radioactive elements also makes it difficult to manage the structure and properties of the membranes, since these can cause variability and complicate the processes of fabrication and application. Furthermore, most membranes made from these materials usually have pore diameters between 0.1 and 5 μm, making them ideal for microfiltration applications. Finally, membrane fouling continues to be a major problem that affects the membranes' long-term effectiveness and performance (Abdullayev, 2022; Al-Shaeli *et al.*, 2022).

Therefore, this work aims to prepare inexpensive and eco-friendly porous ceramic membranes using natural sand and heavy metal leached coal fly ash. This is to achieve a waste-to-resource strategy, use local natural resources, and lower the cost of the ceramic membrane. The effects of the amount of natural sand and sintering temperature on the properties of the prepared coal fly ash-based flat ceramic membrane were studied. Different characterization techniques including X-ray diffraction (XRD), X-ray fluorescence (XRF), Fourier transform infrared (FTIR) spectroscopy, Thermogravimetric analysis (TGA), and scanning electron microscopy (SEM) were utilized to study properties of the prepared ceramic membrane.

4.1 Experimental

4.1.1. Materials

The main starting materials used in the fabrication of the flat ceramic membranes were natural sand from Masvingo, Zimbabwe, and coal fly ash from Harare Thermal Power Station in Zimbabwe. **Table 1** presents the specific chemical compositions of the coal fly ash and natural sand utilized in the study. Natural sand was used to increase the mechanical strength and thermal stability of the membrane, while dextrin and carboxymethyl cellulose (CMC) were used as pore former and binder respectively. These additives were purchased from Merck, South Africa.

4.1.2. Leaching of heavy metals present in coal fly ash

Leaching experiments were evaluated using a modified method reported by Fedje *et al.* (2010). The experiments were carried out in a 1000 mL round bottom flask placed on a magnetic stirrer at 25 ^{o}C. The coal fly ash (10 g) was mixed with 500 mL of 1 mol/ L of acetic acid solution for 4 h under continuous moderate stirring (200 rpm). After the stirring process, the mixture was filtered. The filtrate was discarded while the residue was washed with distilled water to remove any unspent acetic acid and dried at 110 °C for 10 h. Finally, the leaching product was analyzed using ICP-OES.

4.1.3. Ceramic membrane fabrication

The ceramic membranes were fabricated using the pressing method, which is widely used in fabricating flat ceramic membranes (Latwal *et al.*, 2023; Ma *et al.*, 2023). Firstly, the acetic acid-leached coal fly ash, pulverized sand, additives and appropriate amount of water were mixed and stirred uniformly. The formed suspension was thoroughly dried at 110 ^{o}C for 10 h. The dried mixture was ground with a mortar and pestle followed by sieving to 75 μm. The flat ceramic membranes were then prepared by shaping a pre-weighed, mixed precursor powder into a disk with a defined diameter of 40 mm using a uniaxial press under a pressure of 40 MPa for 3 min. The fabricated ceramic membranes were dried in a hot air oven at 110 °C for 10 h for the complete removal of loose moisture. To avoid thermal shocks and cracks, the membrane was then sintered in a furnace at a rate of 5 °C min^{-1} up to a range of temperatures between 800 °C and 1200 °C for 2 h. The composition of the precursor mixture is given in **Table 1** and the detailed steps for the fabrication of coal fly ash/sand ceramic membranes is schematically illustrated in **Fig. 1**.

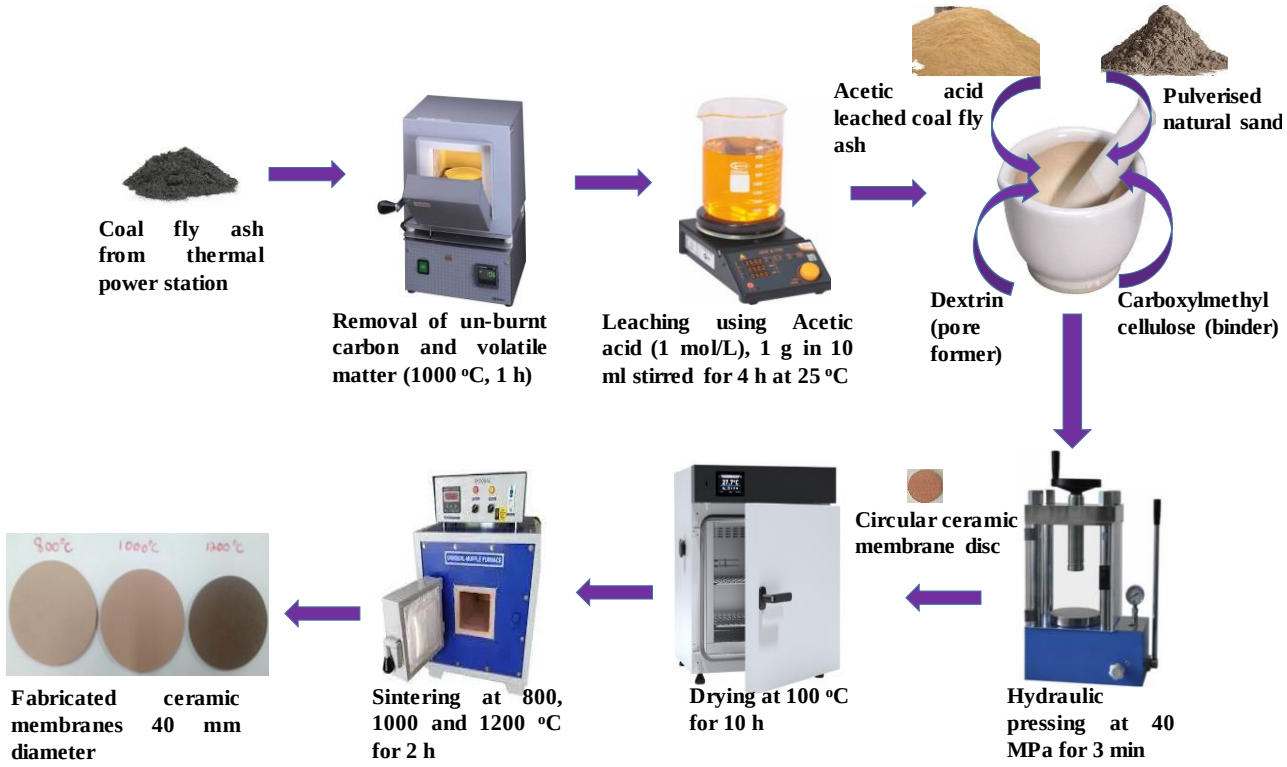


Figure 1: Schematic diagram of the fabrication process of the ceramic membranes by the pressing technique.

Table 1: Formulation of the raw materials and fabrication parameters.

Ceramic membrane (CM)	Coal fly ash (g)	Natural sand (g)	Dextrin (g)	Sodium carboxymethyl cellulose (g)	Distilled water (mL)	Sintering temperature (°C)
A_0	90	0	3	7	150	-
A_1	90	0	3	7	150	800
A_2	90	0	3	7	150	1000
A_3	90	0	3	7	150	1200
B_0	80	10	3	7	150	-
B_1	80	10	3	7	150	800
B_2	80	10	3	7	150	1000
B_3	80	10	3	7	150	1200
C_0	70	20	3	7	150	-
C_1	70	20	3	7	150	800
C_2	70	20	3	7	150	1000
C_3	70	20	3	7	150	1200
D_0	60	30	3	7	150	-
D_1	60	30	3	7	150	800
D_2	60	30	3	7	150	1000

D_3	60	30	3	7	150	1200

4.1.4 Water uptake

The water uptake of the fabricated ceramic membranes was determined using a method reported by Rao *et al.* (2023). The prepared membranes were firstly immersed in distilled water at room temperature and left for 24 h. Thereafter, the immersed ceramic membranes were wiped with paper towel and weighed to give wet weight (*wW*). After that the membranes were dried in a hot air oven at 100 °C for 12 h and the dry weight (*dW*) of the ceramic membranes was noted. Water uptake % was determined using equation 1.

$$\boldsymbol{Percentage\ Water\ uptake} = \frac{\boldsymbol{wW - dW}}{\boldsymbol{wW}} * \mathbf{100}\% \qquad \textbf{(1)}$$

4.1.5 Chemical stability

The chemical stability of the fabricated ceramic membranes was evaluated using hydrochloric acid and sodium hydroxide at the pH of 1.5 and 13 respectively. The as-prepared ceramic membranes were soaked individually into HCl and NaOH for 1 week at room temperature. The chemical resistance of the ceramic membrane was evaluated in terms of weight loss of the ceramic membrane after seven days.

4.1.6 Water absorption and Porosity

The open porosity of the fabricated ceramic membrane was determined by the Archimedes technique (Obada *et al.*, 2023). The dried ceramic membrane was first weighed to give dry weight (**dW**), then immersed in distilled water at 25 ^{o}C. After 24 h, the immersed ceramic membrane was removed from the water, wiped with a paper towel, and weighed to give wet weight (**wW**). The open porosity was calculated using the expressions in equations 2 and 3.

$$\boldsymbol{Percentange\ Membrane\ Porosity}(\boldsymbol{\varepsilon}) = \frac{\boldsymbol{wW - dW}}{\boldsymbol{\rho_W * V_{memb}}} * \mathbf{100} \qquad \textbf{(2)}$$

$$\boldsymbol{V_{memb} = \pi r^2 h} \qquad \textbf{(3)}$$

Where $\mathbf{V_{memb}}$ **(m^3)** is the volume of the fabricated ceramic membrane, **h (m)** is the membrane thickness, **r (m)** radius of the membrane, $\boldsymbol{\rho_W}$ **(kg/m^3)** is the density of water.

4.1.7 Pure water permeation and mean pore radius

Water permeation of the fabricated ceramic membranes was determined using a method reported by Ni *et al.* (2022). The pure water permeation test was evaluated using a dead-end filtration set-up and the filtration process was driven by pressure from N_2 gas. Firstly, a known volume of water was poured into the dead-end column, which was then compressed with nitrogen gas. The time taken to collect all the water permeate was recorded. The water flux was determined using the formula in Equation 4, and the water permeability was calculated using Equation 5.

$$\boldsymbol{J = \frac{V}{A\Delta T}} \quad \textbf{(4)}$$

$$\boldsymbol{J^1 = \frac{V}{A\Delta TP}} \quad \textbf{(5)}$$

Where $\boldsymbol{J}$= pure water flux (L/m^2/h), $\boldsymbol{V}$= Volume of permeate in (L), $\boldsymbol{A}$= the fabricated membrane's effective surface membrane area (m^2), $\boldsymbol{\Delta T}$= time taken to collect the permeate (h), $\boldsymbol{J^1}$= water permeability (L/m^2/h/kPa) and $\boldsymbol{P}$ = transmembrane pressure (kPa).

The mean pore radius of the fabricated ceramic membranes was determined using the filtration velocity method and applying Guerout–Elford–Ferry equation (6) (Mishra & Mukhopadhyay, 2017). The pore size (diameter) of the fabricated ceramic membranes was determined by multiplying the mean pore radius ($\mathbf{r_m}$) by two.

$$\boldsymbol{r_m = \sqrt{\frac{2.9 - 1.7\varepsilon * 8\eta_L Q}{\varepsilon * \Delta P * A}}} \quad \textbf{(6)}$$

Where $\boldsymbol{r_m}$= mean pore radius (µm), $\boldsymbol{\eta}$= water viscosity (8.9×10^{-4} Pa s), $\boldsymbol{\varepsilon}$= porosity of the fabricated ceramic membrane (%), $\boldsymbol{\iota}$= membrane thickness (m), $\boldsymbol{Q}$= volume of permeate water (m^3/s), $\boldsymbol{A}$= the fabricated membrane's effective surface membrane area (m^2) and $\Delta\boldsymbol{P}$= is operational pressure (Pa)

4.1.8 Linear firing shrinkage and loss on ignition

Linear firing shrinkage and loss on ignition of the fabricated ceramic membrane were evaluated after the sintering process. The ceramic membrane's thickness and diameter were measured before and after sintering to give the resultant total linear shrinkage in terms of volume using the expression in Equation 7. Loss on ignition was evaluated as the loss of weight of the ceramic membrane after sintering using the expression given in Equation 8.

$$\boldsymbol{Linear\ firing\ shrinkage = \frac{V_i - V_f}{V_i} * 100} \quad \textbf{(7)}$$

Where V_i is the initial volume of the ceramic membrane before sintering and V_f is the final volume of the ceramic membrane after sintering

$$\textbf{Loss on iginition} = \frac{W_i - W_f}{W_i} * 100 \quad \textbf{(8)}$$

Where W_i is the initial weight of the ceramic membrane before sintering and W_f is the final weight of the ceramic membrane after sintering

4.1.9 Average crystallite size

The average crystallite sizes in the fabricated ceramic membranes were determined using Scherrer's formula (Equation 9).

$$\textbf{Crystallite size } (D) = \frac{K\lambda}{\beta Cos\theta} \quad \textbf{(9)}$$

Where *K* is the Scherrer's constant (Here, taken as 0.94), λ is the wavelength of X-rays (Å), β = F. W. H. M (Full Width at Half Maxima in degrees), θ = Peak position in XRD graph (that is 2θ in degrees).

4.1.10 Ceramic membrane characterization

The composition of coal fly ash and natural sand was evaluated using X-ray fluorescence spectroscopy (Zetium, PANalytical Corporation, Netherlands). Inductively coupled plasma - optical emission spectrometry (PerkinElmer's NexION 2000 ICP-OES) was used to determine the elemental composition of the coal fly ash. Functional groups of the main precursor materials and ceramic membranes were analyzed using an FT-IR spectrophotometer (Bruker alpha-P FTIR spectrophotometer). Phase composition of coal fly ash, natural sand and synthesized ceramic membranes was analyzed using X-ray diffraction (Bruker D8 Advance X-ray diffractometer (Karlsruhe, Germany). The surface morphology and texture of the fabricated ceramic membrane were analyzed using scanning electron microscopy (Quanta FEG 250 Environmental scanning electron microscope (ESEM) coupled with EDX.). Thermal stability properties and weight loss of precursor powder of different compositions were evaluated using a Thermogravimetric Analyzer (SDTQ 600 thermal instrument). The mechanical strength of the ceramic membranes was evaluated using the three-point bending load method reported by Mazel *et al.* (2014). This test involved applying compressive stress to the upper portion of the circular ceramic membrane, which resulted in tensile stress to the lower portion. The membrane breaks due to the highest tensile stress, which was present on the lower face of the sample. The flexural strength (MPa) of the circular flat ceramic membrane was calculated using (Equation 10).

$$\boldsymbol{Flexural\ strength\ (MPa) = \frac{3FL}{2Dh^2}} \quad \textbf{(10)}$$

Where **F=** applied force (N) resulting in the breaking of the membrane, D= the circular ceramic membrane diameter (mm), **h=** is the ceramic membrane thickness (mm) **L= is** the distance between the supports (mm)

4.2 Results and Discussion

4.2.1 X-ray fluorescence (XRF) analysis and Leaching studies

X-ray fluorescence analysis was used to analyze the chemical composition of coal fly ash and natural sand. The chemical composition in weight% is displayed in **Table 2**. It is observed that coal fly ash is generally composed of alumina (33.67%) and silica (48.3%) with traces of alkali and alkaline–earth metal oxides and transition metal oxides. The loss on ignition (LOI) of CFA was 10.2 wt.% and is mainly attributed to the residual carbon content and volatile organic matter in coal fly ash. The formation of pores in ceramic membranes can be considerably aided by the presence of this volatile organic matter and residual carbon content (Zou et al., 2019). Natural sand is mostly composed of silica (86%) and traces of metal oxides. ICP OES analysis revealed that the coal fly ash also contains heavy metals, some of which exceeded WHO limits as shown in **Table 3**. The leaching profile of heavy metals is shown in Table. 3 indicates that acetic acid has a strong leaching ability for As, Cr, Cu, Ni, and Pb at pH 5. This could be attributed to the sublime hydrolysis of metal cations in weak acidic conditions (Geng *et al.*, 2020). The leaching ability of acetic acid can also be due to its coordinative ability with metal ions which results in the formation of a stable ligand that makes the leaching of metals much easier. This occurs when carboxyl functional groups are used to generate soluble organic combinations, which inhibits the adsorption of heavy metals on coal fly ash's surface (Ke *et al.*, 2020; Leelarungroj *et al.*, 2018). Studies by Yan *et al.* (2014) also showed the strong leaching ability of acetic acid toward heavy metals. In their studies, acetic acid proved to be a better option than inorganic acids.

Table 2: Chemical composition of coal fly ash and natural sand expressed as percent by weight.

Materials	**Oxides and their percentage composition**											
	SiO_2	**Al_2O_3**	**Fe_2O_3**	**CaO**	**MgO**	**SO_3**	**Na_2O**	**K_2O**	**Mn_2O_3**	**TiO_2**	**P_2O_5**	**LOI**
CFA_2	45.30	32.67	4.71	11.19	1.04	1.43	1.20	0.92	0.08	1.32	0.70	10.20
NS	86.20	2.50	1.30	6.69	0.23	0.10	0.14	0.44	0.01	0.11	0.02	2.20

LOI mean loss on ignition.

Table 3: Heavy metal concentrations in coal fly ash both before and after leaching studies (unit: ppb).

	Heavy metals and their concentration in (ppb)						
	As	**Cd**	**Cr**	**Cu**	**Ni**	**Pb**	**Hg**
WHO limits	50.00	5.00	50.00	1500.00	100.00	50.00	1.00
CFA_A	112.70	0.08	273.1	91.00	87.00	6.09	0.04
CFA_B	38.79	0.07	55.8	24.9	30.57	3.60	0.11

CFA_A – coal fly ash before the leaching process and **CFA_B** - coal fly ash after the leaching process.

4.2.2 Material composition and appearance of the fabricated ceramic membrane.

Fig. 2 shows the images of the flat ceramic membranes fabricated in this study. The brown colour of the fabricated ceramic membranes changed to chocolate brown when the sintering temperature increased to 1200 ℃. It is also very clear that the diameter of the fabricated membranes reduces as the sintering temperature increases. All these could be a result of overheating of the ceramic membranes and their resultant densification.

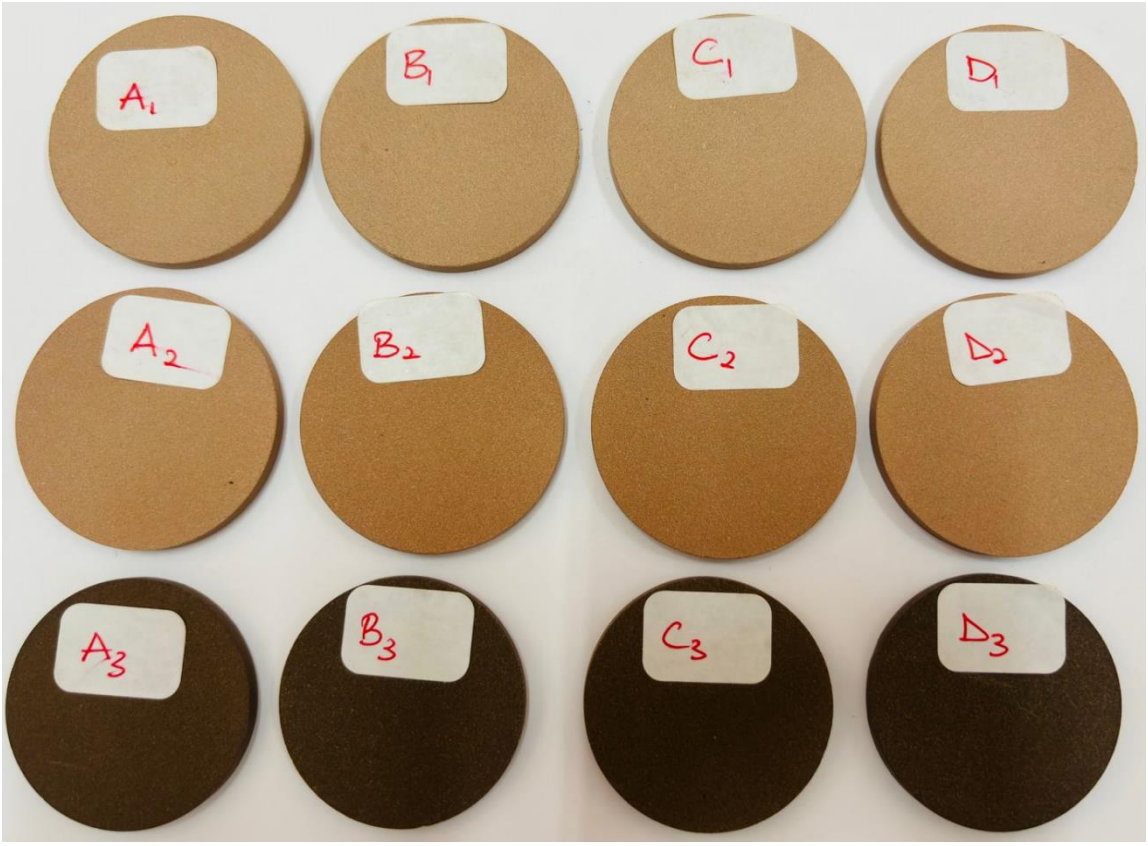


Figure 2: Images of the fabricated ceramic membranes illustrating the typical differences in the visual aspects of different sintering temperatures. (A, B, C and D represents ceramic membranes fabricated

from CFA: NS ratios of 90/0, 80:10, 70:20 and 60:30 respectively while subscripts 1, 2 and 3 represent sintering temperatures of 800, 1000, 1200 ℃ respectively).

4.2.3 Shrinkage and Loss on ignition

Table 4 shows that all samples exhibited an increase in shrinkage behaviour when the sintering temperature was increased from 800 to 1200 ℃. This shows the direct effect of a high sintering temperature on the enhancement of densification of the membrane. Increasing the amount of natural sand content leads to a decrease in the percentage shrinkage from 3.72 to 2.13%. This indicates that natural sand can enhance the densification of ceramic membranes. Table 4 also shows an increase in loss on ignition (LOI) when the sintering temperature increased from 800 - 1000 ℃ in all the starting material compositions. The LOI at 800 ℃ could be attributed to the decomposition of volatile substances in the starting materials, such as organic binders, pore formers, moisture, or carbonates. Above 800 ℃, phase changes in the materials can occur, which may include extensive loss of certain phases and transformation of phases into less stable forms which can release gases or other volatile substances. The results showed a similar trend with previously reported studies (Cipriano *et al.*, 2020).

4.2.4 Water absorption, open porosity and water permeability

The porosity of the fabricated ceramic membranes was measured by Archimedes' principle using water as a wetting liquid. This technique is based on the penetration of water into a membrane's pores under atmospheric pressure. As shown in Table 4, open porosity decreased with increasing sintering temperature. This was due to the melting and fusion of mineral grains, which resulted in the blocking of membrane pores. These values are consistent with other ceramic specimens obtained by the pressing method (Zou et al., 2019). Membranes sintered at 1200 ℃ had porosities less than 30%, thereby rendering them not fit for filtration purposes. This result is consistent with that deduced from the percent of linear shrinkage and water absorption. As water absorption is directly related to porosity (%), the same trend was also observed in increasing the firing temperature. At higher temperatures, the particles tend to agglomerate with each other which leads to a more consolidated ceramic body. Figure 3 shows the permeate flux profiles for double distilled water through four distinct membranes: (A_2) CFA (90%); NS (0%), (B_2) CFA (80%); NS (10%), (C_2) CFA (70%); NS (20%), and (D_2) CFA (60%); NS (30%) at transmembrane pressures of 100, 150, and 200 kPa. The results showed a linear, pressure-dependent regime. Membrane B_2 has the largest water permeability at 200 kPa, 35.32 L/m^2/h, whereas membrane A_2 has the lowest at 100 kPa, 9.02 L/m^2/h. The variation in water flux between membranes could be attributed to the difference in membrane porosities, which are altered by the interactions of individual

particles (Arsuaga *et al.*, 2013; Lalia *et al.*, 2013). The hydraulic pore size of ceramic membranes A_2, B_2, C_2, and D_2 were 0.48, 0.68, 0.64, and 0.58 µm, as determined by Equation 6.

Table 4: Properties of the fabricated ceramic membranes

Ceramic Membrane code	Loss on ignition (%)	Linear firing shrinkage (%)	Water uptake (%)	Open porosity (%)	Crystallite size (nm)	Chemical stability (%) (Acid/ Base)
A_1	9.92	2,28	23,1	38,5	11.39	4.21\1,22
A_2	10.3	3,72	20,0	33,7	32.21	2.98\0,82
A_3	9.41	24.44	5,9	12,6	3.50	2.35/0,61
B_1	9.56	1,16	22,5	37,1	30.66	3.24/1,32
B_2	12.40	3,43	20,7	35,2	39.18	3.2/0,76
B_3	10.10	23,80	3,7	7,9	11.40	2.76/0,7
C_1	9.52	1,03	22,8	37,2	38.35	4.01/0,9
C_2	12.41	2,77	20,4	34,7	67.25	3.1/0,69
C_3	11.11	22.52	6,3	13,5	31.85	2.67/0,59
D_1	8.92	0,80	21,9	36,4	40.30	3.3/0,98
D_2	11.43	2,13	20,2	34,3	43.76	2.78/0,63
D_3	10.92	20,93	5,6	11,7	33.29	1.98/0,6

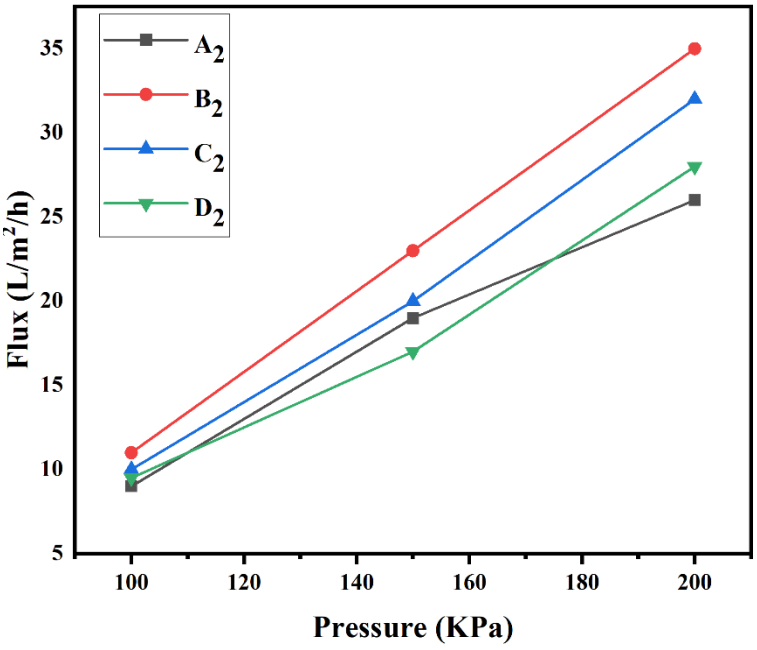


Figure 3: Pure water flux of different fabricated ceramic membranes sintered at 1000 °C for 2 h: (A_2) CFA (90%); NS (0%), (B_2) CFA (80%); NS (10%), (C_2) CFA (70%); NS (20%) and (D_2) CFA (60%); NS (30%).

4.2.5 Chemical and mechanical stability

4.2.5.1 Chemical stability

Table 4 shows the weight loss of 12 different ceramic membranes when evaluated for their chemical stability by immersing them in HCl and NaOH solutions of pH of 1.5 and 13 respectively. Each ceramic membrane exhibited exceptional chemical stability, as evidenced by an average weight loss of less than 3% in the test medium. The results also showed that the fabricated ceramic membranes are more stable in an alkaline environment than acidic environment. The weight loss observed during acidic corrosion tests could be attributed to the presence of calcium oxide, magnesium oxide, and sodium oxide in the membrane morphology, as these oxides are highly reactive with acids (Suresh *et al.*, 2016). Sand's composition and sintering temperature greatly influenced the chemical stability of these membranes, Chemical stability increased when the sand composition, as well as the sintering temperature, increased. This is because the increase in sand composition directly induces silica within the membrane structure, thereby reinforcing the structure of the membrane (Alftessi et al., 2021). High sintering temperatures could have also improved the chemical stability through internal rearrangement of the ceramic membrane by increasing the interlocking of the particles (densification process) (Yang *et al.*, 2024; Zoli *et al.*, 2024).

4.2.5.2 Mechanical stability

Three-point bend tests and flexural strength results of the fabricated ceramic membranes are given in Figure 4. The mechanical properties of the ceramic membranes were evaluated to determine how the composition of coal fly ash and natural sand, as well as the sintering temperature, affected the strength of the ceramic membranes. As shown in Figure 4b, flexural strength increased as sand composition increased. This was due to the increased weakened Si-O-Si bonds in $[SiO_4]^{4-}$ tetrahedrons, thereby enhancing the membrane densification through the formation of strong interactions with different inorganic materials present in coal fly ash. Densification of the ceramic membrane causes a reduction in membrane porosity, which raises the load-bearing area and lowers the stress concentration (Tkaczewska, 2021; Zhang *et al.*, 2024). The mechanical strength of the fabricated ceramic membranes increases as the sintering temperature increases as shown in Figure 4c. This could be ascribed to improved membrane densification via increased particle connectivity and sinter neck development. The presence of liquid phases formed from inorganic oxides such as K_2O, CaO, and MgO at 1200 °C may

have contributed to the increased sintering process that resulted in exhibiting the highest mechanical strength (Zou et al., 2021). High sintering temperatures can also result in reduced membrane porosity, hence reducing defects that act as stress concentration spots (Levänen & Mäntylä, 2002; Li *et al.*, 2016; Wu *et al.*, 2013). Figure 4 (a and c) shows that when the sintering temperature and sand composition increased, the flexural strain values decreased, indicating that the ceramic membranes experienced less bending or deformation when subjected to stress or force (Askarinejad, 2017; Nieto, 2016). Therefore, the optimal sintering temperature for coal fly ash-natural sand ceramic membranes was determined to be 1000 °C. At 1200 °C, the porosity decreased excessively, leading to the formation of cracks. Conversely, at a sintering temperature of 800 °C, the mechanical properties were lower than those observed at the other sintering temperatures.

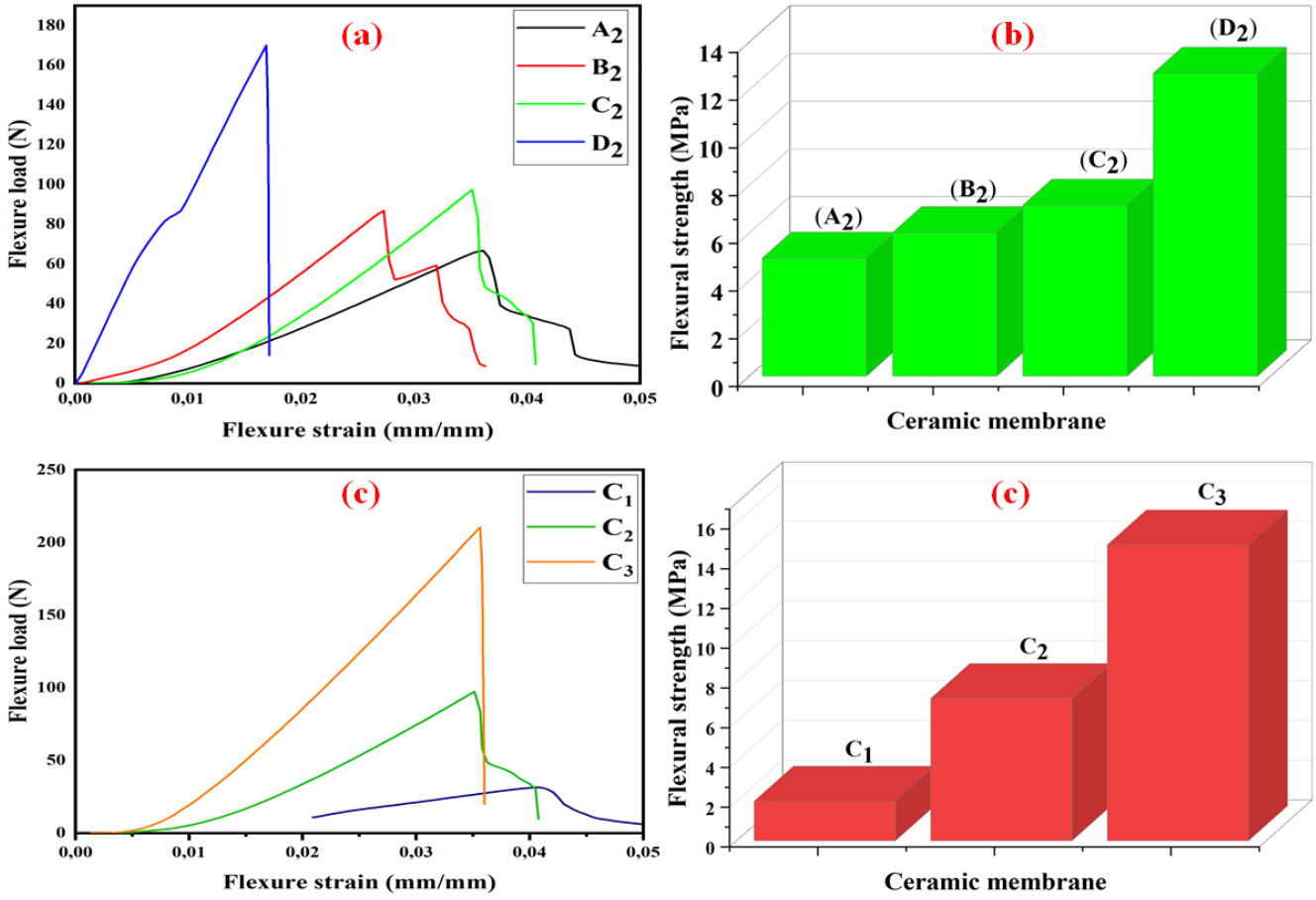


Figure 4: (a) Flexure strain vs. flexure load and (b) Flexural strength of different fabricated ceramic membranes sintered at 1000 °C for 2 h (A_2) CFA (90%); NS (0%), (B_2) CFA (80%); NS (10%), (C_2) CFA (70%); NS (20%) and (D_2) CFA (60%); NS (30%). (c) Flexure strain vs. flexure load and (d) Flexural strength of ceramic membranes fabricated from CFA (70%); NS (20%) and sintered at (C_1) 800 °C, (C_2) 1000 °C and (C_3) 1200 °C for 2 h.

4.2.6 Fourier transform infrared (FTIR) spectroscopic studies

Infra-red spectra of the ceramic membrane samples fabricated from different ratios of coal fly ash (CFA) and natural sand (NS) including CFA (90%), NS (0%); CFA (80%), NS (10%); CFA (70%), NS (20%); and CFA (60%), NS (30%); all sintered at 800, 1000 and 1200 ℃ are presented in Figure 5 (a -d) respectively. The spectrum of natural sand and coal fly ash showed all the characteristic bands of quartz mineral, with the asymmetric stretching vibration bands of Si-O-Si which appeared around 1060 cm^{-1} and the asymmetric bending vibrations bands of Si-O-Si observed around 450 cm^{-1} (Amran *et al.,* 2022). The presence of symmetrical bending vibration of the Si–O group at 680 cm^{-1} displayed by the FTIR spectra of natural sand indicates that the quartz is in crystalline form (Anbalagan *et al.*, 2010). The vibrational band at 600 cm^{-1} in both natural sand and coal fly ash corresponds to the stretching vibration of Si-O-Al (Khan *et al.*, 2014). The peak at 600 cm^{-1} can also confirm the presence of a mullite structure in the mixture (Chathurappan & Anandkumar, 2022). FTIR spectrum of the natural sand also displayed stretching vibrational bands attributed to the Si–O around 777 cm^{-1} (Alsubei *et al.,* 2024). The spectra of the ceramic membranes from all the different compositions before and after sintering showed characteristic bands that are consistent with natural sand and coal fly ash in the range of 450 - 1100 cm^{-1}. Additional peaks at 1608 cm^{-1} for unsintered ceramic membranes may be attributed to the H-O-H bending vibration. Figure 5 (a-c) displays additional peaks in the 1500 - 3000 cm^{-1} range following calcination at 1200 ℃. These could be due to O-H stretching vibrations induced by moisture absorption or surface hydration (Abdulqader *et al.,* 2024). The peaks may also be attributed to metal-oxygen vibrations or interactions due to the existence of complex oxide in both coal fly ash and natural sand (Shilar *et al.,* 2022).

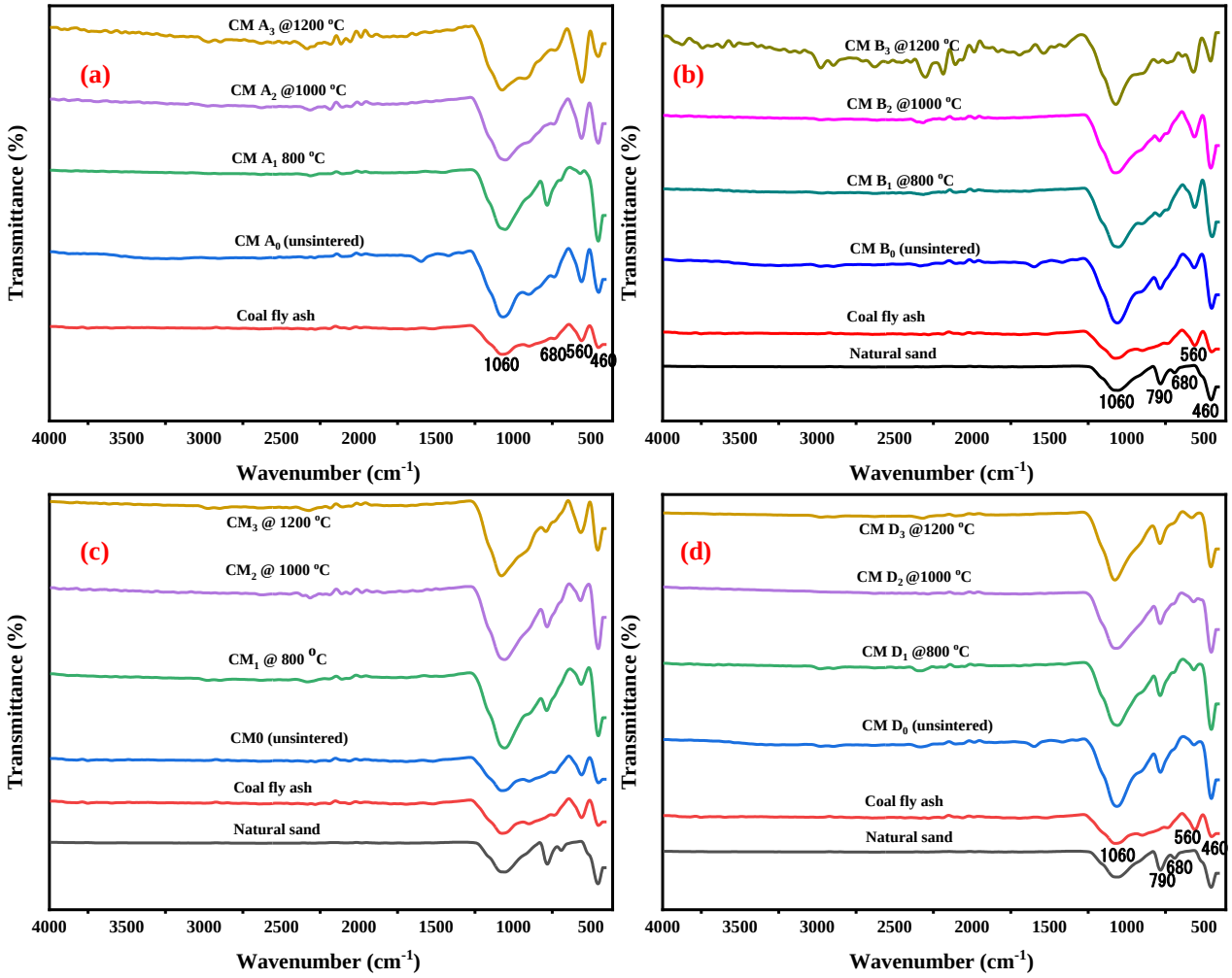


Figure 5: FTIR spectra of ceramic membrane samples fabricated from different ratios of coal fly ash and natural sand, (a) CFA (90%); (b) CFA (80%), NS (10%); (c) CFA (70%), NS (20%); and (d) CFA (60%), NS (30%) all sintered at 800 °C, 1000 °C, and 1200 °C for 2 h.

4.2.7 X-ray diffraction (XRD) analysis

XRD analysis was used to identify the phase transformation behaviour of the fabricated ceramic membranes to comprehend the structural changes that resulted from the incorporation of different sand compositions and sintering processes. The diffraction patterns of the coal fly ash displayed characteristic peaks of (1) α-quartz (SiO_2) at 2θ° values of 21.85, 26.5, 39.6, 49.5, 54.5 and 60.8°, (JCPDS no 46–1045); (2) mullite ($3Al_2O_3{\cdot}2SiO_2$) at 2θ° values of 16.6, 25.9, 30.8, 33.7 35.5, 37.4, 39.2, 52.5, 62.8 and 64.5°, (JCPDS no 84-1205); (3) Hematite (Fe_2O_3) at 2θ° values of 33.8° (JCPDS card no. 84-0311); and (4) corundum (α-Al_2O_3) at 2θ° values of 27 and 36, (JCPDS no 46-1212). The major crystalline phases identified in natural sand were α-quartz, anorthite (JCPDS no 76-0832) and albite. The studied sand and coal fly ash samples had a high crystalline character, which is shown by the sharp peaks of the diffraction pattern. The XRD pattern of ceramic membrane fabricated from prestine coal fly ash and additives sintered at a temperature range of 800– 1200 °C, presented in Fig. 6a, showed

characteristic peaks exhibited in coal fly ash with reduced intensities. The peaks corresponding to quartz and mullite displayed similar intensities from those of the raw materials for all ceramic membranes sintered at 800 ℃, indicating the thermal stability of these phases at this sintering temperature. The emergence of a new peak at 2θ° value of 28.3° corresponding to anorthite ($CaO.Al_2O_3{\cdot}2SiO_2$) after sintering at 1200 ℃ was because of the reaction between CaO with alumina and quartz SiO_2 present in the raw material. This shows that a fabricated membrane can easily be transformed when high sintering temperatures are used. The results showed a similar trend with previously reported studies (Shi *et al.*, 2023).

Figs. 6 (b-d) shows the XRD patterns of the ceramic membrane samples fabricated from the coal fly ash and different proportions of natural sand sintered in the temperature range of 800–1200 °C. An increase in the composition of natural sand in the sintered ceramic membranes resulted in the subsequent disappearance of peaks that were present in both sand and coal fly ash. The intensity of the peaks also decreased. The peaks corresponding to quartz did not change much, indicating the thermal stability of the phase at various sintering temperatures. The disappearance of some of the peaks gave rise to new peaks. The quartz and mullite phases in the initial fly ash and natural sand were slightly reduced for quartz and significantly reduced for mullite in ceramic membranes produced at sintering temperatures above 1000 ℃. This could be ascribed to their transformation into cristobalite (tetragonal SiO_2) phase, with peaks at 2θ values of 22, 28, and 36°) and anorthite phase ($CaO.Al_2O_3{\cdot}2SiO_2$) with peaks at 2θ values of 21.3° (Ahmed & Mir, 2021; Meftah *et al.*, 2023). It is reported that the mullitization reaction of ceramic membranes appears between 1000 and 1200 °C (Dong *et al.*, 2009).

The effect of sintering temperature and natural sand composition on the crystal size of the fabricated ceramic membranes was evaluated using Scherrer's equation **(**Equation 6**)**. Results presented in Table 3 show that the sintering temperature above 1000 ℃ gave rise to a decrease in crystal size, while natural sand composition resulted in increased crystallite size. A decrease in crystal size results in increased interlocking of particles that results in effective densification of the membranes (Vasanth *et al.*, 2011). This improves the mechanical and chemical properties of ceramic membranes. However, the ceramic membrane's porosity and water absorption are reduced.

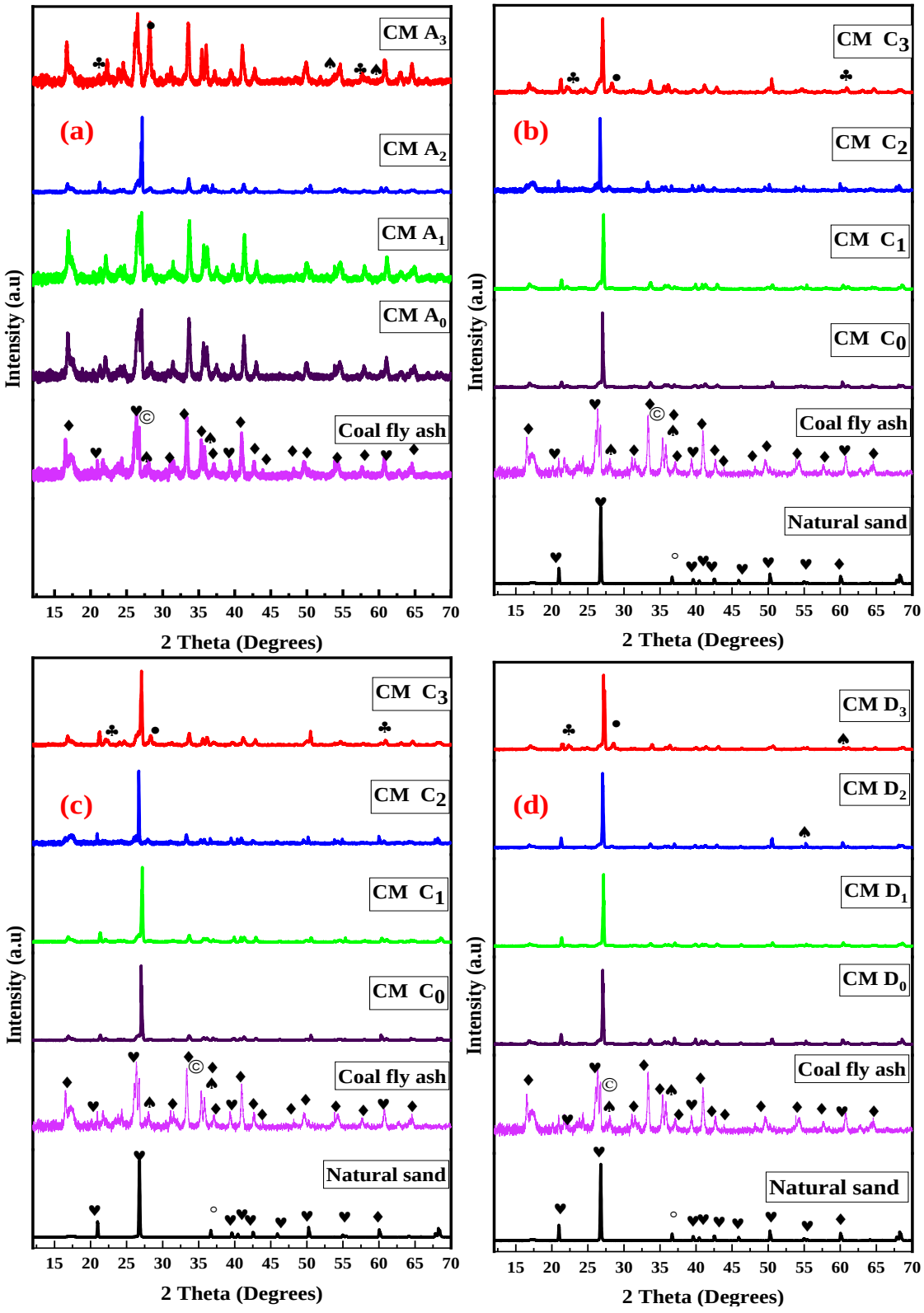


Figure 6: X-ray diffraction patterns of ceramic membrane samples fabricated from different ratios of coal fly ash and natural sand (a) CFA (90%), NS (0%); (b) CFA (80%), NS (10%); (c) CFA (70%), NS (20%); and (d) CFA (60%), NS (30%); all sintered at 800, 1000 and and 1200 °C for 2 h. (α-quartz (♥), mullite (♦), anorthite (●), hematite (©), corundum (♠), cristobalite (♣) and albite (◦)

4.2.8 Thermogravimetric analysis (TGA)

TGA analysis was used to evaluate the thermal stability of the prepared ceramic membranes by monitoring the weight change that occurred as the raw materials mixture was heated between 25-1000 ℃ at a rate of 10 °C/min under nitrogen purge. The TGA-DTG graph in Fig 7 displays three different weight loss zones, with an observed 12% overall weight loss for the sample. A weight loss of about 0.5% at below 100 ℃ may be attributed to the loss due to adsorbed volatiles. About 5% weight loss occurred between 200 and 300 ℃, which can be related to the dihydroxylation process and pre-dehydration process of coal fly ash and natural sand that could cause their layers to reorganize. The weight loss between 400 and 700 °C could be attributed to the thermal decomposition of dextrin and sodium carboxyl methylcellulose, thereby producing CO_2. The DTG curve (Fig. 7) shows two exothermic peaks at 275 and 500 ℃, which can be ascribed to the decomposition of the binder and pore former (Bensalah *et al.*, 2023). The formation of CO_2 increases the porosity of the membrane because it leaves behind long, linked pores in the membrane structure. There was no weight loss after 750 ℃, and this temperature may be assumed as the lowest temperature at which the ceramic membrane can be sintered.

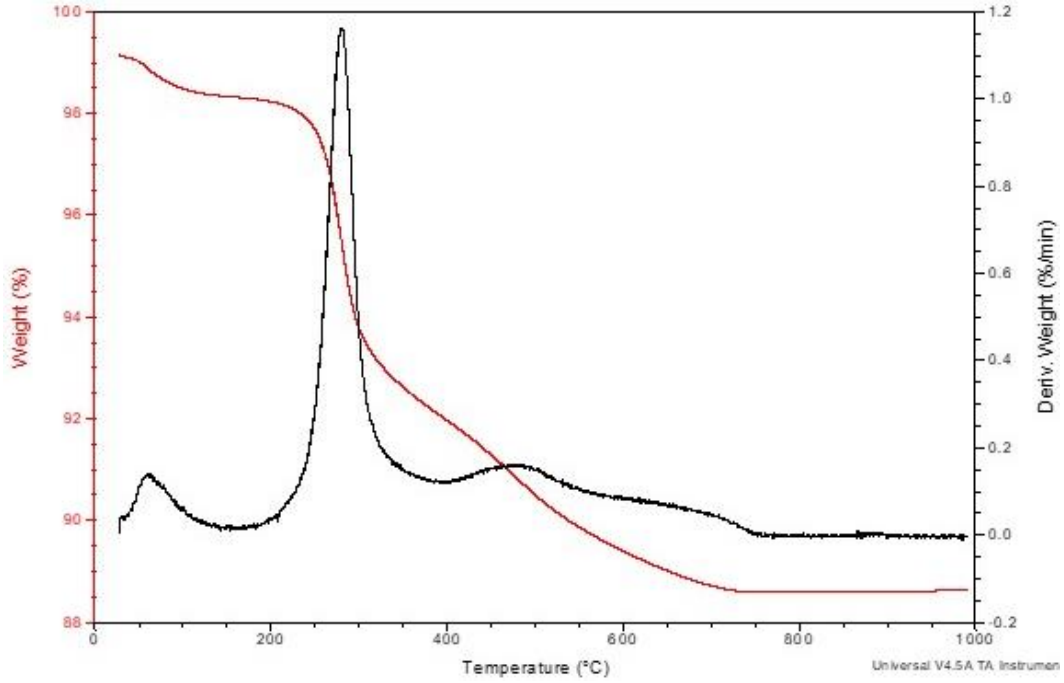
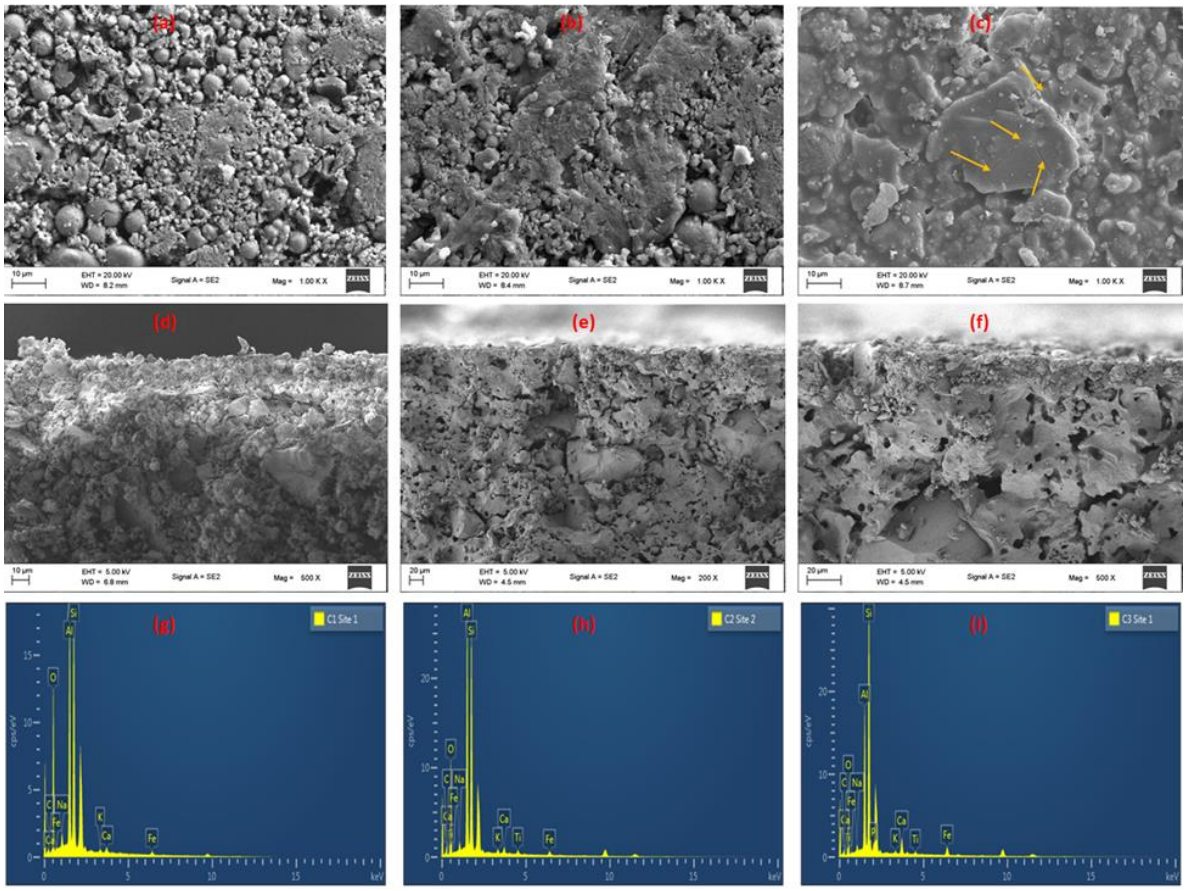


Figure *7*: TGA-DTG curve for the ceramic membrane starting material (60%CFA;20% NS)

4.2.9 Morphological study

4.2.9.1 SEM and EDX analysis of ceramic membranes sintered at different temperatures.

The effect of sintering temperature on the morphology of the synthesized ceramic membranes was investigated and presented in Fig. 8(a–f). The elemental composition of the fabricated ceramic membranes is also shown in Figs. 8(g-i). The SEM micrographs of the ceramic membranes sintered at 800 ℃ are shown in Figs. 8 (a and d) and are dominated by loosely held spherical particles. The presence of these loose particles results in a high membrane porosity because of the many channels that are present between the layers of the particles. However, due to the restricted particle interactions, the mechanical strength of the membrane would be low. There were no visible cracks on the cross-sectional or surface areas. The spherical particles began to agglomerate at a temperature of 1000 °C, as shown in Figs. 8 (b and e), thereby forming a dominating dense structure with pores. This indicates that at 1000 °C, the membranes were sufficiently sintered. Most of the particles transformed into sintering necks when the temperature was raised to 1200 °C due to an increase in the densification process. This caused the ceramic membrane to shrink, thereby increasing its mechanical strength. The membrane's porosity consequently decreases as the sintering temperature increases. Furthermore, as shown by the yellow arrows in Fig. 8c, cracks could be observed on the membrane's surface. Aluminium and silicon were identified as the main elements of the ceramic membranes as shown in the EDX spectra of Fig. 8(g-i), indicating that coal fly ash and natural sand are suitable starting materials for the ceramic membranes.



(j)

	Wt%	Wt% Sigma
C	9.02	1.58
O	48.10	0.89
Na	1.72	0.11
Al	18.25	0.35
Si	20.58	0.40
K	0.39	0.05
Ca	0.71	0.06
Fe	1.23	0.11
Total	100.00	

(k)

	Wt%	Wt% Sigma
C	13.01	1.52
O	38.47	0.76
Na	1.26	0.09
Al	20.39	0.39
Si	22.69	0.44
K	0.64	0.06
Ca	1.06	0.06
Ti	0.88	0.07
Fe	1.58	0.11
Total	100.00	

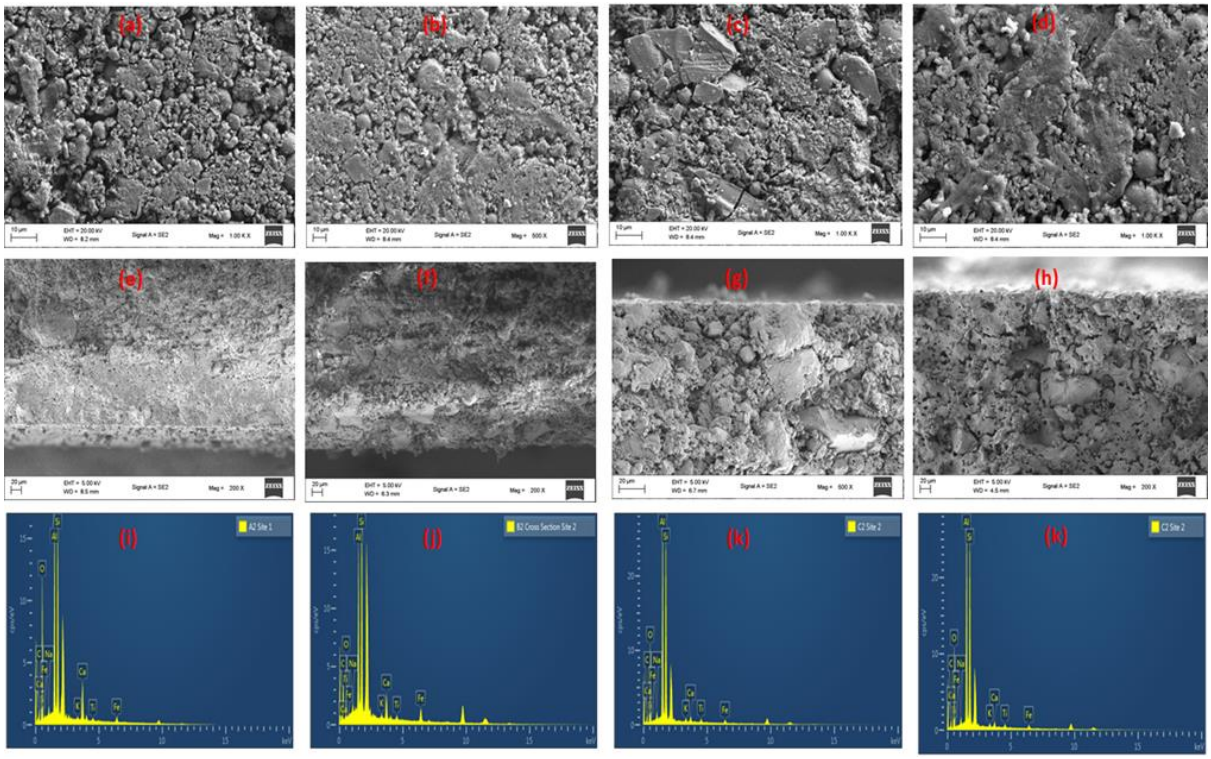
(l)

	Wt%	Wt% Sigma
C	8.35	1.96
O	32.64	0.82
Na	1.25	0.10
Al	15.66	0.37
Si	31.49	0.72
P	1.32	0.15
K	0.41	0.06
Ca	3.50	0.12
Ti	0.73	0.09
Fe	4.65	0.19
Total	100.00	

Figure 8**:** SEM surface micrographs (a-c), SEM cross-sectional micrographs (d-f), EDX spectra (g-i) Table of elements present (j-l) in ceramic membranes fabricated from 30% natural sand and 60% coal fly ash and sintered for 2 h at different temperatures of 800, 100 and 1200 ℃ respectively.

4.2.9.2 SEM and EDX analysis of ceramic membranes fabricated from different natural sand compositions.

The effect of natural sand composition on the morphology of the synthesized ceramic membranes was investigated and presented in Figs. 9(a–h). The elemental composition of the fabricated ceramic membranes is also shown in Figs 9(i-k). The SEM micrographs of ceramic membranes composed of 100% coal fly ash and additives (Figs 9a and e) revealed a morphology mostly dominated by spherical particles, while particle aggregation was observed when the percentage of natural sand was increased. Agglomeration of particles increases the flexural strength by decreasing the membrane porosity. Aluminum and silicon were identified as the main elements in the EDX spectrum Figs. 9(i-k) of the ceramic membranes that were fabricated at different compositions of natural sand. The results also showed that the composition of Si increased as the amount of natural sand increased.



(l)

	Wt%	Wt%
C	16.79	1.39
O	39.70	0.76
Na	1.11	0.09
Al	8.87	0.19
Si	23.57	0.44
K	0.45	0.05
Ca	1.94	0.08
Ti	1.49	0.09
Fe	6.08	0.19
Total	100.00	

(m)

	Wt%	Wt%
C	36.57	1.27
O	27.96	0.74
Na	1.03	0.11
Al	11.36	0.26
Si	14.48	0.33
K	0.40	0.06
Ca	3.08	0.11
Ti	0.72	0.08
Fe	4.40	0.18
Total	100.00	

(n)

	Wt%	Wt% S
C	23.82	2.13
O	35.25	1.11
Na	1.03	0.13
Al	12.62	0.39
Si	18.43	0.56
Cl	0.70	0.08
K	0.42	0.07
Ca	1.57	0.10
Ti	1.89	0.13
Fe	4.28	0.22
Total	100.00	

(o)

	Wt%	Wt%
C	12.89	2.62
O	36.36	1.21
Na	1.13	0.14
Al	14.64	0.48
Si	29.68	0.94
K	0.59	0.09
Ca	1.26	0.11
Ti	0.35	0.12
Fe	3.10	0.23
Total	100.00	

Figure 9: SEM surface micrographs (a-d), SEM cross-sectional micrographs (e-h), EDX spectra (i-k) and Table of elements (i-o) of ceramic membranes fabricated from 0%, 10%, 20%, and 30% natural sand and sintered at 1000 ℃ for 2 h.

Table 5: Comparative study of the properties of the fabricated ceramic membrane utilizing coal fly ash and natural sand against sustainable ceramic membranes reported in earlier studies

Main sustainable starting materials	**Configuration**	**Sintering temperature (℃)**	**Pore size (μm) & porosity (%)**	**Mechanical strength (MPa)**	**Pure water flux(L/m^2/h)**	**Ref.**
Potters' clay & Tea waste	flat	900	0.49 52.51	-	-	(Tai *et al.*, 2019)
Palm oil fuel ash	hallow	700	0.5 33.2	60	28.4	(Tai et al., 2019)
Bauxite	hallow	1450	1.5 46.5	308.1	87	(Ismail *et al.*, 2020)
Cow bone	hallow	1200	0.01 35.4	20.2	80.3	(Hubadillah *et al.*, 2020)
sugarcane bagasse ash	hallow	1000	1.85 42	60	466	(Jamalludin *et al.*, 2018)
Coal fly ash	flat	700	- 40	6	57.8	(Ahmad *et al.*, 2022)
Metakaolin and corn cob ash	hallow	1200	3.26 19.4	41.61	82.4	(Kamarudin *et al.*, 2020)
Silica sand	hallow	1300	0.85 17.2	210	14	(Alftessi et al., 2021)
Linz Donawitz slag	flat	950	8 60	6	800	(Deepti *et al.*, 2020)
Coal fly ash and natural sand	flat	1000	0.64 34.3	7.7	32.23	Present study

4.3 Conclusion

In this study, a sustainable ceramic membrane was successfully fabricated from coal fly ash and natural sand by the uniaxial compaction method. The sintering temperature and composition of natural sand significantly influenced the properties of the fabricated ceramic membranes. The ceramic membrane exhibited greater phase changes, shrinkage, porosity loss, increased mechanical and chemical stability, and decreased water absorption behavior as the sintering temperature increased. Additionally, as shown in Table 5, the optimized coal fly ash-based ceramic membrane displayed comparable properties to the other ceramic membranes fabricated from low-cost materials. A reduction in the shrinking behavior occurred, while an enhancement in the mechanical and chemical stability was observed with the increase in the amount of natural sand content. The ceramic membrane, synthesized from 20% natural sand composition and sintered at 1000 ℃, demonstrated optimal properties. These included a mean pore size of 0.64 μm, an open porosity of 34.7%, and exceptional chemical stability under harsh environmental conditions, coupled with robust mechanical properties. Notably, the membrane exhibited a remarkable water permeability rate of 32.23 $L/m^2/h$. The study shows that coal fly ash and natural sand can be used to successfully establish a multipurpose ultrafiltration membrane that can be used for various water purification applications.

4.4 References

Abdullayev, A. (2022). *Silicate materials for low-cost ceramic membranes: synthesis, processing, and characterization*: Technische Universitaet Berlin (Germany).

Abdulqader, M. A., Suliman, M. A., Ahmed, T. A., Wu, R., Bobaker, A., Tiyasha, T., . . . Al-Areeq, N. (2024). Conversion of chicken rice waste into char via hydrothermal, pyrolysis, and microwave carbonization processes: a comparative study. *AUIQ Complementary Biological System, 1*(1), 1-9.

Addich, M., El Baraka, N., Laknifli, A., Saffaj, N., Fatni, A., El Hammadi, A., . . . Lgaz, H. (2022). New low-cost tubular ceramic microfiltration membrane based on natural sand for tangential urban wastewater treatment. *Journal of Saudi Chemical Society, 26*(4), 101512.

Ahmad, B., Dilshad, M., Haider, B., Anwar, M., Ali, H., Gilani, S., . . . Farooq, M. (2022). Synthesis of novel fly ash based geo-polymeric membranes for the treatment of textile waste water. *International Journal of Environmental Science and Technology*, 1-10.

Ahmed, N., & Mir, F. Q. (2021). Fabrication of a Cost Effective Ceramic Microfiltration Membrane by Utilizing Local Kashmir Clay. *Transactions of the Indian Ceramic Society, 80*(1), 41-46. doi:10.1080/0371750x.2020.1864663

Al-Shaeli, M., Al-Juboori, R. A., Al Aani, S., Ladewig, B. P., & Hilal, N. (2022). Natural and recycled materials for sustainable membrane modification: Recent trends and prospects. *Science of the Total Environment, 838*, 156014.

Alftessi, S. A., Othman, M. H. D., Adam, M. R., Farag, T. M., Ismail, A. F., Rahman, M. A., . . . Hubadillah, S. K. (2021). Novel silica sand hollow fibre ceramic membrane for oily wastewater treatment. *Journal of Environmental Chemical Engineering, 9*(1), 104975. doi:ARTN 104975 10.1016/j.jece.2020.104975

Alftessi, S. A., Othman, M. H. D., Bin Adam, M. R., Farag, T. M., Tai, Z. S., Raji, Y. O., . . . Abu Bakar, S. (2022). Hydrophobic silica sand ceramic hollow fiber membrane for desalination via direct contact membrane distillation. *Alexandria Engineering Journal, 61*(12), 9609-9621. doi:10.1016/j.aej.2022.03.044

Alsubei, M. D., Reid, B., Aljlil, S. A., Coppens, M.-O., & Campos, L. C. (2024). Fabrication and characterization of coated ceramic membranes from natural sources for water treatment applications. *Journal of Membrane Science, 690*, 122226.

Amran, T., Mohd, T., Bohairah, T. A., & Jaafar, M. Z. (2022). Characterization of Quartz Sand as an Adsorbent for Anionic Surfactant Adsorption with Presences of Alkaline and Polymer. *Chemical Engineering Transactions, 95*, 283-288.

Anbalagan, G., Prabakaran, A. R., & Gunasekaran, S. (2010). Spectroscopic Characterization of Indian Standard Sand. *Journal of applied spectroscopy, 77*(1), 86-94. doi:DOI 10.1007/s10812-010-9297-5

Arsuaga, J. M., Sotto, A., del Rosario, G., Martínez, A., Molina, S., Teli, S. B., & de Abajo, J. (2013). Influence of the type, size, and distribution of metal oxide particles on the properties of nanocomposite ultrafiltration membranes. *Journal of Membrane Science, 428*, 131-141. doi:10.1016/j.memsci.2012.11.008

Arumugham, T., Kaleekkal, N. J., Gopal, S., Nambikkattu, J., K, R., Aboulella, A. M., . . . Banat, F. (2021). Recent developments in porous ceramic membranes for wastewater treatment and desalination: A review. *J Environ Manage, 293*, 112925. doi:10.1016/j.jenvman.2021.112925

Askarinejad, S. (2017). Deformation Mechanisms in Bioinspired Multilayered Materials. *Mechanical Engineering*.

Bensalah, H., Derouich, G., Wang, X., Alami Younssi, S., & Bekheet, M. F. (2023). Graphene-Oxide-Grafted Natural Phosphate Support as a Low-Cost Ceramic Membrane for the Removal of Anionic Dyes from Simulated Textile Effluent. *Membranes, 13*(3), 345.

Bobo, A., Manyuchi, M., & Sukdeo, N. Production of Bio Fertilizer from Blending Coal Fly Ash and Vermicompost.

Chathurappan, R., & Anandkumar, J. (2022). Synthesis and Characterization of Coal Fly Ash Based Multipurpose Ultrafiltration Membrane. *Materialia, 25*, 101548. doi:ARTN 101548 10.1016/j.mtla.2022.101548

Cipriano, P. B., Galdino, T., Sá, C., & Ferraz, A. (2020). Study of phases formed during sintering at different temperatures in ceramic composites containing gypsum waste. In.

Deepti, Sinha, A., Biswas, P., Sarkar, S., Bora, U., & Purkait, M. K. (2020). Utilization of LD slag from steel industry for the preparation of MF membrane. *Journal of Environmental Management, 259*, 110060. doi:ARTN 110060 10.1016/j.jenvman.2019.110060

Dong, Y., Zhou, J.-e., Lin, B., Wang, Y., Wang, S., Miao, L., . . . Meng, G. (2009). Reaction-sintered porous mineral-based mullite ceramic membrane supports made from recycled materials. *Journal of hazardous materials, 172*(1), 180-186.

Fedje, K. K., Ekberg, C., Skarnemark, G., & Steenari, B. M. (2010). Removal of hazardous metals from MSW fly ash--an evaluation of ash leaching methods. *J Hazard Mater, 173*(1-3), 310-317. doi:10.1016/j.jhazmat.2009.08.094

Foorginezhad, S., Zerafat, M. M., Mohammadi, Y., & Asadnia, M. (2022). Fabrication of tubular ceramic membranes as low-cost adsorbent using natural clay for heavy metals removal. *Cleaner Engineering and Technology, 10*, 100550. doi:ARTN 100550 10.1016/j.clet.2022.100550

Geng, H., Wang, F., Yan, C., Tian, Z., Chen, H., Zhou, B., . . . Yao, J. (2020). Leaching behavior of metals from iron tailings under varying pH and low-molecular-weight organic acids. *J Hazard Mater, 383*, 121136. doi:10.1016/j.jhazmat.2019.121136

He, Y., Wang, L. J., Chen, Z., Huang, X., Wang, X. M., Zhang, X. Y., & Wen, X. H. (2022). Novel catalytic ceramic membranes anchored with MnMe oxide and their catalytic ozonation performance towards atrazine degradation. *Journal of Membrane Science, 648*, 120362. doi:ARTN 120362 10.1016/j.memsci.2022.120362

Huang, J., Zhang, H., Zhang, Y., Liang, D., & Chen, H. (2022). Recycle coal fly ash for preparing tubular ceramic membranes applied in transport membrane condenser. *Separation and Purification Technology, 282*, 119972.

Huang, J. G., Chen, H. P., Qi, R., Yang, J. H., Li, Z. H., & Zhang, H. (2023). Porous ceramic membranes from coal fly ash with addition of various pore-forming agents for oil-in-water emulsion separation. *Journal of Environmental Chemical Engineering, 11*(3), 109929. doi:ARTN 109929 10.1016/j.jece.2023.109929

Hubadillah, S. K., Othman, M. H. D., Tai, Z. S., Jamalludin, M. R., Yusuf, N. K., Ahmad, A., . . . Harun, Z. (2020). Novel hydroxyapatite-based bio-ceramic hollow fiber membrane derived from waste cow bone for textile wastewater treatment. *Chemical Engineering Journal, 379*, 122396. doi:ARTN 122396 10.1016/j.cej.2019.122396

Ismail, N. J., Othman, M. H. D., Abu Bakar, S., Jaafar, J., & Rahman, M. A. (2020). Fabrication of Ceramic, Hollow-Fiber Membrane: The Effect of Bauxite Content and Sintering Temperature. *Clays and Clay Minerals, 68*(4), 309-318. doi:10.1007/s42860-020-00076-8

Issaoui, M., & Limousy, L. (2019). Low-cost ceramic membranes: Synthesis, classifications, and applications. *Comptes Rendus Chimie, 22*(2-3), 175-187. doi:10.1016/j.crci.2018.09.014

Jamalludin, M. R., Harun, Z., Othman, M. H. D., Hubadillah, S. K., Yunos, M. Z., & Ismail, A. F. (2018). Morphology and property study of green ceramic hollow fiber membrane derived from waste sugarcane bagasse ash (WSBA). *Ceramics International, 44*(15), 18450-18461. doi:10.1016/j.ceramint.2018.07.063

Kamarudin, N. H., Harun, Z., Othman, M. H. D., Abdullahi, T., Bahri, S. S., Kamarudin, N. H., . . . Salleh, W. N. W. (2020). Waste environmental sources of metakaolin and corn cob ash for preparation and characterisation of green ceramic hollow fibre membrane -MCa) for oil-water separation. *Ceramics International, 46*(2), 1512-1525. doi:10.1016/j.ceramint.2019.09.118

Ke, X., Zhang, F. J., Zhou, Y., Zhang, H. J., Guo, G. L., & Tian, Y. (2020). Removal of Cd, Pb, Zn, Cu in smelter soil by citric acid leaching. *Chemosphere, 255*, 126690. doi:10.1016/j.chemosphere.2020.126690

Khan, S. A., Uddin, I., Moeez, S., & Ahmad, A. (2014). Fungus-Mediated Preferential Bioleaching of Waste Material Such as Fly - Ash as a Means of Producing Extracellular, Protein Capped, Fluorescent and Water Soluble Silica Nanoparticles. *PloS one, 9*(9), e107597. doi:ARTN e107597 10.1371/journal.pone.0107597

Khedidja, M., Bechir, M., Feyda, S., & Ali, T. M. (2024). Development of ceramic filtering membranes based on Tunisian clay and phosphate sludge in wastewater treatment. *Solid State Sciences, 148*, 107430.

Kouotou, Y. M., Njoya, A., Mountapbeme, I. C., Njuhou, S., Kamgang, P. S., Mouafon, M., . . . Njopwouo, D. (2024). Properties of ceramic membranes obtained from kaolinitic clay mixed with palm and mango wastes from Cameroon: Application to wastewater treatment from breweries. *International Journal of Ceramic Engineering & Science*, e10229.

Lalia, B. S., Kochkodan, V., Hashaikeh, R., & Hilal, N. (2013). A review on membrane fabrication: Structure, properties and performance relationship. *Desalination, 326*, 77-95. doi:10.1016/j.desal.2013.06.016

Latwal, M., Arora, S., Joshi, A., Irfan, M., & Pandey, G. (2023). Sustainable ceramic membrane for decontamination of water: A cost-effective approach. *Heliyon, 9*(2), e13321. doi:10.1016/j.heliyon.2023.e13321

Leelarungroj, K., Likitlersuang, S., Chompoorat, T., & Janjaroen, D. (2018). Leaching mechanisms of heavy metals from fly ash stabilised soils. *Waste Manag Res, 36*(7), 616-623. doi:10.1177/0734242X18775494

Levänen, E., & Mäntylä, T. (2002). Effect of sintering temperature on functional properties of alumina membranes. *Journal of the European Ceramic Society, 22*(5), 613-623.

Li, L. L., Chen, M. L., Dong, Y. C., Dong, X. F., Cerneaux, S., Hampshire, S., . . . Liu, J. (2016). A low-cost alumina-mullite composite hollow fiber ceramic membrane fabricated via phase-inversion and sintering method. *Journal of the European Ceramic Society, 36*(8), 2057-2066. doi:10.1016/j.jeurceramsoc.2016.02.020

Liang, D. H., Huang, J. G., Zhang, Y. T., Zhang, Z., Chen, H. P., & Zhang, H. (2021). Influence of dextrin content and sintering temperature on the properties of coal fly ash-based tubular ceramic membrane for flue gas moisture recovery. *Journal of the European Ceramic Society, 41*(11), 5696-5710. doi:10.1016/j.jeurceramsoc.2021.04.055

Ma, J., Chen, W. W., Qian, J. J., Shui, A. Z., Du, B., & He, C. (2023). Co-pressing and co-sintering preparation of cost-effective and high-performance asymmetric ceramic membrane for oily wastewater treatment. *Separation and Purification Technology, 323*, 124373. doi:ARTN 124373 10.1016/j.seppur.2023.124373

Mazel, V., Diarra, H., Busignies, V., & Tchoreloff, P. (2014). Study of the validity of the three-point bending test for pharmaceutical round tablets using finite element method modeling. *Journal of Pharmaceutical Sciences, 103*(4), 1305-1308.

Meftah, N., Hani, A., & Merdas, A. (2023). Extraction and Physicochemical Characterization of Highly-pure Amorphous Silica Nanoparticles from Locally Available Dunes Sand. *Chemistry Africa-a Journal of the Tunisian Chemical Society, 6*(6), 3039-3048. doi:10.1007/s42250-023-00688-2

Meldha, Z., Amri, I., Angkoso, M. D. T., & Jumaga, Y. (2023). The utilization of silica sand and clay with the addition of sawdust as raw material for manufacturing ceramic membranes to reduce TSS and TDS levels of peat water. *Materials Today: Proceedings*.

Mishra, G., & Mukhopadhyay, M. (2017). Flux improvement, rejection, surface energy and antibacterial properties of synthesized TiO 2-Mo. HNTs/PVC nanocomposite ultrafiltration membranes. *New Journal of Chemistry, 41*(24), 15049-15057.

Ni, T. L., Kong, L. X., Xie, Z. L., Lin, J. Y., & Zhao, S. F. (2022). Flux vs. permeability: How to effectively evaluate mass transfer performance of membranes in oil-water separation br. *Journal of Water Process Engineering, 49*, 103119. doi:ARTN 103119 10.1016/j.jwpe.2022.103119

Nieto, A. (2016). *Synthesis, Mechanical Behavior, and Multi-Scale Tribological Performance of Carbon Nanoparticle Reinforced Ceramic Composites*: University of California, Davis.

Obada, D. O., Salami, K. A., Alabi, A. A., Oyedeji, A. N., Csaki, S., Hulan, T., & Meher, A. K. (2023). Mechanical behaviour of porous kaolin-based ceramics for potential catalysts support applications. *Journal of the Korean Ceramic Society, 60*(1), 99-112.

Rani, S. L. S., & Kumar, R. V. (2021). Insights on applications of low-cost ceramic membranes in wastewater treatment: A mini-review. *Case Studies in Chemical and Environmental Engineering, 4*, 100149.

Rao, A., Kaushik, A., Kuppurangan, G., & Selvaraj, G. (2023). Characterization and application of novel fly ash blended ceramic membrane in MFC for low-cost and sustainable wastewater treatment and power generation. *Environ Sci Pollut Res Int, 30*(16), 45872-45887. doi:10.1007/s11356-023-25327-8

Raychaudhuri, A., & Behera, M. (2020). Ceramic membrane modified with rice husk ash for application in microbial fuel cells. *Electrochimica Acta, 363*, 137261. doi:ARTN 137261 10.1016/j.electacta.2020.137261

Samadi, A., Gao, L., Kong, L. X., Orooji, Y., & Zhao, S. F. (2022). Waste-derived low-cost ceramic membranes for water treatment: Opportunities, challenges and future directions. *Resources Conservation and Recycling, 185*, 106497. doi:ARTN 106497 10.1016/j.resconrec.2022.106497

Satyannarayana, K. V. V., Rani, S. L. S., Baranidharan, S., & Kumar, R. V. (2022). Indigenous bentonite based tubular ceramic microfiltration membrane: Elaboration, characterization, and evaluation of environmental impacts using life cycle techniques. *Ceramics International, 48*(19), 28843-28855. doi:10.1016/j.ceramint.2022.03.156

Sawunyama, L., Ajiboye, T. O., Oyewo, O., & Onwudiwe, D. C. (2024). Ceramic-polymer composite membranes: Synthesis methods and environmental applications. *Ceramics International, 50*(3), 5067-5079. doi:10.1016/j.ceramint.2023.11.337

Sawunyama, L., Olatunde, O. C., Oyewo, O. A., Bopape, M. F., & Onwudiwe, D. C. (2024). Application of coal fly ash based ceramic membranes in wastewater treatment: A sustainable alternative to commercial materials. *Heliyon, 10*(2), e24344. doi:10.1016/j.heliyon.2024.e24344

Sawunyama, L., Oyewo, O. A., Seheri, N., Onjefu, S. A., & Onwudiwe, D. C. (2023). Metal oxide functionalized ceramic membranes for the removal of pharmaceuticals in wastewater. *Surfaces and Interfaces, 38*, 102787. doi:ARTN 102787 10.1016/j.surfin.2023.102787

Shi, Z. M., Han, C., & Wang, W. B. (2023). Preparation and Properties of Quartz-Anorthite Ceramics Synthesized Using Desert Sand and Coal Fly Ash. *Journal of Materials in Civil Engineering, 35*(8), 04023221. doi:Artn 04023221 10.1061/Jmcee7.Mteng-14712

Shilar, F. A., Ganachari, S. V., Patil, V. B., Khan, T. M. Y., Almakayeel, N. M., & Alghamdi, S. (2022). Review on the Relationship between Nano Modifications of Geopolymer Concrete and Their Structural Characteristics. *Polymers, 14*(7), 1421. doi:ARTN 1421 10.3390/polym14071421

Suresh, K., Pugazhenthi, G., & Uppaluri, R. (2016). Fly ash based ceramic microfiltration membranes for oil-water emulsion treatment: Parametric optimization using response surface methodology. *Journal of Water Process Engineering, 13*, 27-43. doi:10.1016/j.jwpe.2016.07.008

Tai, Z. S., Hubadillah, S. K., Othman, M. H. D., Dzahir, M. I. H. M., Koo, K. N., Tendot, N. I. S. T. I., . . . Abd Aziz, M. H. (2019). Influence of pre-treatment temperature of palm oil fuel ash on the properties and performance of green ceramic hollow fiber membranes towards oil/water separation application. *Separation and Purification Technology, 222*, 264-277. doi:10.1016/j.seppur.2019.04.046

Tkaczewska, E. (2021). Effect of Chemical Composition and Network of Fly Ash Glass on the Hydration Process and Properties of Portland-Fly Ash Cement. *Journal of Materials Engineering and Performance, 30*(12), 9262-9282. doi:10.1007/s11665-021-06129-w

Vasanth, D., Uppaluri, R., & Pugazhenthi, G. (2011). Influence of Sintering Temperature on the Properties of Porous Ceramic Support Prepared by Uniaxial Dry Compaction Method Using Low-Cost Raw Materials for Membrane Applications. *Separation Science and Technology, 46*(8), 1241-1249. doi:Pii 937791489 10.1080/01496395.2011.556097

Wang, Z., Xu, Z., Qiu, D., Chu, Y., & Tang, Y. (2021). Beneficial utilization of Al/Si/O-rich solid wastes for environment-oriented ceramic membranes. *Journal of hazardous materials, 401*, 123427.

Wu, Z. T., Faiz, R., Li, T., Kingsbury, B. F. K., & Li, K. (2013). A controlled sintering process for more permeable ceramic hollow fibre membranes. *Journal of Membrane Science, 446*, 286-293. doi:10.1016/j.memsci.2013.05.040

Xue, Y., Kamali, M., Al-Salem, S., Rossi, B., Appels, L., & Dewil, R. (2024). Naturally derived materials to enhance the membrane properties in (waste) water treatment applications-Mechanisms, scale-up challenges and economic considerations. *Journal of Water Process Engineering, 57*, 104647.

Yan, Y., Gao, J., Wu, J., & Li, B. (2014). Effects of inorganic and organic acids on heavy metals leaching in contaminated sediment. *An interdisciplinary response to mine water challenges, China University of Mining and Technology Press, Xuzhou*.

Yang, F., Zhao, S., Chen, G., Li, K., Fei, Z., Mummery, P., & Yang, Z. (2024). High-strength, multifunctional and 3D printable mullite-based porous ceramics with a controllable shell-pore structure. *Advanced Powder Materials, 3*(1), 100153.

Zhang, Y., Shi, Z., Wang, W., Luo, W., & Liu, Z. (2024). Improvement of Phase Transformation and Densification of SiO2-ZrO2 Ceramics by Using Desert Sand as a SiO2 Source. *Silicon, 16*(3), 1357-1375.

Zhang, Z., Yang, J., Qi, R., Huang, J., Chen, H., & Zhang, H. (2023). Development of Hydrophobic Coal-Fly-Ash-Based Ceramic Membrane for Vacuum Membrane Distillation. *Materials (Basel), 16*(8), 3153. doi:10.3390/ma16083153

Zoli, L., Servadei, F., Bassi, G., Rossi, A., Montesi, M., Vinci, A., . . . Panseri, S. (2024). From outer space to inside the body: ultra-high temperature ceramic matrix composites for biomedical applications. *Journal of the European Ceramic Society, 44*(2), 729-737.

Zou, D., Fan, W., Xu, J. R., Drioli, E., Chen, X. F., Qiu, M. H., & Fan, Y. Q. (2021). One-step engineering of low-cost kaolin/fly ash ceramic membranes for efficient separation of oil-water emulsions. *Journal of Membrane Science, 621*, 118954. doi:ARTN 118954 10.1016/j.memsci.2020.118954

Zou, D., Qiu, M. H., Chen, X. F., Drioli, E., & Fan, Y. Q. (2019). One step co-sintering process for low-cost fly ash based ceramic microfiltration membrane in oil-in-water emulsion treatment. *Separation and Purification Technology, 210*, 511-520. doi:10.1016/j.seppur.2018.08.040

CHAPTER 5

TiO_2-ZnO functionalized low-cost ceramic membranes from coal fly ash for the removal of tetracycline from water under visible light

5.0. Introduction

The use of ceramic membranes in filtration technology for wastewater treatment applications has evolved rapidly on a global scale due to its excellent filtration effectiveness, longer service life, lower susceptibility to fouling, and chemical and thermal stability (Samaei, Gato-Trinidad et al. 2018, Bottino, Capannelli et al. 2020). However, high energy requirements for sintering, high operational cost and limited performance in the mineralization of contaminants are identified as major drawbacks in real industrial utilization (Ajiboye, Sawunyama et al. 2023, Sawunyama, Oyewo et al. 2023, Xie, Wang et al. 2024). This has, thus, directed research to focus on the fabrication of ceramic membranes using inexpensive and easily accessible materials. For example, studies revealed that clay, bentonite, kaolin, sand, and other materials were successfully used for the fabrication of ceramic membranes (Issaoui and Limousy 2019, Zou, Fan et al. 2021, Samadi, Gao et al. 2022, Sawunyama, Olatunde et al. 2024). These materials contain substantial amounts of SiO_2, CaO, and Al_2O_3, making them an ideal precursor for ceramic membrane fabrication (Alsubei, Reid et al. 2024). In our previous study, fabrication of a ceramic membrane from coal fly ash and natural sand at a sintering temperature that was lower than that of commercial starting materials was reported. The membrane demonstrated good water absorption capabilities in addition to good thermal and chemical durability (Sawunyama, Oyewo et al. 2024).

To overcome the inefficiency of ceramic membranes in degrading contaminants in wastewater, the functionalization of ceramic membranes with photocatalysts has recently been explored. This hybrid method is based on exploring the combined advantages of photocatalysis and ceramic membrane technologies in order to maximize their benefits and minimize their drawbacks, hence reducing adverse effects on the economy and environment (Li, Sun et al. 2020). Metal oxide semiconductors are the major photocatalysts used to functionalize ceramic membranes (Al-Abri, Al-Ghafri et al. 2024), due to the generation of reactive species such as superoxide and hydroxyl radicals, which possess strong oxidizing capabilities and can effectively degrade organic pollutants (Zaleska-Medynska 2018, Prakruthi, Ujwal et al. 2022, Chiromo and Chiromo 2023). Metal oxides such as ZnO and TiO_2 are widely regarded as safe and environmentally friendly materials. These give them advantage over advanced materials such as MXenes, Layered Double Hydroxides and covalent organic frameworks

(COFs), whose environmental implications of synthesis procedure are still under investigation. These advanced materials often involve more complex synthesis and handling processes, which can hinder their scalability and practical applications(Janjhi, Ihsanullah et al. 2023, Farhan, Khalid et al. 2024). Another key advantage of metal oxide photocatalysts is their ease of fabrication compared to other photocatalytic options. This simplicity makes them a viable choice for large-scale applications. Additionally, their straightforward production facilitates their integration into existing technologies, such as coatings and composite materials. However, the limited absorption of solar light, poor adsorption characteristics, and high recombination rates impede photocatalytic activity of these metal oxide semiconductors. Consequently, semiconductor hybridization to form heterojunctions and elemental doping have been extensively and effectively studied to meet the necessary properties for industrial applicability (Ghosh, Sahu et al. 2020, Sawunyama, Oyewo et al. 2023) (Karthikeyan, Arunachalam et al. 2020, Danish, Estrella et al. 2021). However, only relatively few studies exist on the removal of contaminants such as pharmaceuticals from wastewater by utilizing metal oxide functionalized ceramic membranes. For example, Li, Lu et al. (2022) reported the degradation of diclofenac, naproxen, and carbamazepine utilizing graphene oxide-titanium dioxide photocatalytic ceramic membranes. In a similar study, Ghaderi, Lahafchi et al. (2023) successfully decomposed diphenhydramine (DPH) with a CuO-TiO_2 functionalized ceramic membrane. Studies involving antibiotics degradation by employing a functionalized ceramic membrane is not well explored, hence the focus of this study.

Antibiotics are a class of pharmaceutical products that are widely used in aquaculture, agriculture, and human and animal therapy due to their effectiveness and affordable price (Zhao, Yang et al. 2021). However, excessive use of these antibiotics combined with improper environmental discharge can lead to very serious consequences for the environment. Tetracycline as a model antibiotic, which could cause harm to humans', microorganisms', and animals' health when misused (Done, Venkatesan et al. 2015, Liu, Steele et al. 2017). Trace levels of tetracycline in drinking water can lead to significant adverse effects on humans' health and aquatic lives over extended periods. In humans, exposure can result in permanent discoloration of teeth in foetuses and children under eight years old, as well as impairments in foetal long bone growth (Shutter and Akhondi 2019). In plants, tetracycline has been shown to restrict growth, affect oxidative responses, and alter phytochemical composition (Margas, Piotrowicz-Cieslak et al. 2019). In terrestrial and aquatic systems, it significantly impacts growth and reproduction (Zhang, Cheng et al. 2015). With tetracycline consumption projected to increase by 30% by 2030 (Balakrishnan, Chinthala et al. 2023), and given that it is the second most consumed pharmaceutical drug, its residues in wastewater are not effectively removed by conventional treatment methods employed in most wastewater treatment plants. The challenge of removing tetracycline from wastewater is compounded by its coexistence with other pharmaceutical contaminants, heavy metals, and organic pollutants, such as dyes. The presence of electron-donor groups in tetracycline allows it to form stable compounds with

various ions, making removal more difficult (Jezowska-Bojczuk, Lambs et al. 1993). Additionally, its complex chemical structures and their low concentrations in wastewater also make it difficult to remove it from wastewater (Liao, Rong et al. 2021). This highlights the urgent need for the development of cost-effective and efficient wastewater treatment techniques capable of degrading tetracycline.

Therefore, this study focuses on the fabrication of novel sustainable photocatalytic ceramic membranes using TiO_2-ZnO heterojunction, natural sand, and coal fly ash for the removal of tetracycline. The photocatalytic ceramic membrane was fabricated through the co-pressing and co-sintering methods. The operating parameters including pH, tetracycline concentration, pressure and catalyst concentration were also investigated to evaluate the filtration and photocatalytic processes of the functionalized ceramic membrane on the removal of tetracycline. The feasibility studies on the industrial applicability of this synthesized functionalized membrane were also evaluated.

5.1. Experimental

5.1.1 Materials

TiO_2-ZnO heterojunction was prepared using zinc acetate [$Zn(CH_3COO)_2{\cdot}2H_2O$, ≥98%], titanium tetra-isopropoxide [$Ti(OCH(CH_3)_2)_4$, 98 %], acetic acid [$C_2H_4O_2$, > 99%], and sodium hydroxide [NaOH, 98%], that were procured from Merck, South Africa. The primary starting materials for ceramic membrane production were coal fly ash (CFA) and natural sand (NS) from Zimbabwe's Harare Thermal Power Station. Carboxymethylcellulose sodium salt and dextrin $(C_6H_{12}O_6)x$ were acquired from Merck in South Africa and used as additions to bind raw ingredients and produce pores respectively. Merck, South Africa supplied tetracycline (TC), which served as the pharmacological model for the photocatalytic degradation test.

5.1.2. Synthesis of TiO_2-ZnO heterojunction

TiO_2-ZnO heterojunction was prepared according to our previous work (Sawunyama, Oyewo et al. 2023) with some modifications. The heterojunction photocatalyst was synthesized using titanium tetra-isopropoxide and zinc acetate solutions. Firstly, ZnO sol was prepared by dissolving pre-weighed zinc acetate in 100 mL of distilled water. About 100 mL of 0.5 M NaOH was added to the mixture under vigorous stirring for 2 h. TiO_2 sol was prepared by adding (in drops) the measured volume of titanium tetra-isopropoxide into 100 mL of distilled water with continuous stirring for 30 min at 80 °C. Then, 50 mL of ethanol was added in drops to the white precipitate solution. The resultant mixed solution was further stirred for 2 h at 25 °C. After 24 h of continuous stirring with a magnetic stirrer, the produced

ZnO and TiO_2 sol were transformed into a gel-like solution. The resultant TiO_2-ZnO gel was centrifuged and rinsed with distilled water, followed by drying at 120 °C for 8 h. Thereafter, the crumps were crushed into a fine powder with a pestle and mortar before calcining for 2 h at 850 °C in a muffle furnace.

5.1.3 Thermal Treatment of Coal Fly Ash and Leaching of Heavy Metals from Coal Fly Ash

Pre-weighed coal fly ash was thermally treated in a muffle furnace set at 1000 °C for 1 h to remove any unburnt carbon and volatile matters. The leaching experiments were conducted according to the procedure reported in our previous work (Sawunyama, Oyewo et al. 2024). Specifically, 1 g of thermally treated coal fly ash was added to 50 mL of 1 mol/L acetic acid solution and stirred continuously at a moderate speed for 6 h. Following this, the mixture was allowed to stand at room temperature for 24 h and then filtered. The resulting residue was washed with distilled water to eliminate any residual acetic acid and subsequently dried at 110 °C for 10 h.

5.1.4. Preparation of TiO_2-ZnO functionalized CFA/NS ceramic membrane

The compositional ratios of the starting materials used in the fabrication of pristine coal fly ash-based ceramic membranes (PM) and functionalized coal fly ash based ceramic membranes (PCM) A, B and C are presented in Table 1. The photocatalytic ceramic membranes were fabricated using the co-pressing and co-sintering method, which has not been extensively used in fabricating functionalized ceramic membranes (Fig. 1). About 1 g of the precursor material was mixed with a pre-weighed, un-calcinated TiO_2-ZnO photocatalyst, and the mixture was pulverized. The photoactive layer was formed by placing the grounded mixture on the mold's base, and the supporting layer was formed by adding pre-weighed ceramic membrane precursor material to the mold. The resultant mixture was uniaxially pressed for 3 min at a pressure of 40 MPa, resulting in a flat ceramic membrane with a defined diameter of 40 mm. The fabricated photocatalytic ceramic membranes were dried in a hot air oven at 110 °C for 10 h for complete removal of loose moisture. To avoid thermal shocks and cracks, the membrane was then sintered in a furnace at a rate of 5 °C min^{-1} up to 850 °C and maintained for 2 h. Thereafter, the membranes were cleaned in an aqueous ultrasonic bath to eliminate of any loose particles that had stuck to the surface of the membrane.

Table. 1. The compositional ratios of the Materials used to fabricate the photocatalytic ceramic membranes

Raw materials	**Weight of different raw materials used for various fabricated membranes**			
	PM	**PCM A**	**PCM B**	**PCM C**
Ceramic membrane precursor material (g) (Mixture of coal fly ash (70g), natural sand (20g), dextrin (3g) and sodium carboxymethyl cellulose (7g))	9	8.75	8.50	8.25
TiO_2-ZnO (g)	-	0.25	0.50	0.75

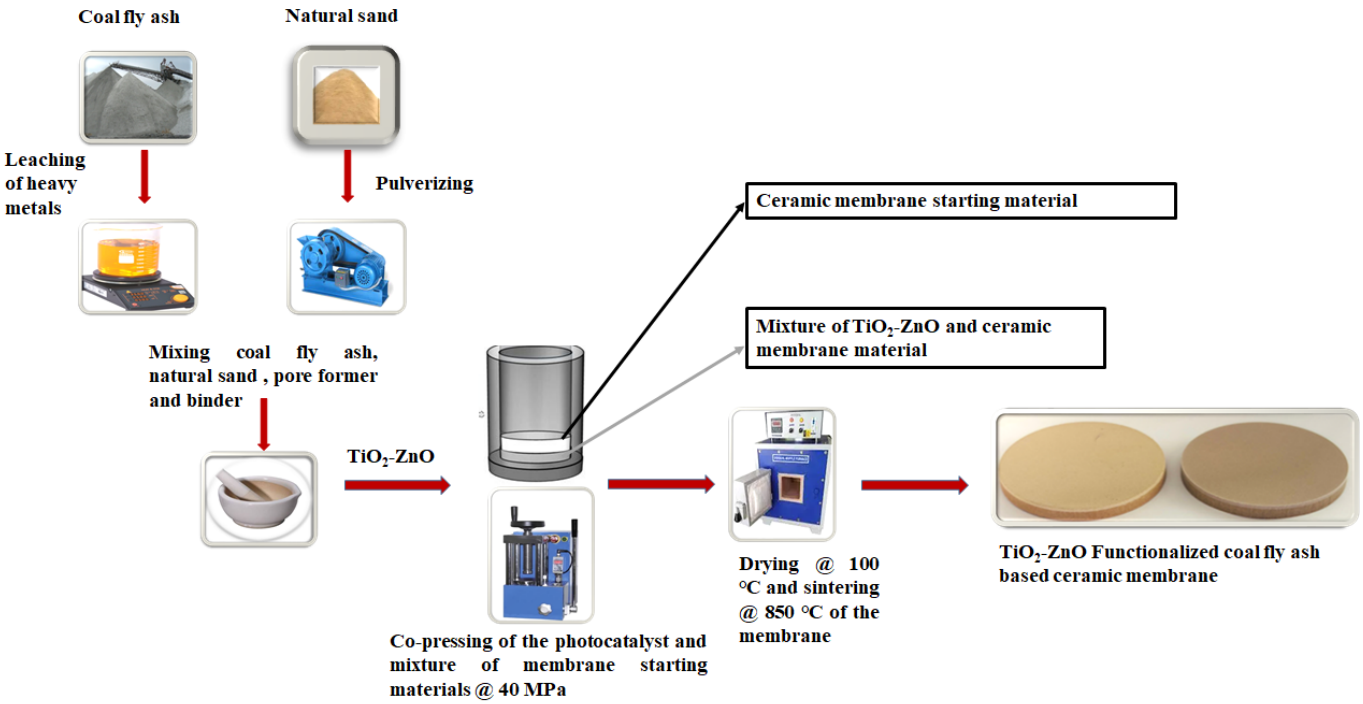


Figure 1: Schematic diagram of the fabrication process of TiO_2-ZnO functionalized coal fly ash based ceramic membranes by the co-pressing and co-sintering technique

5.1.5. Characterization of the photocatalytic ceramic membranes

Quanta FEG 250 Environmental scanning electron microscope (ESEM) coupled with EDX was utilized to characterize the morphology and elemental composition of the fabricated membranes. TG-DTA (TG/DTA 6300, Seiko Co., Ltd.) was used to evaluate the thermal stability of the ceramic membrane. X-ray diffraction (Bruker D8 Advance X-ray diffractometer (Karlsruhe, Germany) was used to determine the phase composition of the membranes. Fourier transform infrared spectroscopy (Bruker alpha-P FTIR spectrophotometer) was used to determine the functional groups present in the membrane and the photocatalyst. The three-point bending load method was used to assess the mechanical strength of the ceramic membranes.

5.1.6 Water absorption, Porosity and Pore size

The water absorption and porosity of the fabricated functionalized ceramic membranes were determined using the gravimetric method. First, the ceramic membranes were weighed to obtain their dry weight (***dw***). The membranes were then submerged in distilled water at room temperature for 24 h. After this process, they were removed, wiped to remove excess water, and reweighed to obtain the wet weight (***ww***). Water absorption and porosity were calculated using the Archimedes principle. Average membrane pore size was determined using the filtration velocity method and calculated using the Guerout–Elford–Ferry equation 3.

$$Water\ absorption\ (\%) = \frac{ww-dw}{ww} * 100 \qquad (1)$$

$$Membrane\ porosity\ (\text{Ɛ}) = \frac{ww-dw}{A*\rho*\text{L}} * 100 \qquad (2)$$

$$Membrane\ mean\ pore\ radius\ (r_{m)=}\sqrt{\frac{2.9-1.7\varepsilon*8\eta\text{L}Q}{\text{Ɛ}*\Delta P*A}} \qquad (3)$$

Where ***ww***= wet weight of the membrane sample (g), ***dw***= dry weight of the membrane sample (g), ***A***= the fabricated membrane's effective surface membrane area (m^2), $\boldsymbol{\rho}_{=\text{is}}$ the density of water **(kg/m^3),** ***ι*= membrane thickness **(m),** rm= mean pore radius (μm), ***η***= water viscosity (8.9×10^{-4} Pa s), ***Q***= volume of permeate water (m^3/s), and $\Delta\boldsymbol{P}$= is operational pressure (Pa)

5.1.7 Chemical and Mechanical stabilities

Chemical stability of the fabricated ceramic membrane was evaluated using hydrochloric acid and sodium hydroxide at pH of 1.5 and 13 respectively. First, the ceramic membranes were weighed to obtain their initial weight (***iw***). The membranes were then submerged in test medium (HCI and NaOH) at room temperature for 1 week. After this period, they were removed, wiped to remove excess test medium, and dried at 100 °C for 12 h followed by reweighed to obtain the final weight (***fw***). The chemical resistance of the ceramic membrane was evaluated in terms of weight loss using equation 4. The mechanical strength of the fabricated functionalized ceramic membranes was evaluated using three-point bending test, as shown in Fig. 1. The flexural strength (MPa) of the circular flat ceramic membrane was calculated using equation 5.

$$Chemical\ stability\ (\%) = \frac{iw-fw}{iw} * 100 \qquad (4)$$

$$Flexural\ \ strength\ (MPa) = \frac{3FL}{2Dh^2} \qquad (5)$$

The chemical stability of the fabricated ceramic membrane was evaluated using hydrochloric acid and sodium hydroxide at pH of 1.5 and 13 respectively (Obada, Salami et al. 2023). First, the ceramic membranes were weighed to obtain their initial weight (***iw***). They were then submerged in a test medium (HCI and NaOH) at room temperature for 1 week. After this period, they were removed, wiped to remove excess test medium, and dried at 100 °C for 12 h, and then reweighed to obtain the final weight (***fw***). The chemical resistance of the ceramic membrane was evaluated in terms of weight loss using Equation 4. The mechanical strength of the fabricated functionalized ceramic membranes was evaluated using a three-point bending test, as shown in Fig. 2. The flexural strength (MPa) of the circular flat ceramic membrane was calculated using equation 5.

$$Chemical\ stability\ (\%) = \frac{iw-fw}{iw} * 100 \qquad (4)$$

$$Flexural\ \ strength\ (MPa) = \frac{3FL}{2Dh^2} \qquad (5)$$

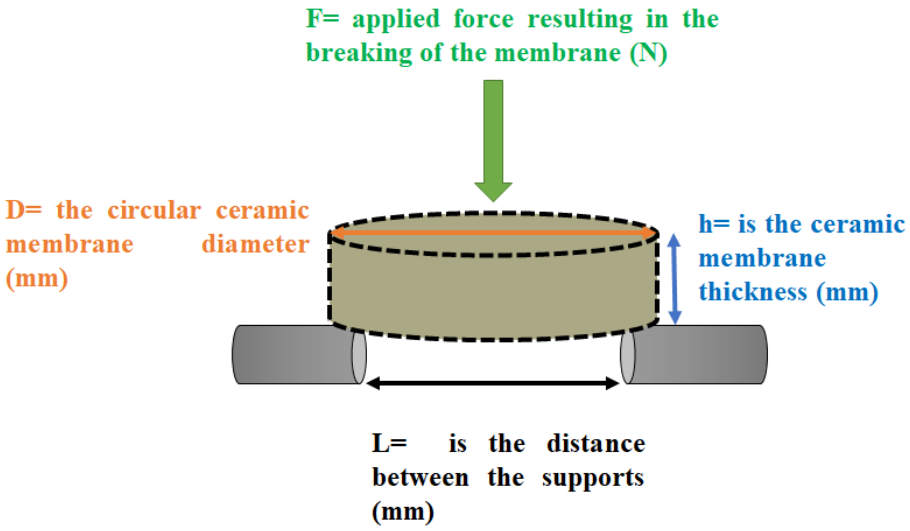


Figure. 2. Schematic representation of the three-point bending test

5.1.8 Pure water permeability and Tetracycline removal by filtration studies

A laboratory dead-end filtration setup was employed to evaluate the pure water permeation and tetracycline removal efficiency of the fabricated membranes (Fig 3). The filtration process was driven by pressure generated from nitrogen gas. Pure water flux (L/m^2/h) and water permeability (L/m^2/h/kPa) were calculated using Equations 6 and 7 respectively. The removal efficiency of tetracycline by both the pristine and functionalized ceramic membranes was assessed under uniform pressure conditions. The permeate was subsequently analyzed using a UV spectrophotometer, and the percent rejection (%R) was calculated using equation 8.

$$Pure\ water\ flux\ (J) = \frac{V}{A\Delta T} \quad (6)$$

$$Water\ permeability\ (J^1) = \frac{V}{A\Delta TP} \quad (7)$$

Where $\boldsymbol{V}$ is the volume of permeate in (L), $\boldsymbol{A}$ is the fabricated membrane's effective surface membrane area (m^2), $\boldsymbol{\Delta T}$ is the time taken to collect the permeate (h), and $\boldsymbol{P}$ is the transmembrane pressure (kPa).

$$R(\%) = \frac{C_0 - C_t}{C_0} * 100 \quad (8)$$

Where $\boldsymbol{C_0}$ and $\boldsymbol{C_t}$ are the initial concentrations of Tetracycline and the concentration at time *t*, respectively.

5.1.9 Procedure for photocatalytic degradation of tetracycline

Evaluation of the photocatalytic degradation of tetracycline by TiO_2-ZnO functionalized coal fly ash-based ceramic membrane was performed in a photocatalytic reactor system by irradiating with light source from a 300 W of Xe lamp (Fig 3). To attain equilibrium before the reaction, the fabricated ceramic membrane was immersed in a solution of tetracycline and kept in the dark for 30 min. The suspension was constantly agitated while exposed to light. Analyte solutions were collected in 5 mL aliquots at 30-min intervals, instantly filtered through a microporous membrane, and the concentration of the permeate solutions was evaluated using a UV-vis spectrophotometer in the range of 200-900 nm wavelength. Equation 9 was used to calculate the percentage of tetracycline eliminated.

$$Degradation\ efficiency\ (\%) = (1 - \frac{C_i}{C_f}) * 100 \qquad (9)$$

Where C_i and C_f are tetracycline concentrations before and after photocatalysis respectively.

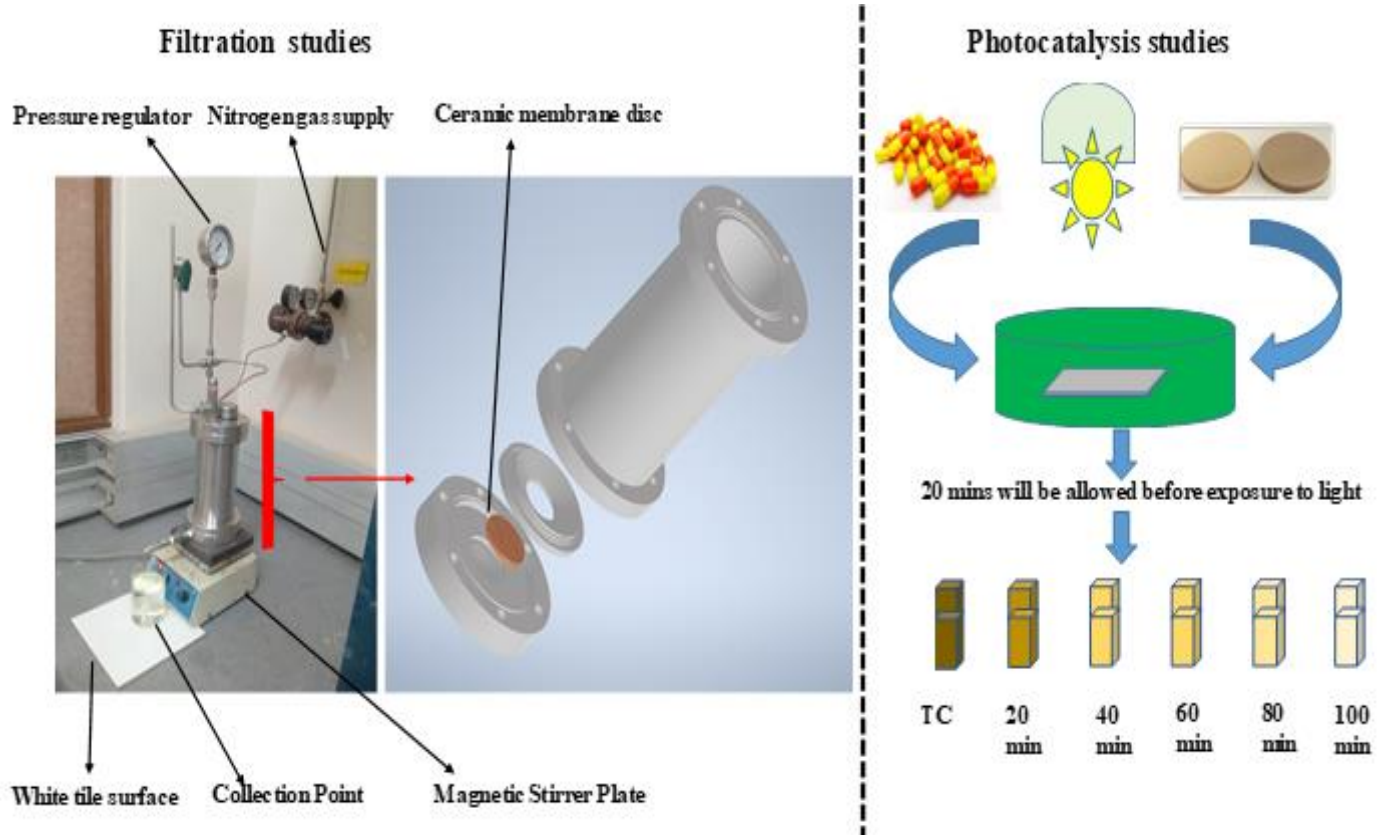


Figure. 3. Schematic representation of the filtration and photocatalytic set-up.

5.2 Results and discussion

5.2.1 Physical observations

Fig. 4 shows a picture of pristine coal fly ash-based ceramic membrane (a & e) and TiO_2-ZnO functionalized coal fly ash-based ceramic membranes at different photocatalyst loading of (b & f) 0.25 g, (c & g) 0.50 g, and (d & h) 0.75 g. A slight but observable structural difference exist between the pristine and functionalized ceramic membranes. The pristine membrane is expected to exhibit a single-layered structure, whereas the functionalized membranes display a two-layered structure. The thickness of the surface-active layer of the functionalized ceramic membranes also increased proportionally with higher photocatalyst loading as shown in Table 2. The surface of the photocatalyst-functionalized ceramic membrane may be less coarse compared to the pristine membranes. This is due to the TiO_2-ZnO incorporating into the matrices and chemically interacting with the ceramic membrane material, hence contributed to a more uniform surface.

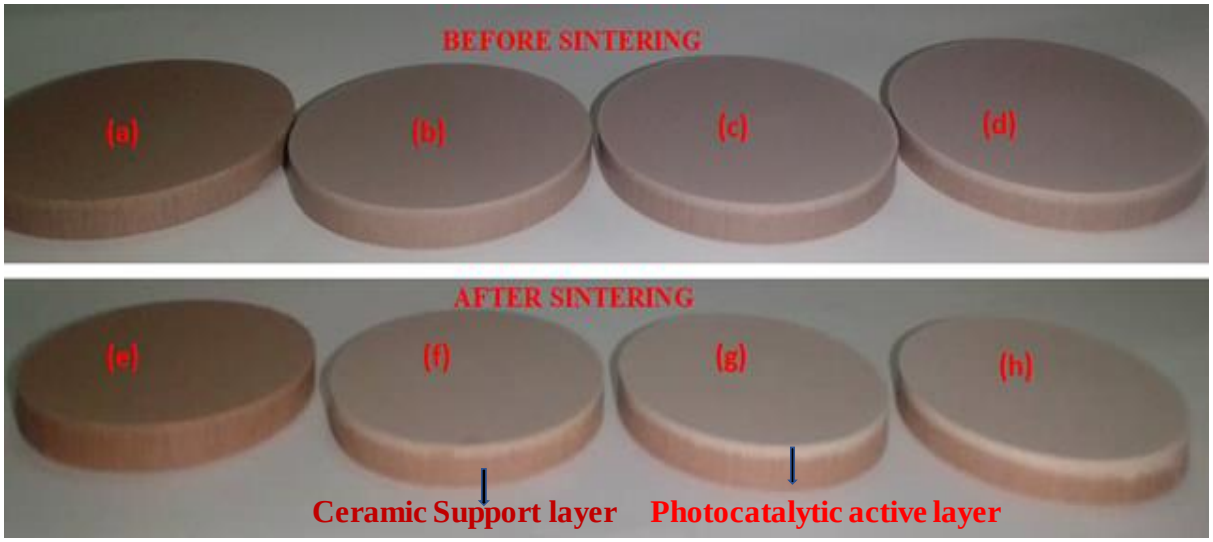


Figure. 4. Pristine and functionalized ceramic membrane before and after sintering. Pristine coal fly ash-based ceramic membrane (a & e) and TiO_2-ZnO functionalized coal fly ash-based ceramic membranes at different photocatalyst loading of (b & f) 0.25 g, (c & g) 0.50 g, and (d & h) 0.75 g.

5.2.2 Water absorption, Porosity and Pore size

The porosity and water absorption characteristics of the fabricated ceramic membranes were evaluated using Archimedes' principle with water as the wetting liquid. As shown in Table 2, pristine coal fly ash-based ceramic membranes exhibited higher water absorption and porosity levels as compared to the functionalized ceramic membranes. As the loading of the TiO_2-ZnO photocatalyst increased on the

functionalized membranes, both porosity and water absorption decreased. This trend could be attributed to the increased occupation of available voids by the photocatalyst, thereby reducing the overall pore radius of the functionalized ceramic membranes (Li, Zhang et al. 2021). The functionalization of the ceramic membranes can alter the membrane's selectivity and permeability, thereby impacting its filtration efficiency or separation applications (Ewis, Ismail et al. 2021). Conversely, functionalizing ceramic membranes with nanoscale materials can facilitate the production of membranes with smoother surfaces. This has the potential to mitigate fouling and enhances the cleaning ability of the membrane, thereby improves the overall membrane performance. A study conducted by Alias et al., (Alias, Harun et al. 2018), revealed a consistent findings regarding the influence of functionalizing ceramic membranes on pore radius, porosity, water absorption, and density. Table 2 also shows the water flux of pristine coal fly ash-based ceramic membrane and TiO_2-ZnO at different catalyst loading of 0.25, 0.50 and 0.75 g. The water flux of these fabricated membranes evaluated at the transmembrane pressure of 100 KPa followed the order of PM > PCM 0.25> PCM 0.50> PCM 0.75. The decrease in water flux occurred as the catalyst loading increased from 0.25 g to 0.75 g, and could be attributed to the significant reduction in pore size. This might be caused by the deposition of nanoparticles which occupied the membrane pores, thereby reduced their effective diameter and the membrane's overall permeability. This blockage also reduces the available space for contaminants to interact with the catalyst. Furthermore, a higher concentration of the catalyst could cause an increase in aggregation, lowering pore diameters and impeding water flow (Wang, Zhao et al. 2013). The reduction in porosity has a more substantial impact on water flux than the expected increase in hydrophilicity from the functionalization of the ceramic membrane with TiO_2-ZnO nanoparticles. Marzouk, Naddeo et al. (2021), reported similar findings, highlighting the influence of photocatalyst concentration on the water flux of functionalized ceramic membranes.

Table 2. A summary of pristine and functionalized ceramic membrane properties.

Membrane code	**Thickness of surface active layer (mm)**	**Thickness of ceramic support layer (mm)**	**Water absorption (%)**	**Open porosity (%)**	**Crystallite size (nm)**	**Pore diameter (nm)**	**Water-Flux ($L/m^2/h$)**
PM	-	3.90	24.16	39.45	30.68	720	40.6
PCM 0.25	0.02	3.88	22.09	36.20	33.17	169	18.6
PCM 0.50	0.04	3.86	21.96	34.94	36.17	140	14.2
PCM 0.75	0.06	3.84	21.32	34.26	37.60	108	9.3

5.2.3 Chemical and mechanical Properties

The result of the acid-base stability of the fabricated ceramic membranes is shown in Fig. 5a. Both the pristine and functionalized coal fly ash-based ceramic membranes exhibited high chemical stability in both test media. This could be attributed to the high sintering temperature that promotes the shrinking of grains and decomposition of acid and base leachable compounds. It is also related to its ability to drive off impurities or residual organic compounds that are present in the ceramic material (Li and Ye 2005, Chaim, Levin et al. 2008). The lower porosity limits the pathways through which chemicals can penetrate and react with the ceramic matrices. Results in Fig 5 (a) also show that the stability towards the acidic condition is lower as compared to the basic condition. Functionalized coal fly ash-based ceramic membranes showed higher weight loss in acidic environments compared to pristine ceramic membranes due to the presence of ZnO, MgO, CaO, and Na_2O which are reactive with concentrated acids (Abo-Naf, El Batal et al. 2003). Fig 5 (b) shows that pristine coal fly ash-based ceramic membranes had lower mechanical strength compared to functionalized ceramic membranes. Flexural strength increased from 4.30 MPa to 5.21 MPa when the number of TiO_2-ZnO nanoparticles loaded increased from 0.25 g to 0.75 g. The observed trend could be attributed to the rise in crosslinking points between the uniformly distributed smaller TiO_2-ZnO photocatalyst particles and the ceramic matrices (Alkahtany 2016). The enhancement in crosslinking resulted to an increase in the rigidity of the surface of the functionalized ceramic membrane. The increase in mechanical strength could also be ascribed to the reduction of voids within the functionalized membranes, which led to a denser and more cohesive structure. However, there are not much difference between the mechanical strength of the pristine and the functionalized ceramic membranes. This could be due to their supporting layer being made from the same material composition.

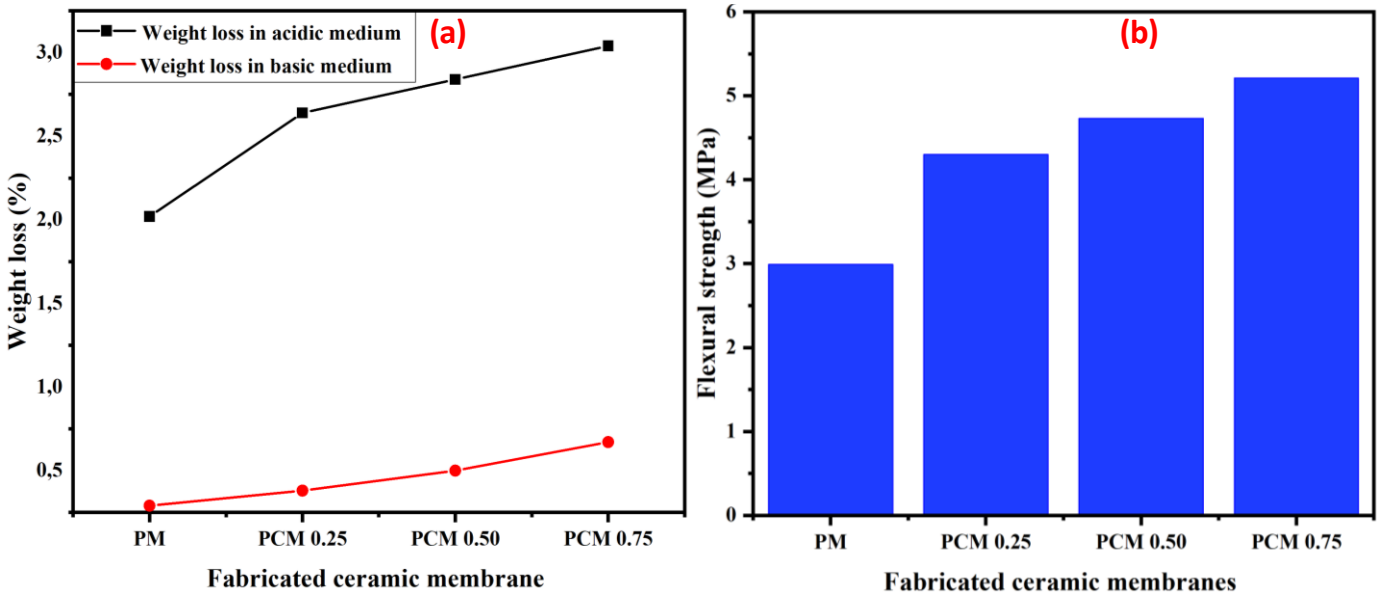


Figure 5: (a) Chemical stability and (b) Flexural strength of coal fly ash based ceramic membrane (PM)

and functionalized ceramic membranes at different photocatalyst loading of 0.25g (PCM 0.25), 0.50g (PCM 0.50) and 0.75g (PCM 0.75) sintered at 850 ℃ for 2 h

5.2.4 Fourier transform infrared spectra

Fig 6 presents the infra-red spectra of TiO_2-ZnO (black), pristine coal fly ash ceramic membrane (red), and functionalized ceramic membranes at different photocatalyst loading of 0.25 g, 0.50 g, and 0.75 g. The spectrum of TiO_2-ZnO showed characteristic peaks around 850, 627, and 502 cm^{-1} which could be ascribed to the vibrational mode of Zn–O–Ti, vibration of Ti−O−Ti, and vibration of M−O linkages (where M represents Zn or Ti) respectively (Moradi, Aberoomand-Azar et al. 2016, Kurniawan and Yuliati 2021). The pristine ceramic membrane's FTIR spectrum displays asymmetric stretching vibration bands attributed to Si-O-Si around 1082 and 452 cm^{-1}. Further, the pristine ceramic membranes also showed peaks at 612 and 778 cm^{-1}, due to the stretching vibration of Al–O–Si (Ahmad, Dilshad et al. 2022). The functionalized ceramic membranes' spectra showed peaks consistent with pristine coal fly ash-based ceramic membrane and TiO_2-ZnO nanoparticles, indicating the successful fabrication of photocatalytic ceramic membranes.

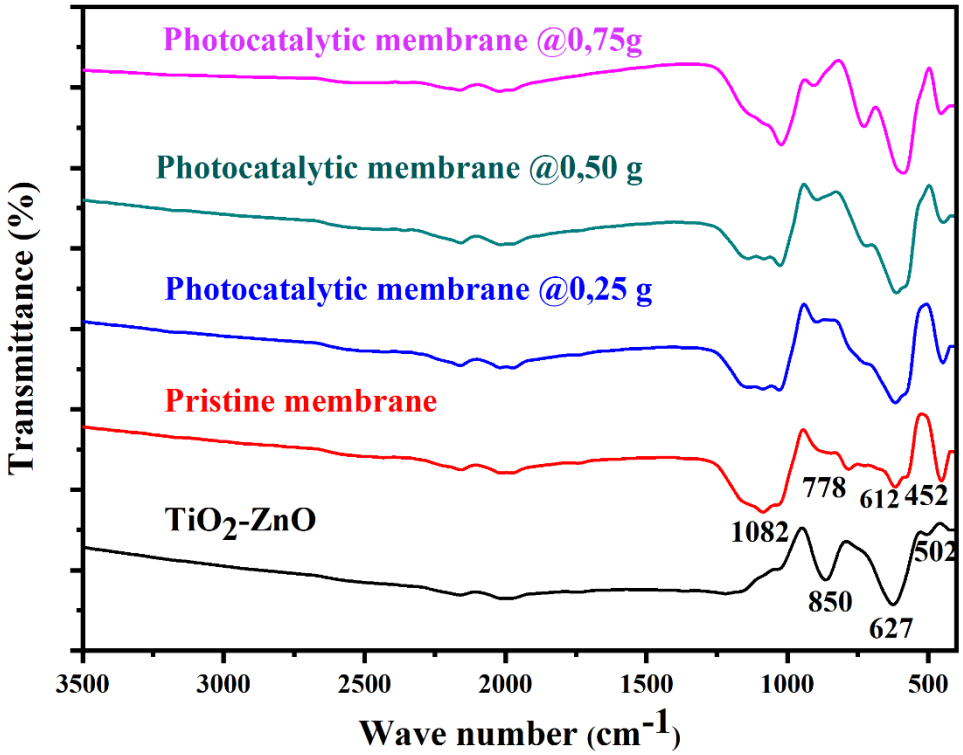


Figure 6: The FTIR spectra of TiO_2-ZnO (black), pristine coal fly ash ceramic membrane (red) and functionalized ceramic membranes at different photocatalyst loading of 0.25 g (blue), 0.50 g (green) and 0.75 g (pink)

5.2.5 Structural studies

The X-ray diffraction patterns of TiO_2-ZnO (black), pristine coal fly ash ceramic membrane (green), and photocatalytic ceramic membranes at different photocatalyst loading of 0.25g (red), 0.50g (blue), and 0.75g (purple) are presented in Fig. 7. The diffraction patterns of the TiO_2-ZnO heterojunction system confirmed the presence of rutile TiO_2, hexagonal $ZnTiO_3$, and Zincite ZnO. The peaks for hexagonal $ZnTiO_3$ appeared at 25, 34, 36, 43, 50, 54, 58, 63, and 64 ^{o} and are in good agreement with JCPDS No. 26-1500 (Faisal, Jalalah et al. 2021). The characteristic peaks of rutile TiO_2 were observed at 2θ = 27, 36, and 54 ^{o} (JCPDS Card No. 21-1276) (Jia, Dong et al. 2018), while the characteristic peaks of Zincite ZnO were observed at 2θ = 33, 36, and 38 ^{o} (JCPDS No. 65-3411) (Danwittayakul, Jaisai et al. 2013). The sharp peaks confirm that the heterojunction photocatalyst contains crystalline components. The XRD patterns of the pristine coal fly ash-based ceramic membrane is composed of three major crystalline phases which are α-quartz (SiO_2), cristobalite (tetragonal SiO_2), and mullite ($3Al_2O_3{\cdot}2SiO_2$). The peaks for α-quartz (SiO_2) are observed at 2θ values of 21.85, 26.85, 39.6, 49.5, 54.5, and 60.8 ^{o}. The peaks due to the mullite and cristobalite were observed at 2θ values of (25.9, 33.7, 37.4, and 52.5 ^{o}) and (22 and 36 ^{o}) respectively. The presence of quartz and mullite phases confirmed the high thermal stability of the fabricated ceramic membrane. All the TiO_2-ZnO peaks and those of pristine coal fly ash-based ceramic membranes were evident in the as-synthesized photocatalytic ceramic membranes demonstrating the success in functionalizing coal fly ash-based ceramic membranes with TiO_2-ZnO photocatalyst. The crystallite size of the functionalized ceramic membranes estimated from the Scherrer equation (Equation 10) was higher than that of the pristine ceramic membrane.

$$D\left(Crystallite\ size\ (nm)\right) = \frac{K\lambda}{\beta Cos\theta} \qquad 10$$

Where K is the Scherrer's constant (Shape factor) (0.94), λ is the Wavelength of X-rays (Å), β = F. W. H. M (Full Width at Half Maxima in degrees), θ = Peak position in XRD graph (that is 2θ in degrees)

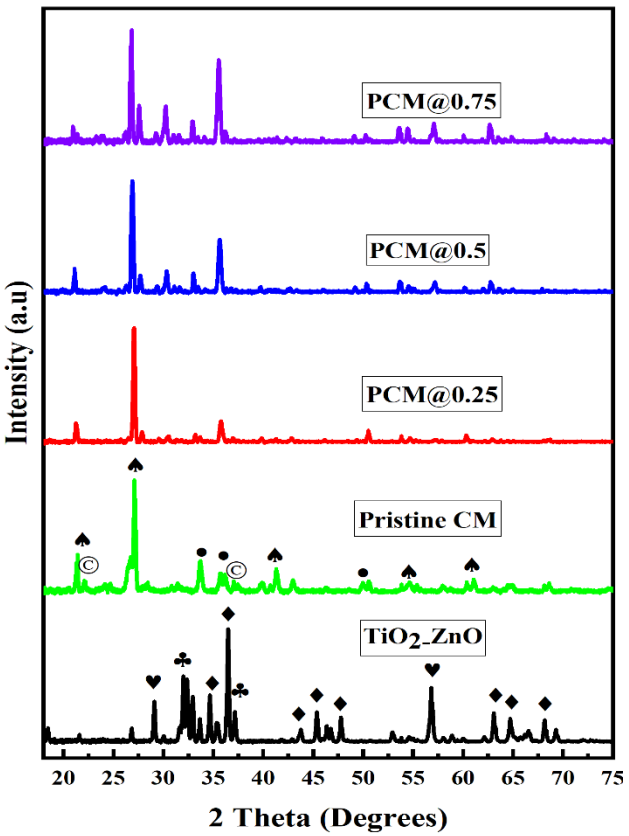


Figure 7: X-ray diffraction spectra of TiO_2-ZnO (black), pristine coal fly ash ceramic membrane (green) and functionalized ceramic membranes at different photocatalyst loading of 0.25g (red), 0.50g (blue) and 0.75g (purple). (TiO2 rutile (♥), ZnTiO3 (♦), Zincite ZnO (♣), mullite (●), cristobalite (©) and α-quartz (♠)

5.2.6 Thermal analysis

The thermal stability properties of the materials were studied using Thermogravimetric analysis (TGA) and differential scanning calorimetry (DSC), and the results are shown in Fig. 8. The precursor material's TGA graph (Fig. 8) reveals a significant weight loss in two phases, with a total weight loss of almost 18%. The first loss observed below 450 °C was due to the removal of the adsorbed water and the decomposition of volatile organic matter, dextrin (pore former) and sodium carboxyl methyl cellulose (binder). This process was accompanied by a weak endothermic peak noted around 336 °C in the DSC thermogram (Fig. 8b). The increase in temperature from 450 to 1000°C resulted in a weight loss of around 7%. A weak exothermic peak noted at 659 °C in the DSC curve is likely attributed to the incineration of unburnt carbon and mineral degradation. When the temperature was further increased to

1200 °C, a narrow endothermic peak appeared in the DSC curve, which could be due to the phase transformation of quartz (Rakcho, Mouiya et al. 2023, Gao, Yan et al. 2024).

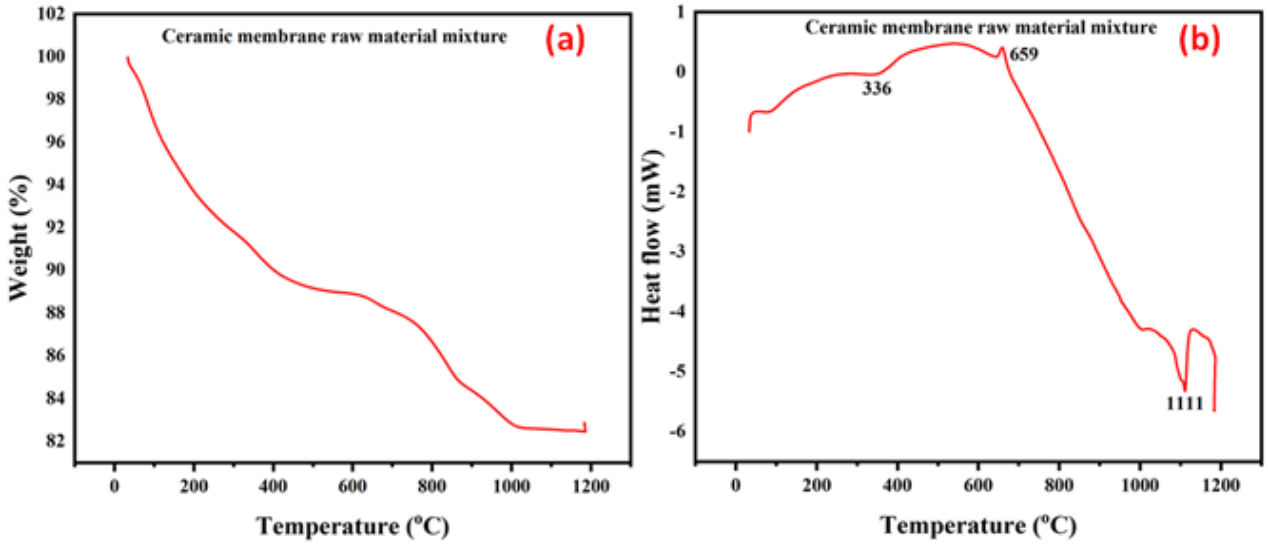
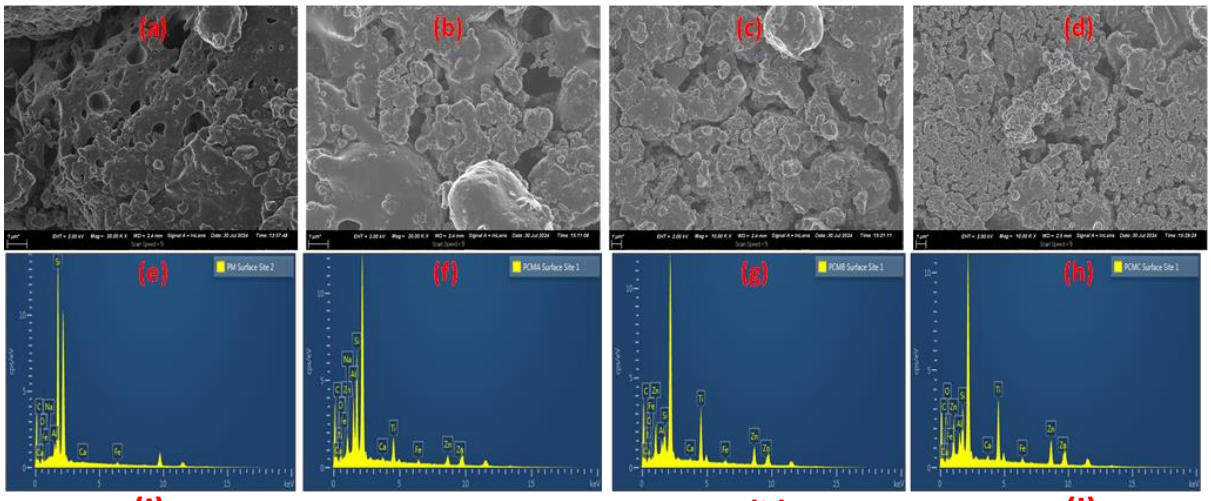


Figure 8: Thermogravimetric (TG) and (b) Differential scanning calometry (DSC) graphs of ceramic membrane raw material mixture

5.2.7 Morphological studies

The morphological changes of the synthesized membranes with varying loads of TiO_2-ZnO and their respective elemental composition are presented in Fig. 9a-h. The micrograph of the pristine ceramic membranes reveals a distinct and well-distributed pore structure. In contrast, upon functionalization, there is a noticeable reduction in pore size and distribution as the TiO_2-ZnO load was gradually increased from 0.25 to 0.75 g. This pattern, thus, indicates that a larger surface coverage with densely packed spherical particles was obtained due to the increase of TiO_2-ZnO on the surface, thereby decreasing the overall pore density. The transition in surface morphology from the pristine ceramic membranes' darker appearance to the lighter appearance of the functionalized membranes further corroborates the successful functionalization process (Fig 9 (a-d). The observed colour change indicates the effective deposition of the TiO_2-ZnO particles on the membrane surface. Cross-sectional micrographs reveal additional insights into the structural changes induced by functionalization. Since the pristine ceramic membranes are characterized by a single-layered structure, functionalized membranes exhibit a distinct two-layered structure. Notably, the thickness of the photocatalytic active layer increases with the TiO_2-ZnO particles, demonstrating a successful integration of the photocatalyst into the matrices of the ceramic membrane. Furthermore, the surface micrographs of the base of both pristine and functionalized ceramic membranes show uniformity in colour and pore distribution, indicating that the functionalization process primarily affected the top surface morphology. The EDX

spectra of the fabricated membranes are displayed in Figs 9 (e-h). Si, Al, Fe, and Ca are the major elements found in the pristine coal fly ash-based ceramic membranes. The additional Ti and Zn that appeared on the surface of functionalized coal fly ash-based ceramic membranes are due to the functionalization. This further confirms the successful incorporation of TiO_2-ZnO heterojunction incorporation into the ceramic matrix.



(i)

	Wt%	Wt% Sigma
C	40.42	2.40
O	20.85	1.12
Na	0.24	0.16
Al	2.30	0.16
Si	34.28	1.41
Ca	0.21	0.11
Fe	1.69	0.22
Total	100.00	

(j)

	Wt%	Wt% Sigma
C	32.58	3.25
O	19.71	1.34
Na	3.03	0.40
Al	8.76	0.47
Si	15.01	0.77
Ca	0.68	0.10
Ti	7.32	0.40
Fe	2.07	0.21
Zn	10.84	0.68
Total	100.00	

(k)

	Wt%	Wt% Sigma
C	28.73	2.89
O	18.45	1.36
Al	2.96	0.23
Si	4.21	0.25
Ca	0.53	0.11
Ti	17.77	0.79
Fe	1.84	0.23
Zn	25.51	1.19
Total	100.00	

(l)

	Wt%	Wt% Sigma
C	24.81	3.06
O	16.00	1.20
Al	4.00	0.24
Si	6.97	0.34
Ca	0.90	0.11
Ti	17.07	0.75
Fe	2.40	0.22
Zn	27.85	1.26
Total	100.00	

Figure 9: SEM surface micrographs of (a) pristine coal fly ash ceramic membrane and functionalized ceramic membranes at different photocatalyst loading of (b) 0.25g (c) 0.50g and (d) 0.75g, EDX spectra (e) of pristine coal fly ash ceramic membrane and functionalized ceramic membranes at different photocatalyst loading of (f) 0.25g (g) 0.50g and (h) 0.75g and Table of elements present in (i) of pristine coal fly ash ceramic membrane and functionalized ceramic membranes at different photocatalyst loading of (j) 0.25g (k) 0.50g and (l) 0.75g

5.2.8 Photocatalytic activity of the functionalized ceramic membranes

5.2.8.1 Effect of solution pH

Solution pH is an important factor in photocatalytic degradation study. This is because it influences the surface electrical charge that is characteristic of the catalyst and dictates the ionization state of the catalyst's surface (Hanafi and Sapawe 2020). Fig. 10 shows the effect of pH on the degradation of tetracycline using a TiO_2-ZnO functionalized coal fly ash-based ceramic membrane. A model solution of tetracycline with a concentration of 25 mg/L and a coal fly ash-based ceramic membrane functionalized with 0.5g of TiO_2-ZnO heterojunction were used. The study was conducted over 100 min. The initial 20 min was for a steady-state adsorption-desorption equilibrium to be established, while the remaining 80 min were used to facilitate the photocatalytic degradation process. It is evident from the results that pH significantly affects the degradation of TC by the functionalized ceramic membranes as pH of 4,7 and 9 resulted in degradation efficiency of 25, 29 and 77.6% respectively (Fig 10 (d)). The results corroborate well with previously reported studies that used black TiO_2-ZnO (Sawunyama, Oyewo et al. 2023) and nanosized TiO_2 (Zhu, Wang et al. 2013). The pH of the solution changes the surface charges of tetracycline and influences the adsorption process, so an increase in adsorption and photocatalytic activity at pH 9 could be attributed to the electrostatic interaction between the charges of TC species and the functionalized ceramic membrane (Qiao, Li et al. 2020). This could also be attributed to tetracycline deprotonation, which increases its adsorption onto the photocatalytic surface. Furthermore, the increased availability of hydroxyl radicals at alkaline pH enhances the degradation process (Liu, Zhou et al. 2023). Tetracycline is an amphoteric molecule with pKa values of 3.32, 7.78, and 9.58, and it exists in three forms depending on the pH. At pH < 3.32, it is primarily cationic, between pH 3.32 and 7.78 it is zwitterionic and above pH 7.78, it becomes anionic (Nezamzadeh-Ejhieh and Shirzadi 2014). Tetracycline molecules with negative charge generate reactive species such as $OH^{\bullet}$ due to high electrical density on the ring system, thereby enhancing the degradation efficiency of tetracycline. The optimization of pH in real wastewater treatment applications is important since changes in pH can affect both the ionization state of pollutants and the surface charge of the photocatalyst, which may lead to reduced adsorption and, consequently, decreased degradation efficiency. The pH of 10 was therefore chosen for the subsequent evaluation of the photocatalytic degradation of TC in this study.

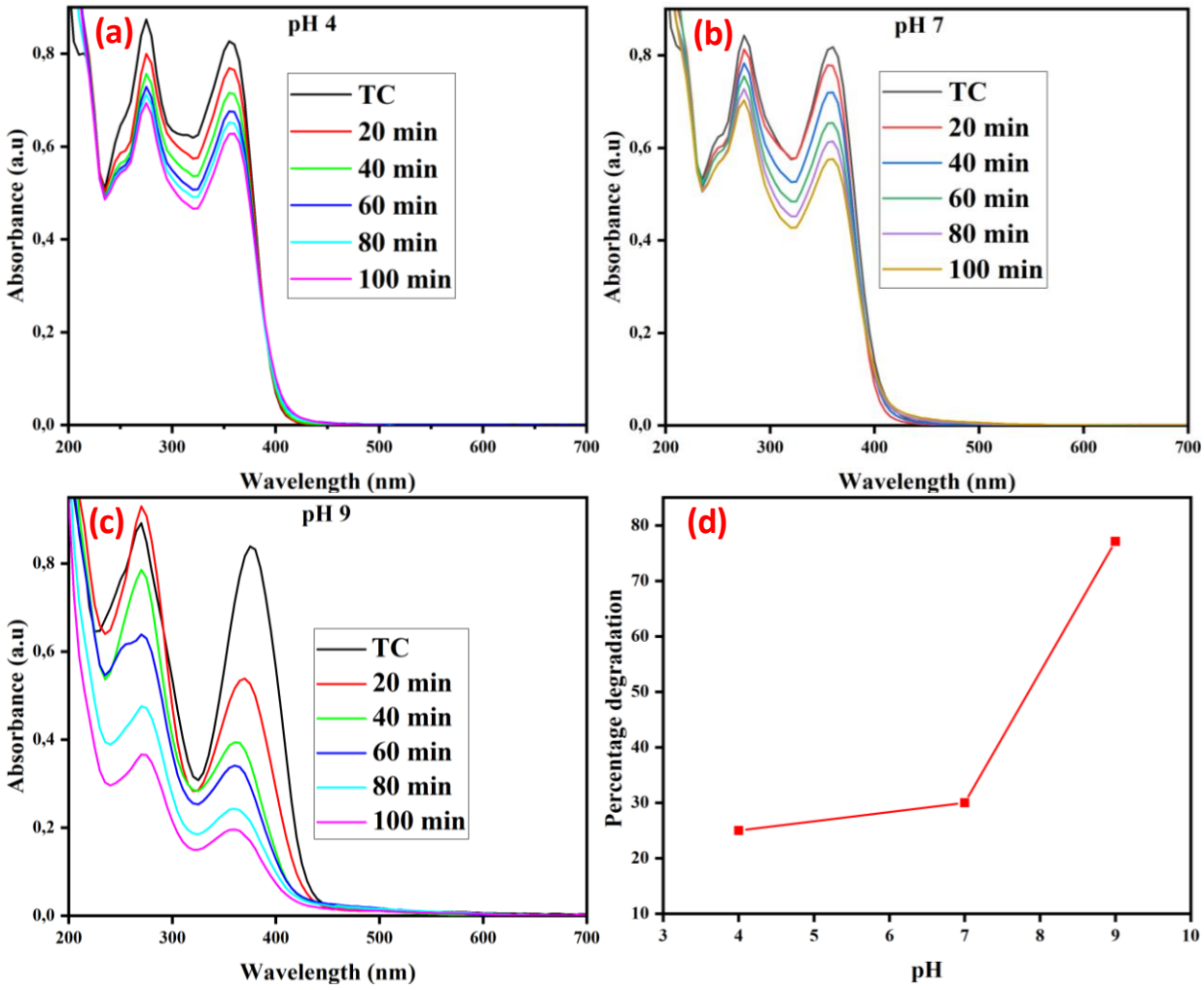


Figure 10: Photocatalytic degradation profile of Tetracycline by TiO_2-ZnO functionalized coal fly ash based ceramic membranes at different pH (a) 4, (b) 7, (c) 9, (d) Percentage degradation of TC under visible light (TC initial concentration: 25 mg/L)

5.2.8.2. Effect of Tetracycline concentration

Fig 11 shows the effect of initial TC concentration on the degradation efficiency of the process. TiO_2-ZnO functionalized coal fly ash-based ceramic membranes demonstrated effective TC degradation across the entire concentration range examined. However, degradation efficiencies decreased as TC concentration increased reaching 82%, 77.6%, and 68.8% at 10, 25, and 50 mg/L, respectively. The reaction rate constants also decreased as the initial concentration of tetracycline increased, and at 10, 25, and 50 mg/L, they were 0.016, 0.014, and 0.013 min^{-1}, respectively. The observed decline in degradation efficiency and reaction rates at higher concentrations may be attributed to several factors. At high tetracycline (TC) concentrations, TC ions dominate the photocatalyst's active sites, which hinders photons from reaching the functionalized ceramic membrane surface. This reduces the photocatalytic activity due to a decrease in the amount of hydroxyl radicals produced. Since the

photocatalytic ceramic membrane and the tetracycline (TC) model wastewater exists in different phases, the rate of photocatalytic degradation is significantly influenced by mass transfer and diffusion between these phases. Therefore, the system also changes from a kinetic control domain, where reaction rates are driven by intrinsic kinetics at low concentrations, to a mass transfer-limited regime at high concentrations, where the reaction rate is limited by the efficiency of reactant delivery to the reaction site (Safari, Hoseini et al. 2015). As the concentration of TC increases, mass transfer limitations may become more pronounced, potentially reducing the availability of TC at the active surface of the photocatalytic membrane (Li, Wang et al. 2023). High TC concentrations can create thicker concentration gradients near the membrane, which can limit the effective mass transfer and hinder their interaction with the photocatalyst. The effectiveness of the degradation process may be impacted by the intermediates that tetracycline molecules may generate during photocatalytic activities. These intermediates may compete with the catalyst's surface for photocatalytic and adsorption sites (Shi, Yang et al. 2024). These results are similar to those reported by Pourshaban-Mazandarani and Nasiri (2024) and Deng, Li et al. (2023).

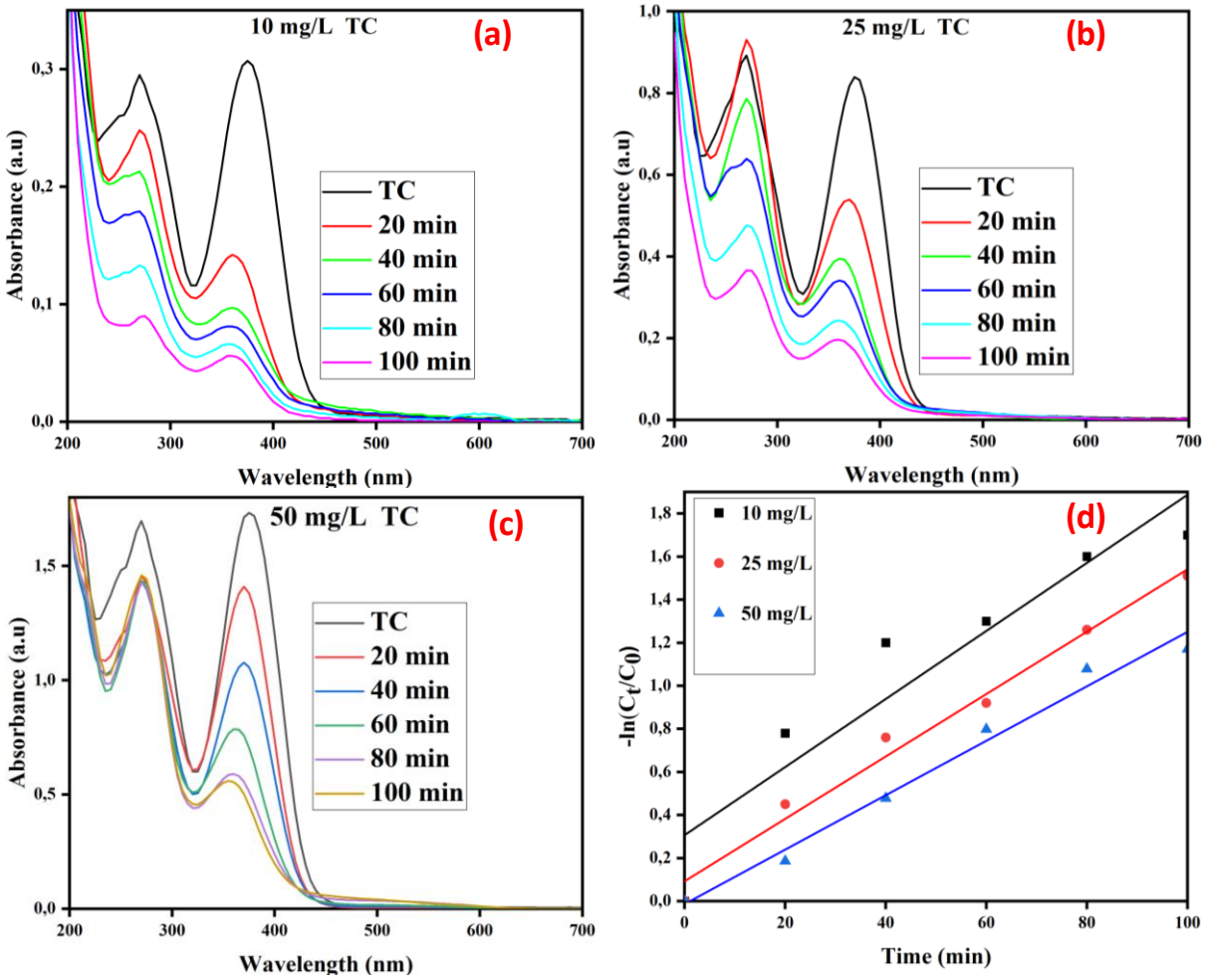


Figure 11: Effect of Tetracycline concentration at (a) 10 mg/L, (b) 25 mg/L and (c) 50 mg/L on the

photocatalytic degradation of Tetracycline by TiO_2-ZnO functionalized coal fly ash based ceramic membranes and (d) the kinetic plots for the effect of antibiotic concentration on the photocatalytic degradation of Tetracycline.

5.2.8.3 Effect of photocatalyst loading

The effect of varied photocatalyst loadings on the breakdown of 25 mg/L tetracycline was investigated using a functionalized coal fly ash-based ceramic membrane. Fig. 13a depicts an increase in the rate of tetracycline degradation as the photocatalyst loading increased from 0.25 to 0.75 g. The enhanced rate of photocatalytic degradation was caused by a rise in the number of surface-active sites, which resulted in the increased creation of photoactive species (Ajiboye, Imade et al. 2022). However, the increase in photocatalyst loading resulted in reduced adsorption of tetracycline during the initial 20-min adsorption-desorption equilibrium. This reduction may be attributed to the saturation of available adsorption sites on the photocatalyst or possible steric hindrance that limits the access of tetracycline molecules to the ceramic membrane surface (Ahmed, Ahmed et al. 2023). Additionally, a higher photocatalyst concentration may lead to more competitive interactions, hindering effective adsorption of the tetracycline onto the catalyst surface (Minale, Gu et al. 2020). Similar results were reported during the photocatalytic degradation of tetracycline hydrochloride over AgBr nanoparticles decorated GO/Bi_2WO_6 photocatalyst (Guan, Li et al. 2021).

5.2.8.4 Synergistic effect of adsorption and photocatalysis

Figures 12 a and b show Tetracycline removal efficiency by the pristine coal fly ash-based ceramic membrane and TiO_2-ZnO functionalized ceramic membrane. During the first 20 min of the adsorption studies, the pristine coal fly ash-based ceramic membrane showed a higher tetracycline removal efficiency of 49% compared to the functionalized ceramic membrane, which achieved only 35%. This suggests that the pristine membrane may have a greater affinity for tetracycline in the initial stages, possibly due to its surface properties or pore structure that favors adsorption (Doran 1995, Jiang, Tan et al. 2022). The Si-O-Si and Al-O-Si groups found in pristine ceramic membranes can generate a surface with polar characteristics. Since tetracycline is a polar organic molecule, it can interact more favorably with these functional groups, resulting in enhanced adsorption through dipole-dipole interactions (Massaro, Colletti et al. 2018). After exposure to visible light, the functionalized ceramic membrane exhibited a marked improvement in tetracycline removal efficiency, reaching 77.6% after 100 min of irradiation. This indicates that the TiO_2-ZnO functionalization significantly enhances the photocatalytic activity of the ceramic membrane, facilitating the degradation of tetracycline under visible light exposure. In contrast, the pristine coal fly ash ceramic membrane's degradation efficiency

declined after the initial adsorption phase, with its removal efficiency after 100 min being lower than the initial 49%. This suggests a paucity of photocatalytic activity and demonstrates that the pristine membrane is predominantly functional through adsorption. The subsequent increase in tetracycline concentration following adsorption reflects a desorption process in which tetracycline is released back into the solution rather than mineralized or further degraded. The results corroborate the hypothesis that ceramic membranes do not mineralize pollutants; rather, pollutants appear to shift from one phase (adsorbed) to another (dissolved). The effect of photolysis was also evaluated in Fig. 12 c. The results showed an insignificant impact of direct photolysis of tetracycline at pH of 9 as evidenced by degradation efficiency of less than 12%.

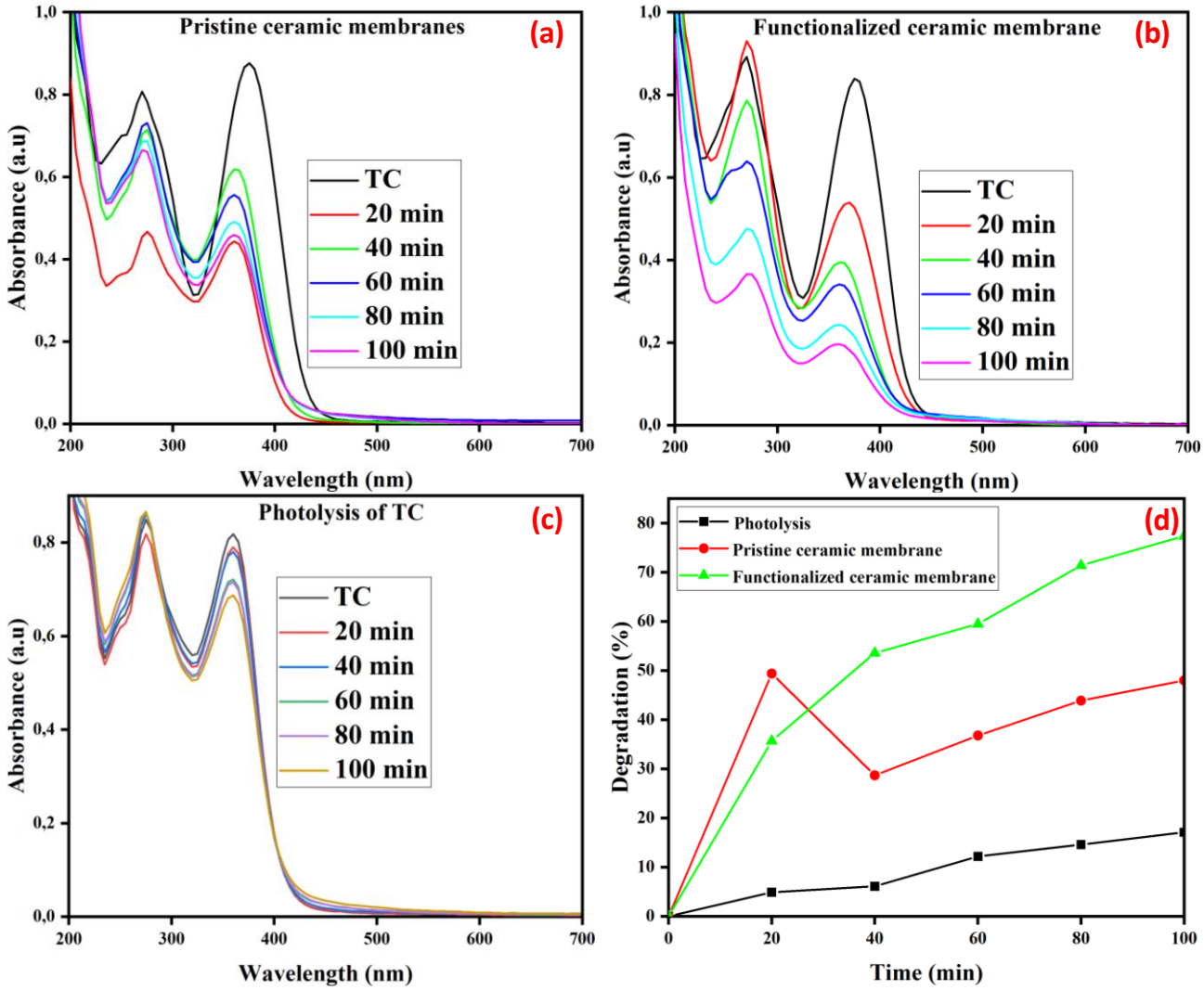


Figure 12: Degradation profile of (a) Pristine coal fly ash based ceramic membrane, (b) TiO2-ZnO functionalized coal fly ash based ceramic membrane, (c) Photolysis of Tetracycline and (d) Percentage degradation of TC under visible light

5.2.8.5 Reusability of the functionalized ceramic membrane

The reusability of the membrane was assessed by 5-cycle runs and Fig 13b shows the results obtained from the functionalized coal fly ash-based ceramic membrane using 25 mg/L TC concentration. After each cycle, the functionalized ceramic membrane was washed with water and then dried at 150 °C for 10 h. The membrane showed high stability and reusability by achieving 73% degradation efficiency after the 5th photocatalytic cycle. This effective reusability can be attributed to the limited loss of the photocatalyst since it is not directly recovered from the solution (Wu, Xu et al. 2019).

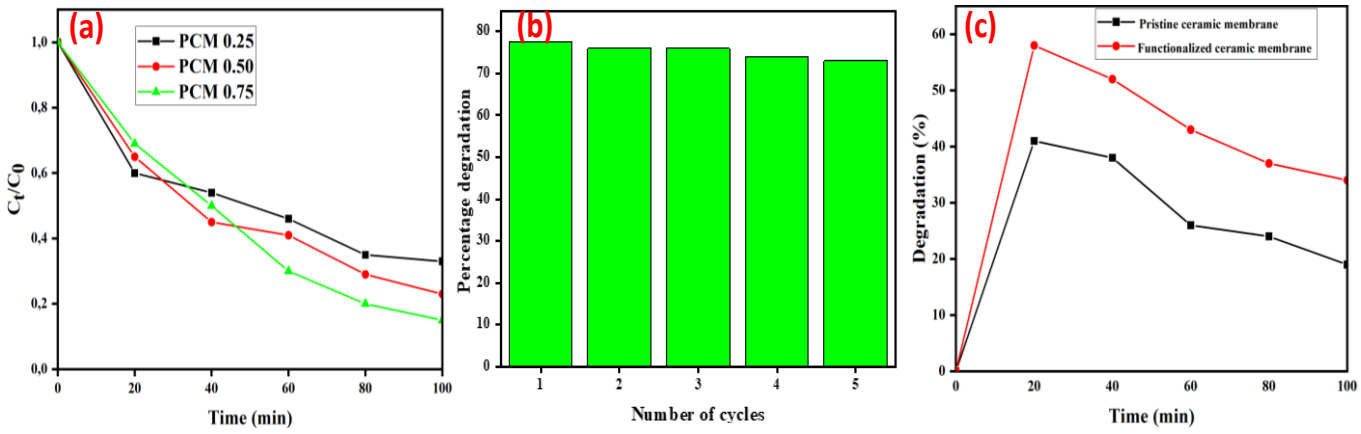


Figure 13. (a) Rate of TC removal with varying TiO_2-ZnO loadings on coal fly ceramic membranes, (b) Reusability of TiO_2-ZnO functionalized coal fly ash-based ceramic membrane for tetracycline degradation, (c) Tetracycline removal efficiency by pristine coal fly ash-based ceramic membrane and TiO_2-ZnO (0.5g) functionalized coal fly ash-based ceramic membrane through adsorption and filtration (TC concentration 25 mg/L, solution pH= 9, time 100 min)

5.2.9 Synergistic effect of adsorption and filtration performance

In Fig 13c, the Tetracycline removal efficiency by pristine coal fly ash-based ceramic membrane and TiO_2-ZnO functionalized coal fly ash-based ceramic membrane (through adsorption and filtration) are shown. During the first 20 min, both membranes showed excellent removal effectiveness, with the functionalized ceramic membrane outperforming the pure coal fly ash-based ceramic membrane. This was due to the presence of nano-sized pores, which provide a larger surface area and more active sites for filtration, allowing for more effective contaminants removal, whereas the pristine coal fly ash-based membrane has pores in the micrometer range, resulting in fewer and less effective filtration sites, causing a lower initial removal efficiency compared to the functionalized ceramic membrane. The decrease in removal efficiency after 20 min by both membranes can be attributed to the saturation of the adsorption sites on the membrane surfaces and the passage of the trapped elements in the pores into

the permeate (Saikia, Sarmah et al. 2019, Lagdali, Miyah et al. 2023). The deposition of particles on the membrane surface and the pores leads to the fouling of the membrane (Jang, Kang et al. 2024).

5.2.10 Photocatalytic mechanism

A photocatalytic degradation mechanism of the tetracycline by TiO_2-ZnO functionalized ceramic membrane has been proposed and presented in Fig. 14. Firstly, the tetracycline molecules are attracted to and adhere to the surface of the photocatalytic membrane. Upon exposure to visible light, the photocatalysts TiO_2 and ZnO absorb some photons, generating electrons and holes. The energy from the light excites electrons from the valence band to the conduction band, and the generated electrons react with dissolved oxygen to form superoxide anion radicals. Simultaneously, holes can oxidize water or hydroxyl ions to form hydroxyl radicals. These superoxide anions and hydroxyl radicals then attack the adsorbed tetracycline molecules, breaking down their structures into less harmful compounds. The intermediate products are further oxidized, ultimately leading to the complete mineralization of tetracycline into carbon dioxide and water (H_2O). After the degradation process, some of the remaining by-products may still be adsorbed on the membrane surface after filtration (Ajiboye, Kuvarega et al. 2020, Chiromo, Nyakuchena et al. 2023).

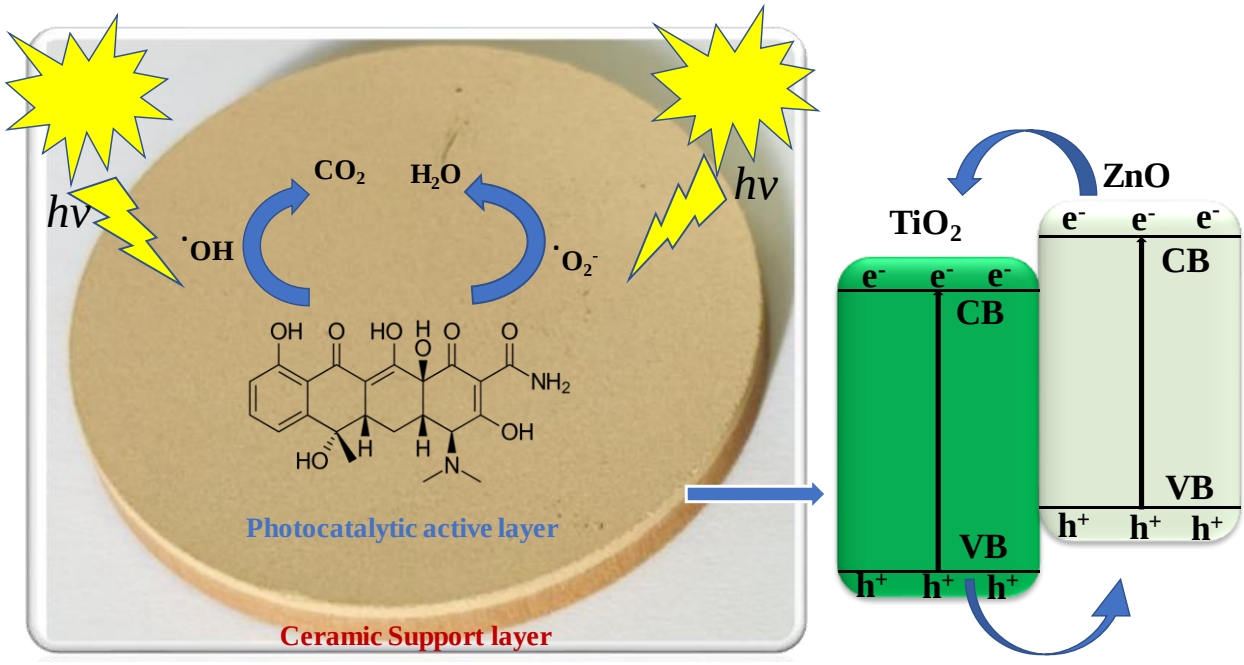


Figure 14. Photocatalytic degradation mechanism of Tetracycline by TiO_2-ZnO functionalized coal fly ash-based ceramic membrane.

5.3 Conclusion

A sustainable and cost-effective ceramic membrane functionalized with TiO_2-ZnO heterojunction photocatalyst was fabricated using co-pressing and co-sintering methods. Coal fly ash and natural sand were used as the main starting materials. The functionalized coal fly ash-based ceramic membrane exhibited nanoscale pore sizes on its photocatalytic surface and excellent thermal, chemical, and mechanical stability. The functionalized ceramic membrane showed 77.6% removal efficiency by photocatalysis and 57% removal efficiency by filtration for model wastewater containing 25 mg/L concentration of tetracycline. In filtration studies, tetracycline was simply adsorbed and filtered without the degradation complicating desorption from surface-active areas. This requires special desorption techniques to regenerate the membrane is expensive and involves high re-sintering temperatures to break down the retained tetracycline. This has the potential to cause environmental problems. Therefore, the fabricated functionalized ceramic membrane could be used in a hybrid photocatalysis and filtration reactor system to optimize its synergistic photocatalytic, adsorption, and filtration properties. Future studies could also investigate the photocatalytic degradation of a broader range of emerging contaminants, including pharmaceuticals (e.g., antibiotics other than TC), personal care products, organic dyes, and endocrine-disrupting compounds. This would provide a more comprehensive understanding of the efficiency of this hybrid wastewater treatment.

5.3 References

Ahmad, B., Dilshad, M., Haider, B., Anwar, M., Ali, H., Gilani, S., . . . Farooq, M. (2022). Synthesis of novel fly ash based geo-polymeric membranes for the treatment of textile waste water. *International Journal of Environmental Science and Technology*, 1-10.

Ahmed, M. A., Ahmed, M. A., & Mohamed, A. A. (2023). Adsorptive removal of tetracycline antibiotic onto magnetic graphene oxide nanocomposite modified with polyvinylpyrroilidone. *Reactive and Functional Polymers, 191*, 105701.

Ajiboye, T. O., Imade, E. E., Oyewo, O. A., & Onwudiwe, D. C. (2022). Silver functionalized gC3N4: Photocatalytic potency for chromium (VI) reduction, and evaluation of the antioxidant and antimicrobial properties. *Journal of Photochemistry and Photobiology A: Chemistry, 432*, 114107.

Ajiboye, T. O., Sawunyama, L., Ravele, M. P., Rasheed-Adeleke, A. A., Seheri, N. H., Onwudiwe, D. C., & Mhlanga, S. D. (2023). Synthesis approaches to ceramic membranes, their composites, and application in the removal of tetracycline from water. *Environmental Advances, 12*, 100371.

Al-Abri, M. Z., Al-Ghafri, B. N., & Al-Husaini, I. S. (2024). Permeation performance analysis of advanced ceramic and polymeric-based photocatalytic membrane (flux and rejection). *Advanced Ceramics for Photocatalytic Membranes*, 317-353.

Alias, S. S., Harun, Z., & Latif, I. S. A. (2018). Characterization and performance of porous photocatalytic ceramic membranes coated with TiO2 via different dip-coating routes. *Journal of Materials Science, 53*(16), 11534-11552.

Alkahtany, M. (2016). Color Stability, Physical Properties and Antifungal Effects of ZrO2 and TiO2 Nanoparticle Additions to Pigmented Polydimethylsiloxanes.

Alsubei, M. D., Reid, B., Aljlil, S. A., Coppens, M.-O., & Campos, L. C. (2024). Fabrication and characterization of coated ceramic membranes from natural sources for water treatment applications. *Journal of Membrane Science, 690*, 122226.

Bottino, A., Capannelli, G., Comite, A., Costa, C., Firpo, R., Jezowska, A., & Pagliero, M. (2020). Treatment of Olive Mill Wastewater through Integrated Pressure-Driven Membrane Processes. *Membranes (Basel), 10*(11), 334. doi:10.3390/membranes10110334

Chaim, R., Levin, M., Shlayer, A., & Estournes, C. (2008). Sintering and densification of nanocrystalline ceramic oxide powders: a review 2. *Advances in Applied Ceramics, 107*(3), 159-169. doi:10.1179/174367508x297812

Chiromo, H., & Chiromo, H. (2023). *Modified Metal Organic Frameworks Supported Ni Single Atom Catalyst for Enhanced Photocatalytic Hydrogen Evolution Reaction.* Paper presented at the Electrochemical Society Meeting Abstracts 243.

Danish, M. S. S., Estrella, L. L., Alemaida, I. M. A., Lisin, A., Moiseev, N., Ahmadi, M., . . . Senjyu, T. (2021). Photocatalytic Applications of Metal Oxides for Sustainable Environmental Remediation. *Metals, 11*(1), 80. doi:ARTN 80 10.3390/met11010080

Danwittayakul, S., Jaisai, M., Koottatep, T., & Dutta, J. (2013). Enhancement of Photocatalytic Degradation of Methyl Orange by Supported Zinc Oxide Nanorods/Zinc Stannate (ZnO/ZTO) on Porous Substrates. *Industrial & Engineering Chemistry Research, 52*(38), 13629-13636. doi:10.1021/ie4019726

Deng, C. X., Li, S., Khattak, K. N., Li, F., Yang, H. Y., Tang, F. L., & Yang, X. P. (2023). Photocatalytic degradation performance and mechanism of tetracycline by Pd-loaded titanium dioxide. *Journal of Environmental Chemical Engineering, 11*(5), 110433. doi:ARTN 110433 10.1016/j.jece.2023.110433

Done, H. Y., Venkatesan, A. K., & Halden, R. U. (2015). Does the recent growth of aquaculture create antibiotic resistance threats different from those associated with land animal production in agriculture? *The AAPS journal, 17*, 513-524.

Doran, P. M. (1995). *Bioprocess engineering principles*: Elsevier.

Ewis, D., Ismail, N. A., Hafiz, M., Benamor, A., & Hawari, A. H. (2021). Nanoparticles functionalized ceramic membranes: fabrication, surface modification, and performance. *Environ Sci Pollut Res Int, 28*(10), 12256-12281. doi:10.1007/s11356-020-11847-0

Faisal, M., Jalalah, M., Harraz, F. A., El-Toni, A. M., Labis, J. P., & Al-Assiri, M. S. (2021). A novel Ag/PANI/ZnTiO ternary nanocomposite as a highly efficient visible-light-driven photocatalyst. *Separation and Purification Technology, 256*, 117847. doi:ARTN 117847 10.1016/j.seppur.2020.117847

Gao, J. M., Yan, Z. W., Wang, B., Ma, Z. B., & Guo, Y. X. (2024). Preparation of whisker mullite ceramic membrane from coal fly ash for efficient oil-water separation. *Ceramics International, 50*(18), 32727-32736. doi:10.1016/j.ceramint.2024.06.082

Ghaderi, S., Lahafchi, R. T., & Jamshidi, S. (2023). Performance evaluation of PdO/ CuO TiO2 photocatalytic membrane on ceramic support for removing pharmaceutical compounds from water. *J Environ Health Sci Eng, 21*(2), 389-401. doi:10.1007/s40201-023-00866-x

Ghosh, R., Sahu, R. P., Ganguly, R., Zhitomirsky, I., & Puri, I. K. (2020). Photocatalytic activity of electrophoretically deposited TiO2 and ZnO nanoparticles on fog harvesting meshes. *Ceramics International, 46*(3), 3777-3785. doi:10.1016/j.ceramint.2019.10.100

Guan, Z. L., Li, X. M., Wu, Y., Chen, Z., Huang, X. D., Wang, D. B., . . . Zhao, H. (2021). AgBr nanoparticles decorated 2D/2D GO/Bi WO photocatalyst with enhanced photocatalytic performance for the removal of tetracycline hydrochloride. *Chemical Engineering Journal, 410*, 128283. doi:ARTN 12828310.1016/j.cej.2020.128283

Issaoui, M., & Limousy, L. (2019). Low-cost ceramic membranes: Synthesis, classifications, and applications. *Comptes Rendus Chimie, 22*(2-3), 175-187. doi:10.1016/j.crci.2018.09.014

Jang, H., Kang, S., & Kim, J. (2024). Identification of Membrane Fouling with Greywater Filtration by Porous Membranes: Combined Effect of Membrane Pore Size and Applied Pressure. *Membranes (Basel), 14*(2), 46. doi:10.3390/membranes14020046

Jezowska-Bojczuk, M., Lambs, L., Kozlowski, H., & Berthon, G. (1993). Metal ion-tetracycline interactions in biological fluids. 10. Structural investigations on copper (II) complexes of tetracycline, oxytetracycline, chlortetracycline, 4-(dedimethylamino) tetracycline, and 6-desoxy-6-demethyltetracycline and discussion of their binding modes. *Inorganic Chemistry, 32*(4), 428-437.

Jia, C. C., Dong, T., Li, M., Wang, P., & Yang, P. (2018). Preparation of anatase/rutile TiO/SnO hollow heterostructures for gas sensor. *Journal of alloys and compounds, 769*, 521-531. doi:10.1016/j.jallcom.2018.08.035

Jiang, Y., Tan, P., Liu, X. Q., & Sun, L. B. (2022). Process-Oriented Smart Adsorbents: Tailoring the Properties Dynamically as Demanded by Adsorption/Desorption. *Accounts of Chemical Research, 55*(1), 75-86. doi:10.1021/acs.accounts.1c00555

Karthikeyan, C., Arunachalam, P., Ramachandran, K., Al-Mayouf, A. M., & Karuppuchamy, S. (2020). Recent advances in semiconductor metal oxides with enhanced methods for solar photocatalytic applications. *Journal of alloys and compounds, 828*, 154281. doi:ARTN 154281 10.1016/j.jallcom.2020.154281

Kurniawan, Y. S., & Yuliati, L. (2021). Activity Enhancement of P25 Titanium Dioxide by Zinc Oxide for Photocatalytic Phenol Degradation. *Bulletin of Chemical Reaction Engineering and Catalysis, 16*(2), 310-319. doi:10.9767/bcrec.16.2.10319.310-319

Lagdali, S., Miyah, Y., El-Habacha, M., Mahmoudy, G., Benjelloun, M., Iaich, S., . . . Sinan, F. (2023). Performance assessment of a phengite clay-based flat membrane for microfiltration of real-wastewater from clothes washing: Characterization, cost estimation, and regeneration. *Case Studies in Chemical and Environmental Engineering, 8*, 100388.

Li, C., Lu, Z., Ao, X., Sun, W., & Huang, X. (2022). Degradation kinetics and removal efficiencies of pharmaceuticals by photocatalytic ceramic membranes using ultraviolet light-emitting diodes. *Chemical Engineering Journal, 427*, 130828.

Li, C., Sun, W., Lu, Z., Ao, X., & Li, S. (2020). Ceramic nanocomposite membranes and membrane fouling: A review. *Water Res, 175*, 115674. doi:10.1016/j.watres.2020.115674

Li, C. J., Zhang, Y. J., Chen, H., He, P. Y., Zhang, Y., & Meng, Q. (2021). Synthesis of fly ash cenospheres-based hollow ABW zeolite for dye removal via the coupling of adsorption and photocatalysis. *Advanced Powder Technology, 32*(10), 3436-3446. doi:10.1016/j.apt.2021.07.029

Li, J. G., & Ye, Y. P. (2006). Densification and grain growth of AlO nanoceramics during pressureless sintering. *Journal of the American Ceramic Society, 89*(1), 139-143. doi:10.1111/j.1551-2916.2005.00654.x

Liao, Q., Rong, H., Zhao, M., Luo, H., Chu, Z., & Wang, R. (2021). Interaction between tetracycline and microorganisms during wastewater treatment: A review. *Sci Total Environ, 757*, 143981. doi:10.1016/j.scitotenv.2020.143981

Liu, X., Steele, J. C., & Meng, X. Z. (2017). Usage, residue, and human health risk of antibiotics in Chinese aquaculture: A review. *Environ Pollut, 223*, 161-169. doi:10.1016/j.envpol.2017.01.003

Marzouk, S. S., Naddeo, V., Banat, F., & Hasan, S. W. (2021). Preparation of TiO/SiO ceramic membranes via dip coating for the treatment of produced water. *Chemosphere, 273*, 129684. doi:ARTN 129684 10.1016/j.chemosphere.2021.129684

Minale, M., Gu, Z., Guadie, A., Kabtamu, D. M., Li, Y., & Wang, X. (2020). Application of graphene-based materials for removal of tetracyclines using adsorption and photocatalytic-degradation: A review. *J Environ Manage, 276*, 111310. doi:10.1016/j.jenvman.2020.111310

Moradi, S., Aberoomand-Azar, P., Raeis-Farshid, S., Abedini-Khorrami, S., & Givianrad, M. H. (2016). The effect of different molar ratios of ZnO on characterization and photocatalytic activity of TiO2/ZnO nanocomposite. *Journal of Saudi Chemical Society, 20*(4), 373-378. doi:10.1016/j.jscs.2012.08.002

Nezamzadeh-Ejhieh, A., & Shirzadi, A. (2014). Enhancement of the photocatalytic activity of Ferrous Oxide by doping onto the nano-clinoptilolite particles towards photodegradation of tetracycline. *Chemosphere, 107*, 136-144. doi:10.1016/j.chemosphere.2014.02.015

Pourshaban-Mazandarani, M., & Nasiri, A. (2024). Photocatalytic Degradation of Tetracycline in Wastewater with Bio-based Matrix Magnetic Heterogeneous Nanocatalyst: Performance and Mechanism Study. *Journal of Polymers and the Environment*, 1-25. doi:10.1007/s10924-024-03340-3

Prakruthi, K., Ujwal, M. P., Yashas, S. R., Mahesh, B., Kumara Swamy, N., & Shivaraju, H. P. (2022). Recent advances in photocatalytic remediation of emerging organic pollutants using semiconducting metal oxides: an overview. *Environ Sci Pollut Res Int, 29*(4), 4930-4957. doi:10.1007/s11356-021-17361-1

Qiao, D. S., Li, Z. H., Duan, J. Y., & He, X. P. (2020). Adsorption and photocatalytic degradation mechanism of magnetic graphene oxide/ZnO nanocomposites for tetracycline contaminants. *Chemical Engineering Journal, 400*, 125952. doi:ARTN 125952 10.1016/j.cej.2020.125952

Rakcho, Y., Mouiya, M., Bouazizi, A., Abouliatim, Y., Sehaqui, H., Mansouri, S., . . . Abourriche, A. (2023). Treatment of seawater and wastewater using a novel low-cost ceramic membrane fabricated with red clay and tea waste. *Arabian Journal of Chemistry, 16*(11), 105277. doi:ARTN 10527710.1016/j.arabjc.2023.105277

Safari, G. H., Hoseini, M., Seyedsalehi, M., Kamani, H., Jaafari, J., & Mahvi, A. H. (2015). Photocatalytic degradation of tetracycline using nanosized titanium dioxide in aqueous solution. *International Journal of Environmental Science and Technology, 12*(2), 603-616. doi:10.1007/s13762-014-0706-9

Saikia, J., Sarmah, S., Bora, J. J., Das, B., & Goswamee, R. L. (2019). Preparation and characterization of low cost flat ceramic membranes from easily available potters' clay for dye separation. *Bulletin of Materials Science, 42*(3), 1-13. doi:ARTN 104 10.1007/s12034-019-1767-7

Samadi, A., Gao, L., Kong, L. X., Orooji, Y., & Zhao, S. F. (2022). Waste-derived low-cost ceramic membranes for water treatment: Opportunities, challenges and future directions. *Resources Conservation and Recycling, 185*, 106497. doi:ARTN 106497 10.1016/j.resconrec.2022.106497

Samaei, S. M., Gato-Trinidad, S., & Altaee, A. (2018). The application of pressure-driven ceramic membrane technology for the treatment of industrial wastewaters - A review. *Separation and Purification Technology, 200*, 198-220. doi:10.1016/j.seppur.2018.02.041

Sawunyama, L., Oyewo, O., Onwudiwe, D. C., & Makgato, S. S. (2023). Photocatalytic degradation of tetracycline using surface defective black TiO(2)-ZnO heterojunction photocatalyst under visible light. *Heliyon, 9*(11), e21423. doi:10.1016/j.heliyon.2023.e21423

Sawunyama, L., Oyewo, O. A., Seheri, N., Onjefu, S. A., & Onwudiwe, D. C. (2023). Metal oxide functionalized ceramic membranes for the removal of pharmaceuticals in wastewater. *Surfaces and Interfaces, 38*, 102787. doi:ARTN 102787 10.1016/j.surfin.2023.102787

Shi, J. H., Yang, T. T., Zhao, T., Pu, K. K., Shi, J. T., Zhou, A. J., . . . Xue, J. B. (2024). Insights on the efficiency and contribution of single active species in photocatalytic degradation of tetracycline: Priority attack active sites, intermediate products and their toxicity evaluation. *Journal of Environmental Management, 367*, 121970. doi:ARTN 121970 10.1016/j.jenvman.2024.121970

Wu, H., Xu, X., Shi, L., Yin, Y., Zhang, L. C., Wu, Z., . . . Sun, H. (2019). Manganese oxide integrated catalytic ceramic membrane for degradation of organic pollutants using sulfate radicals. *Water Res, 167*, 115110. doi:10.1016/j.watres.2019.115110

Xie, X. Y., Wang, L. J., Wei, J., He, H. Y., Guo, Z., Wang, C., . . . Song, Y. H. (2024). Progress in ceramic membrane coupling ozonation process for water and wastewater treatment: A critical review. *Chemical Engineering Journal, 493*, 152475. doi:ARTN 152475 10.1016/j.cej.2024.152475

Zaleska-Medynska, A. (2018). *Metal oxide-based photocatalysis: fundamentals and prospects for application*: Elsevier.

Zhao, Y., Yang, Q. E., Zhou, X., Wang, F.-H., Muurinen, J., Virta, M. P., . . . Zhu, Y.-G. (2021). Antibiotic resistome in the livestock and aquaculture industries: Status and solutions. *Critical Reviews in Environmental Science and Technology, 51*(19), 2159-2196.

Zhu, X. D., Wang, Y. J., Sun, R. J., & Zhou, D. M. (2013). Photocatalytic degradation of tetracycline in aqueous solution by nanosized TiO2. *Chemosphere, 92*(8), 925-932. doi:10.1016/j.chemosphere.2013.02.066

Zou, D., Fan, W., Xu, J. R., Drioli, E., Chen, X. F., Qiu, M. H., & Fan, Y. Q. (2021). One-step engineering of low-cost kaolin/fly ash ceramic membranes for efficient separation of oil-water emulsions. *Journal of Membrane Science, 621*, 118954. doi:ARTN 118954 10.1016/j.memsci.2020.118954

Chapter 6

Conclusion and recommendation

6.0 Conclusion

The photocatalytic and filtration properties of the TiO_2-ZnO functionalized coal fly ash-based ceramic membrane fabricated through co-pressing and co-sintering method is reported in this thesis. The intrinsic properties of the fabricated materials were characterized by chemical and physical properties such as chemical stability, mechanical stability, water absorption, and porosity. The shape, crystallinity, thermal characteristics, and functional groups were also determined using SEM, XRD, TGA, and FTIR studies. The effects of reaction parameters, including sintering temperature, and precursor ratios, on the properties of the fabricated materials were examined across various chapters. Additionally, the impact of process parameters such as catalyst dosage, pH, and contaminant concentration was also discussed.

In chapter 3, visible light-driven photocatalytic degradation of tetracycline using surface defective black TiO_2-ZnO heterojunction photocatalyst was investigated. The studies revealed that the TiO_2-ZnO heterojunction photocatalyst effectively degraded tetracycline under visible light. The optimal conditions for the photocatalytic degradation process were found to be a pH of 7, a tetracycline concentration of 50 mg/L, and a photocatalyst dosage of 100 mg. The study also confirmed that solution pH plays a critical role in the degradation process. A pH of $\geq$ 10 resulted in enhanced photocatalytic degradation, while a new absorption peak at 550 nm indicated the formation of by-products.

In chapter 4, low cost and sustainable ceramic membranes were successfully fabricated from coal fly ash, an industrial solid waste product, and natural sand, a commonly available and inexpensive natural material. Dextrin and carboxymethyl cellulose (CMC) were used as pore former and binder respectively. These ceramic membranes were fabricated by the uniaxial compaction technique using a manual hydraulic pressing machine. X-ray fluorescence (XRF) analysis of the starting materials confirmed the presence of SiO_2 and Al_2O_3, two key inorganic materials required for the fabrication of ceramic membranes. Heavy metals present in the raw coal fly ash were leached out before the fabrication process. The membrane, fabricated with 20 wt% sand content and sintered at 1000 °C, had a pore size of 0.64 µm and a porosity of 34.7%. It demonstrated good mechanical strength (7.71 MPa) and exceptional chemical stability. Additionally, the membrane exhibited a remarkable water permeability of 32.23 $L/m^2/h$.

In chapter 5, the prepared TiO_2-ZnO functionalized coal fly ash-based ceramic membrane and pristine coal fly ash-based ceramic membrane were evaluated on the removal efficiency of tetracycline in

synthetic wastewater by photocatalysis and filtration. The study's results demonstrated that the asymmetric functionalized coal fly ash-based ceramic membranes demonstrated remarkable efficacy in the tetracycline degradation process, indicating a significant advancement in the field of environmental remediation. The TiO_2-ZnO heterojunction nanocomposite facilitates efficient visible light absorption and charge separation, leading to effective tetracycline degradation. Additionally, the coal fly ash-based ceramic membrane offers a high surface area, enhancing tetracycline adsorption and improving photocatalytic degradation. The functionalized coal fly ash-based ceramic membrane also demonstrated commendable stability and reusability, making it a promising candidate for practical applications in wastewater treatment. Reusability studies of TiO_2-ZnO functionalized coal fly ash-based ceramic membranes showed that they retained over 73% of their efficiency after five cycles. This study contributes to the development of advanced materials for remediating antibiotic-contaminated water sources, addressing environmental concerns related to pharmaceutical pollutants.

6.1 Recommendation

Although the specific objectives of the study were achieved, additional issues that require further examination for the scale-up of photocatalytic ceramic membranes and their utilization in real industrial applications are:

1. The removal efficiency of tetracycline by the functionalized coal fly ash-based ceramic membranes was assessed through independent photocatalysis and filtration processes. It is therefore recommended that further studies explore the use of the fabricated photocatalytic ceramic membrane in a hybrid photocatalysis and filtration reactor system, to optimize its synergistic photocatalytic, adsorption, and filtration properties, rather than evaluating these processes separately.
2. To fully assess the effectiveness of the fabricated photocatalytic ceramic membrane, it is recommended that evaluation be extended to a diverse range of water contaminants. This should include not only pharmaceuticals but also organic dyes, metals, and microbial organisms.
3. Further studies are recommended to investigate the mechanism of degradation, the nature of degradation products, and the toxicity of these degradation products resulting from the photocatalytic degradation of tetracycline using a TiO_2-ZnO functionalized coal fly ash-based ceramic membrane.